This work is financed by Fundos FEDER from Programa Operacional Factores do Competitividade (COMPETE) and Fundos Nacionais from Fundação para a Ciência e a Tecnologia (FCT) within the scope of the project SFRH/BD/80537/2011 and by the European Union (FEDER funds through COMPETE) and National Funds (FCT), through project Pest-C/EQB/LA0006/2013. Part of the research was carried out with the equipment purchased thanks to the financial support of the European Regional Development Fund in the framework of the Polish Innovation Economy Operational Program (contract no. POIG.02.01.00-12-023/08). To all financing sources the authors are greatly indebted.

Acknowledgments

I would like to express my deepest, sincere and special gratitude towards all the people who made this big step in my life possible.

To Dr. Sónia Figueiredo and Dr. Olga Freitas for "*if you need any help, you know where to find us*", for their valuable guidance, constant care, friendly attitude, and for their patience in correcting my uncountable spelling mistakes.

To Dr. Agnieszka Węgrzyn without whom I would not be where I am today; for her support and dedication, for pushing me to the limits, and for the long hours spent in the laboratory.

To Paula Paíga for always being ready to help.

To Dr. Cristina Deluere-Matos, Dr. Teresa Teles, and Prof. Dr. hab. Lucjan Chmielarz for their support.

"Understand that friends come and go, but for the precious few you should hold on."
-Mary Schmich-

Therefore, last but not least, many thanks to Leonel Março, Monica Avila Garcia, Bartosz Borowicz, Cláudia Mendes, Shashank Gaur, André Teixeira, Paulo Pimenta, Pedro Martins, Luisa Correia de Sá and Paula Paíga for holding on.

Author's publications related to this thesis

Published papers

Wojciech Stawiński, Olga Freitas, Lucjan Chmielarz, Agnieszka Węgrzyn, Kamila Komędera, Artur Błachowski, Sónia Figueiredo, *The influence of acid treatments over vermiculite based material as adsorbent for cationic textile dyestuffs.*
Chemosphere, 153 (2016), pp. 115 – 129.

Wojciech Stawiński, Agnieszka Węgrzyn, Tomasz Dańko, Olga Freitas, Sónia Figueiredo, Lucjan Chmielarz, *Acid-base treated vermiculite as high performance adsorbent: Insights into the mechanism of cationic dyes adsorption, regeneration, recyclability and stability studies*.
Chemosphere, 173 (2017), pp. 107 – 115.

Wojciech Stawiński, Agnieszka Węgrzyn, Olga Freitas, Lucjan Chmielarz, Grzegorz Mordarski, Sónia Figueiredo, *Simultaneous removal of dyes and metal cations using an acid, acid-base and base modified vermiculite as a sustainable and recyclable adsorbent.*
Science of the Total Environment, 576 (2017), pp. 398-408.

Submitted manuscripts

Wojciech Stawiński, Agnieszka Węgrzyn, Olga Freitas, Lucjan Chmielarz, Sónia Figueiredo, *Dual-function hydrotalcite-derived adsorbents with sulfur storage properties: dyes and hydrotalcite fate in adsorption-regeneration cycles.*
Submitted to Microporous and Mesoporous Materials on 21st of June 2016.

Wojciech Stawiński, Agnieszka Węgrzyn, Grzegorz Mordarski, Zofia Piwowarska, Michał Skiba, Olga Freitas, Sónia Figueiredo, *Sustainable adsorbent obtained from byproduct of acid activation of vermiculite and composite clay-LDH hybrid adsorbent for removal of industrial dyes and metal cations.*
Submitted to Green Chemistry on 15th of March 2017.

Abstract

The quality of water is an issue of the uttermost importance, which is vital to the maintenance of the hydrological environment and to human health. Therefore this scarce good should be preserved and protected from the effects of pollution. Colored wastewater is created as a result of the production of dyes and as well as a direct consequence of its use in textile and related industries. Metals are found among the most common pollutants and often accompany dyes in wastewaters. Among many available treatment techniques adsorption has been getting more interest due to its good efficiency, ease of operation, wide application, and possibility of regeneration and reuse of many adsorbents. The most desired adsorbent should be derived from inexpensive and easily available materials, they should be produced on a sustainable way and do not pose hazards to the environment. Double layered materials (LDMs), such as clays and layered double hydroxides (LDHs), owning to their specific properties may be applied in this field. LDMs can be subjected to various modifications in order to enhance their adsorption capacities.

Adsorption studies using a clay (vermiculite), a LDH (hydrotalcite) and their modified derivatives were performed in batch system and in column. Two well-known equilibrium models, Langmuir's and Freundlich's models, and two commonly used kinetic models, pseudo 1^{st} and pseudo 2^{nd} order models, were adjusted to the data gathered during the experiments. Moreover, the performance of such prepared adsorbents was tested in packed bed column, with constant flow, and evaluated by adjusting Yan's, Thomas', and Yoon-Nelson's models. The adsorbents derived from vermiculite were tested additionally in bi and tricomponent solutions containing cationic dyes and Cu^{2+} cations. The hybrid composite vermiculite-hydrotalcite-like LDH and hydrotalcite-like LDHs were tested in batch system and adsorption capacities were determined. All materials were characterized by X-ray diffraction (XRD), Attenuated Total Reflectance Spectroscopy (ATR), Diffuse Reflectance Infrared Fourier Transform Spectroscopy (DRIFT), X-ray fluorescence (XRF), Scanning Electron Microscopy (SEM), Scanning Electron Microscopy with Energy Dispersive Spectroscopy (SEM-EDS), UV–vis-Diffuse Reflectance Spectroscopy (UV-vis-DRS) and Thermogravimetric Analysis (TGA). The determination of point of zero charge (PZC) and specific surface area by Brunauer, Emmett and Teller (BET) technique were also performed.

Vermiculite was subjected to modifications based on acid, combined acid-base and base activation. The first modification consisting of treatment with 1.8 M nitric acid and 10% (m/v) citric acid resulted in an increase of the adsorption capacity for the cationic dyes, Methylene Blue (MB) from 55 ± 2 to 150 ± 4 mg g^{-1} and Astrazon Red (AR) from 54 ± 1 to 100.8 ± 0.8 mg g^{-1} in column operation (feed concentration of 50 mg L^{-1}). However, the capacity for Cu^{2+} decreased from 15 ± 1 to 5.28 ± 0.09 mg g^{-1} in batch system with initial Cu^{2+} concentration equal to 25 mg L^{-1}. The second modification (acid-base activation) resulted in further increase of the capacity for the dyes to 127 ± 2 mg g^{-1}

and 203 ± 4 mg g^{-1} for AR and MB, respectively. Moreover, the capacity for Cu^{2+} was regained and returned to 24 ± 1 mg g^{-1} in column operation with the feed concentration of 50 mg L^{-1} in the case of the dyes, and 25 mg L^{-1} in the case of Cu^{2+}. The third modification (base activation) did not change the adsorption capacity of vermiculite for dyes; however a significant increase to 51 ± 1 mg g^{-1} occurred in the case of Cu^{2+} in column operation (feed concentration 25 mg L^{-1}). All presented capacity values were estimated through column experiments. Regeneration experiments showed that a mixture of 1 M NaCl and ethanol (1:1 v/v) was efficient in desorbing dyes from the material, whereas 0.5 M HNO_3 was efficient for desorbing metal cations. Subsequent application of the above mentioned eluents allowed separation of both adsorbates.

Hydrotalcite was subjected to thermal treatment that resulted in the formation of mixed oxides, which regenerate the layer structure in aqueous solution. Upon annealing at 450 °C the maximum adsorption capacity for the anionic dye Levafix Amber increased from 179 ± 5 to 291 ± 8 mg g^{-1} at pH 3.5. The cationic dye AR reached maximum adsorption capacities, at pH 8.0, of 6 ± 2 and 48 ± 2 mg g^{-1}, respectively before and after calcination of the materials based on the equilibrium experiments. Thermal regeneration of this material was efficient; however some sulfuric compounds were accumulated in the material in each desorption cycle.

Hydrotalcite-like LDH materials were synthesized from the by-product of acid activation of raw (W) and expanded (Ve) vermiculites and subjected to thermal treatment at 450 °C, which enhanced their adsorption capacities. The highest removal was obtained for the materials derived from W after treatment with 3.2 M nitric acid for the anionic dye Congo Red (CR) and Cu^{2+} reaching capacities of 289 ± 2 and 64 ± 2 mg g^{-1}, respectively. For the materials derived from W by treatment with 1.8 M nitric acid capacities of 38.2 ± 0.6 and 137 ± 2 mg g^{-1} were obtained for the cationic dye AR and the anionic dye Reactive Red 184 (R), respectively.

A composite hybrid vermiculite-hydrotalcite-like LDH adsorbent was formed by joining the acid activated vermiculite with the by-product of that activation in one-pot synthesis. Thermal treatment was applied to increase the adsorption capacities of prepared materials. The highest levels of removal were obtained on the material derived from W subjected to activation with 3.2 M nitric acid, reaching capacities of 44 ± 1, 238 ± 3, 111 ± 2 and 72 ± 3 mg g^{-1}, respectively for AR, CR, R and Cu^{2+}. The presented results were obtained in batch system with concentration 200 mg L^{-1} for dyes and 30 mg L^{-1} for Cu^{2+}. Moreover, a strong synergic effect on adsorption was observed in this group of materials (up to 400%), based on analysis of materials' composition. The values obtained in the experiments were higher than the theoretical capacities of adsorbents prepared by mixing *ex situ* of the acid activated vermiculite with the hydrotalcite-like LDHs in appropriate proportions.

Keywords: adsorption, activation, dyes, hydrotalcite, metals, regeneration, vermiculite.

Resumo

A qualidade da água é uma questão de extrema importância, que é vital para a manutenção do ambiente hidrológico e para a saúde humana. Portanto, este bem escasso deve ser preservado e protegido dos efeitos da poluição. As águas residuais coradas têm origem na produção de corantes e são também originadas como consequência directa da utilização de corantes na indústria têxtil e afins. Os metais encontram-se entre os poluentes mais comuns e aparecem muitas vezes em simultâneo com corantes nas águas residuais. Entre as várias técnicas de tratamento disponíveis a adsorção tem despertado mais interesse devido à sua elevada eficiência, facilidade de operação, aplicação abrangente, e possibilidade de regeneração e reutilização dos adsorventes. O adsorvente ideal deve ser derivado de materiais baratos e facilmente disponíveis, ser produzido de forma sustentável e que não apresente perigosidade para o ambiente. Os materiais de camada dupla (LDMs), tais como as argilas e os hidróxidos duplos lamelares (LDHs), devido às suas propriedades específicas, podem ser utilizados nesta área. Podem ser aplicadas várias modificações aos LDMs de forma a aumentar as suas capacidades de adsorção.

Estudos de adsorção usando uma argila (vermiculite), um LDH (hidrotalcite) e as suas formas modificadas foram realizados em sistema fechado e em coluna. Os dados recolhidos durante as experiências foram ajustados a dois modelos de equilíbrio bem conhecidos, o de Langmuir e o de Freundlich, e a dois modelos cinéticos muito utilizados, os modelos de pseudo-primeira e de pseudo-segunda ordem. Além disso, o desempenho de tais adsorventes foi testado em coluna de leito fixo com fluxo constante, e avaliado com base nos ajustes aos modelos de Yan, Thomas e Yoon-Nelson. Os adsorventes derivados da vermiculite foram testados adicionalmente em sistemas bi e tricomponente, contendo corantes catiónicos e catiões Cu^{2+}. Os materiais híbridos constituídos por vermiculite-LDH tipo-hidrotalcite e LDHs tipo-hidrotalcite foram testados em sistema fechado e foram determinadas as respetivas capacidades de adsorção. Todos os materiais foram caracterizados por difração de raios X (XRD), espectroscopia de reflectância total atenuada (ATR), espectroscopia de transformada de Fourier no infravermelho de reflexão difusa (DRIFT), fluorescência de raios X (XRF), microscopia eletrónica de varrimento (SEM), microscopia eletrónica de varrimento - espectroscopia de Dispersão de Energia (SEM-EDS), espectroscopia de reflexão UV-vis-Difusa (UV-vis-DRS) e análise termogravimétrica (TGA). Foram também realizadas as determinações do ponto de carga zero (PZC) e da área superficial específica pela técnica de Brunauer, Emmett e Teller (BET).

A vermiculite foi sujeita a activação ácida, combinação de activação ácida e alcalina, e activação alcalina. A primeira modificação, consistiu no tratamento com ácido nítrico 1,8 M e posterior tratamento com ácido cítrico a 10% (m/v), tendo produzido um aumento na capacidade de adsorção dos corantes catiónicos Azul de Metileno (MB) e Astrazon Red (AR), em coluna de leito fixo (concentração de alimentação de 50 mg L^{-1}), de 55 ± 2 para 150 ± 4 mg g^{-1} e de 54 ± 1 para 100,8 ± 0,8 mg g^{-1}, respetivamente.

Contudo, a capacidade de adsorção do Cu^{2+}, determinada em sistema fechado para uma concentração inicial de 25 mg L^{-1}, diminuiu de 15 ± 1 para 5,28 ± 0,09 mg g^{-1}.

A segunda modificação (activação ácida-alcalina) resultou num aumento adicional da capacidade para os corantes AR e MB, obtendo-se valores de 127 ± 2 mg g^{-1} e 203 ± 4 mg g^{-1}, respetivamente. Além disso, a capacidade de Cu^{2+} retomou um valor semelhante ao obtido para o material sem tratamento, 24 ± 1 mg g^{-1} nos ensaios em coluna com as concentrações iniciais de 50 mg L^{-1} para os corantes e de 25 mg L^{-1} para o Cu^{2+}. A terceira modificação (ativação alcalina) não alterou a capacidade de adsorção da vermiculite para os corantes, contudo ocorreu um aumento significativo para 51 ± 1 mg g^{-1} no caso de Cu^{2+} (concentração de alimentação à coluna de 25 mg L^{-1}). As experiências de regeneração mostraram que o eluente constituído pela mistura de NaCl 1 M e etanol (1:1 v/v) era eficiente na dessorção de corantes do material, enquanto que para a dessorção de catiões Cu^{2+} era eficiente a solução HNO_3 0,5 M. A aplicação subsequente dos eluentes acima mencionados permitiu a separação de ambos os adsorvatos.

A hidrotalcite foi submetida a um tratamento térmico, que resultou na formação de óxidos mistos que, em solução aquosa, regeneram a estrutura em camadas. Após calcinação a 450 °C a capacidade máxima para o corante aniónico Levafix Amber aumentou de 179 ± 5 para 291 ± 8 mg g^{-1} a pH 3,5. O corante catiónico AR atingiu capacidades máximas, com base nos ensaios de equilíbrio, a pH 8,0, de 6 ± 2 e 48 ± 2 mg g^{-1} antes e após calcinação, respetivamente. A regeneração térmica deste material foi eficiente, contudo observou-se uma acumulação de alguns compostos sulfúricos no material em cada ciclo de dessorção.

Os materiais de LDH tipo-hidrotalcite foram sintetizados a partir do subproduto da activação ácida de vermiculite bruta (W) e expandida (Ve), e submetidos a tratamento térmico a 450 ° C, o que aumentou as suas capacidades de adsorção. A remoção mais elevada foi obtida para os materiais derivados de W após tratamento com ácido nítrico 3,2 M para o corante aniónico Congo Red (CR) e Cu^{2+}, alcançando capacidades de 289 ± 2 e 64 ± 2 mg g^{-1}, respectivamente. Para os materiais derivados de W por tratamento com ácido nítrico 1,8 M obtiveram-se capacidades de 38,2 ± 0,6 e 137 ± 2 mg g^{-1} para o corante catiónico AR e para o corante aniónico Reactive Red 184 (R), respetivamente.

O compósito híbrido de vermiculite-LDH tipo-hidrotalcite foi sintetizado pela junção de vermiculite activada com ácido com o subproduto dessa activação. Foi aplicado um tratamento térmico para aumentar as capacidades de adsorção dos materiais preparados. Os níveis de remoção mais elevados foram obtidos para o material derivado de W que foi submetido a ativação com ácido nítrico 3,2 M, atingindo capacidades de 44 ± 1, 238 ± 3, 111 ± 2 e 72 ± 3 mg g^{-1}, respetivamente para AR, CR, R e Cu^{2+}. Os resultados apresentados foram obtidos para os ensaios em sitema fechado com concentrações iniciais de 200 mg L^{-1} para os corantes e 30 mg L^{-1} para o Cu^{2+}.Além disso, neste grupo de materiais observou-se um forte efeito sinérgico na adsorção (até 400%), com base na análise da composição dos materiais. Os valores obtidos nas experiências foram superiores às capacidades teóricas dos adsorventes preparados, misturando *ex situ* nas proporções adequadas a vermiculite activada com ácido com LDH tipo-hidrotalcite.

Palavras-chave: adsorção, ativação, corantes, hidrotalcite, metais, regeneração, vermiculite.

Abstrakt

Jakość wody jest strategicznym elementem wpływającym na prawidłowe funkcjonowanie ekosystemu i na zdrowie człowieka, dlatego kwestia jej ochrony jest sprawą pierwszorzędnej wagi. Zanieczyszczenie wód barwnikami powstaje bezpośrednio w wyniku ich produkcji jak i ich użytkowania. Co więcej, w ściekach często towarzyszą im metale ciężkie, które same w sobie są jednym z najbardziej rozpowszechnionych zanieczyszczeń. Pośród wielu dostępnych metod oczyszczania ścieków, adsorpcja jest szczególnie interesująca ze względu na wydajny i nieskomplikowany proces oczyszczania, szerokie pasmo zastosowań i możliwość regeneracji i ponownego wykorzystania większości adsorbentów. Pożądany adsorbent powinien byś otrzymany z niedrogiego i łatwo dostępnego materiału na zrównoważonej drodze i charakteryzować się dobrą pojemnością sorpcyjną oraz nie stwarzać zagrożenia dla środowiska. Materiały o strukturze warstwowej (double layered materails – LDMs) takie jak minerały ilaste i warstwowe podwójne wodorotlenki (double layered hydroxides – LDHs) stwarzają dobre perspektywy jako adsorbenty. Ponadto materiały te mogą zostać poddane rożnym modyfikacjom, skutkującym zmianami w ich właściwościach i często znacznym wzrostem pojemności sorpcyjnej.

Właściwości sorpcyjne minerału ilastego wermikulitu i warstwowego podwójnego wodorotlenku, hydrotalkitu oraz ich modyfikowanych wersji zostały przetestowane w reaktorze okresowym (tbatch) i przepływowym (kolumna). Dwa powszechnie stosowanie równania do modelowania procesów kinetycznych tj. równanie pseudo-pierwszo- i pseudo-drugorzędowe, oraz równanie izoterm Langmuira i Freundlicha zostały doładowane do otrzymanych danych. Model Yana, Thomasa i Yoon-Nelsona zostały dopasowane do danych otrzymanych z badań w reaktorze przepływowym. Adsorbenty uzyskane z wermikulitu zostały dodatkowo przetestowane w układach zawierających barwniki i Cu^{2+} w dwu i trzy składnikowym systemie. Materiały powstałe z hydrotalkitu oraz hybrydy zawierające wermikulit i hydrotalkit zostały zbadane jedynie w systemie typu „batch". Wszystkie próbki zostały scharakteryzowane przy użyciu następujących metod: rentgenografia strukturalna (XRD), spektroskopia odbicia rozproszonego w podczerwieni (DRIFT), fluorescencja rentgenowska (XRF), skaningowa mikroskopia elektronowa (SEM), skaningowa mikroskopia elektronowa z dyspersją energii (SEM-EDS), spektroskopia odbicia promieniowania UV-Vis (UV-Vis-DRS), analiza termograwimetryczna (TGA). Ponadto oznaczony został punk izoelektryczny (PZC) i powierzchnia właściwa materiałów metodą BET.

Wermikulit został poddany modyfikacjom opartym na aktywacji kwasem, kwasem i zasadą oraz zasadą. Aktywacja kwasowa polegająca na traktowaniu 1.8 M HNO_3 i 10% (m/v) kwasem cytrynowym poskutkowała zwiększeniem pojemności adsorpcyjnej materiału dla barwników kationowych – Błękitu Metylenowego (MB) z 55 ± 2 mg g^{-1} do 150 ± 4 mg g^{-1} oraz Astrazon Red (AR) z 54 ± 1 do 100.8 ± 0.8 mg g^{-1} (kolumna, steżenie barwników równe 50 mg L^{-1}). Jednocześnie zaobserwowano spadek pojemności dla kationów Cu^{2+} z 15 ± 3 do 5.28 ± 0.09 mg g^{-1} (batch, steżnie początkowe

równe 25 mg L^{-1}). Traktowanie kwasowo-zasadowe spowodowało znacznie większym wzrostem pojemności adsorpcyjnej materiału do 127 ± 2 mg g^{-1} i 203 ± 4 mg g^{-1} dla odpowiednio AR i MB. Co więcej, pojemność dla Cu^{2+} została zregenerowana i osiągnęła poziom materiału wyjściowego (kolumna, 50 mg L^{-1} dla barwników i 25 mg L^{-1} dla Cu^{2+}). Modyfikacja oparta na traktowaniu zasadą nie zmieniła pojemności adsorpcyjnej dla barwników, jednakże widoczny wzrost do 51 ± 1mg g^{-1} odnotowano dla kationów miedzi (kolumna 25 mg L^{-1}). Badania nad regeneracją tak przygotowanych adsorbentów wykazały, iż mieszanina 1M roztworu NaCl z etanolem (1:1 v/v) jest odpowiednia do desorpcji barwników, a 0.5 M roztwór HNO_3 sprawdza się przy desorpcji kationów miedzi. Ponadto naprzemienne użycie obu eluentów pozwoliło na rozdzielenie barwników od kationów metalu.

Hydotalkit został poddany modyfikacjom termicznym. Kalcynacja w 450 °C poskutkowała utworzeniem mieszanych podwójnych tlenków, które były w stanie odtworzyć warstwową strukturę materiału wyjściowego. Tak przygotowany adsorbent charakteryzował się zwiększoną pojemnością adsorpcją dla anionowego barwnika Levafix Amber (AMB), która wzrosła z 179±5 do 291±8 mg g^{-1} w pH 3.5. Kationowy barwnik AR był adsorbowany na tym materiale w pH 8.0 na poziomie 6±2 mg g^{-1} przed kalcynacją i na poziomie 48±2 mg g^{-1} po kalcynacji (wyniki na podstawie izoterm) Materiał ten został poddany skutecznej regeneracji termicznej, jednakże zaobserwowano akumulację związków siarki powstałych w wyniki rozkładu AMB.

Materiały hydrotalkitowe (LHDs) zostały zsyntetyzowane wykorzystując produkt uboczny powstały przy aktywacji kwasowej wermikulitów: surowego (W) i ekspandowanego (Ve). Kalcynacja w 450 °C poskutkowała zwiększeniem ich pojemności adsorpcyjnej. Materiał otrzymany z produktu aktywacji W w 3.2 M HNO_3 charakteryzował się największą pojemnością dla anionowego barwnika – Czerwieni Kongo (CR) i Cu^{2+} osiągając odpowiednio poziom 289 ± 2 i 64 ± 2 mg g^{-1}. Adsorbent otrzymany z produktu ubocznego aktywacji W w 1.8 M HNO_3 osiągnął wysoki poziom adsorpcji dla anionowego barwnika – Reactive Red 184 (R) (137 ± 2 mg g^{-1}) i kationowego AR (38.2 ± 0.6 mg g^{-1}).

Hybrydowy adsorbent zawierający LDH i wermikulit został zsyntezowany przez połączenie produktu ubocznego aktywacji z aktywowanym wermikulitem w syntezie jednonaczyniowej. Otrzymany materiał został poddany obróbce termicznej w 450 °C. Największy poziom adsorpcji został odnotowany dla materiału otrzymanego z surowego wermikulitu po aktywacji w 3.2 M HNO_3 osiągając pojemność 44±1, 238±3, 111±2 i 72±3 mg g^{-1} odpowiednio dla AR, CR, R i Cu^{2+}. Co więcej, ta grupa materiałów wykazała silny efekt synergiczny na adsorpcję, która wzrosła nawet o 400 % w porównaniu do teoretycznej pojemność adsorbentów otrzymanych przez zmieszanie ex situ aktywowanego wermikulitu i LDH w proporcjach wynikających z analizy XRF otrzymanych hybryd. Przedstawione wyniki w oparciu o wyniki z system batch przy poczatkwoych steżeniach barnikow rownych 200 mg L^{-1} I metalu 25 mg L^{-1}.

Słowa-klucze: adsorpcja, aktywacja, barwniki, hydrotalkit, metale, regeneracja, vermikulit

Table of content

CHAPTER 3 *Acid-base treatment of vermiculite*

CHAPTER 5 *Hydrotalcite*

CHAPTER 6 *Hybrids*

CHAPTER 7 *General conclusions and suggestions for future work*

List of figures

CHAPTER 1

CHAPTER 2

Appendix A.2

CHAPTER 3

Supplementary Material S.3

CHAPTER 4

Appendix A.4

Supporting material S.4

CHAPTER 5

Appendix A.5

CHAPTER 6

List of tables

CHAPTER 1

CHAPTER 2

Appendix A.2

CHAPTER 3

Supplementary Material S.3

CHAPTER 4

Appendix A.4

CHAPTER 5

Appendix A.5

CHAPTER 6

List of abbreviations

C_e	equilibrium concentration in liquid phase (mg L^{-1})
F	flow rate (mL min^{-1})
k_1	pseudo 1st order kinetic rate constant (min^{-1})
k_2	pseudo 2nd order kinetic rate constant (g mg^{-1} min^{-1})
K_F	Freundlich's constant ((mg g^{-1})(L mg^{-1})$^{1/n}$)
K_L	Langmuir's constant related to energy of adsorption (L mg^{-1})
K_{Th}	Thomas's constant (mL (mg min)$^{-1}$)
a_Y	Yan´s constant (dimensionless)
k_{YN}	Yoon-Nelson´s constant (min^{-1})
M	amount of adsorbent in Thomas's model (mg)
m	adsorbent mass (mg; g)
n	Freundlich's constant (dimensionless)
q	adsorption capacity (mg g^{-1})
Q_0	maximum solid-phase solute concentration in Thomas's model (mg g^{-1})
q_e	adsorption capacity at equilibrium (mg g^{-1})
q_m	Langmuir's model maximum adsorption capacity (mg g^{-1})
q_t	adsorption capacity at time t (mg g^{-1})
q_y	maximum adsorption capacity in Yan model (mg g^{-1})
r^2	determination coefficient
s^2	variance coefficient
t	time (min)
τ	time required for 50% adsorbate breakthrough (min)
V	volume (mL)
XRD	X-ray diffraction (),
ATR	Attenuated Total Reflectance Spectroscopy
DRIFT	Diffuse Reflectance Infrared Fourier Transform Spectroscopy
XRF	X-ray fluorescence
SEM	Scanning Electron Microscopy
SEM-EDS	Scanning Electron Microscopy with Energy Dispersive Spectroscopy
UV-vis-DRS	UV–vis-Diffuse Reflectance Spectroscopy
TGA	Thermogravimetric Analysis
PZC	point of zero charge
BET	specific surface area by Brunauer, Emmett and Teller technique
MB	Methylene Blue
AR	Astrazon Red
CR	Congo Red
MO	Methyl Orange
AMB	Levafix Amber
R	Reactive Red 184

List of tested materials

HT	AlMg-hydrotalcite
HToxC300 AMB	hydrotalcite regenerated from mixed oxides obtained at 300 °C, saturated with the dye Levafix Amber (AMB)
HToxC300	mixed oxides obtained from hydrotalcite calcined at 300 °C
HToxC450 AMB	hydrotalcite regenerated from mixed oxides obtained at 450 °C, saturated with the dye Levafix Amber (AMB)
HToxC450	mixed oxides obtained from hydrotalcite calcined at 450 °C
HToxC600 AMB	hydrotalcite regenerated from mixed oxides obtained at 600 °C, saturated with the dye Levafix Amber (AMB)
HToxC600	mixed oxides obtained from hydrotalcite calcined at 600 °C
HToxC750 AMB	hydrotalcite regenerated from mixed oxides obtained at 750 °C, saturated with the dye Levafix Amber (AMB)
HToxC750	mixed oxides obtained from hydrotalcite calcined at 750 °C
HT-REF	reference AlMgFe-hydrotalcite-like material
Ve NaCl 1M	expanded vermiculite treated with 1.0 M NaCl
Ve Act	expanded vermiculite treated with acetone
Ve Clmf	expanded vermiculite treated with chloroform
Ve EtOH	expanded vermiculite treated with ethanol
Ve EtOH+HNO_3	expanded vermiculite treated with a mixture of ethanol and 0.5 M HNO_3 (1:1 v/v)
Ve EtOH+NaCl	expanded vermiculite treated with a mixture of ethanol and 1 M NaCl (1:1 v/v)
Ve H_2O COLD	expanded vermiculite treated with cold water
Ve H_2O HOT	expanded vermiculite treated with hot water
Ve HCl 0.1M	expanded vermiculite treated with 0.1 M HCl
Ve MeOH	expanded vermiculite treated with methanol
Ve NaCl 0.5M	expanded vermiculite treated with 0.5 M NaCl
Ve NaCl 5M	expanded vermiculite treated with 5.0 M NaCl
Ve Perox	expanded vermiculite treated with 30% hydrogen peroxide
Ve	expanded vermiculite
VeC1%	expanded vermiculite treated with 1% citric acid (2h)
VeC10%	expanded vermiculite treated with 10% citric acid (2h)
VeCl0.8	expanded vermiculite treated with 0.8 M HCl (2h)
VeH2O	expanded vermiculite treated with water (2h)

Ve-L-1.2	hydrotalcite-like material obtained from by-product of acid activation with 1.2 M HNO_3 (2h) of expanded vermiculite
Ve-L-3.2	hydrotalcite-like material obtained from by-product of acid activation with 3.2 M HNO_3 (2h) of expanded vermiculite
Ve-LS-1.2	hybrid vermiculite-hydrotalcite obtained after treatment of expanded vermiculite with 1.2 M HNO_3 (2h)
Ve-LS-3.2	hybrid vermiculite-hydrotalcite obtained after treatment of expanded vermiculite with 3.2 M HNO_3 (2h)
VeN0.8 24h	expanded vermiculite treated with 0.8 M HNO_3 (24h)
VeN0.8	expanded vermiculite treated with 0.8 M HNO_3 (2h)
VeN1.2	expanded vermiculite treated with 1.2 M HNO_3
VeN2.5	expanded vermiculite treated with 2.5 M HNO_3 (24h)
VeN2.5C10%	expanded vermiculite treated with 2.5 M HNO_3 (2h) and 10% citric acid (2h)
VeS0.4	expanded vermiculite treated with 0.4M H_2SO_4 (2h)
Ve-S-1.2	expanded vermiculite treated in 1.2 HNO_3 (2h)
Ve-S-3.2	expanded vermiculite treated in 3.2 HNO_3 (2h)
W AR Cu	raw vermiculite saturated with astrazon red and copper cations
W AR	raw vermiculite saturated with astrazon red
W Cu	raw vermiculite saturated with copper cations
W MB AR Cu	raw vermiculite saturated with methylene blue, astrazon red and copper cations
W MB Cu	raw vermiculite saturated with methylene blue and copper cations
W MB	raw vermiculite saturated with methylene blue
W	raw vermiculite
W24h	raw vermiculite treated with 1 M NaOH (24h)
W2h	raw vermiculite traded with 1 M NaOH (1h)
WC10%	raw vermiculite treated with 10% citric acid (2h)
W-L-1.8	hydrotalcite-like material obtained from by-product of acid activation with 1.8 M HNO_3 (2h) of raw vermiculite
W-L-3.2	hydrotalcite-like material obtained from by-product of acid activation with 3.2 M HNO_3 (2h) of raw vermiculite
W-LS-1.8	hybrid vermiculite-hydrotalcite obtained after treatment of raw vermiculite with 1.8 M HNO_3 (2h)
W-LS-3.2	hybrid vermiculite-hydrotalcite obtained after treatment of raw vermiculite with 3.2 M HNO_3 (2h)
WN0.01	raw vermiculite treated in 0.01 M HNO_3 (2h)

WN0.05	raw vermiculite treated in 0.05 M HNO_3 (2h)
WN0.1	raw vermiculite treated in 0.1 M HNO_3 (2h)
WN0.5	raw vermiculite treated in 0.5 M HNO_3 (2h)
WN1.0	raw vermiculite treated in 1.0 M HNO_3 (2h)
WN1.5	raw vermiculite treated in 1.5 M HNO_3 (2h)
WN1.5C10%	raw vermiculite treated with 1.5 M HNO_3 (2h) and 10% citric acid (2h)
WN1.8	raw vermiculite treated in 1.8 M HNO_3 (2h)
WN1.8C10%	raw vermiculite treated with 1.8 M HNO_3 (2h) and 10% citric acid (2h)
WN2.0	raw vermiculite treated in 2.01 M HNO_3 (2h)
WN2.0C10%	raw vermiculite treated with 2.0 M HNO_3 (2h) and 10% citric acid (2h)
WN3.2C10%	raw vermiculite treated with 3.2 M HNO_3 (2h) and 10% citric acid (2h)
WNaOH AR Cu	raw vermiculite treated with 2.0 M NaOH (4h) saturated with astrazon red and copper cations
WNaOH AR	raw vermiculite treated with 2.0 M NaOH (4h) saturated with astrazon red
WNaOH Cu	raw vermiculite treated with 2.0 M NaOH (4h) saturated with copper cations
WNaOH MB AR Cu	raw vermiculite treated with 2.0 M NaOH (4h) saturated with methylene blue, astrazon red and copper cations
WNaOH MB Cu	raw vermiculite treated with 2.0 M NaOH (4h) saturated methylene blue and copper cations
WNaOH MB	raw vermiculite treated with 2.0 M NaOH (4h) saturated with methylene blue
WNaOH	raw vermiculite treated with 2.0 M NaOH (4h)
WNaOH0.005	raw vermiculite treated with 0.005 M NaOH (2h)
WNaOH0.01	raw vermiculite treated with 0.01 M NaOH (2h)
WNaOH0.05	raw vermiculite treated with 0.05 M NaOH (2h)
WNaOH0.1	raw vermiculite treated with 0.1M NaOH (2h)
WNaOH0.5	raw vermiculite treated with 0.5 M NaOH (2h)
WNaOH1	raw vermiculite treated with 1.0 M NaOH (2h)
WNaOH1.5	raw vermiculite treated with 1.5 M NaOH (2h)
WNaOH2	raw vermiculite treated with 2.0 M NaOH (2h)
WNaOH2-H1	raw vermiculite treated with 2.0 M NaOH (1h)

WNaOH2-H2	raw vermiculite treated with 2.0 M NaOH (2h)
WNaOH2-H24	raw vermiculite treated with 2.0 M NaOH (24h)
WNaOH2-H4	raw vermiculite treated with 2.0 M NaOH (4h)
WNaOH2-H72	raw vermiculite treated with 2.0 M NaOH (72h)
WNaOH3	raw vermiculite treated with 3.0 M NaOH (2h)
WNaOH4	raw vermiculite treated with 4.0 M NaOH (2h)
WNaOH5	raw vermiculite treated with 5.0 M NaOH (2h)
WNaOH6	raw vermiculite treated with 6.0 M NaOH (2h)
WNaOH6-H1	raw vermiculite treated with 6.0 M NaOH (1h)
WNaOH6-H2	raw vermiculite treated with 6.0 M NaOH (2h)
WNaOH6-H24	raw vermiculite treated with 6.0 M NaOH (24h)
WNaOH6-H4	raw vermiculite treated with 6.0 M NaOH (4h)
WNaOH6-H72	raw vermiculite treated with 6.0 M NaOH (72h)
WNC EtOH	raw vermiculite treated with 1.8 M HNO_3 (2h) and 10% citric acid (2h) and with ethanol
WNC EtOH+NaCl	raw vermiculite treated with 1.8 M HNO_3 (2h) and 10% citric acid (2h) and with a mixture of ethanol and 1M NaCl (1:1 v/v)
WNC H20 COLD	raw vermiculite treated with 1.8 M HNO_3 (2h) and 10% citric acid (2h) and with cold water
WNC	raw vermiculite treated with 1.8 M HNO_3 (2h) and 10% citric acid (2h)
WNC24h	raw vermiculite treated with 1.8 M HNO_3 (2h), 10% citric acid (2h) and 1 M NaOH (24h)
WNC2h	raw vermiculite treated with 1.8 M HNO_3 (2h), 10% citric acid (2h) and 1 M NaOH (1h)
WN-OH AR Cu	raw vermiculite treated with 1.8M HNO_3 (2h), 10% citric acid (2h) and 0.5 M NaOH (1h) saturated with astrazon red and copper cations
WN-OH AR	raw vermiculite treated with 1.8 M HNO_3 (2h), 10% citric acid (2h) and 0.5 M NaOH (1h) saturated with astrazon red
WN-OH Cu	raw vermiculite treated with 1.8 M HNO_3 (2h), 10% citric acid (2h) and 0.5 M NaOH (1h) saturated with copper cations
WN-OH MB AR Cu	raw vermiculite treated with 1.8 M HNO_3 (2h), 10% citric acid (2h) and 0.5 M NaOH (1h) saturated with methylene blue, astrazon red and copper cations
WN-OH MB Cu	raw vermiculite treated with 1.8 M HNO_3 (2h), 10% citric acid (2h) and 0.5 M NaOH (1h) saturated methylene blue and copper cation

WN-OH MB	raw vermiculite treated with 1.8 M HNO_3 (2h), 10% citric acid (2h) and 0.5 M NaOH (1h) saturated with methylene blue
WN-OH	raw vermiculite treated with 1.8 M HNO_3 (2h), 10% citric acid (2h) and 0.5 M NaOH (1h)
W-S-1.8	raw vermiculite treated in 1.8 HNO_3 (2h)
W-S-3.2	raw vermiculite treated in 3.2 HNO_3 (2h)

CHAPTER 1

Introduction

1.1 General introduction

Life on Earth in the form that we know relies on water as it plays a vital role in the proper functioning of the Earth's ecosystem (Gupta and Ali, 2012). It is the most essential and precious, out of all natural resources that is crucial for sustainable and wholesome development of mankind. It is not only the fundamental element in the social realm for direct consumption, but also in the sphere of integral economic growth for many types of industries (Mishra and Clark, 2013a; Sharma, 2013). Water makes up more than 70% of every adult human body and represents 50–90% of plants and animals. Out of the total enormous quantity of water available on the Earth, barely a small fraction of it is potable. It is estimated that approximately 1% water is available as Earth's freshwater for all our day-to-day uses and out of this more than one-third of it is used for agricultural, industrial, and domestic uses (Sharma and Sanghi, 2012; Mishra and Clark, 2013b)

The essential role of water has long been recognized and water was worshipped in many countries and civilizations. The water of oceans, rivers and lakes have enticed many poets and artists (Mishra and Clark, 2013b, a). Also in many religions it is considered sacred, Christians, Muslims, and Hindus sprinkle holy water on a newborn child (Mishra and Clark, 2013b).

In recent times, water has been the most exploited natural resource (Srinivasan, 2013a) which caused a serious water quality crisis across the world (Mishra and Clark, 2013a). Many factors contribute to the continuous deterioration of water quality, including domestic activities, rapid population growth, widespread urbanization, industrial proliferation, increasing living standards, wide spheres of human activities and expanding and intensifying food production with the use of modern methods of agriculture (Gupta and Ali, 2012; Mishra and Clark, 2013a; Srinivasan, 2013a). Also massive industrialization causes the release of significant amounts of pollutants into the environment while extracting some useful and meaningful substances (Mishra and Clark, 2013b). UN studies show that high-income developed nations treat about 70 % of their wastewater, while only 8 % of wastewater undergoes any kind of treatment in low-income developing nations (Monsalvo, 2016). Scientific assessments show that about 80% of diseases and one third of the total death toll in the developing countries are caused by the low quality of the drinking water. Water-transmitted diseases can seriously undermine regional security and economic development and even provoke social conflicts. Many rivers in Europe and in other parts of the world are significantly polluted by insufficiently treated or untreated wastewater discharge (Hlavinek et al., 2011). According to United Nations (UN) World Water Development Report (United Nations,

2016), around 2 million tons of waste are discharged into water bodies per day including industrial wastes, dyes and chemicals, human waste and agricultural wastes.

This way water has become one of the scarcest commodities in some parts of the world and in many other places the gross abuse of water has threatened the very process of obtaining potable water from the hydrosphere. Worldwide, the need for drinkable water is increasing while the supply is decreasing. Inadequate access to clean water is one of the most pervasive problems afflicting people throughout the world, and those problems are expected to grow worse in the upcoming decades (Mishra and Clark, 2013b, a). Almost all the sources of water supply around the world are highly polluted with substances varying from simple nutrients to highly toxic hazardous chemicals (Srinivasan, 2013a). Securing an adequate supply of fresh, clean water is essential to the health of humankind and the functioning of modern society (Howe et al., 2012). Today, quality of surface water is not only an issue for scientists, but also for policymakers, politicians, and the public in general (Sharma and Sanghi, 2012). Water pollution presents a global threat with both immediate and long-term consequences for aquatic ecosystems and human health (Mishra and Clark, 2013a).

Our water resources are limited and degradation of its quality due to pollution has taken centre stage in global reflection as a serious and threatening phenomenon. Hence, rational treatment of wastewaters and recycling methods are very topical issues as alternatives for getting fresh water in the coming decades (Gupta and Ali, 2012; Sharma and Sanghi, 2012; Sharma, 2013).

1.2 Selected legislation regarding water quality in European Union

Environmental policy is one of the greatest social challenges faced by the public authorities and all sectors of economy. Manufacturing industry is continuously facing the need to address the requirement to satisfy the demands of increasingly stringent legislation and controls introduced by governments and enforced by regulatory agencies to ensure compliance with environmental issues. The environmental policy in the EU has arguably led the way in terms of introducing the strictest environmental legislation. The principal EU policy objectives may be summarized as (Christie, 2014):

- protecting environmental quality;
- protecting human health;
- promoting prudent use of natural resources;
- promoting international measures to deal with environmental problems.

The broad objectives of EU environmental policy as set out in Articles 174–176 of the Treaty establishing the European Community (EC) in 1957, provide it with legal competence to act in all areas of environmental policy. However, this competence is not

exclusive and it is shared with the Member States. European Union environmental legislation includes mainly directives, regulations and decisions. Most EU environmental laws are directives that are binding on all Member States but may contain differing requirements due to different environmental and economic conditions in each Member State. Framework directives set out general principles, procedures and requirements for legislation and other 'daughter' directives must conform to the framework directive. Regulations are directly binding in Member States and supersede any conflicting national laws. They require further national measures for implementation and Member States may not transpose them into national law. Decisions are individual legislative acts which are binding in their entirety upon the parties to whom they are addressed. They are usually very specific in nature and less common in the environmental field (Cattoor, 2007).

1.2.1 Integrated Pollution Prevention and Control (IPPC)

The Council Directive 96/61/EC of 24 September 1996, concerning integrated pollution prevention and control (IPPC) laid down measures designed to prevent or reduce pollution of the air, water and soil. It also related to the quantities of waste arising from industrial and agricultural installations in order to ensure a high level of environmental protection taken as a whole. It is also known as the IPPC-Directive and it has been amended four times since it entered in force and has been codified (Directive 2008/1/EC of the European Parliament and of the Council of 15 January 2008 concerning integrated pollution prevention and control). It has been replaced with effect from 7 January 2014 by Directive 2010/75/EU on industrial emissions. It defined obligations that highly polluting industrial and agricultural activities must comply. It establishes a procedure for authorizing these activities and sets minimum requirements to be included in all permits, particularly in terms of pollutants released. The permits must take into account the whole environmental performance of the plant, including emissions to air, water and land, generation of waste, use of raw materials, energy efficiency, noise, prevention of accidents, risk management. It must be released based on the "best available techniques", which are the most effective and advanced stage in the development of activities and their methods of operation. The Directive also ensures the right of the public to participate in the decision making process. It also set up the European Pollutant Release and Transfer Register (E-PRTR) reporting industrial emissions into air and water and providing information on what the industrial installations do with their waste and wastewater to ensure public information about the amount of pollution that different installations are responsible for (Cattoor, 2007).

1.2.2 Water Framework Directive (WFD)

The EU Water Framework Directive (WFD), formally called Directive 2000/60/EC of the European Parliament and of the Council establishing a framework for the Community action in the field of water policy was adopted in 2000. It establishes a holistic and innovative approach to protecting the whole body of water, its source, tributaries, and river mouth. The WFD addressed protection of inland surface waters, transitional waters, coastal waters and groundwater.

The system is based on management within river basins, the natural geographical and hydrological formations covering the entire river system, from the sources of small tributaries to the estuary, including its groundwater. It created a legal framework to protect and restore clean water across Europe and ensure its long term, sustainable use. The purpose of the WFD was to prevent further deterioration, protect and enhance the status of aquatic ecosystems, and to promote sustainable water use based on a long-term protection of available water resources ensuring the progressive reduction of pollution of groundwater and prevent its further pollution.

After the WFD came into force, Member States had to define their river basin districts geographically, and identify the authorities responsible for water management. The next task was to undertake a joint economic and environmental analysis. Then countries had to launch water-monitoring networks. Under the WFD, Member States have to hold extensive consultations with the public and interested parties to identify the problems, the solutions and their costs, to be included in the river basin management plans.

The WFD has been partially repealed by the 2006/11/EC Directive related with priority substances. It has been submitted to some changes too, by 2455/2001/EC Decision (priority substances), 2008/32/EC (implementing powers), 2008/105/EC (environmental quality standards), 2009/31/EC (carbon dioxide geological storage), 2013/39/EU (priority substances) and 2014/101/EU (framework for Community action in the field of water policy) Directives.

1.2.3 Registration, Evaluation, Authorization of Chemicals (REACH)

Regulation EC No 1907/2006 – REACH of 18 December 2006 concerning the Registration, Evaluation, Authorization and Restriction of Chemicals (REACH) and establishing a European Chemicals Agency is an EU law on chemicals and their safe use that aims to protect human health and the environment from the risks arising from the use of chemicals while maintaining the free movement of goods in the EU (Christie, 2014). REACH is very wide in its scope covering both existing and new substances. It

requires manufacturers and importers to register the chemicals used, and to establish and make public the hazards posed by each substance, with reference to their entire life-cycle. This information is registered by The European Chemicals Agency (ECHA). The purpose of this Regulation is to ensure a high level of protection of human health and the environment, including the promotion of alternative methods for assessment of hazards of substances, as well as the free circulation of substances on the internal market while enhancing competitiveness and innovation. Although this regulation has been submitted to small changes it keeps its original aim, contribute to reduced pollution of air, water and soil as well as to reduced pressure on biodiversity. However improved control of persistent bio-accumulative and toxic substances is needed to ensure that these substances are prevented from polluting the environment (REACH in brief, 2007).

1.3 Dyes

A dye or dyestuff is usually a colored organic compound that may be used to impart color by selective adsorption of light to a substrate. They are soluble or go into solution during the application process and attach firmly to the fiber by chemical and/or physical bonding between of the dye and the fiber (Ejder-Korucu et al., 2015; Gürses et al., 2016). Owing to their versatility, they have been widely used in various areas of high technology including textiles, paper, leather, plastic, biological staining, lasers, liquid crystalline displays and ink-jet printers. Additionally they have found use in specialized applications such as food, drug, cosmetic and photochemical production. The industries that use and manufacture dyes have become massive today and often produce wastewaters containing dyes, which cause serious problems (Gürses et al., 2016).

Colorants that are used in textile industry may have an adverse effect on all forms of life, and the toxic nature of some dyes has long been recognized (Hunger, 2007). Depending on exposure time they can have acute or chronic effect on organisms and owning to their high thermal and photo resistance, as well as to their synthetic nature and mostly aromatic structure, that renders most of them non-biodegradable, dyes can remain in the environment for an extended period of time. Many of them and can cause allergies, dermatitis, and skin irritation, moreover, they can have carcinogenic and mutagenic action, cause dysfunctions of kidneys, liver, brain, reproductive system and central nervous system (Hunger, 2007; Hijazi et al., 2015; Gürses et al., 2016). These effects might manifest as acute, as a result of a short-term exposure to the substance, or chronic, after regular exposure over a prolonged period of time. In the first case regarding the azo dyes, the problems are reported to be connected with the ability of the reactive groups present in the dyes to react with human serum albumin causing allergic reactions. The chronic effect of these dyes is related with carcinogenicity, which

is attributed to their metabolism by reductive cleavage of the azo group. Some of the primary aromatic amines used in color manufacture are recognized as carcinogenic having the potential to react with nucleophilic sites of DNA. Some anthraquinone dyes express genotoxicity by intercalation, which occurs via insertion of the planar anthraquinone portion of the dye between adjacent base pairs of the DNA helix. Some disperse dyes can cause acute reaction due to migration to the skin via perspiration in certain tight-fitting garments made from synthetic fibers(Gregory, 2007; Christie, 2014).

The textile effluent may be toxic not only because of the of dyes but also due to the presence of substances like sulfur, naphthol, nitrates, acetic acid, soaps, enzymes, chromium compounds and heavy metals like copper, arsenic, lead, cadmium, mercury, nickel, cobalt and certain auxiliary chemicals (Kant, 2012). Also of a great environmental concern is the fact that dyes absorb part of sunlight entering the water reducing the photosynthetic activity of algae, which might contribute to extinction of living organisms and upset the food chain. At the same time, the public perception of water quality is greatly influenced by color due to the presence of dyes and pigments, which is visible even when they are in very low concentrations (Gürses et al., 2016). Although this effect is more aesthetically displeasing than hazardous it attracts the critical attention of the public and local authorities (Hunger, 2007; Christie, 2014).

1.3.1 Dyeing and textile industry nowadays

It is estimated by Global Industry Analysts, Inc. (GIA) that by the year 2017 the global market for colorants will reach 9.9 million tons and $26.53 billion, driven by the growth of key end-use industries (Paint & Coating Industries, 2015). Depending on the particular dye class in use, the percentage of dye that remains unfixed to the fiber during the dyeing process, and finds its way into
the effluent, can range from 5 to 50% (Hardin, 2007), having the reactive dyestuffs as the most used and the ones with lowest fixation level (Cooper et al., 1995). The global dyes and pigments market is projected to grow at a CAGR (Compound Annual Growth Rate) of 3.6% from 2013 to 2018 and reach 11 million metric tons by 2018 (MNM, 2013). In the past 25 years, the production of dyes in the United States, Western Europe and Japan has decreased significantly. The factors restraining the growth of colorants market were raw material price volatility, fierce price competition and globalization of world trade and environmental concerns. At the same time production in Asian countries, particularly in China, India, Thailand and Indonesia, has thriving economies and rapidly expanding manufacturing bases. In the colorants market, Asia-Pacific accounts for the largest share becoming one of the key markets for dyes and pigments production. China now accounts for 40–45% of world consumption. India has also increased its presence, now accounting

for about 10% of world consumption. These two countries are also major exporters of dyes to other countries. Consumption of textiles is the largest end-use market for dyestuffs (MNM, 2013; IHS Markit, 2014). According to The European Apparel and Textile Confederation, in 2015, the overall size of the Textile & Clothing industry (T&C) in the 28 European Union countries represented a turnover of 169 billion € and investments of around 4 billion €. There was approximately 174 000 T&C companies that employed over 1.7 million workers. EU external trade reached 45 billion € of T&C products exported and 109 billion € imported from Third markets (Euratex, 2015).

The world's population will increase by around 30% by 2050 (UN/DESA, 2015). This population growth and the ongoing economic growth in the developing countries will create significant increase in textile production and consumption. This in turn, will drive significant increases in the textile industry's productions and consumption of dyes resulting in increased environmentally harmful emissions.

1.3.2 Classification of dyes

Due to the wide variety in kind and number of colorants their classification became mandatory. For this reason they can be classified according to many parameters, such as chemical structure, color, application, fastness, manufacturer, synthesis route or date of invention (Clark, 2011). However, the most common classification bases on their chemical structure or application (Hunger, 2007; Ejder-Korucu et al., 2015; Gürses et al., 2016).

1.3.2.1 Chemical classification

One possible system of classification is chemical. It readily identifies dyes as belonging to a group that has characteristic properties and there is a manageable number of groups. This classification is most widely used by both the synthetic dye chemist and the dye technologist (Hunger, 2007). Some of the major chemical classes are azo, anthraquinone, indigoid, phthalocyanine, sulfur, nitro and nitroso dyes, which are described below.

1.3.2.1.1 Azo dyes

Azo dyes are the most important and widely used dyes and represent over 60% of the total dyes (Gürses et al., 2016). This group of dyes is characterized by the presence of at least one azo group (Fig.1.1) which is attached to two groups of which at least one, but usually both, are aromatic (Hunger, 2007; Gürses et al., 2016). Due to the simple nature of the synthesis, usually in aqueous medium, and the almost unlimited

choice of starting products, an extremely wide variety of azo dyes is possible. The number of combinations is further increased by the fact that a dye molecule can contain several azo groups. This diversity and relatively inexpensive production permits a wide spectrum of shades and fastness properties suitable for use on a variety of substrates (Hunger et al., 2011). Those dyes are intensively used in the textile industry for dyeing cellulosic fibbers, especially cotton (Ejder-Korucu et al., 2015), pharmaceutical, plastic, leather, paper, and printing industries and they do not occur naturally (Gürses et al., 2016)

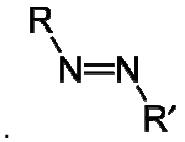

Figure1.1 Structure of the azo group.

1.3.2.1.2 Anthraquinone dyes

This group represents the second most important class of dyes, after azo dyes, basing on the anthraquinone structure as a building block (Fig.1.2). Anthraquinone dyes are one of the oldest types of dyes. They have been found in the wrappings of mummies dating back over 4000 years. In contrast to azo dyes that have no natural counterparts, all the important natural red dyes belong to this group. They are commonly found in bacteria, fungi, lichens and plants. They are characterized by good brightness and fastness properties and excellent photo stability. However, the importance of anthraquinone dyes has declined due to quite complicated syntheses and low tinctorial (coloring) strengths that make their production more costly (Hunger, 2007; Gürses et al., 2016).

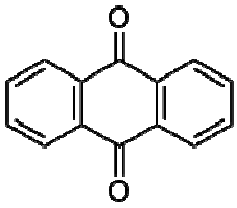

Figure 1.2 The structure of anthraquinone.

1.3.2.1.3 Indigoid dyes

This group bases on the structure of indigo (Fig.1.3) which represent one of the oldest known organic dye, used in textile dyeing for almost 5000 years. Nowadays it is used almost exclusively to give color to denim jeans and jackets. Although many indigoid dyes have been synthesized, only indigo is of any major importance today (Gürses et al., 2016).

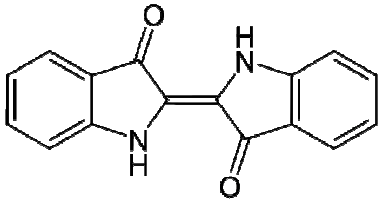

Figure 1.3 The structure of indigo.

1.3.2.1.4 Phthalocyanine Dyes

Those dyes are based on phthalocyanides (Fig.1.4) which belong to a class of macrocyclic compounds that form intensely colored complexes with most elements, especially metals such as Cu, Fe, Si, Ge and As. phthalocyanides have exceptional stability, they are bright, tinctorially strong and are probably the most stable of all the colorants in use today (Gürses et al., 2016).

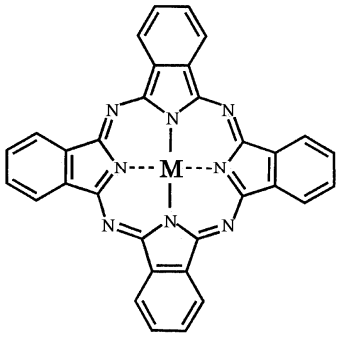

Figure 1.4 The phthalocyanine structure.

1.3.2.1.5 Sulfur Dyes

Those dyes, with only a few exceptions, are exclusively used for producing deeper muted shades, especially black, dark blue, olive, brown, and green on cellulosic fiber and its blends with synthetic fibers. They are also used to a limited extent to dye polyamide fibers, silk, leather, paper, and wood (Hunger, 2007; Gürses et al., 2016). Sulfur dyes possess neither well defined chemical structures nor consistent in composition. They are basically complex mixture of polymeric molecular species comprising of large proportion of sulfur in the form of sulfide (–S–), disulphide (–S–S–) and polysulfide (–Sn–) links in heterocyclic rings. Amongst synthetic dyes, they have the dullest range of colors of all dyestuff classes, are inexpensive and exhibit excellent washing and good light fastness (Gürses et al., 2016).

1.3.2.1.6 Nitro and Nitroso Dyes

These dyes are now of minor commercial importance. They have one or more nitro or nitroso group (Fig.1.4A and B) conjugated with an electron donating group via an aromatic system (Gürses et al., 2016). They are nitro derivatives of phenols or naphthols. The most important nitro dyes are the nitrodiphenylamines whose small molecules are ideal for penetrating dense fibers such as polyester. The early nitro dyes were used for dyeing natural animal fibers such as wool and silk they are cost-effective because of their easy synthesis from inexpensive intermediates. Nitroso dyes are metal-complex derivatives of naphthols or o-nitrosophenols The only nitroso dyes important commercially are the iron complexes of sulfonated 1-nitroso-2-naphthol, used mainly for coloring paper (Hunger, 2007).

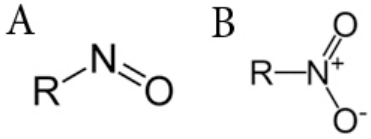

Figure 1.5 The structure of nitro (A) and nitroso (B) group.

1.3.2.2 Classification according to application methods

Classification by usage or application is the principal system adopted by the Color Index. They may be also subdivided as water soluble (e.g. reactive, acid, basic, direct) or not soluble (e.g. disperse, vat, solvent). These main classes are presented below.

1.3.2.2.1 Reactive dyes

This class of dyes is characterized by the presence of one or more specific functional reactive groups in their structure, normally attached to the chromophore via a bridging group such as –NH–, –CO–, and SO_2–. Owning to that, the dyes are capable of forming a covalent bond with compatible groups such as –OH, –SH, and –NH_2 present on the fiber, on the way of addition or substitution (Hunger, 2007; Gürses et al., 2016). Due to this strong chemical bond they present very good fastness to washing and to light. Moreover their bright colors and its easy application make these dyestuffs the most used for dyeing cellulosic fibers and wool. Their main disadvantage is that they present low fixation levels to the fiber, when compared with other classes, between 50 and 90% (Cooper et al., 1995).

1.3.2.2.2 Acid dyes

The term acid dye derives from the dyeing process, which is carried out in an acidic aqueous solution (pH 2-6). The most common commercially available forms are sodium salts of the sulfonic acid. They exhibit good water solubility. These dyes present natural affinity by proteic fibers (wool and silk) and for polyamide being used for their dyeing. They may be used also for modified acrylic, and polypropylene fibers as well as blends of the mentioned fibers with other fibers such as cotton, rayon, and polyester, regular acrylic fiber. The anionic azo dyes constitute the most widely used group of this class of dyes (Hunger, 2007; Gürses et al., 2016).

1.3.2.2.3 Basic dyes (cationic dyes)

Basic or cationic dyes derive their name from the fact that the dye molecules dissociate in water to a cation, with either localized or delocalized charge, that is the colored portion of the dye, and to colorless anion that is a low molecular mass inorganic or organic acid. They are water soluble and are applied to paper, poly-acrylonitrile, modified nylons, and modified polyesters. Many of these dyes can be converted into water-insoluble dye bases by addition of alkali. For this reason, they were formerly called basic dyes (Hunger, 2007; Gürses et al., 2016).

1.3.2.2.4 Direct dyes

Direct dyes are water-soluble dyes, easily applied to cellulosic fibers. The essential requirement for classification of a dye in this group is its substantivity, i.e., its absorption from an aqueous salt-containing solution onto cellulosic materials. Since both dyestuff and fiber become negatively charged in aqueous solution the electrolyte is essential to promote its affinity. Direct dyes are mainly used to dye materials made from natural or regenerated cellulose (e.g., cotton, jute, viscose or paper) without employing mordants (dye fixative) as auxiliaries (Hunger, 2007; Gürses et al., 2016).

1.3.2.2.5 Disperse dyes

Disperse dyes are colorants with low water solubility that, in their disperse colloidal form, are suitable for dyeing and printing hydrophobic fibers and fabrics such as nylon, polyamide, polyester and acrylic fiber. They generally contain azo, anthraquinone, nitro groups (Hunger, 2007; Gürses et al., 2016).

1.3.2.2.6 Vat dyes

Most vat dyes are indigoid or anthraquinone and usually have between five and ten aromatic rings. These dyes are water-insoluble however, due to a chemical reduction in alkaline solution they convert into water-soluble form with substantivity for cotton and other cellulose fibers. Once the reduced dye has diffused into the fiber, it is oxidized and becomes water insoluble again. Despite their high cost and their muted colors, these dyes are extremely important for certain textiles for demanding applications because of their superior fastness against washing and other environmental impacts such as light or chlorine bleach. Despite that, there has been a decrease in their usage that might be due to their fairly complex application process and a corresponding lack of know-how in many textile dye houses (Hunger, 2007; Gürses et al., 2016).

1.3.2.2.7 Solvent dyes

This group comprises water-insoluble but solvent-soluble dyes, which are used for colored plastics, gasoline, oils, and waxes (Hunger, 2007).

1.4 Heavy metals

The term heavy metal has no one coherent and clear definition and has never been defined by IUPAC. Moreover, the available lists of heavy metals significantly differ from one to another, which raises the question about their definition (Banfalvi, 2011). Generally, heavy metals is a collective term applied to any metal or metalloid that is characterized by relatively high atomic density. However, there is no consensus in this matter and the density separating light form heavy metals is reported to lie between 3 and 5 g cm^{-3} (Banfalvi, 2011; Chen, 2012; Gautam et al., 2015). Another definition bases on the atomic mass and states that every metal with the atomic mass above 40 should be classified as heavy (Chen, 2012). Yet, another one points the presence of *d*-orbitals in the structure of a metal to make it heavy (Banfalvi, 2011). Although, there is an agreement on the fact that heavy metals are toxic or poisonous even at low concentrations. Chronic low exposures can pose a threat to nature in general and to humans in particular especially when heavy metals are present in soluble form as they lead to severe environmental and health disturbances. In spite of that, it should be noticed that some of them are essential for life and ecosystems, and play an important role in the metabolism, e.g. as active centers of enzymes, however at trace level concentrations (Ho and El-Khaiary, 2009; Küpper, 2011; Gautam et al., 2015).

Some other common characteristics of heavy metals are listed below (Chen, 2012):

- good conductors of electricity,
- eclectic resistance is directly proportional to the absolute temperature,
- high thermal conductivity,
- malleability and ductility, without which it cannot be drawn into sheets and wires
- has oxidation numbers or valences such as 0, +1, +2, +3, +6,
- zero-valent metals are present in solid form. Mercury is the only exception as it is in the form of liquid,
- may exist in nature as metal oxides, metal carbonates, or metal sulfates,
- may be present in nature as soluble species, in the form of complexes.

The hazardous nature of heavy metals has been recognized also because of their bioaccumulative nature. Unlikely like many organic pollutants that are susceptible to biological degradation, heavy metals cannot be degraded into harmless end products and will tend to accumulate in biotic systems (Küpper, 2011; Chen, 2012; Gautam et al., 2015). Because of the relevance of these phenomena, heavy metal contamination has become one of the most important environment problems in the world that have been a subject of intensive research since many years (Ho and El-Khaiary, 2009; Küpper, 2011; Chen, 2012). Moreover, they often accompany dyes in the wastewaters. The European Union has addressed a number of issues related to heavy metals and due to international and national regulations and improvement in available technologies emission of heavy metals from point sources, mostly industrial, has been considerably reduced over the last few decades. Nonetheless, emissions from diffused sources, i.e. agriculture, traffic, combustions etc., have either reminded stable or increased and heavy metals are among the most common pollutants found in wastewater (Scoullos et al., 2012; Gautam et al., 2015).

The main source of heavy metals is that from metal–complex dyes, which are widely used, but mainly to improve the light fastness of the dyes. Heavy metals are widely used in the dyeing industry. Derivatives of mercury are used as catalyst in the sulfonation of anthraquinone, an essential first step in production of anthraquinone dyes. There are many inorganic pigments based on lead (chromates and molybdates) and cadmium (sulfides and sulfoselenides) that are still important commercially. There are toxicological and environmental issues associated with several other metals, such as copper, cadmium, arsenic, cobalt, lead and nickel, used to a certain extent in colorants and that accompany dyes in wastewaters (Christie, 2007; Kant, 2012; Christie, 2014). A brief description of each of them is presented in the subsection below.

1.4.1 Characteristics of selected heavy metals

1.4.1.1 Copper

Copper naturally occurs as free metal, most of its compounds have +1 or 2+ valence states. It is primarily used as a metal or alloy (e.g., brass, bronze, gun metal). Copper sulfate is used as a fungicide, algaecide, and nutritional supplement. Copper particles are released to into the environment by windblown dust, volcanic eruptions, natural withering of soil and rocks, and from anthropogenic sources, mostly copper smelters and ore processing families, and as effluent from sewage treatment plants.

Copper is an essential nutrient that is incorporated into a number of metalloenzymes involved in hemoglobin formation, carbohydrate metabolism, catecholamine biosynthesis, and cross linking of collagen, elastin, and hair keratin. Excessive exposure to copper can result in a number of adverse health effects which include anemia, immunotoxicity, developmental toxicity and kidney and liver damage (ATSDR, 2004b).

1.4.1.2 Lead

Although lead occurs naturally in the environment most of its emissions have anthropogenic origin. Before the ban on the use of leaded gasoline, most of the lead found throughout the environment came from car gaseous emissions. Most of the lead in inner city soils, aside from automobiles, comes from old houses painted with paint containing lead. Landfills may contain lead coming from lead ore mining, ammunition manufacturing, or industries that handle lead such as battery production and iron and steel manufacturers. Moreover, mining wastes that have been used for construction of sandlots, driveways, and roadbeds might contribute to pollution with this metal, as well as degradation of some chemicals containing lead by sunlight, air and water.

The main target for lead toxicity is the nervous system, and at some levels of exposure it can severely damage the brain and kidneys. (ATSDR, 1993b; Scoullos et al., 2012).

1.4.1.3 Mercury

Mercury naturally occurs in the environment in several forms, the most common are metallic mercury, mercuric sulfide (cinnabar ore), mercuric chloride, and methylmercury. The latter form is of particular concern because it can accumulate in certain fish and marine mammals that can build it up to levels that are many times greater than levels in surrounding water. Mercury enters naturally the environment as a

result of weathering of rocks and soils and volcanic activity, which have remained relatively steady in recent history. Anthropogenic activities cause release primarily from fossil fuels combustion, mining and smelting, solid waste incineration (especially medical waste), fertilizers, fungicides containing mercury, and improper disposal of municipal solid waste (containing for example discarded batteries, electrical switches, or thermometers).

The major target organs for mercury are the kidneys (acute renal failure) and the central nervous system (profound neurotoxicity), however respiratory, cardiovascular, and gastrointestinal effects may also occur (ATSDR, 1989; Scoullos et al., 2012).

1.4.1.4 Arsenic

Arsenic naturally is widely distributed in Earth's crust. It is classified as a metalloid, having both properties of a metal and nonmetal. It occurs naturally in soil and many kinds of rock, especially in minerals and ores that contain copper and lead. Its compounds are used as anti-rotting and anti-decay agents in preservation of wood, as well as in alloys in lead-acid batteries for automobiles, and in semiconductors and light-emitting diodes. It finds its way to the environment as a result of soil and rock weathering, eruptions of volcanoes, during the mining and smelting of copper and lead ores and as a discharge of industrial waters. Fish arsenic is a common name for arsenobeatine – an organic form of arsenic that builds up in tissues of certain fish and shellfish.

Arsenic is a potent toxicant that may exist in several oxidation states and in a number of inorganic and organic forms. Skin is the most sensitive noncancer target of oral exposure of this metal. It is also known to be a human carcinogen with respiratory system being the primary tumor type followed by the liver, skin and digestive tract (ATSDR, 2007).

1.4.1.5 Cobalt

Cobalt is a naturally occurring element with similar properties to iron and nickel. There is only one stable isotope, ^{59}Co, and many unstable or radioactive isotopes, with ^{60}Co and ^{57}Co having the highest commercial importance. A small amount of this metal is naturally found in rocks, soil, water, plants and animals. It may enter air and water, and settle on land from wind-blown dust, seawater spray, volcanic eruptions, and forests fires. Small amount may be generated in coal-fired power plants and industrial activities related to the mining and processing of cobalt-containing ores, and the production of cobalt alloys and chemicals. Radionuclides may be emitted to the environment as a

result of nuclear accidents, radioactive waste dumping and nuclear power plant operations.

Cobalt is usually mixed with other metals to form alloys that are hard or resistant to wear and corrosion. Cobalt compounds are used as colorants in glass, ceramics, and paints (characteristic blue color), as catalysts, and paint driers. It is also found as trace element additive in agriculture and medicine. Radioactive isotopes are used as a source of gamma radiation for sterilizing medical equipment and consumer products (extending shelf-life of food by destroying pathogens), radiation therapy for treating cancer patients and for manufacturing plastics.

Cobalt is essential in the body as it is a component of cyanocobalamin (vitamin B12) that plays an important role in the metabolism. However, in case of overexposure, cobalt can cause various adverse effects including lung effects, cardiomyopathy, liver and kidney congestion, visual disturbances, thyroid effects, dermatitis and sensitization. Exposure to radionuclides of cobalt can cause damages characteristic of gamma radiation (ATSDR, 2004a)

1.4.1.6 Nickel

Nickel naturally occurs in large amounts in Earth's crust, most often combined with other elements. It is released to the environment during nickel mining and by industries that make nickel alloys or nickel compounds. These industries may also discharge nickel in waste water. Smaller amounts find their way to the atmosphere due to oil-burning power plants and municipal solid waste incinerators. Nickel is used to produce goods like plumbing, marine equipment, petrochemical equipment, heat exchangers, pumps, and electrodes for welding. Nickel alloys mostly with iron, copper chromium, and zinc are used in making metal coins and jewelry. Most nickel is however used to make stainless steel, nevertheless some of its compounds are also used for nickel plating, to color ceramics, produce batteries and catalysts.

Nickel is essential to animals and humans, in trace levels. The most common adverse effect of this element in humans is an allergic reaction, most commonly a skin rash however, cases of hand eczema and asthma attracts have been reported. It can be reasonably anticipated carcinogenic as cases of lungs and nasal sinus cancer have been reported in people exposed to high nickel contamination (ATSDR, 2005).

1.4.1.7 Cadmium

Cadmium is not usually present in the environment as a pure metal but it rather occurs as oxides, sulfides, and carbonates usually in zinc, lead, and copper ores. Rarely

is it present in the form of chlorides and sulfates. About half of the amount of cadmium released to the environment comes from weathering of rocks into river water. Forest fires and volcanoes also release considerable amount of this element into the environment. The major contributor from anthropogenic sources is mining, burning of fossil fuels and household waste, and application of some fertilizers in the agriculture. Due to strict restrictions only a small amount of cadmium enters water from the disposal of domestic and industrial wastewater. However, cigarettes followed by food are the main sources of cadmium exposure for. Smokers may even double their daily intake of that metal compared to nonsmokers.

Exposure to cadmium can seriously damage the lungs, build up in the kidneys, severely irritate the stomach, and also cause fragile bones (ATSDR, 1993a).

1.5 Water treatment

Water treatment might be defined as a process to achieve determined quality standards set by the end user or a community through its regulatory agencies (Howe et al., 2012). Legislation defines the quality level needed depending on the water use.

Water treatment methods may be classified according to its nature, physical, chemical, electrical, thermal or biological (Gupta and Ali, 2012; Sun et al., 2012). The treatment is often technically and economically challenging as some of the methods are not effective and excessively expensive (Sharma, 2013; Srinivasan, 2013b). Usually a combination of various methods has to be applied as no single method can completely remove all contaminants and impurities from the water (Mishra and Clark, 2013a). It is very important not to cause further secondary pollution (Sharma et al., 2012) since some of the methods generate toxic sludge, the disposal of which is still a problem, and produce toxic by-products that prevents their wide acceptance (Teng and Low, 2012; Sharma, 2013; Srinivasan, 2013b). Although a number of successful processes have been applied, cost-effective removal of color and metals from effluents remains a challenge in industrial wastewater treatment (Sun et al., 2012; Teng and Low, 2012).

It is essential to develop sustainable, non-intrusive, low-cost, ecologically benign, and socially accepted technologies for water treatment in order to reduce the deleterious after-effects on the environment during cleanup processes, known as the ‘‘footprint’’ of remediation (Mishra and Clark, 2013a; Sharma, 2013).

1.5.1 Methods for dyestuffs and metals removal

Many treatments based on different methods are applied to remove dyes and metal ions for waste.

Biological treatment is suitable for elimination of biodegradable dyestuffs, but some dyes are reluctant to biological breakdown and the stability of the microorganism cultures may be upset in presence of high concentrations of some pollutants or by the presence of toxic substances, such as metals.

Nano and ultrafiltration or reverse osmosis, were effective, for both dyes and metal cations, but dye molecules caused frequent clogging of membrane pores. The high working pressures leads to significant energy consumption and the short life time of membranes, which as expensive, make the process costly and limit the application of those techniques.

Oxidation processes are widely used for decolonization purposes. However decomposition of some dyes requires long time and some solutions remain still colored after the process. Moreover, that treatment method may cause release of metals from metal complex dyes. Some of the techniques, such as electrochemical oxidation using Fenton's reagent, are effective but they produce large volume of sludge that requires further treatment and adequate disposal because they usually contain toxic compounds. Ozonation technique is efficient in removal of some dyes, however the products of such treatment might be more toxic than parent dyes (Hassan and Hawkyard, 2007; Philippis and Micheletti, 2009).

Coagulation/flocculation has been used widely for treating textile wastewaters, however, it gives only partial removal of color and metals and generates a chemical sludge that has to be properly managed increasing the operation costs. It also has the disadvantage of possible over-feeding of chemicals to the waste stream, which may contaminate the decolorized effluent (Hardin, 2007; Philippis and Micheletti, 2009). A particular case of coagulation/flocculation is chemical precipitation therefore having the same disadvantages. Although it is the most common technology applied to removal of metal cations, it is not always efficient. Since most of the wastes contain various metal cations, it might be difficult to remove them all because the optimum pH condition for precipitation of one may cause another metal to solubilize. Moreover, it requires large amounts of chemicals to reduce the concentration of metals to an acceptable level.

1.5.1.1 Adsorption

Among the various techniques of water treatment, the adsorption process has been proved to be one of the most promising, effective and attractive approach for water treatment (Gupta and Ali, 2012; Teng and Low, 2012; Pejman Hadi et al., 2015). For many applications, this process has been proven to be superior to other techniques for a variety of reasons, including the simplicity of design, easy operation, low cost, high removal efficiency, wide range of applications and availability. Further, it can remove different type of pollutants, organic as well as inorganic ones. Thus, it has a wider applicability in water pollution control (Gupta and Ali, 2012; Pejman Hadi et al., 2015). Molecules and atoms (adsorbates) can attach to solid surfaces (adsorbents) by physical or chemical interactions, physisorption is mainly due to van der Waals interactions and in chemisorption a chemical bonds are formed, usually covalent bonds (Atkins and de Paula, 2010). During the adsorption process, the adsorbate diffuses into the porous solid adsorbent and is then adsorbed onto its surface (Howe et al., 2012).

Activated carbon produced from carbonaceous material by chemical activation or gas activation is considered an universal adsorbent for water and wastewater treatment because of its highly porous structure and large specific surface area that result in very good removal efficiencies. However, its application is restricted due to high costs (Gupta and Ali, 2012; Howe et al., 2012; Teng and Low, 2012; Worch, 2012; Chowdhury et al., 2015).

Ion exchange is similar to adsorption, except that it involves the exchange of ions with the same net charge. It is applied efficiently for the removal of metals however it may be really expensive due to the price of synthetic ion exchange resins (Philippis and Micheletti, 2009). Therefore, there is a need to search for alternatives, cheaper and effective adsorbents that may offer a lot of promising benefits for commercial use in future (Teng and Low, 2012).

A material could be assumed to be low cost if it is abundant in nature, inexpensive, requires little processing, and is effective in the treatment process. Low-cost adsorbents could be obtained from any agriculture and industry by-products, natural materials, and biosorbents that contain high surface area and porosity (Teng and Low, 2012). Attempts that have been undertaken for this purpose has focused on the use of waste or by-products from industries and agricultural operations, natural materials, microbial and non-microbial biomass (Chowdhury et al., 2015). Typical natural adsorbents are clay minerals, natural zeolites, oxides, or biopolymers. Clays have a special position among them because of their low cost, relatively large specific surface area, excellent physical and chemical stability, and other advantageous structural and

surface properties (Worch, 2012; Tolga Depci and Çelik, 2015). Clays and their modified forms have been used as adsorbents, and are considered by some researchers as an ideal adsorbent (Tolga Depci and Çelik, 2015).

1.6 Layered minerals

There are many families of laminar solids, however only few of them exhibit good adsorption properties, which they owe to the ability of intercalation of guest molecules. At the forefront of such materials are clays and layered double hydroxides (LDH) (Pinnavaia, 2004). Moreover, layered minerals can be a subject to various modifications in order to change their properties (Ruiz-Hitzky et al., 2004; Bergaya and Lagaly, 2006; de Roy et al., 2006; Heller-Kallai, 2006; Komadel and Madejova, 2006; Lagaly et al., 2006).

1.6.1 Clays

Clay has been known to, and used by, humans since antiquity. It is an abundant raw material which has an amazing variety of uses and properties that are largely dependent on their mineral structure and composition. Clays are utilized in agricultural applications, engineering and construction applications, environmental remediation, geology and industrial processes, such as production of porcelain, bricks, tiles and sanitary ware. They also are an essential constituent of many plastics, paints, paper, rubber and cosmetics (Fuchs, 2004; Bergaya and Lagaly, 2006; Murray, 2006).

Clays are formed in processes of dissolution and recristallisation of rocks (silicate minerals) as a result of their interaction with dilute aqueous solutions of varying composition and pH. They are the finest, often colloidal, part of the weathering material. They have a special physical structure, which is very different from that of the pre-existing minerals, and gives them very specific characteristics of chemical and physical reactivity. Clays are stable only at the surface of the earth or within several hundreds of meters of the Earth's crust. Along with increasing temperature they transform into another minerals, either different clays or other mineral structures (Velde, 1995; Carroll, 2012).

There is no uniform nomenclature for clay and clay material. Geologists, mineralogists, chemists, and soil scientists all approach the terms clay and clay mineral somewhat differently (Carrado, 2004; Bergaya and Lagaly, 2006). Some of the definitions are presented below.

- Clay minerals are any of a group of important hydrous aluminum silicates with a layer (sheetlike) structure, and very small particle size (Encyclopædia Britannica Online, 2015).
- Clays are soil separate comprising mineral particles less than 2 µm in diameter. Whereas clay minerals are hydrous aluminum silicates with layered structure, members of the phyllosilicates (sheet silicates) with related chemistry (Allaby, 2013).
- Clay minerals are hydrous aluminum silicates that are extremely small crystals with structural units of silica tetrahedra and alumina octahedra that are bonded together into bands or layers (Carroll, 2012).
- Clays are aggregates of minerals, soils or rocks that commonly show plasticity. These materials contain not only minerals belonging to the clay family but also very fine particles with various proportions of quartz, feldspar, mica, and organic material. Clay minerals are a diverse group of hydrous layer aluminosilicates that constitute the greater part of the phyllosilicate family of minerals. They are commonly >2 µm, or even 4 µm in at least one dimension, and they are the major constituent of fine-grained sediments and rocks (Huggett, 2004).
- A clay is a natural, earthy, fine-grained material which develops plasticity when mixed with a limited amount of water. It is composed primarily of silica, alumina, and water, often with iron, alkalies, and alkaline earths. A clay mineral is one of a group of finely crystalline, hydrous silicates with a layer crystal structure. It is one of the major components of clays (McGraw-Hill, 2003).
- Clays are naturally occurring phyllosilicate minerals composed primarily of fine-grained minerals, and minerals which impart plasticity to clay at appropriate water contents, and which harden upon drying or firing (Guggenheim and Martin, 1995)
- Clays are any fine-grained, natural, earthy, argillaceous material of extremely small crystalline particles that belong to a group of minerals that are commonly known as the clay minerals (Grim, 1962; Grim, 1968).

Bailey and Rieder (Bailey and Chairman, 1980; Rieder et al., 1998) presented a classification of silicates based on their structure (Fig. 1.5).

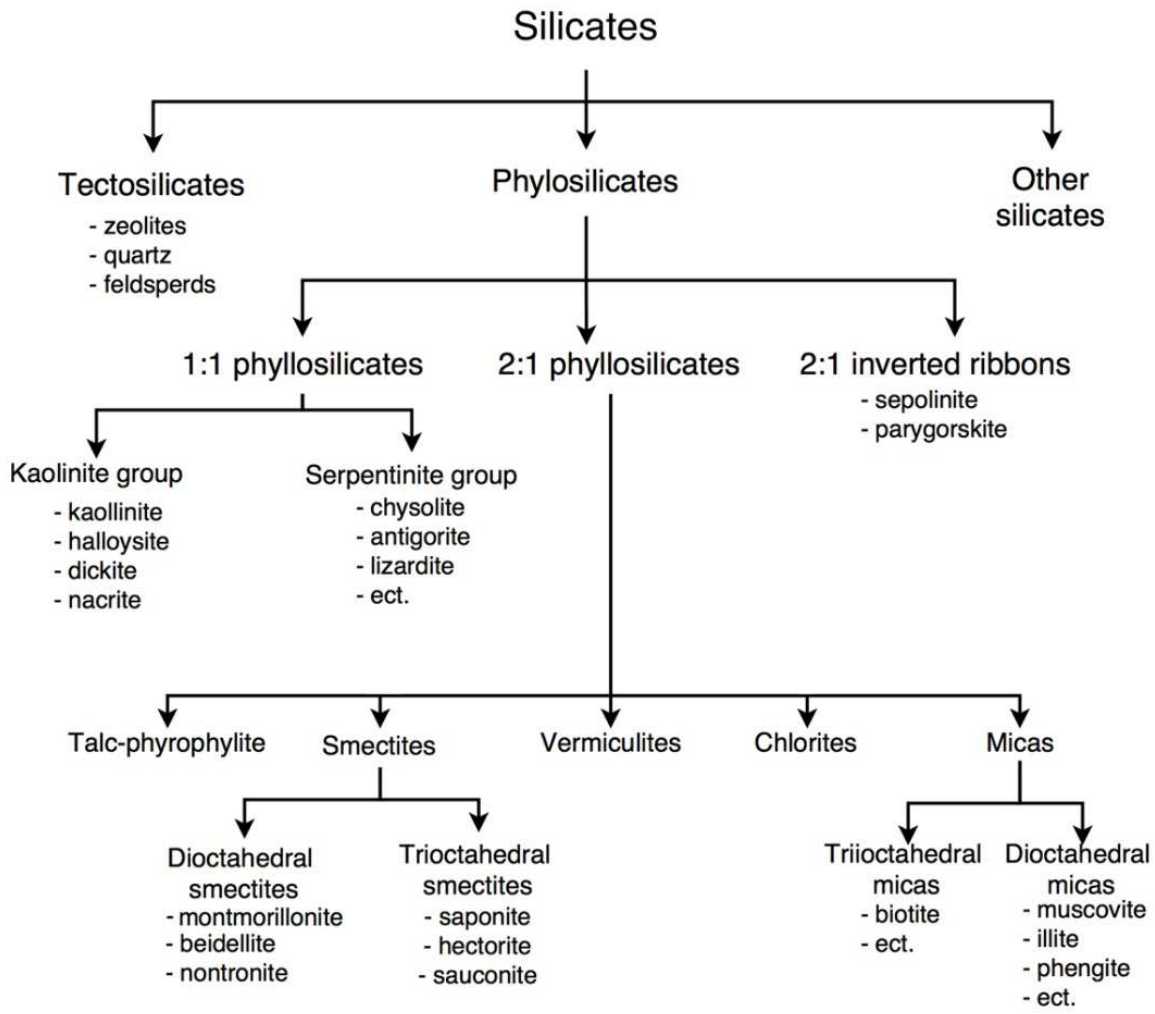

Figure 1.6 Classification of silicates according to Bailey and Chairman (1980) and Rieder et al. (1998).

Clays ideally contain a continuous tetrahedral sheet or tetrahedral and octahedral sheet. Each tetrahedron consists of a cation, coordinated to four oxygen atoms, and linked to adjacent tetrahedra by sharing three corners to form an infinite two-dimensional 'hexagonal' mesh pattern. The general formula for the tetrahedra is T_2O_5, where T is mainly Si^{4+}, but Al^{3+} frequently (and Fe^{3+} less frequently). The octahedral sheet comprises two planes of close-packed oxygen ions with cations occupying the resulting octahedral sites between the two planes. In this sheet connections between each octahedron to neighboring octahedra are made by sharing edges. Octahedral cations are usually Al^{3+}, Fe^{3+}, Mg^{2+} and Fe^{2+}, but cations of other transition elements can occur. The composite layer formed by linking one tetrahedral and one octahedral sheet is called 1:1 or T-O layer (Fig.1.6A), while a composite layer of one octahedral layer sandwiched between two tetrahedral layers (both with the tetrahedra pointing towards the octahedral layer) in known as a 2:1 or T-O-T layer structure (Fig.1.6B).

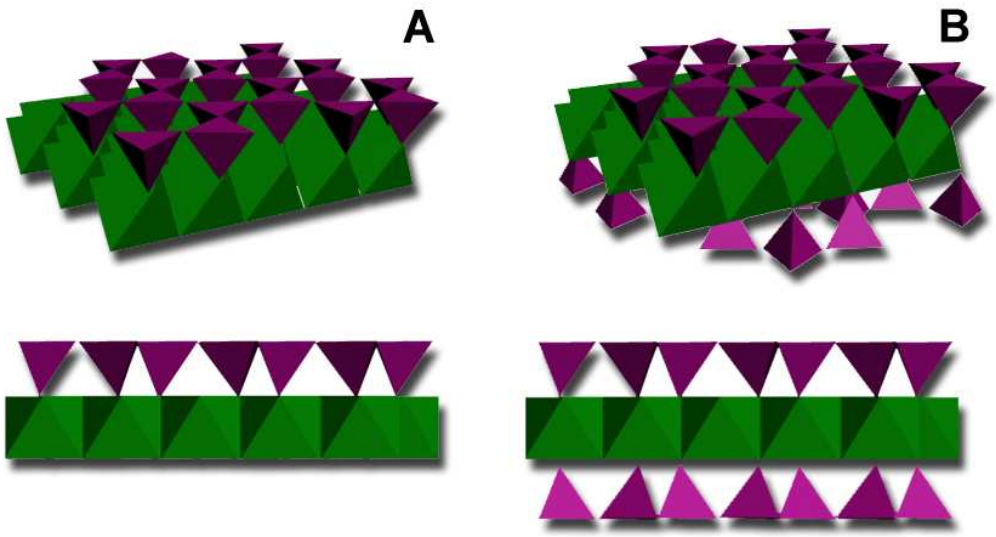

Figure 1.7 The structure of 1:1 (T-O) (A) and 2:1 (T-O-T) (B) layer.

When the tetrahedral and octahedral sheets are joined in a layer, the resulting structure can be either electrically neutral or negatively charged due to the partial replacement of Si^{4+} (in tetrahedral positions) and/or Al^{3+}(in octahedral sites) by cations of similar size and coordination but usually) of lower valency. If a charge is present on the sheets, it is balanced by an ion located in between the sheets. This charge variability is recognized as one of the most important features of 2:1 phyllosilicates, because it induces occupancy of the interlayer space by exchangeable cations. Clays can easily exchange these ions what results in very good ion-exchange properties of the material (Velde, 1995; Huggett, 2004; Bergaya and Lagaly, 2006; Brigatti et al., 2006; Theng, 2012).

Vermiculite is a clay mineral belonging to the 2:1 group. In its structure some Fe^{3+} are replaced for Mg^{2+} and some Al^{3+} for Si^{4+}. This substitution results in charge balanced by interlayer cations, most commonly Mg^{2+}, however forms with Ca^{2+} and Na^{+} also occur. Fig.1.7 presents the structure of that mineral. Vermiculite is formed in hydrothermal alternation of biotite and phlogopite and from alternation of ultrabasic rocks (Huggett, 2004; Brigatti et al., 2006; Allaby, 2013).

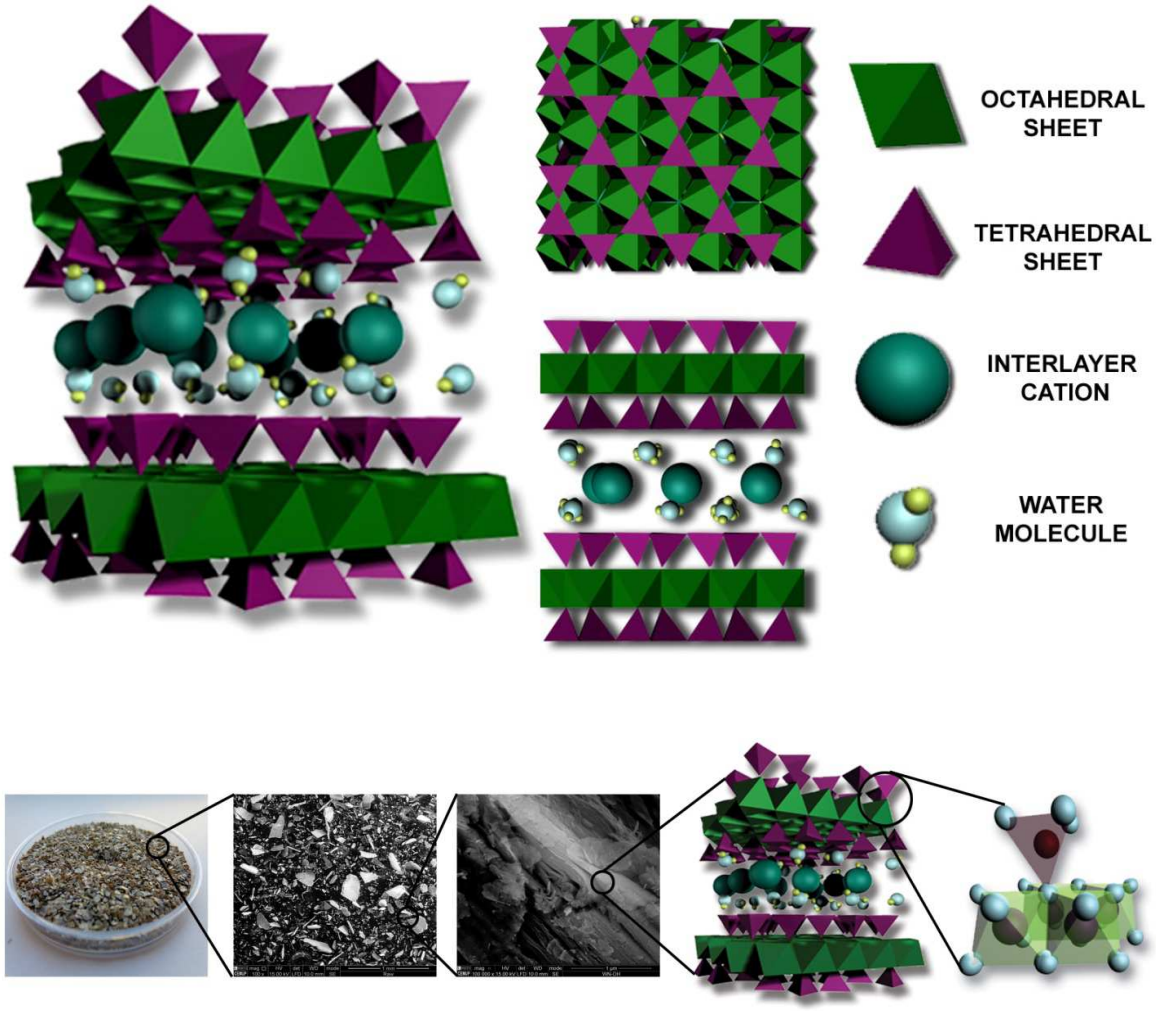

Figure 1.8 The structure of vermiculite.

1.6.1.1 Acid treatment of clays

Acid activation or acid treatment of clays and clay minerals has been used for decades both for industrial and scientific purposes. The manufactured materials are widely available, relatively inexpensive and effective in a number of industrially significant reactions and processes. Acid activation of clays, which consists of the treatment of clay with a mineral acid solution, is one of the most common chemical modifications of clays. During the process interlayer cations are exchanged by protons and metals from the layers are leached causing changes in the structure of the material The main task is to obtain a partly dissolved material resulting into an increased specific surface area, porosity and surface acidity. The resulting product may also contain unaltered layers and amorphous three-dimensional cross-linked, protonated and hydrated silica, depending on the extent of acid activation. Optimal conditions for activation can be achieved by combining different acid strengths and reaction times. A careful selection of the level of acid treatment is necessary to optimize the surface area,

pore volume, surface acidity and thermal stability of the final product. The optimum level of acid treatment corresponds to a removal between 19 and 35% of the octahedral cations. However, these values depend on the original clay mineral. This procedure results in the production of bleaching earths, clays suitable for a range of bleaching or decolorizing applications, they are also used to prepare clay-modified electrodes, adsorbents and catalysts (Komadel and Madejova, 2006; Maqueda et al., 2007; Maqueda et al., 2009; Santos et al., 2015).

1.6.2 Layered double hydroxides (LDH)

Layered double hydroxides (LDHs) are also called hydrotalcite-like compounds (HTI), hydrotalcite-type materials (HTM) or anionic clays (known as anion exchanging clays). Those are the commonest names applied to a large group of synthetic and natural lamellar hydroxides with two kinds of metallic cations in the main layers and interlayer domains containing anionic species. They are readily produced when suitable mixtures of metal salts are exposed to base.

The LDHs consist of layers, containing hydroxides of two (sometimes more) different kinds of metal cations, in most cases in the +2 and +3 oxidation states. Each cation is surrounded, approximately octahedrally, by hydroxide ions. These octahedral units form layers by edge-sharing, with the hydroxide ions sitting perpendicular to the plane of the layers. The layers stack on top of one another and form three-dimensional structure. Owning to the substitution of a part of divalent cations by trivalent ones, the layers acquire a positive charge, which density is proportional to the trivalent to divalent metal ratio. This charge is neutralized by incorporated exchangeable anion which nature can be almost freely selected (Fig.1.8).

The possibility of varying the identity and relative proportions of the layers building cations, as well as the identity of the interlayer ions, gives rise to a large variety of materials with different characteristics that belong to the LDHs family. The principal areas of interest include their use as catalysts and catalyst supports, adsorbents, anion scavengers, anion exchangers, polymer stabilizers, antacids, antipeptins, stabilizers and delivery systems for pharmaceuticals (Braterman et al., 2004; Evans and Slade, 2005; Rives, 2006).

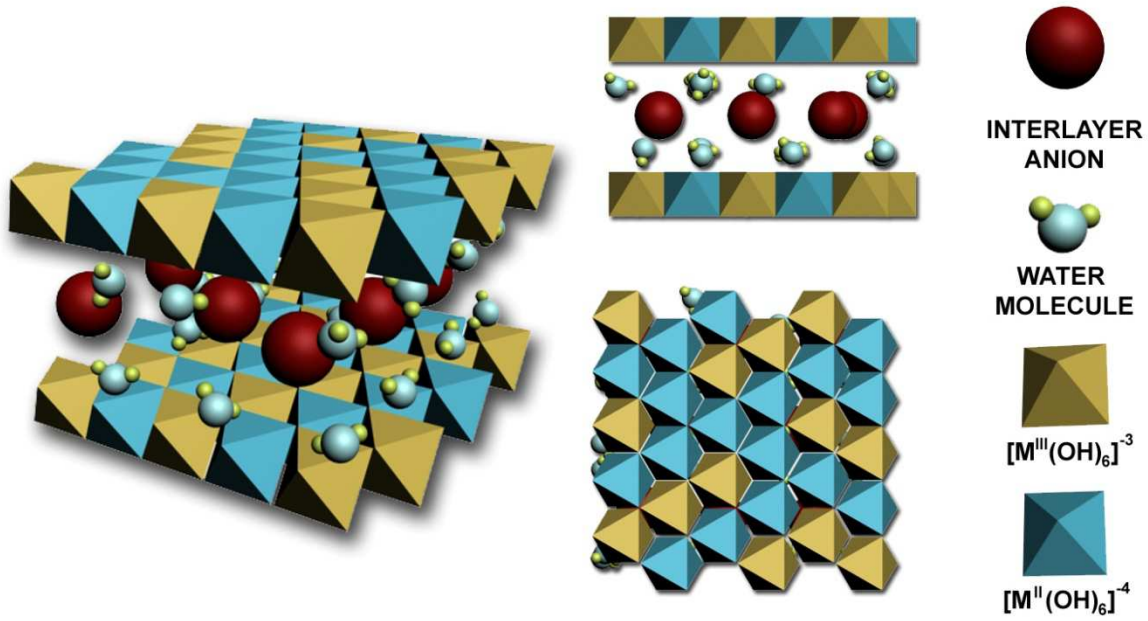

Figure 1.9 The structure of a layered double hydroxide.

1.6.2.1 Thermal treatment of LDHs

A unique property of layered double oxides is that after thermal decomposition, under mild conditions, they are able to regenerate the layered structure when exposed to water and anions (Rives, 2006). The conversion of the mixed metal oxides into LDHs has been variously referred to as regeneration, reconstruction, restoration, rehydration or "calcination-rehydration process", "structural memory effect" or simply "memory effect" (He et al., 2005).

When most of LDHs are subjected to thermal treatment, surface water molecules are the first to be removed from the structure, then the water molecules present in the interlayer gallery (Fig.1.9B), and finally, the water corresponding to the dehydroxylation of the main layers, leading to the collapse of the structure (Fig.1.9C). Depending on the nature of the interlamellar anions, they can remain or be removed at different temperatures. Further rise in temperature results in formation of a new phase of quasi-amorphous mixed-oxides (Fig.1.9D) that generally displays a relatively high specific surface area compared to the as-prepared LDHs. When the calcination temperature increases more, a process of solid-state diffusion of cations into tetrahedral positions occurs progressively forming a stable spinel phase (Fig.1.9E). This phase is resistant to rehydration, has a general formula of $M^{II}M^{III}_2O_4$, and also contains divalent metal oxides (He et al., 2005; de Roy et al., 2006).

After moderate calcination to pre-spinel oxide, LDH can be reconstructed in a solution containing anions or in air. In that case water molecules and anions (carbonates) are provided by atmosphere. Water is absorbed to reform the hydroxyl layers, and together with anions it is incorporated into the interlayer galleries (de Roy et al., 2006). The anions used to regenerate the structure do not necessarily need to be the same as those from the original LDH material. This phenomenon is important in synthesis of various inorganic and organic forms of LDHs (He et al., 2005) and opens the possibility of effective regeneration of LDHs based adsorbents.

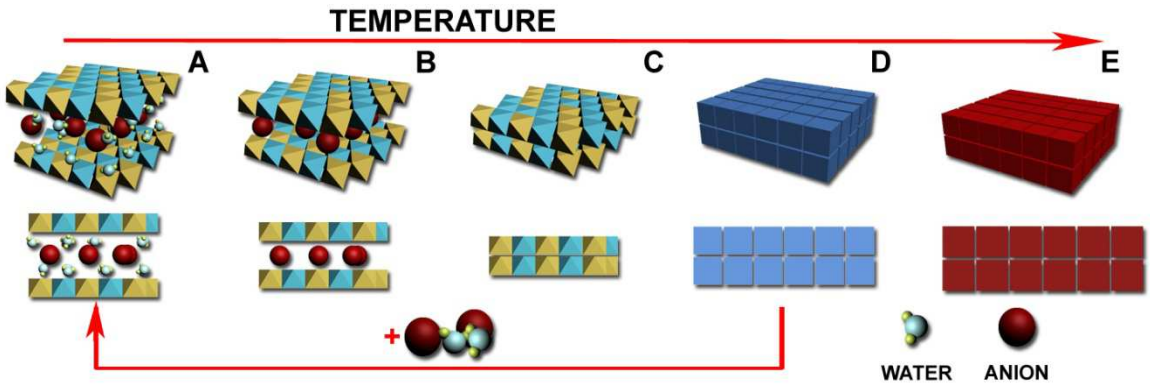

Figure 1.10 Changes occurring in hydrotalcite during its thermal treatment.

1.7 State-of-the-art

During the period of approximately two last decades some research on adsorption onto vermiculite have been carried out. However, most authors focused on adsorption onto the material without its modifications, with exception to thermal exfoliation. None of the authors applied subsequent acid-base treatment, not base treatment to the material in order to enhance its maximum adsorption capacity. Adsorption of dyes onto MgAl-hydrotalcite is studied more than onto vermiculite. However, focus on the fate of spent adsorbent it marginal.

Usage of waste produced during acid activation of vermiculite, or producing hydrotalcite-vermiculite composite adsorbents is a novelty that has not been reported in the literature. However, some attempts to producing such hybrids have been taken in the past, but this topic still requires a lot of research.

1.7.1 Removal of dyes by vermiculite and acid activated vermiculite

Clay minerals have been broadly used for adsorption of dyes but only certain studies address their removal using vermiculite. The great majority of them focused of the material as it is, without any modifications except thermal exfoliation. Literature

review on adsorption of dyestuffs by vermiculite in different forms, raw, expanded, expanded and washed and acid activated, is presented in Table 1.1, where the maximum adsorption capacities obtained in batch studies are presented. The origin of the material used in each study is identified.

Table 1.1 Application of vermiculite for removal of dyestuffs.

Vermiculite origin and/or treatment	**Dye**	**Maximum adsorption capacity** ($mg\ g^{-1}$)		**Reference**
Shanghai, China	Basic Red 9	17		Duman et al. (2015)
Shanghai, China (expanded 500 °C)		20		
Shanghai, China (expanded and washed with water for 24 h)		22		
Dharampuri, India	Basic Red 12	20		Khosla (2015)
Kovodor, Russia		raw	activated	
Kovodor, Russia (activated, 12.5% HCl)	Brilliant Green	45	166	Shapkin et al. (2014)
	Bromophenol Blue	12	30	
Karamürsel, Turkey	Pyronine Y	2		Toprak et al. (2014)
Karamürsel, Turkey	Pyronine Y	30		Toprak and Halisdemir (2015)
Karamürsel, Turkey (activated, 2.0 M H_3PO_4)		33		
Hebei, China	Methylene Blue	19		Yu et al. (2015)
	Crystal Violet	27		
Xinjiang, China	Methylene Blue	7		Zhao et al. (2008)
Xinjiang, China (activated, 2 M HCl, 12 h)		12		
Chugchong, Korea	Cationic Blue	107		Choi and Cho (1996)

Considerably more literature exists on the topic of removal of heavy metals cations using vermiculite as adsorbent, although again, not counting organic modifications that are not discussed here, only thermal treatment of the material is utilized to enhance adsorption capacity, but the application of not modified material prevails. Literature review on removal of metal ions using vermiculite based adsorbents is presented in Table 1.2. All studies were performed in batch system.

Table 1.2 Application of vermiculite for removal of metal cations.

Vermiculite (origin and treatment)	Metal	Adsorption capacity (mg g^{-1})	Reference
Piauí, Brasil (expanded for 1 min at 1000 °C)	Ni^{2+}	30	Marcos and Rodríguez (2016)
China (expanded for 1 min at 1000 °C)		160	
Red Sea, Egypt	Cd^{2+}	Cd 15, Pb 15	Hashem et al. (2015)
Red Sea, Egypt (treated with 0.5 HCl)	Pb^{2+}	Cd 21, Pb 21	
Red Sea, Egypt (treated with H_2O_2)		Cd 23, Pb 23	
Red Sea, Egypt	Cd^{2+}	Cd / Pb	Hashem et al. (2015)
Red Sea, Egypt (treated with 0.5 HCl)		15 / 15	
Red Sea, Egypt (treated with H_2O_2)	Pb2+	21 / 21	
		23 / 23	
Sigma–Aldrich	Hg^{2+}	20	Tran et al. (2015)
Chennai, India	Pb^{2+}	49	Vijayaraghavan and Raja (2015)
	Cd^{2+}	11	
	Cu^{2+}	13	
	Ni^{2+}	6.8	
Malatya, Turkey	Cr^{3+}	18	Sis and Uysal (2014)
	Pb^{2+}	49	
	Zn^{2+}	11	
China	Cr^{3+}	0.074	Marcos and Rodríguez (2014)
Guilan Province, Iran	Cu^{2+}	20	Dizadji et al. (2013)
Antalya-Turkey	Ag^{+}	46	Sarı and Tüzen (2013)
Kwangjoo, Korea (exfoliated in microwave at 440 W for 330 s)	Cd^{2+}	0.569	Lee (2012)
	Cr^{3+}	0.0009	
	Cu^{2+}	0.457	
	Pb^{2+}	0.725	
	Zn^{2+}	0.54	
North Transvaal, Africa Rochester N.I.	Cr^{3+}	25	Badawy et al. (2010)
	Cu^{2+}	15	
Mediterranean origin	Ni^{2+}	18	Katsou et al. (2010)
Sigma-Aldrich	Cd^{2+}	38	Abollino et al. (2008)
	Cu^{2+}	21	
	Mn^{2+}	27	
	Ni^{2+}	25	
	Pb^{2+}	64	
	Zn^{2+}	23	
Antalya, Turkey	Cr^{4+}	88	Sari and Tuzen (2008)
China	Pb^{2+}	109	Liu et al. (2007)
Institute of Geology & Mineral Exploration	Cu^{2+}	11	Stylianou et al. (2007)
Piauí, Brazil	Cd^{2+}	1.5	Abate and Masini (2005)
	Pb^{2+}	5	
Bikita, Zimbabwe	Hg^{2+}	20	Brigatti et al. (2005)
Paraíba, Brazil	Co^{2+}	45	da Fonseca et al. (2005)
	Cu^{2+}	53	
	Ni^{2+}	54	
	Pb^{2+}	122	
Askos, Greece / South Africa		Greece / South	Álvarez-Ayuso and García-Sánchez (2003)
	Cu^{2+}	26 / 8.6	
	Cd^{2+}	24 / 8.4	
	Ni^{2+}	19 / 5.9	

n.a. not analyzed

1.7.2 Removal of dyes by MgAl-hydrotalcite and hydrotalcite derived mixed oxides

MgAl-hydrotalcite and hydrotalcite derived mixed oxides have been used to remove dyes from aqueous solutions by some authors. The tested materials differed in the ration of Mg:Al, calcination temperature and time. Some example of research and their results from the last decade are presented in Table 1.3.

Table 1.3 Adsorption of dyes by hydrotalcite like adsorbents, raw (HT), calcined (HTC), after synthesis subjected to hydrothermal treatment and calcination (HTTC), HTC submitted to additional grounding after synthesis (HTCG), and hydrotalcite available commercially (HTCM).

Adsorbent	Dye	Maximum adsorption capacity (mg g^{-1})		Reference
HT (Mg:Al= 1)	Congo Red	130		Li et al. (2016)
HTC (700 °C, 3.5h)		143		
HTCM commercial		HTC	HTS	Heraldy et al. (2015)
	Eosin Yellow	32	7	
HT (Mg:Al= 2)	Methyl Orange	32	11	
	Methylene Blue	4	8	
HT (Mg:Al= 2)	Reactive Red	60		Shan et al. (2015)
	Congo Red	37		
	Acid Red 1	108		
HT (Mg:Al= 3)	Brilliant Red X-3B	47		Zhang et al. (2014)
HT (Mg:Al= 3)	Acid Green 68:1	99		Santos et al. (2013)
HTC (550 °C, 4h)		155		
HT (Mg:Al= 3)	Acid Orange 10	n.a.		Extremera et al. (2012)
HTC (500 °C, 3h)		209		
HTTC (80 °C, 24 h; 500 °C, 3 h)		634		
HTCG		407		
HT (Mg:Al= 2)	Orange II	1236		Mustapha Bouhent et al. (2011)
HT (Mg:Al= 3)	Astrazon Remazol Brilliant Blue	HTC: quicker retention of dyes		Flores et al. (2011)
HTC (450°C, 4h)	Direct Red	Capacity for DR greater than for ARBB		
HT (Mg:Al= 2)	Benzopurpurine 4B	154		Drici Setti et al. (2010)
HTC (500 °C, 4h)		417		
HT (Mg:Al= 2)	Brilliant Red K-2BP	658		Li et al. (2009)
HT (Mg:Al= 2)	Indigo Carmine	n.a.		El Gaini et al. (2009)
HTC (600 °C, 6h)		1786		
HT (Mg:Al= 5.6)	Acid Blue 9	48 [1]		Auxilio et al. (2009)
HTC (500 °C, 4h)		183 [2]		
		139 [3]		
HT (Mg:Al= 2)	Acid Blue 113	47		Bascialla and Regazzoni (2008)
HTC (500 °C, over night)		2544		
HT (Mg:Al= 2)	Brilliant Blue R	66		Zhu et al. (2005)
HTC (500 °C, 8h)		614		

[1] adsorption from 20% (v/v) glycerol-H_2O; [2] adsorption from 20% (v/v) glycerol-H_2O;[3] adsorption from H_2O

1.7.3 Adsorption from multicomponent solution

There are some research studies about simultaneous adsorption of metals. However to author's best knowledge no publications on the topic of adsorption in multicomponent system of dyes or dyes and metals onto vermiculite exist.

Interaction of vermiculite with Pb^{2+}, Cd^{2+}, Cu^{2+} and Ni^{2+} ions in quaternary mixtures was investigated by Vijayaraghavan and Raja (2015). Experimental results revealed that severe competition existed between metal ions during the adsorption with Pb^{2+} being the most favorable adsorbate, followed by Cu^{2}, Ni^{2+} and Cd^{2+}. Anjos et al. (2014) studied adsorption of various metal cations from multicomponent solution onto vermiculite (obtained from São Paulo, Brazil) and found the affinity of adsorbates to vermiculite to be classified as indicated: $Pb^{2+} \geq Cd^{2+} > Zn^{2+} \geq Mn^{2+} > Co^{2+} \geq Ni^{2+} \geq Cu^{2+} > Cr^{3+} > Sr^{2+} > V^{5+} \geq As^{5+} \geq Ba^{2+}$. Co-adsorption of Pb^{2+} and Cu^{2+} onto vermiculite (from Virginia, USA) was investigated by Padilla-Ortega et al. (2013). The results showed that the presence of Cu^{2+} increased the affinity of Pb^{2+} toward the adsorbent. Competitive adsorption of Ag^{+}, Cd^{2+}, Pb^{2+} Ni^{2+} ions on vermiculite (from China) in a binary, ternary, and quaternary mixture was investigated in batch experiments by Liu et al. (2010). The results indicated that Pb^{2+} ions always favorably adsorbed on the material over Ag^{+}, Cd^{2+} and Ni^{2+}. El-Bayaa et al. (2009) investigated competition in adsorption of Cr^{3+}, Cu^{2+}, Ni^{2+} and Co^{2+} onto vermiculite (supplied by the North Transvaal, Africa Rochester N.I.). It was found that divalent cations competed for adsorption sites, however trivalent metal cation had the strongest affinity to the adsorbent and caused desorption of divalent cations after it was added to the solution. Vieira dos Santos and Masini (2007) studied adsorption of Pb^{2+}, Cd^{2+} and Cu^{2+} from wastewaters on vermiculite (obtained from Piauí, Brazil) and its expanded version. The results showed that adsorption of Pb^{2+} was favored, and competition with Fe^{3+} cation and organic matter present in the sample interfered with the removal efficiency. Coadsorption experiments of Cd^{2+}, Cr^{3+}, Cu^{2+}, Ni^{2+}, Pb^{2+} and Zn^{2+} using vermiculite (from Süd-Chemie, Spain) conducted by Covelo et al. (2007) revealed that Cu^{2+} and Zn^{2+} were preferentially adsorbed onto the material.

1.7.4 Clay/hydrotalcite composites

To the author's best knowledge, there are no reports in the literature on synthesizing hydrotalcite like material from waste products resulting from acid activation of clays. A few studies deliver information about hydrotalcite-clay composite and their applications in waste water treatment.

Tian et al. (2016) produced a hierarchical MgAl–layered double hydroxide on the external and interlayer surfaces of vermiculite and used it to remove Cr^{6+} cations. Such

prepared adsorbent showed increased maximum adsorption capacity due to its 3D hierarchical structure. The same element was removed by Pérez et al. (2015) using nano-MgAl-hydrotalcite particles supported on silica. Tao et al. (2011) used amorphous silica coated with MgAl-hydrotalcite to remove basic dyes, Crystal Violet and Leuco-crystal Violet. Deng and Shi (2015) synthesized mesoporous modified kaolin clay by loading MgAl-hydrotalcite onto kaolin clay through co-precipitation method and applied it for adsorption of phosphate from aqueous solution.

1.7.5 Regeneration of adsorbent

Only a few authors investigate the possibility of regeneration of the adsorbent they study. In most of the cases ethanol or methanol are applied to desorb dyes, and low concentrated acids to remove metals from vermiculite. Thermal regeneration is considered suitable to regenerate hydrotalcite adsorbents as well as clays.

Toprak and Halisdemir (2015) used methanol for that purpose, regeneration his adsorbent after adsorption of Pyronin B. Duman et al. (2015) and Zhao et al. (2008) applied ethanol for regeneration of their adsorbent saturated with Basic Red 9 and Methylene Blue, respectively. Liu et al. (2010) used 1.0 M HNO_3 while Anjos et al. (2014) applied HCl to desorb metals from vermiculite. Choi and Cho (1996) regenerated their adsorbent by thermal treatment in temperatures above 550 °C after removal of Cationic Blue. Teixeira et al. (2014) and Drici Setti et al. (2010) applied successfully thermal regeneration at 500 °C to hydrotalcite adsorbent. Extremera et al. (2012) touched the problem of regeneration of spent adsorbent and recovery of adsorbed dye for further use. The dye was successfully desorbed in aqueous solution containing carbonates. However, an attempt to regenerate such treated adsorbent by calcination did not give good results and the adsorption capacity was not regained.

1.8 References

96/61/EC, Council Directive of 24 September 1996 concerning integrated pollution prevention and control. Official Journal L 257 , 10/10/1996 P. 0026 - 0040.

2000/60/EC, Directive of the European Parliament and of the Council of 23 October 2000 establishing a framework for Community action in the field of water policy. Official Journal L 327, 22.12.2000, 1–73.

2006/11/EC, Directive of the European Parliament and of the Council of 15 February 2006 on pollution caused by certain dangerous substances discharged into the aquatic environment of the Community. Official Journal, L 64, 4.3.2006, p. 52–59.

2008/1/EC, Directive of the European Parliament and of the Council of 15 January 2008 concerning integrated pollution prevention and control. Official Journal, L 24, 29.1.2008, p. 8–29.

2008/32/EC, Directive of the European Parliament and of the Council amending Directive 2000/60/EC establishing a framework for Community action in the field of water policy, as regards the implementing powers conferred on the Commission. Official Journal, L 81, 20.03.2008, p. 60-61.

2008/105/EC, Directive of the European Parliament and of the Council of 16 December 2008 on environmental quality standards in the field of water policy, amending and subsequently repealing Council Directives 82/176/EEC, 83/513/EEC, 84/156/EEC, 84/491/EEC, 86/280/EEC and amending Directive 2000/60/EC of the European Parliament and of the Council. Official Journal, L 348, 24.12.2008, p. 84–97

2009/31/EC, Directive of the European Parliament and of the Council of 23 April 2009 on the geological storage of carbon dioxide and amending Council Directive 85/337/EEC, European Parliament and Council Directives 2000/60/EC, 2001/80/EC, 2004/35/EC, 2006/12/EC, 2008/1/EC and Regulation (EC) No 1013/2006. Official Journal, L 140, 5.6.2009, p. 114–135.

2010/75/EU, Directive of the European Parliament and of the Council of 24 November 2010 on industrial emissions (integrated pollution prevention and control). Official Journal, L 334, 17.12.2010, p. 17–119

2013/39/EU, Directive of the European Parliament and of the Council of 12 August 2013 amending Directives 2000/60/EC and 2008/105/EC as regards priority substances in the field of water policy. Official Journal, L 226, 24.8.2013, p. 1–17.

2014/101/EU, Commission Directive of 30 October 2014 amending Directive 2000/60/EC of the European Parliament and of the Council establishing a framework for Community action in the field of water policy. Official Journal, L 311, 31.10.2014, p. 32–35.

2455/2001/EC, Decision of the European Parliament and of the Council of 20 November 2001 establishing the list of priority substances in the field of water policy and amending Directive 2000/60/EC. Official Journal, L 331, 15.12.2001, p. 1–5.

Abate, G., Masini, J.C., 2005. Influence of pH, ionic strength and humic acid on adsorption of Cd(II) and Pb(II) onto vermiculite. Colloids Surf. Physicochem. Eng. Aspects 262, 33-39.

Abollino, O., Giacomino, A., Malandrino, M., Mentasti, E., 2008. Interaction of metal ions with montmorillonite and vermiculite. Appl. Clay Sci. 38, 227-236.

Allaby, M., 2013. A Dictionary of Geology and Earth Sciences. OUP Oxford.

Álvarez-Ayuso, E., García-Sánchez, A., 2003. Removal of heavy metals from waste waters by vermiculites. Environ. Technol. 24, 615-625.

Anjos, V.E., Rohwedder, J.R., Cadore, S., Abate, G., Grassi, M.T., 2014. Montmorillonite and vermiculite as solid phases for the preconcentration of trace elements in natural waters: Adsorption and desorption studies of As, Ba, Cu, Cd, Co, Cr, Mn, Ni, Pb, Sr, V, and Zn. Appl. Clay Sci. 99, 289-296.

Atkins, P., de Paula, J., 2010. Atkins' Physical Chemistry. OUP Oxford.

ATSDR, 1989. Toxicological Profile for Mercury. Agency for Toxic Substances and Disease Registry, U.S. Public Health Service.

ATSDR, 1993a. Toxicological profile for cadmium. U.S. Dept. of Health and Human Services, Public Health Service, Agency for Toxic Substances and Disease Registry.

ATSDR, 1993b. Toxicological Profile for Lead. U.S. Department of Health and Human Services, Public Health Service, Agency for Toxic Substances and Disease Registry.

ATSDR, 2004a. Toxicological Profile for Cobalt. U.S. Department of Health and Human Services, Public Health Service, Agency for Toxic Substances and Disease Registry.

ATSDR, 2004b. Toxicological Profile for Copper. U.S. Department of Health and Human Services, Public Health Service, Agency for Toxic Substances and Disease Registry.

ATSDR, 2005. Toxicological Profile for Nickel. Agency for Toxic Substances and Disease Registry.

ATSDR, 2007. Toxicological Profile for Arsenic. Agency for Toxic Substances and Disease Registry, U.S. Public Health Service.

Auxilio, A.R., Andrews, P.C., Junk, P.C., Spiccia, L., 2009. The adsorption behavior of C.I. Acid Blue 9 onto calcined Mg–Al layered double hydroxides. Dyes Pigm. 81, 103-112.

Badawy, N.A., El-Bayaa, A.A., Abd AlKhalik, E., 2010. Vermiculite as an exchanger for copper(II) and Cr(III) ions, kinetic studies. Ionics 16, 733-739.

Bailey, S.W., Chairman, 1980. Summary of recommendations of AIPEA nomenclature committee on clay minerals. Am. Mineral. 65, 1-7.

Banfalvi, G., 2011. Heavy Metals, Trace Elements and Their Cellular Effects. in: Banfalvi, G. (Ed.). Cellular Effects of Heavy Metals. Springer Netherlands.

Bascialla, G., Regazzoni, A.E., 2008. Immobilization of anionic dyes by intercalation into hydrotalcite. Colloids Surf. Physicochem. Eng. Aspects 328, 34-39.

Bergaya, F., Lagaly, G., 2006. General introduction: clays, clay minerals, and clay science. in: Bergaya, F., Theng, B.K.G., Lagaly, G. (Eds.). Handbook of Clay Science. Elsevier Ltd.

Braterman, P.S., Xu, Z.P., Yarberry, F., 2004. Layered double Hydroxides (LDHs). in: Auerbach, S.M., Carrado, K.A., Dutta, P.K. (Eds.). Handbook of Layered Materials. Marcel Dekker, U.S.A.

Brigatti, M.F., Colonna, S., Malferrari, D., Medici, L., Poppi, L., 2005. Mercury adsorption by montmorillonite and vermiculite: a combined XRD, TG-MS, and EXAFS study. Appl. Clay Sci. 28, 1-8.

Brigatti, M.F., GALAN, E., Theng, B.K.G., 2006. Structures and mineralogy of clay minerals. in: Bergaya, F., Theng, B.K.G., Lagal, G. (Eds.). Handbook of Clay Science. Elsevier Ltd.

Carrado, K.A., 2004. Introduction: Clay Structure, Surface Acidity, and Catalysis. in: Auerbach, S.M., Carrado, K.A., Dutta, P.K. (Eds.). Handbook of Layered Materials. Marcel Dekker, U.S.A.

Carroll, D., 2012. Rock Weathering. Springer US.

Cattoor, T., 2007. European legislation relating to textile dyeing. in: Christie, R.M. (Ed.). Environmental Aspects of Textile Dyeing. Elsevier Science.

Chen, J.P., 2012. Decontamination of Heavy Metals: Processes, Mechanisms, and Applications. Taylor & Francis.

Choi, Y.S., Cho, J.H., 1996. Color Removal from Dye Wastewater Using Vermiculite. Environ. Technol. 17, 1169-1180.

Chowdhury, S., Balasubramanian, R., Das, P., 2015. Novel Carbon-Based Nanoadsorbents for Removal of Synthetic Textile Dyes from Wastewaters. in: Sharma, S.K. (Ed.). Green Chemistry for Dyes Removal from Waste Water: Research Trends and Applications. Wiley.

Christie, R., 2014. Colour Chemistry. Royal Society of Chemistry.

Christie, R.M., 2007. Environmental Aspects of Textile Dyeing. Elsevier Science.

Clark, M., 2011. Fundamental principles of dyeing. in: Clark, M. (Ed.). Handbook of Textile and Industrial Dyeing: Principles, Processes and Types of Dyes. Elsevier Science.

Cooper, P., Dyers, S.o., Colourists, 1995. Colour in Dyehouse Effluent. Society of Dyers and Colourists.

Covelo, E.F., Vega, F.A., Andrade, M.L., 2007. Competitive sorption and desorption of heavy metals by individual soil components. J. Hazard. Mater. 140, 308-315.

da Fonseca, M.G., de Oliveira, M.M., Arakaki, L.N.H., Espinola, J.G.P., Airoldi, C., 2005. Natural vermiculite as an exchanger support for heavy cations in aqueous solution. J. Colloid Interface Sci. 285, 50-55.

de Roy, A., Forano, C., Besse, J.P., 2006. Layered double hydroxides: synthesis and post-synthesis modification. in: Rives, V. (Ed.). Layered Double Hydroxides: Present and Future Nova Science Publishers, Inc., New York.

Deng, L., Shi, Z., 2015. Synthesis and characterization of a novel Mg–Al hydrotalcite-loaded kaolin clay and its adsorption properties for phosphate in aqueous solution. J. Alloys Compd. 637, 188-196.

Dizadji, N., Rashtchi, M., Dehpouri, S., Nouri, N., 2013. Experimental Investigation of Adsorption of Copper from Aqueous Solution using Vermiculite and Clinoptilolite. International Journal of Environmental Research 7, 887-894.

Drici Setti, N., Jouini, N., Derriche, Z., 2010. Sorption study of an anionic dye – benzopurpurine 4B – on calcined and uncalcined Mg–Al layered double hydroxides. J. Phys. Chem. Solids 71, 556-559.

Duman, O., Tunç, S., Polat, T.G., 2015. Determination of adsorptive properties of expanded vermiculite for the removal of C. I. Basic Red 9 from aqueous solution: Kinetic, isotherm and thermodynamic studies. Appl. Clay Sci. 109–110, 22-32.

EC 1907/2006, Regulation of the european parliament and of the council of 18 December 2006 concerning the Registration, Evaluation, Authorisation and Restriction of Chemicals (REACH),. Official Journal L 396/1 , 30.12. 2006.

EEC Treaty, 1957. Treaty establishing the European Economic Community,- original text (non-consolidated version).

Ejder-Korucu, M., Gürses, A., Doğar, Ç., Sharma, S.K., Açıkyıldız, M., 2015. Removal of Organic Dyes from Industrial Effluents: An Overview of Physical and Biotechnological Applications. in: Sharma, S.K. (Ed.). Green Chemistry for Dyes Removal from Waste Water: Research Trends and Applications. Wiley.

El-Bayaa, A.A., Badawy, N.A., AlKhalik, E.A., 2009. Effect of ionic strength on the adsorption of copper and chromium ions by vermiculite pure clay mineral. J. Hazard. Mater. 170, 1204-1209.

El Gaini, L., Lakraimi, M., Sebbar, E., Meghea, A., Bakasse, M., 2009. Removal of indigo carmine dye from water to Mg–Al–CO3-calcined layered double hydroxides. J. Hazard. Mater. 161, 627-632.

Encyclopædia Britannica Online, 2015. clay mineral. Encyclopædia Britannica. Encyclopædia Britannica Inc.

Euratex, 2015. Key Figures 2015 - The EU-28 Textile and Clothing Industry in the year 2015. The European Apparel and Textile Confederation, http://euratex.eu/fileadmin/user_upload/documents/key_data/Euratex_KeyFigures_-_2015.pdf.

Evans, D.G., Slade, R.C.T., 2005. Structural aspects of layered double hydroxides. in: Duan, X., Evans, D.G. (Eds.). Layered Double Hydroxides. Springer.

Extremera, R., Pavlovic, I., Pérez, M.R., Barriga, C., 2012. Removal of acid orange 10 by calcined Mg/Al layered double hydroxides from water and recovery of the adsorbed dye. Chem. Eng. J. 213, 392-400.

Flores, J., Lima, E., Maubert, M., Aduna, E., Rivera, J.L., 2011. Clean-up of wastes from the textile industry using anionic clays. Clays Clay Miner. 58.

Fuchs, Y., 2004. Clays, economic uses, Encyclopedia of geology: Vol. 1. in: Cocks, R., Selley, R.C., Cocks, L.R.M., Plimer, I.R. (Eds.). Encyclopedia of geology: Vol. 1. Elsevier Science.

Gautam, R.K., Sharma, S.K., Mahiya, S., Chattopadhyaya, M.C., 2015. Contamination of heavy metals in aquatic media: transport, toxixity and technologies for remediation. in: Sharma, S.K. (Ed.). Heavy metals in water. Presence, removal and safety. The Royal Society of Chemistry, Cambridge.

Gregory, P., 2007. Toxicology of textile dyes in: Christie, R.M. (Ed.). Environmental Aspects of Textile Dyeing. Elsevier Science.

Grim, R.E., 1962. Applied Clay Mineralogy. McGraw-Hill, Ney Yourk.

Grim, R.E., 1968. Clay Mineralogy, 2nd Edition. McGraw-Hill, New York.

Guggenheim, S., Martin, R.T., 1995. Definition of clay and clay mineral: joint report of the AIPEA nomenclature and CMS nomenclature committees. Clays and Clay Minerals 43, Clay Minerals 30.

Gupta, V.K., Ali, I., 2012. Environmental Water: Advances in Treatment, Remediation and Recycling. Elsevier.

Gürses, A., Açıkyıldız, M., Güneş, K., Gürses, M.S., 2016. Dyes and Pigments. Springer International Publishing.

Hardin, I.R., 2007. Chemical treatment of textile dye effluent. in: Christie, R.M. (Ed.). Environmental Aspects of Textile Dyeing. Elsevier Science.

Hashem, F.S., Amin, M.S., El-Gamal, S.M.A., 2015. Chemical activation of vermiculite to produce highly efficient material for Pb2 + and Cd2 + removal. Appl. Clay Sci. 115, 189-200.

Hassan, M.M., Hawkyard, C.J., 2007. Decolorisation of effluent with ozone and re-use of spent dyebath. in: Christie, R.M. (Ed.). Environmental Aspects of Textile Dyeing. Elsevier Science.

He, J., Wei, M., Li, B., Kang, Y., Evans, D.G., Duan, X., 2005. Preparation of LayeredDouble Hydroxides. in: Duan, X., Evans, D.G. (Eds.). Layered Double Hydroxides. Springer.

Heller-Kallai, L., 2006. Thermally Modified Clay Minerals. in: Bergaya, F., Theng, B.K.G., Lagaly, G. (Eds.). Handbook of Clay Science. Elsevier Ltd.

Heraldy, E., Santosa, S.J., Triyono, T., Wijaya, K., 2015. Anionic and cationic dyes removal from aqueous solutions by adsorption onto synthetic mg/al hydrotalcite-like compound. Indonesian Journal of Chemistry 15.

Hijazi, A., Mcheik, A., Rammal, H., Rammal, W., Annan, H., Toufaily, J., Hamieh, T., 2015. Biosorption of methylene blue from waste water using lebanese cymbopogon citratus (citronelle). European Scientific Journal 11.

Hlavinek, P., Winkler, I., Marsalek, J., Mahrikova, I., 2011. Advanced Water Supply and Wastewater Treatment: A Road to Safer Society and Environment. Springer Netherlands.

Ho, Y.S., El-Khaiary, M.I., 2009. Metal Research Trends in the Environmental Field. in: Wang, L.K., Chen, J.P., Hung, Y.T., Shammas, N.K. (Eds.). Heavy Metals in the Environment. CRC Press.

Howe, K.J., Hand, D.W., Crittenden, J.C., Trussell, R.R., Tchobanoglous, G., 2012. Principles of Water Treatment. Wiley.

Huggett, J.M., 2004. Clay minerals, Encyclopedia of geology: Vol. 1. in: Cocks, R., Selley, R.C., Cocks, L.R.M., Plimer, I.R. (Eds.). Encyclopedia of geology: Vol. 1. Elsevier Science.

Hunger, K., 2007. Industrial Dyes: Chemistry, Properties, Applications. Wiley.

Hunger, K., Mischke, P., Rieper, W., 2011. Azo Dyes. Ullmann's Encyclopedia of Industrial Chemistry, 40 Volume Set. Ullmann's Encyclopedia of Industrial Chemistry, 40 Volume Set, Wiley.

IHS Markit, 2014. Chemical Economics Handbook: Dyes. https://www.ihs.com/products/dyes-chemical-economics-handbook.html.

Kant, R., 2012. Textile dyeing industry an environmental hazard. Natural Science 4, 22-26.

Katsou, E., Malamis, S., Haralambous, K.J., Loizidou, M., 2010. Use of ultrafiltration membranes and aluminosilicate minerals for nickel removal from industrial wastewater. J. Membr. Sci. 360, 234-249.

Khosla, E., 2015. Natural Clay -An Adsorbent for Basic Dye. Journal of Chemistry & Applied Biochemistry.

Komadel, P., Madejova, J., 2006. Acid Activation of Clay Minerals. in: Bergaya, F., Theng, B.K.G., Lagaly, G. (Eds.). Handbook of Clay Science. Elsevier Ltd.

Küpper, H., 2011. Foreword. in: Sherameti, I., Varma, A. (Eds.). Detoxification of Heavy Metals. Springer Berlin Heidelberg.

Lagaly, G., Ogava, M., Dekany, I., 2006. Clay Mineral Organic Interactions. in: Bergaya, F., Theng, B.K.G., Lagaly, G. (Eds.). Handbook of Clay Science. Elsevier Ltd.

Lee, T., 2012. Removal of heavy metals in storm water runoff using porous vermiculite expanded by microwave preparation. Water, Air, Soil Pollut. 223, 3399-3408.

Li, B., Zhang, Y., Zhou, X., Liu, Z., Liu, Q., Li, X., 2016. Different dye removal mechanisms between monodispersed and uniform hexagonal thin plate-like MgAl–CO32--LDH and its calcined product in efficient removal of Congo red from water. J. Alloys Compd. 673, 265-271.

Li, Y., Gao, B., Wu, T., Wang, B., Li, X., 2009. Adsorption properties of aluminum magnesium mixed hydroxide for the model anionic dye Reactive Brilliant Red K-2BP. J. Hazard. Mater. 164, 1098-1104.

Liu, Y., Li, H., Zhu, X.-H., 2010. Competitive Adsorption of Ag+, Pb2+, Ni2+, and Cd2+ Ions on Vermiculite. Sep. Sci. Technol. 45, 277-287.

Liu, Y., Xiao, D., Li, H., 2007. Kinetics and Thermodynamics of Lead (II) Adsorption on Vermiculite. Sep. Sci. Technol. 42, 185-202.

Maqueda, C., Perez-Rodriguez, J.L., Šubrt, J., Murafa, N., 2009. Study of ground and unground leached vermiculite. Appl. Clay Sci. 44, 178-184.

Maqueda, C., Romero, A.S., Morillo, E., Pérez-Rodríguez, J.L., 2007. Effect of grinding on the preparation of porous materials by acid-leached vermiculite. J. Phys. Chem. Solids 68, 1220-1224.

Marcos, C., Rodríguez, I., 2014. Some effects of trivalent chromium exchange of thermo-exfoliated commercial vermiculite. Appl. Clay Sci. 90, 96-100.

Marcos, C., Rodríguez, I., 2016. Thermoexfoliated commercial vermiculites for Ni2 + removal. Appl. Clay Sci. 132–133, 685-693.

McGraw-Hill, 2003. Dictionary of Geology & Mineralogy. McGraw-Hill Education.

Mishra, A., Clark, J.H., 2013a. Greening the Blue: How the World is Addressing the Challenge of Green Remediation of Water. in: Mishra, A., Clark, J.H. (Eds.). Green

Materials for Sustainable Water Remediation and Treatment. Royal Society of Chemistry.

Mishra, A., Clark, J.H., 2013b. Preface. in: Mishra, A., Clark, J.H. (Eds.). Green Materials for Sustainable Water Remediation and Treatment. Royal Society of Chemistry.

MNM, 2013. Dyes and Pigments Market - Dyes (Reactive, Disperse, Acid, Direct, Basic, VAT), Organic Pigments (Azo, Phthalocyanines, High Performance) & Inorganic Pigments (TiO2, Iron Oxide, Carbon Black & Others) - Global Trends & Forecast to 2018. MarketsandMarkets.com, http://www.marketsandmarkets.com/Market-Reports/colorants-tinting-systems-paints-coatings-market-875.html.

Monsalvo, V.M., 2016. Introduction. in: Monsalvo, V.M. (Ed.). Water treatment in developed and developing nations. An international perspective. CRC Proess, Apple academic Proess.

Murray, H.H., 2006. Applied Clay Mineralogy: Occurrences, Processing and Applications of Kaolins, Bentonites, Palygorskitesepiolite, and Common Clays. Elsevier Science.

Mustapha Bouhent, M., Derriche, Z., Denoyel, R., Prevot, V., Forano, C., 2011. Thermodynamical and structural insights of orange II adsorption by MgRAlNO3 layered double hydroxides. J. Solid State Chem. 184, 1016-1024.

Padilla-Ortega, E., Leyva-Ramos, R., Flores-Cano, J.V., 2013. Binary adsorption of heavy metals from aqueous solution onto natural clays. Chem. Eng. J. 225, 535-546.

Paint & Coating Industries, 2015. Growth in key industries drives pigments and dyes market. http://www.pcimag.com/articles/96518-growth-in-key-industries-drives-pigments-and-dyes-market.

Pejman Hadi, P., Sharma, S.K., Gordon McKay, G., 2015. Removal of Dyes from Effluents Using Biowaste-Derived Adsorbents. in: Sharma, S.K. (Ed.). Green Chemistry for Dyes Removal from Waste Water: Research Trends and Applications. Wiley.

Pérez, E., Ayele, L., Getachew, G., Fetter, G., Bosch, P., Mayoral, A., Díaz, I., 2015. Removal of chromium(VI) using nano-hydrotalcite/SiO2 composite. Journal of Environmental Chemical Engineering 3, 1555-1561.

Philippis, R., Micheletti, E., 2009. Heavy Metal Removal with Exopolysaccharide-Producing Cyanobacteria. in: Wang, L.K., Chen, J.P., Hung, Y.T., Shammas, N.K. (Eds.). Heavy Metals in the Environment. CRC Press.

Pinnavaia, T.J., 2004. Foreword. in: Auerbach, S.M., Carrado, K.A., Dutta, P.K. (Eds.). Handbook of Layered Materials. Marcel Dekker, U.S.A.

REACH in brief, E.C., 2007. Environment Directorate General, http://ec.europa.eu/environment/chemicals/reach/pdf/publications/2007_02_reach_in_brief.pdf.

Rieder, M., Cavazzini, G., D'yakonov, Y.S., Frank-Kamenetskii, V.A., Gottardi, G., Guggenheim, S., Koval, P.V., Müller, G., Neiva, A.M.R., Radoslovich, E.W., Robert, J.-L., Sassi, F.P., Takeda, H., Weiss, Z., Wones, D.R., 1998. Nomenclature of micas. Clays Clay Miner. 46, 586-595.

Rives, V., 2006. Preface. in: Rives, V. (Ed.). Layered Double Hydroxides: Present and Future. Nova Science Publishers, Inc., New York.

Ruiz-Hitzky, E., Aranda, P., Saerratosa, J.M., 2004. Clay-organic interactions: organoclay complexes and polymer-clay nanocomposites. in: Auerbach, S.M., Carrado, K.A., Dutta, P.K. (Eds.). Handbook of layered materials. Marcal Dekker, New York.

Santos, R.M.M., Gonçalves, R.G.L., Constantino, V.R.L., da Costa, L.M., da Silva, L.H.M., Tronto, J., Pinto, F.G., 2013. Removal of Acid Green 68:1 from aqueous solutions by calcined and uncalcined layered double hydroxides. Appl. Clay Sci. 80–81, 189-195.

Santos, S.S.G., Silva, H.R.M., de Souza, A.G., Alves, A.P.M., da Silva Filho, E.C., Fonseca, M.G., 2015. Acid-leached mixed vermiculites obtained by treatment with nitric acid. Appl. Clay Sci. 104, 286-294.

Sari, A., Tuzen, M., 2008. Removal of Cr(VI) From Aqueous Solution by Turkish Vermiculite: Equilibrium, Thermodynamic and Kinetic Studies. Sep. Sci. Technol. 43, 3563-3581.

Sarı, A., Tüzen, M., 2013. Adsorption of silver from aqueous solution onto raw vermiculite and manganese oxide-modified vermiculite. Microporous Mesoporous Mater. 170, 155-163.

Scoullos, M., Vonkeman, G.H., Thornton, I., Makuch, Z., 2012. Mercury — Cadmium — Lead Handbook for Sustainable Heavy Metals Policy and Regulation. Springer Netherlands.

Shan, R.-r., Yan, L.-g., Yang, Y.-m., Yang, K., Yu, S.-j., Yu, H.-q., Zhu, B.-c., Du, B., 2015. Highly efficient removal of three red dyes by adsorption onto Mg–Al-layered double hydroxide. Journal of Industrial and Engineering Chemistry 21, 561-568.

Shapkin, N.P., Maiorov, V.I., Leont'ev, L.B., Shkuratov, A.L., Shapkina, V.Y., Khal'chenko, I.G., 2014. A study of the adsorption properties of modified layered silicate. Colloid J. 76, 746-752.

Sharma, R.K., 2013. Green Materials for Sustainable Remediation of Metals in Water. in: Mishra, A., Clark, J.H. (Eds.). Green Materials for Sustainable Water Remediation and Treatment. Royal Society of Chemistry.

Sharma, S.K., Sanghi, R., 2012. Advances in Water Treatment and Pollution Prevention. Springer Netherlands.

Sharma, S.K., Sanghi, R., Mudhoo, A., 2012. Green Practices to Save Our Precious "Water Resource". in: Sharma, S.K., Sanghi, R. (Eds.). Advances in Water Treatment and Pollution Prevention. Springer Netherlands.

Sis, H., Uysal, T., 2014. Removal of heavy metal ions from aqueous medium using Kuluncak (Malatya) vermiculites and effect of precipitation on removal. Appl. Clay Sci. 95, 1-8.

Srinivasan, R., 2013a. Natural Polysaccharides as Treatment Agents for Wastewater. in: Mishra, A., Clark, J.H. (Eds.). Green Materials for Sustainable Water Remediation and Treatment. Royal Society of Chemistry.

Srinivasan, R., 2013b. Role of Plant Biomass in Heavy Metal Treatment of Contaminated Water. in: Mishra, A., Clark, J.H. (Eds.). Green Materials for Sustainable Water Remediation and Treatment. Royal Society of Chemistry.

Stylianou, M.A., Inglezakis, V.J., Moustakas, K.G., Malamis, S.P., Loizidou, M.D., 2007. Removal of Cu(II) in fixed bed and batch reactors using natural zeolite and exfoliated vermiculite as adsorbents. Desalination 215, 133-142.

Sun, J., Ji, Y., Cai, F., Jing Li, J., 2012. Heavy Metal Removal Through Biosorptive Pathways. in: Sharma, S.K., Sanghi, R. (Eds.). Advances in Water Treatment and Pollution Prevention. Springer Netherlands.

Tao, Y.F., Lin, W.G., Gao, L., Yang, J., Zhou, Y., Yang, J.Y., Wei, F., Wang, Y., Zhu, J.H., 2011. Low-cost and effective phenol and basic dyes trapper derived from the porous silica coated with hydrotalcite gel. J. Colloid Interface Sci. 358, 554-561.

Teixeira, T.P.F., Aquino, S.F., Pereira, S.I., Dias, A., 2014. Use of calcined layered double hydroxides for the removal of color and organic matter from textile effluents: kinetic, equilibrium and recycling studies. Brazilian Journal of Chemical Engineering 31, 19-26.

Teng, T.T., Low, L.W., 2012. Removal of Dyes and Pigments from Industrial Effluents. in: Sharma, S.K., Sanghi, R. (Eds.). Advances in Water Treatment and Pollution Prevention. Springer Netherlands.

Theng, B.K.G., 2012. Formation and Properties of Clay-polymer Complexes. Elsevier.

Tian, W., Kong, X., Jiang, M., Lei, X., Duan, X., 2016. Hierarchical layered double hydroxide epitaxially grown on vermiculite for Cr(VI) removal. Mater. Lett. 175, 110-113.

Tolga Depci, T., Çelik, M., S,, 2015. Dye Adsorption on Expanding Three-Layer Clays. in: Sharma, S.K. (Ed.). Green Chemistry for Dyes Removal from Waste Water: Research Trends and Applications. Wiley.

Toprak, M., Halisdemir, E., 2015. Removal of Pyronin B from aqueous solutions using raw and modified vermiculite. Res. Chem. Intermed. 41, 8289-8306.

Toprak, M., Salci, A., Demirkiran, A.R., 2014. Comparison of adsorption performances of vermiculite and clinoptilolite for the removal of pyronine y dyestuff. Reaction Kinetics, Mechanisms and Catalysis 111, 791-804.

Tran, L., Wu, P., Zhu, Y., Yang, L., Zhu, N., 2015. Highly enhanced adsorption for the removal of Hg(II) from aqueous solution by Mercaptoethylamine/Mercaptopropyltrimethoxysilane functionalized vermiculites. J. Colloid Interface Sci. 445, 348-356.

UN/DESA, 2015. World population prospects: The 2015 revision summary and key findings. United Nations, Department of Economic and Social Affairs

United Nations, 2016. The United Nations World Water Development Report 4: Managing Water under Uncertainty and Risk, (World Water Assessment Programme). in: UNESCO (Ed.).

Velde, B., 1995. Origin and Mineralogy of Clays: Clays and the Environment. Springer Berlin Heidelberg.

Vieira dos Santos, A.C., Masini, J.C., 2007. Evaluating the removal of Cd(II), Pb(II) and Cu(II) from a wastewater sample of a coating industry by adsorption onto vermiculite. Appl. Clay Sci. 37, 167-174.

Vijayaraghavan, K., Raja, F.D., 2015. Interaction of Vermiculite with Pb(II), Cd(II), Cu(II) and Ni(II) Ions in Single and Quaternary Mixtures. CLEAN – Soil, Air, Water 43, 1174-1180.

Worch, E., 2012. Adsorption Technology in Water Treatment: Fundamentals, Processes, and Modeling. De Gruyter.

Yu, X., Wei, C., Wu, H., 2015. Effect of molecular structure on the adsorption behavior of cationic dyes onto natural vermiculite. Sep. Purif. Technol. 156, Part 2, 489-495.

Zhang, C., Yang, S., Chen, H., He, H., Sun, C., 2014. Adsorption behavior and mechanism of reactive brilliant red X-3B in aqueous solution over three kinds of hydrotalcite-like LDHs. Appl. Surf. Sci. 301, 329-337.

Zhao, M., Tang, Z., Liu, P., 2008. Removal of methylene blue from aqueous solution with silica nano-sheets derived from vermiculite. J. Hazard. Mater. 158, 43-51.

CHAPTER 2

Acid treatment of vermiculite

Chemosphere 153 (2016) 115–129

Contents lists available at ScienceDirect

Chemosphere

journal homepage: www.elsevier.com/locate/chemosphere

The influence of acid treatments over vermiculite based material as adsorbent for cationic textile dyestuffs

Wojciech Stawiński[a], Olga Freitas[a], Lucjan Chmielarz[b], Agnieszka Węgrzyn[b,*], Kamila Komędera[c], Artur Błachowski[c], Sónia Figueiredo[a,*]

[a] *REQUIMTE, LAQV, Instituto Superior de Engenharia do Porto, Instituto Politécnico do Porto, Rua Dr. António Bernardino de Almeida 431, 4200-072 Porto, Portugal*
stawor@gmail.com; omf@isep.ipp.pt; saf@isep.ipp.pt

[b] *Faculty of Chemistry, Jagiellonian University, ul. Ingardena 3, 30-060 Krakow, Poland*
wegrzyn@chemia.uj.edu.pl; chamielar@chemia.uj.edu.pl

[c] *Mössbauer Spectroscopy Laboratory, Pedagogical University, ul. Podchorążych 2, 30-084Kraków, Poland*
kamilakom@op.pl; sfblacho@cyf-kr.edu.pl

Abstract

The influence of different acid treatments over vermiculite was evaluated. Equilibrium, kinetic and column studies have been conducted. The results showed that vermiculite first treated with nitric acid and then with citric acid has higher adsorption capacity, presenting maximum adsorption capacities in column experiments: for Astrazon Red (AR), 100.8 ± 0.8 mg g^{-1} and 54 ± 1 mg g^{-1} for modified and raw material, respectively; for Methylene Blue (MB) 150 ± 4 mg g^{-1} and 55 ± 2 mg g^{-1} for modified and raw material, respectively. Materials characterization by X-ray diffraction, UV–vis-diffuse reflectance spectroscopy, diffuse reflectance infrared Fourier transform spectroscopy, X-ray fluorescence, N_2 adsorption and CEC determination, has been performed. The results suggest the existence of exchange of interlayer cations, leaching of metals from vermiculite's sheets and formation of an amorphous phase in the material. Adsorption follows pseudo 2nd order model kinetics for both dyestuffs and equilibrium occurs accordingly to Langmuir's model for AR and Freundlich's model for MB. In column systems Yan's model is the best fit. The enhanced properties of acid treated vermiculite offer new perspectives for the use of this adsorbent in wastewater treatment.

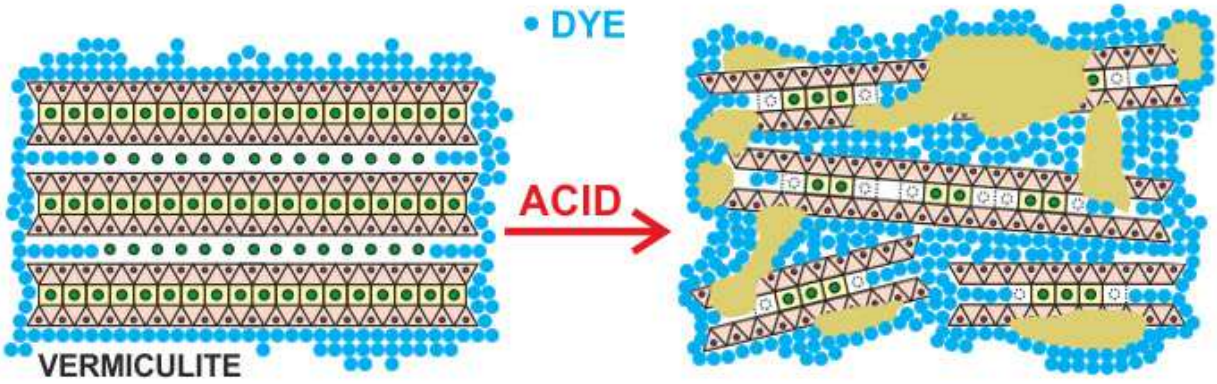

Keywords: vermiculite, acid treatment; citric acid; nitric acid; adsorption; column

2.1 Introduction

According to ‘‘Water for People Water for Life’’ United Nations World Water Development Report UNESCO the demand for fresh water has greatly increased with domestic, industrial and agricultural sector consuming 8, 22 and 70% of the available fresh water respectively, what is directly linked with the generation of large amount of wastewaters (Lehr et al., 1980; Helmer and Hespanhol, 1997). The quality of water is a very important issue, which is vital to the maintenance of a hydrological environment and to human health. In accordance to the water Framework-Directive 2000/60/CE and subsequent changes, by Decision 2455/2001/CE and Directives 2006/11/CE, 2008/32/CE, 2008/105/CE, 2009/31/CE and 2013/39/UE, emissions of priority substances should be decreased and finally eliminated. The discharge of colored effluents, namely in textile industry, is an important issue. The removal of dyestuffs from textile effluents contributes to achieve the ultimate goal of the directive, “good ecological and chemical status” for all community waters.

Colored wastewater is created as a result of the production of the dye and as well as a direct consequence of its use in the textile and related industries. It is estimated that approximately 10%–20% of dyes in the textile dying process will be lost in residual dyeing baths through incomplete exhaustion and washing operations. Therefore, hundreds tons of dyestuffs daily find their way into the environment, primarily dissolved or suspended in water (Allen et al., 2004). Effluents which are colored might be interfering with light penetrating in receiving water bodies and disturb the natural biological processes, moreover some dyestuffs might exhibit toxic effects towards microorganisms or toxic/carcinogenic effects to mammals. Most of the textile dyestuffs are poorly biodegradable, have a complex molecular structure and are difficult to remove from wastewaters by conventional treatments (Reife and Freeman, 1996; Forgacs et al., 2004; Bhatnagar and Jain, 2005).

Physico-chemical processes are often applied to treat colored wastewater, namely coagulation/flocculation. However, most of these processes present high operation costs (Mall et al., 2005). Increasing stringent legislation on the purity of water resources has created a growing interest in the cleansing of water, wastewater and polluted effluents by adsorption processes (Leitão and Serrão, 2005). Adsorption is a process in which dissolved molecules are attached to the surface of an adsorbent by physical or chemical forces (Noroozi and Sorial, 2013). It is a method that generates high-quality treated effluent. Lots of adsorbents might be recycled due to reversible nature of most of the adsorption processes (Pan et al., 2009). It is very efficient in the

treatment of industrial effluents (Vinod and Anirudhan, 2003). Layered minerals (clay minerals) seem to be interesting precursors for adsorbents preparation.

Clays are naturally occurring minerals, composed primarily of fine-grained minerals that have layer structure based on a tetrahedral (T) and an octahedral (O) phyllosilicate sheets, that may condense in either a 1:1 or 2:1 proportion to form T-O or T-O-T layer. The layers may be negatively charged, positively charged or uncharged, depending on their composition (Bergaya and Lagaly, 2006). If the layers are charged, this charge is balanced by interlayer cations. In any case the interlayer may also contain water. Interlayer cations can be exchanged, which explains that the whole group of clay minerals is characterized by very good ion-exchange properties (Chmielarz et al., 2003). Depending on the type of layered mineral, cations and also anions can be removed from wastewater. Vermiculite is a clay mineral classified as 2:1 phyllosilicate (Bailey and Chairman, 1980; Rieder et al., 1998). It is very abundant and much cheaper in comparison with other clays. Due to its remarkable features, vermiculite is widely used in agricultural, industrial and environmental applications (Duman and Tunç, 2008; Duman et al., 2015) Studies have shown that treatment of vermiculites with mineral acids resulted in an increase of specific surface area and porosity (Chmielarz et al., 2010; Santos et al., 2015), which enhances their adsorption capacity. Clay minerals modified in this way were recognized to have various applications: selective adsorbents for specific contaminants from wastewater (Polubesova et al., 2006), support to luminescent complexes (Silva et al., 2014), selective catalyst for NO reduction (Chmielarz et al., 2010) therefore application of such materials for adsorption of textile dyestuffs is expected to be also effective. Systematic study about the influence of activation with different acids is still rare and only few studies focus on treatment with nitric acid. The combination of nitric and citric acid for adsorbents preparation was not reported before in scientific literature.

2.2 Materials and Methods

2.2.1 Materials

The basic dyestuffs Methylene Blue (MB), CI 52015, supplied by Riedel de Haen and Astrazon Red FBL 200% (AR), CI 85496-37-3, supplied by Dystar, have been used. Their structural and molecular formulas are presented in Fig.2.A.6 in the Appendix. The pH values of the solutions were adjusted with hydrochloric acid and sodium hydroxide. All reagents (nitric acid 65%, sulfuric acid 96%, hydrochloric acid 36%, citric acid) were of analytical grade.

Vermiculite from South Africa in its natural form (raw vermiculite, W) and its expanded version (Ve) were kindly supplied by ROMINCO POLSKA Sp. z o.o. The adsorbent has been ground and sieved. The fraction below 355 □m was collected and used for further experiments.

Prior to the preliminary adsorption screening experiments the material was treated following the procedure given below: 250 mL of 0.4 M sulfuric (VI) acid or 0.8 M hydrochloric acid or 0.8 M nitric (V) acid were placed into round-bottom flasks equipped with reflux condenser. In each flask a weighted portion of 25 g of expanded vermiculite was added and boiled at 98 °C for two hours at constant stirring. In the next step material was repeatedly washed with water and centrifuged (5 cycles, 10 min each at 4000 rpm). The rinsing water, containing traces of heavy metals, was collected and a concentrated solution of NaOH was added drop wise to precipitate hydroxides of the metals present in the solution. After that the solution was filtrated and its pH neutralized. The sediment was disposed of as a hazardous substance. Samples were left to dry (at 50 °C) and powdered again in a grinder.

Extensive optimization of activation parameters was performed for nitric acid according to the following procedure: 250 mL of HNO_3 solutions of concentrations ranging from 0.8 M to 6.5 M, were placed in round-bottom flasks equipped with reflux condenser. Weighted portion of 25 g of starting vermiculite was placed into each flask (five solutions for raw vermiculite (W) and six solutions for expanded one (Ve)), treated for 2 h at 98 °C at constant stirring, and centrifuged (10 minutes, 4000 rpm). Half of each sediment was transferred to a beaker, stirred for 2 h in 200 mL of citric acid at room temperature (concentrations ranged from 0.01% to 10% for Ve and from 0.5% to 15% for W) and subsequently washed with water and centrifuged (5 cycles, 10 min, 4000 rpm). The remaining portions the sediment, without any further modifications, were washed in distilled water and separated in the same manner. Samples were left to dry (at 50 °C) and powdered in a grinder again.

Each sample was named according to the following rule: the first part of the name refers to the starting material (Ve or W for expanded and raw vermiculite, respectively), the second part stands for mineral acid used in activation process (N, S or Cl for nitric, sulfuric (VI), and hydrochloric acid, respectively), the third part represents the mineral acid concentration (M) and the last part, if exists, indicates the usage of citric acid (C) and its concentration (%). If treatment time was different than 2 hours it is indicated at the end of the sample name (treatment time in hours). The codes of the samples and feed composition are presented in Table A.2.4 in the Appendix.

2.2.2 Characterization

Materials have been characterized by X-ray diffraction (XRD), UV–vis-diffuse reflectance spectroscopy (UV-vis-DRS) and diffuse reflectance infrared Fourier transform spectroscopy (DRIFT) methods. The results are presented in the Appendix.

Particle size distribution was assessed using test sieves with openings varying from 45 to 355 µm. A weighted portion of vermiculite was passed through sieves, each separated fraction weighted and percentage of mass calculated (wt%). Cation exchange capacity (CEC) of the material was determined by the ammonium acetate method (Steudel, 2008). The textural parameters of the samples were determined by N_2 adsorption at −196 °C using a 3Flex v1.00 (Micromeritics) automated gas adsorption system. The samples before the analysis were degassed under vacuum at 350 °C for 24 h. The specific surface area (S_{BET}) was determined using BET (Brunauer–Emmett–Teller) model. Contribution of micropore, mesopore and external surface area was obtained from t-plot analysis. Results of textural characterization are shown in Table 2.1 and Table A.2.5 in the Appendix. Chemical composition of samples was determined using atomic absorption spectroscopy (AAS) (Analitic Jena High-Resolution Continuum Source Atomic Absorption Spectrometer, ContrAA 700) and X-ray fluorescence spectroscopy (XRF) (Ampec X-123SDD X-Ray Spectrometer) methods. Prior to AAS analysis samples were digested in hot plate method in which 100 mg of each sample was placed in 10 mL of a solution of nitric and hydrochloric acids (molar ratio 1:3) and digested at 90 °C for 5 h. The supernatant was collected, centrifuged (10 min in 4500 rpm) and analyzed to determinate content of metals (Li, Na, Mg, K, Ca, Cr, Co, Ni, Cu, Zn). The results for the most abundant elements (>0.025 wt. %) are presented in Table 2.1.

Table 2.1 Physical and chemical properties of the materials used in adsorption experiments.

Sample	S_{BET}*	CEC	Chemical composition (wt%)		
	(m^2 g^{-1})	meq/100g	AAS	XRF	
			MgO	Al_2O_3	Fe_2O_3
Ve	9	38	n.d.	10.3	10.4
VeC1%	6	50	n.d.	4.5	9.5
VeN1.2	146	57	n.d.	5.2	7.2
W	21	93	14.8	12.2	9.7
WN1.5	318	44	n.d.	5.6	7.1
WN1.5C10%	n.d.	46	n.d.	6.3	7.2
WN1.8	333	41	6.5	20.5	7.6
WN1.8C10%	338	49	6.9	4.4	6.1
WN2.0	459	28	n.d.	5.7	4.7
WN2.0C10%	449	26	n.d.	4.5	4.1
WN3.2C10%	525	11	n.d.	6	0.7
Particle size distribution (wt%)					
Fraction [µm]	**355-180**	**180-125**	**125-65**	**65-45**	**<45**
W	15	42	10	9	24
WN1.8C10%	9	11	39	17	23

n.d. – not determined *extended data is presented in Table A.2.5 in the Appendix.

Acid activation produced an increase of the specific surface area of the samples. Decrease of CEC was observed for a set of samples obtained from natural vermiculite (W) but not expanded vermiculite (Ve) (Table 2.1). In the latter case acid treatment resulted in regeneration of cation exchange properties. Content of Fe, Mg and Al was decreased due to leaching of the above mentioned metals. On the other hand, percentage content of Si which is not leached increased.

Adsorption experiments in batch and column systems were performed for both dyestuffs, MB and AR. Adsorbate concentration was measured using UV-VIS spectrophotometer (Thermo Scientific, Evolution 300) at the maximum absorbance wavelength (665 nm for MB and 531 nm for AR).

2.2.3 Batch screening experiment

Batch screening experiments were carried out in 250 mL Erlenmeyer's flasks. 100 mL of MB with concentrations of 100 mg L^{-1}, 55 mg L^{-1} and 22 mg L^{-1} was added to 100 mg or 50 mg of each sample, stirred for 2 h at room temperature (20 °C) and centrifuged (10 min in 4000 rpm) (Sartorius, Sigma 2-16). Each adsorption experiment was made in 3 repetitions.

2.2.4 Kinetic experiments

Kinetic studies were performed at room temperature (20 °C), without pH adjustment, using a magnetic stirrer (Velp, Multistirrer 15). Initial concentration of dyestuff solution was 100 mg L^{-1} and 500 mL of solution was added to 250 mg of adsorbent. The samples were collected in selected time intervals using a micropipette and immediately centrifuged (1 min in 4500 rpm) (Sartorius, Sigma 2-16) to separate the adsorbent. Then dyestuff concentration in supernatant was evaluated spectrophotometrically (Thermo Scientific, Evolution 300).

2.2.5 Equilibrium experiments

Equilibrium studies were performed in a set of 100 mL Erlenmeyer's flasks (with caps) containing 50 mL of dyestuff solution (initial concentrations of 50 or 100 mg L^{-1}) and varying amount of adsorbent (from 10 mg to 250 mg). Agitation was performed using a magnetic stirrer (Velp, Multistirrer 15) for 2 h, then the samples were taken and centrifuged (10 min in 4000 rpm) (Sartorius, Sigma 2-16). Dyestuff concentration was determined using a spectrophotometer (Thermo Scientific, Evolution 300).

2.2.6 Column experiments

Colum experiments were performed using a glass column (Omnifit), with 2.5 cm inside diameter and 15 cm height, and a peristaltic pump (Gilson, Minipuls 3).

In the case of adsorption of AR on WN1.8C10% the following conditions were used: 50 mg L^{-1} dyestuff concentration at room temperature (20 °C); 4.0 g of the sample mixed with 24.0 g of washed quartz sand and a flow rate of 0.8 mL min^{-1}. In other experiments, 0.5 g sample mixed with 24.0 g of washed quartz sand and a flow rate of dyestuff solution (50 mg L^{-1}, 20 °C) of 2 mL min^{-1} were used.

2.3 Results

2.3.1 Optimization of acid treatment

Adsorption properties after treatment of vermiculite using three mineral acids (nitric, sulfuric and hydrochloric), obtained in preliminary screening, were calculated according to Eq. (1):

$$q_{m=}\frac{(C_0-C_{eq})\,V}{m} \qquad (1)$$

where q_m is adsorption capacity (mg g^{-1}), C_0 and C_{eq} initial and final concentrations (mg L^{-1}) respectively, V volume of adsorbate (mL), m adsorbent mass (mg). Obtained results showed that vermiculite treated with nitric acid has the best adsorption properties.

Moreover, shorter treatment with this acid (2 h) gave better results than longer (24 h), for which the capacity decreased. It was also observed that additional treatment of the samples with citric acid (sample VeN2.5C10%) resulted in an increase of adsorption capacity and that boiling only in distilled water (sample VeH_2O) significantly decreases adsorption capacity compared to untreated material (Ve). Moreover, treatment only with citric acid did not result in an increase of the adsorption capacity (WC10% and VeC10%). Selected results of screening with MB at concentration of 22 mg L^{-1} in case of different acids treatment and results for MB at concentration of 55 mg L^{-1} in case of citric acid treatment are shown in Table 2.2.

Table 2.2 Results of preliminary screening of adsorption properties.

Sample	Adsorption capacity (mg g^{-1})
Ve	27 ± 4
VeH_2O	15 ± 1
VeS0.4	9.6 ± 0.7
VeCl0.8	10.0 ± 0.2
VeN0.8	11.5 ± 0.3
VeN0.8 24h	10.2 ± 0.4
VeN2.5	39 ± 1
VeN2.5C10%	42 ± 1
VeC10%	37 ± 2
W	33 ± 5
WN1.8	66 ± 2
WN1.8C10%	86 ± 2
WC10%	42 ± 2

The optimization results from subsequent application of both nitric and citric acids are shown in Figs. 2.1 and 2.2. It was found that the optimum concentration of nitric acid in the first step of treatment for expanded vermiculite was 1.2 M and for citric acid, as the secondary component, the best concentration was 1%. The same procedure was applied to optimize concentrations of the acids for raw vermiculite; the optimal nitric acid concentration was 1.5 M, however, when the sample is treated with citric acid the optimal concentration for nitric acid in the first step shifts to a higher concentration, 1.8 M (Fig. 2.3). With raw (W), nitric acid activated vermiculite four concentrations of citric acid were investigated, only 10% concentration produced a significant increase in adsorption capacity (Fig. 2.4).

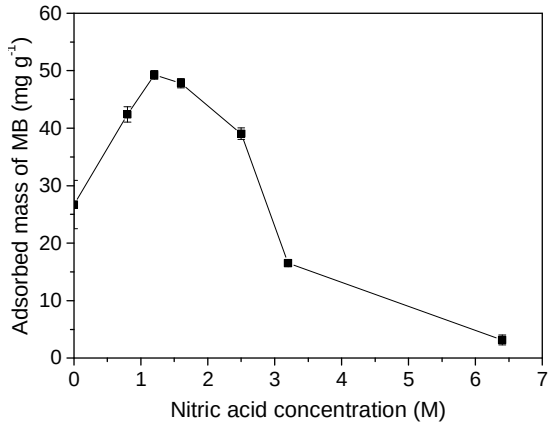

Figure 2.1 Optimization of nitric acid concentration for expanded vermiculite treatment.

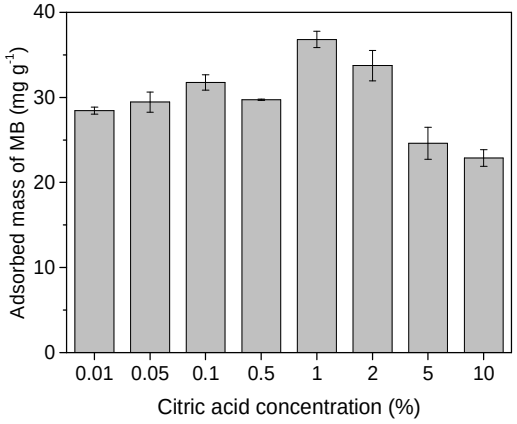

Figure 2.2 Optimization of citric acid concentration with expanded nitric acid treated vermiculite.

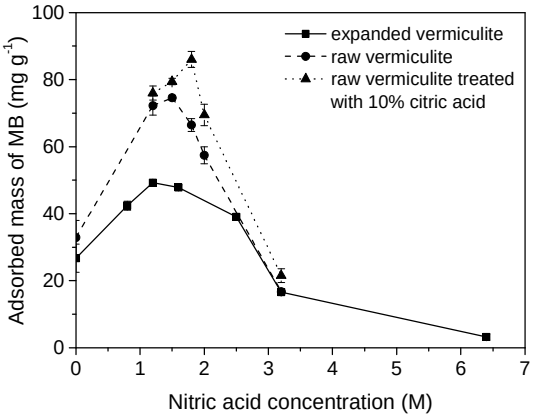

Figure 2.3 Optimization of treatment conditions for expanded and raw vermiculite.

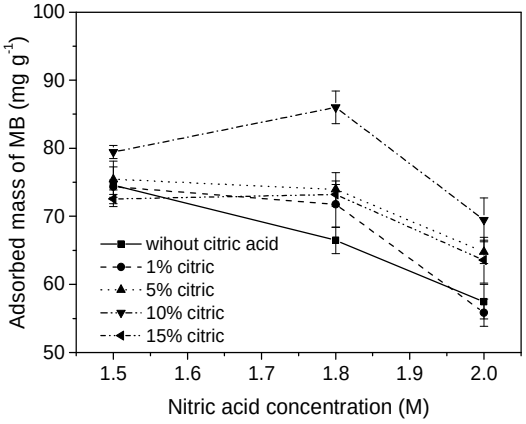

Figure 2.4 Optimization of citric acid concentration in nitric acid treated vermiculite.

The results of the optimization experiments showed a significant difference between adsorption capacities of expanded and raw vermiculite, which increases when the samples are treated with nitric acid and then with citric acid. For expanded vermiculite treated with the optimal nitric acid concentration, 1.2 M, the adsorption capacity of 49.3 ± 0.7 mg g^{-1} was achieved; for raw vermiculite treated with the optimal nitric acid concentration, 1.5 M, the adsorption capacity of 74.6 ± 0.7 mg g^{-1} was obtained; for raw vermiculite treated with 1.8 M nitric acid and additionally with 10% citric acid the capacity reached the value of 86 ± 2 mg g^{-1} (Fig. 2.3).

2.3.2 Kinetic experiments

To describe the adsorption kinetics for studied vermiculites, two models were selected. Pseudo 1st (Lagergren's model) and pseudo 2nd (Ho's model) order models were used. Pseudo 1st order model equation is (Lagergren, 1898) expressed by Eq. (2) (Ho, 2004):

$$q_t = q_e\left(1 - e^{-k_1 t}\right) \qquad (2)$$

q_e and q_t (mg g^{-1}) are adsorption capacities at equilibrium and at time t (min), respectively, and k_1 is the pseudo 1st order kinetic rate constant of the model (min^{-1}). This Eq. can describe typical diffusion dependent kinetics following the Langmuir model, as well as it may also describe kinetics of adsorption on energetically heterogeneous surfaces (Marczewski, 2010).

Pseudo 2nd order model (Ho and McKay, 1999) is expressed by Eq. (3):

$$q_t = \frac{q_e^2 k_2 t}{1 + q_e k_2 t} \qquad (3)$$

Where k_2 is the pseudo 2nd order kinetic rate constant (g mg^{-1} min^{-1}).

That formula reflects some properties of the Langmuir's rate equation if the change of the concentration during the experiment is highly significant. It may also be used for systems where heterogeneity of various origin exists (Ho and McKay, 1999).

Experimental data and fitted models (non-linear regression) are shown in Fig. 2.5 and respective parameters of the models with confidence intervals are presented in Table 2.3, where s^2 is the variance coefficient and r^2 is the determination coefficient. Equilibrium was reached approximately after 60 min. Variances and correlation coefficients were determined and compared using F and AIC tests. In all cases the pseudo 2nd order kinetic model was the best fit according to Akaike's information criterion (AIC) although Fisher's (F) test did not show statistically significant differences between the models in case of AR on WN1.8C10% and MB on W.

Comparing raw and treated material, k_2 kinetic constants are quite similar for MB and AR (0.005 ± 0.002 and 0.003 ± 0.001 g mg^{-1} min^{-1} for raw and modified vermiculite with AR, and 0.007 ± 0.002 and 0.004 ± 0.001 g mg^{-1} min^{-1} for raw and modified material with MB, respectively).

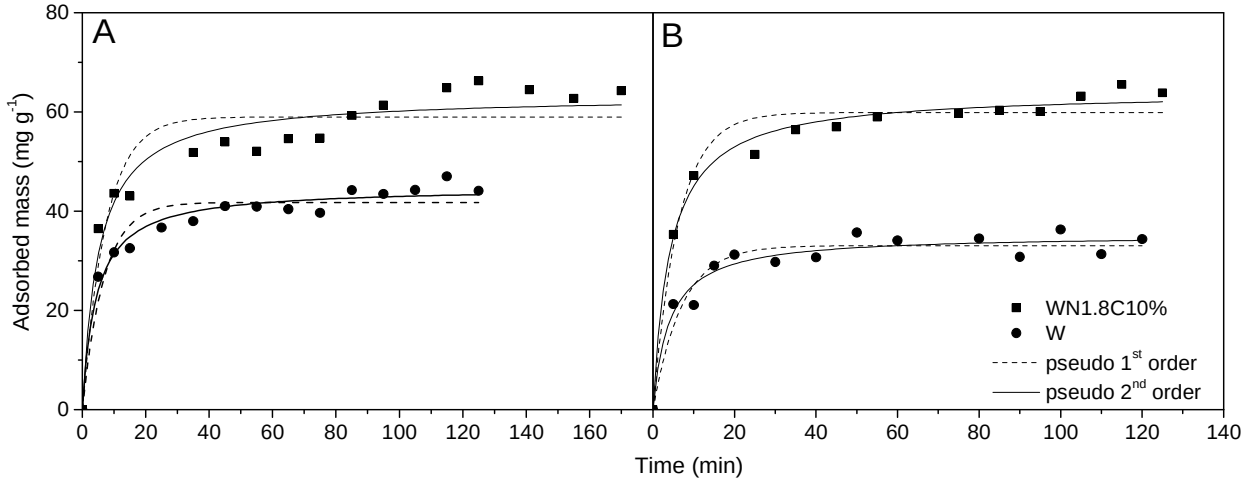

Figure 2.5 Kinetic models fitted for AR (A) and MB (B) over raw and treated vermiculite.

Table 2.3 Parameters of kinetic equations obtained in adsorption of AR and MB on raw and treated vermiculites.

Model	Parameters	AR on W	AR on WN1.8C10%	MB on W	MB on WN1.8C10%
Pseudo 1st order	k_1 (min^{-1})	0.15 ± 0.04	0.13 ± 0.06	0.14 ± 0.04	0.16 ± 0.04
	q_e (mg g^{-1})	41 ± 2	59 ± 2	33 ± 2	60 ± 4
	s^2	10.13	31.44	6.64	12.57
	r^2	0.924	0.883	0.926	0.959
Pseudo 2nd order	k_2 (g (mg min)$^{-1}$)	0.005 ± 0.002	0.003 ± 0.001	0.007 ± 0.002	0.004 ± 0.001
	q_e (mg g^{-1})	45 ± 2	63 ± 4	35 ± 2	64 ± 4
	s^2	3.76	14.93	5.09	3.89
	r^2	0.972	0.945	0.943	0.988
Model comparison	Fisher's test	pseudo 2nd	no difference	no difference	pseudo 2nd
	AIC	pseudo 2nd	pseudo 2nd	pseudo 2nd	pseudo 2nd

2.3.3 Equilibrium experiments

Two models were selected to fit the experimental data. The Langmuir's model (Langmuir, 1918) is based on several basic assumptions (Greluk and Hubicki, 2010): adsorption takes place on specific homogeneous sites within the adsorbent; one dye molecule occupies one site; the adsorbent has a limited capacity for the adsorbate; adsorbents are structurally homogeneous. The model is expressed by Eq. (4):

$$q = \frac{q_m K_L C_e}{1 + K_L C_e} \qquad (4)$$

The Freundlich's model (Freundlich, 1906) is applied to adsorption on heterogeneous surfaces with the interaction between the adsorbed molecules. The model suggests that the adsorption energy exponentially decreases as the adsorption proceeds. This model also predicts that the dye concentration on the material will increase as long as there is an increase of the dye concentration in the solution (multilayer adsorption) (Greluk and Hubicki, 2010).

Freundlich's equation is shown below:

$$q = K_F C_e^{\frac{1}{n}} \qquad (5)$$

The parameters used in the equilibrium models are: q (mg g^{-1}) is the amount of dyestuff adsorbed per unit weight of adsorbents; C_e (mg L^{-1}) is the equilibrium concentration; q_m (mg g^{-1}) and K_L (L mg^{-1}) are the Langmuir's constants related to the affinity of the binding sites and energy of adsorption, respectively; $\frac{1}{n}$ and K_F ((mg g^{-1})(L mg^{-1})$^{1/n}$) are the Freundlich's constants related to adsorption intensity and adsorption capacity, respectively.

Experimental equilibrium data and fitted models (non-linear regression) are shown in Fig. 2.6. Variances and correlation coefficients were determined and compared using F and AIC tests. Model parameters are presented in Table 2.4. According to the Fisher's test there was no difference in fitting both models to experimental data except in case of MB on WN1.8C10%, where the Freundlich's model fits better. AIC shows that the Langmuir's model fits better the experiments with AR, and the Freundlich's model fits better the experiments with MB.

The equilibrium experiments showed that the material modified with nitric and citric acid presents higher adsorption capacity for both dyestuffs (comparison based in Langmuir model) 44 ± 2 mg g^{-1} and 60 ± 4 mg g^{-1} for AR on raw and modified material, respectively, and 53 ± 5 mg g^{-1} and 66 ± 7 mg g^{-1} for MB on raw and modified material, respectively.

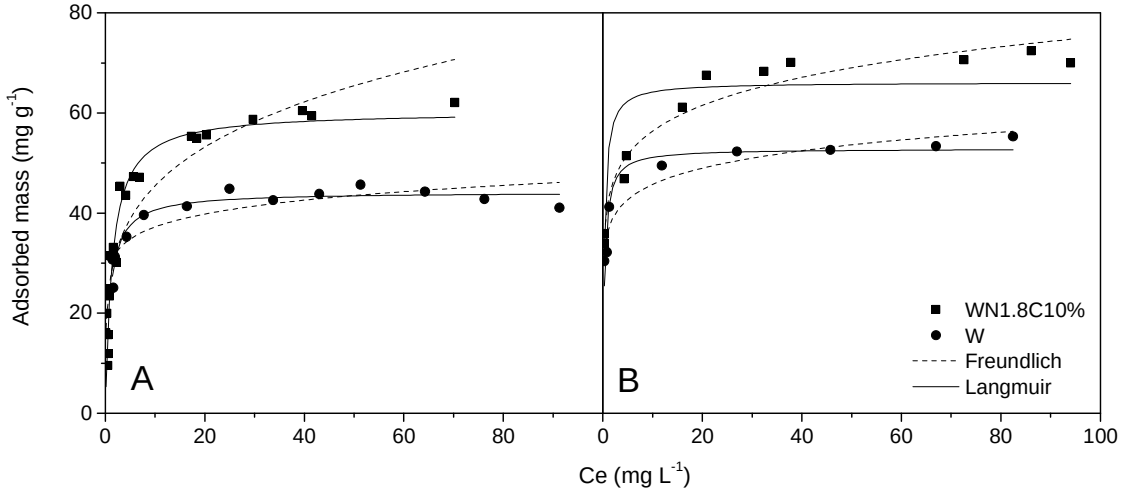

Figure 2.6 Adsorption isotherms for AR (A) and MB (B) over raw and treated vermiculite.

Table 2.4 Parameters of Langmuir's and Freundlich's isotherms obtained by fitting (non-linear) equations for adsorption of AR and MB on raw and treated vermiculites.

Model	Parameters	AR on W	AR on WN1.8C10%	MB on W	MB on WN1.8C10%
Langmuir	q_m (mg g^{-1})	44 ± 2	60 ± 4	53 ± 5	66 ± 7
	K_L (L mg^{-1})	1.1 ± 0.4	0.7 ± 0.2	3 ± 2	3 ± 2
	s^2	4	21.94	11.11	54.42
	r^2	0.903	0.928	0.888	0.739
Freundlich	K_F ((mg g^{-1})(L $mg^{-1})^{1/n}$)	30 ± 4	27 ± 4	36 ± 5	42 ± 5
	n	10 ± 4	4.4 ± 0.9	10 ± 2	8 ± 2
	s^2	10	37.84	8.37	11.43
	r^2	0.761	0.875	0.915	0.945
Model comparison	Fisher's test	no difference	no difference	no difference	Freundlich
	AIC	Langmuir	Langmuir	Freundlich	Freundlich

2.3.4 Column experiments

Three models were selected to describe the behavior of the systems, Thomas's, Yoon-Nelson's and Yan's model.

Thomas's model (Cavas et al., 2011) is one of the most widely used column performance models which allows to predict the relationship between concentration of the effluent and time (Thomas, 1944). The model is represented by Eq.(6):

$$\frac{C}{C_0} = \frac{1}{1+exp\left(\frac{k_{Th}Q_0 m}{F} - k_{Th}C_0 t\right)} \qquad (6)$$

Where, k_{Th} is Thomas's model constant (L mg^{-1} min), Q_0 is the maximum concentration of adsorbate adsorbed on solid phase (mg g^{-1}), m is the amount of adsorbent (mg), F is flow rate (mL min^{-1}) and t is the time (min), C and Co are the concentrations of feed and effluent (mg L^{-1}), respectively.

Yan's model (Yan et al., 2001) is more accurate than Thomas's. It helps to overcome some the draw-backs like serious deficiency in predicting the effluent concentration with respect to time zero. Yan's Eq. (7) was found to better describe the breakthrough curves in fixed bed columns (Lodeiro et al., 2006). The equation is as follows:

$$\frac{C}{C_0} = 1 - \frac{1}{1+\left(\frac{FC_0 t}{q_Y M}\right)^{a_Y}} \qquad (7)$$

Where, a_Y is the Yan's model constant (dimensionless), q_Y is the maximum adsorption capacity (mg g^{-1}) and M is the adsorbent mass (mg).

Yoon-Nelson model (Yoon and Nelson, 1984) is a relatively simple model, which does not require detailed data about characteristics of adsorbate, type of adsorbent or physical properties of the adsorption bed (Lodeiro et al., 2006). This model is expressed as follows, Eq.(8):

$$\frac{C}{C_0 - C} = \exp\left(k_{YN}t - \tau k_{YN}\right) \qquad (8)$$

Where, k_{YN} is the Yoon-Nelson's model constant (min^{-1}), τ is the time required for 50% adsorbate removal (min) and t is the time.

Fig. 2.7 illustrates the experimental data, and corresponding fitted models (non-linear regression). The parameters and statistics of applied models are shown in Table 2.5. All selected models fitted well to the experimental data, although the best fit was the Yan's model (AIC indicates that model as the best fit in all cases). The Fisher's test did not show any difference between models with materials used with MB. The results showed higher adsorption capacities than predicted by equilibrium isotherms. The capacities reached the value of 52 ± 1 and 98.9 ± 0.6 mg g^{-1} for AR for raw and modified material, respectively, and 53.8 ± 0.2 and 147 ± 2 mg g^{-1} for MB for raw and modified material, respectively. Similar capacities were predicted by Thomas' model 54 ± 1 and 100.4 ± 0.8 mg g^{-1} for AR with raw and modified vermiculite, respectively, and 55 ± 2 and 150 ± 4 mg g^{-1} for MB with raw and modified material, respectively. From Yoon-Nelson's model the breakthrough times for 50% removal were estimated, being 271 ± 6 and 10039 ± 71 min for AR and 274 ± 11 and 816 ± 17 min for MB, with raw vermiculite and modified material, respectively.

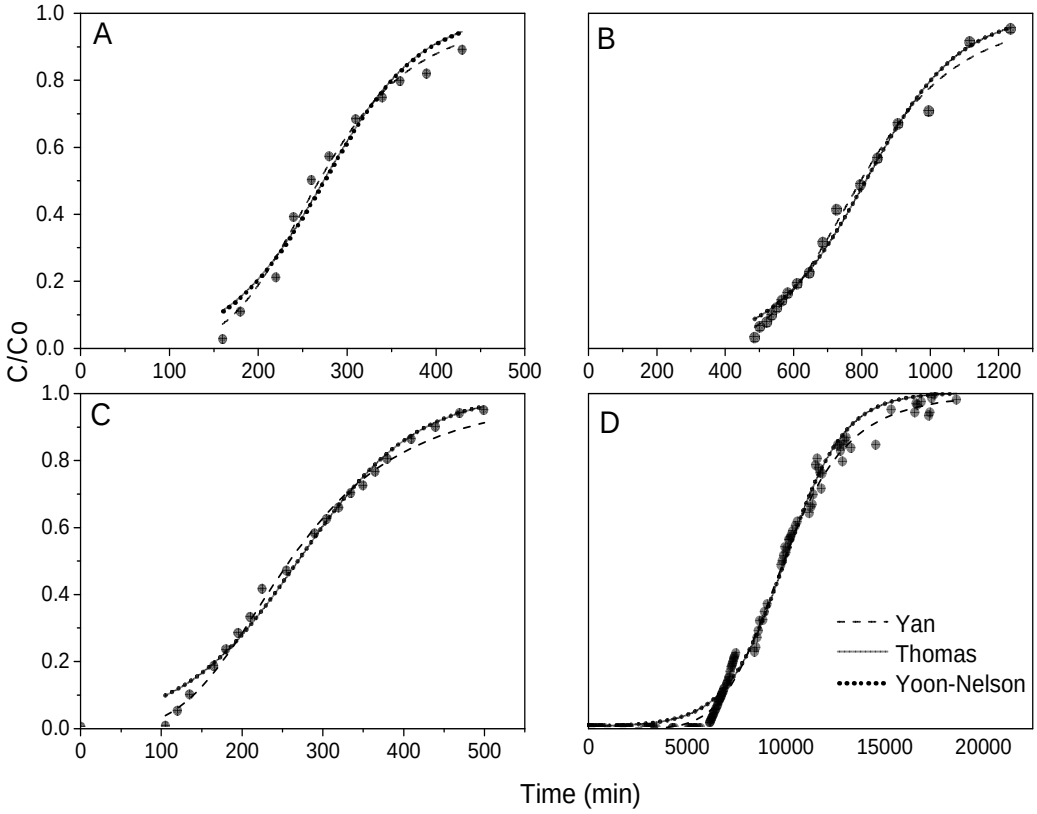

Figure 2.7 Breakthrough curves of adsorption obtained for MB on raw (A) and treated vermiculite (B) and AR on raw (C) and treated vermiculite (D).

Table 2.5 Parameters obtained in modeling of breakthrough curves for AR and MB adsorption on raw and modified vermiculites.

Model	Parameters	AR on W	AR on WN1.8C10%	MB on W	MB on WN1.8C10%
Yoon-Nelson	k_{YN} (min^{-1})	0.014 ± 0.001	0.00066 ± 0.00002	0.018 ± 0.005	0.0073 ± 0.0009
	τ_{YN} (min)	271 ± 6	10039 ± 71	274 ± 11	816 ± 17
	s^2	0.0012	0.00108	0.00346	0.00123
	r^2	0.988	0.991	0.962	0.987
Thomas	k_{TH} ($mL(mg\ min)^{-1}$)	0.27 ± 0.02	0.0133 ± 0.0006	0.37 ± 0.09	0.16 ± 0.02
	q_{TH} ($mg\ g^{-1}$)	54 ± 1	100.4 ± 0.8	55 ± 2	150 ± 4
	s^2	0.012	0.0011	0.00345	0.00123
	r^2	0.988	0.991	0.962	0.988
Yan	a_Y	3.6 ± 0.2	6.1 ± 0.2	5.0 ± 0.7	5.6 ± 0.4
	q_Y ($mg\ g^{-1}$)	52 ± 1	98.9 ± 0.6	53.8 ± 0.2	147 ± 2
	s^2	0.0006	0.0006	0.00129	0.0008
	r^2	0.994	0.995	0.986	0.992
Model comparison	Fisher's test	Yan	Yan	no difference	no difference
	AIC	Yan	Yan	Yan	Yan

2.4 Discussion

In present work it has been proven that mineral acid treatment of vermiculite followed by washing with citric acid results in a significant increase in the adsorption capacity of the material. Compared to other studies where the capacity reached a level of 11.7 mg g^{-1} after treatment in 2 M HCl (Zhao et al., 2008) the capacity has increased from 33 ± 5 to 86 ± 2 mg g^{-1} for starting material and activated one, respectively. The results presented herein provide clear evidence that both acids concentrations influence greatly the potential adsorption capacity of the material. The changes are probably due to partial leaching of Al^{3+}, Mg^{2+} and Fe^{3+} ions from the octahedral sheets and structural changes of the material as well as to exchange of interlayer ions (for example Mg^{2+}, Ca^{2+}, K^{+}, Na^{+}) (Komadel and Madejova, 2006; Santos et al., 2015). In the first step protons replace the exchangeable cations and then they attack the layers. The second effect is the leaching of Al, Mg and Fe from the octahedral and tetrahedral sheets, due to the dehydratation of the structural OH groups, what results in corrosion of the sheets, however the SiO_4 groups of the tetrahedral sheet stay almost intact (Steudel et al., 2009; Pentrák et al., 2012).

Vermiculites are characterized by high layer charge, which makes the ion exchange more difficult to proceed. Strong interaction between layers and cations results in limited diffusion of ions between layers. Acid treatment caused leaching of octahedral layers by protonating the oxygen atoms, which explains the increase of heterogeneity of OH species in the structure, and decreases layer charge facilitating ion exchange (Schoonheydt and Johnston, 2006). The changes in the material described above facilitate adsorption of dyestuff molecules. Ionic radius of hydrogen is bigger than the one of magnesium. It is known that the smaller the radius and the higher the valence, the higher is the polarizing power of a cation, therefore the magnesium cation has higher polarizing power than a proton. Ions with higher polarizing power are preferred during ion exchange (Sparks, 2003; Molina, 2013) thus it is easier for a dye molecule to exchange with H^{+}. As mentioned above, it is known that high layer charge in vermiculites leads to difficulties in ion exchange process. Decrease of CEC observed in acid treated samples (Table 2.1) could facilitate adsorption of dye molecules via ion exchange mechanism (Schoonheydt and Johnston, 2006). When concentrated acid was used, excessive leaching of layer components and loss of CEC may be compensated by increasing specific surface area and formation of adsorption centers, e.g. via interaction of dye molecules with surface hydroxyl groups in silica (Komadel and Madejova, 2006; Zhao et al., 2008; Hajjaji and El Arfaoui, 2009).

Furthermore, acid treatment results in both delamination of the structure and development of porosity. UV-Vis spectra showed that Fe species in bulk form, possibly located outside layers, which is a result of grinding and acid activation, what together with creation of amorphous silica residue increases specific surface of the material (Maqueda et al., 2007; Maqueda et al., 2009). This is a result of changes in the crystalline structure of the material (Santos et al., 2015), which becomes amorphous and more porous as well as leaching of elements from octahedral layer. Micropores and small mesopores are created and specific surface area increases with increasing acid concentration (Table 2.1). Decreased interactions between layers, as a result of delamination and formation of "house of cards" structure, may facilitate intercalation of bigger chemical species, like dyes, what might be concluded from the obtained XRD patterns for the spent materials (Fig.A.2.5).

Citrate, as other small organic anions may catalyze dissolution of minerals by formation of metal-organic complex what increases the solubility of metals such as Al (Huang and Keller, 1971; Stumm and Furrer, 1987; Welch and Ullman, 1993). Organic anions may also act as chelating agents towards the exchangeable cations balancing the charge of layers (Muir and Nesbitt, 1991; Huang and Longo, 1992; Fein, 1994). This process may open sites for H^+ attack by removing the charge balancing cations (Muir and Nesbitt, 1991). Furthermore, when amorphous phases are present in the material, strong organic complexation occurs and material can undergo fast reductive dissolution (Zinder et al., 1986; Waite, 1986.; Torn et al., 1997). Therefore, the influence of organic acids on mineral dissolution is rather an indirect than a direct effect (Kubicki et al., 1999). Citric acid is generally a weakly adsorbed ligand on clays oppositely to the strong tendency for Al and citric acid to form complexes in solution (Hue et al., 1986). Citrate tends to form multidentate ligands (Powell and Heath, 1996), as exchange of a COO^- group for H_2O at three sites may be possible in solution but not on a mineral surface (Kubicki et al., 1999). No traces of organic matter were found in the IR spectra, what can be explained by the fact that organic acid are weakly adsorbed onto vermiculite and rinsing with distilled water removes them from the structure (Kubicki et al., 1999).

Kinetic experiments showed that adsorption onto the material correlates with pseudo 2^{nd} order kinetic model based on the assumption that the rate-limiting step may be chemisorption involving valency forces through sharing or exchanging electrons between adsorbent and adsorbate. Approximately 60 min was enough in each case to reach the equilibrium and adsorption on raw material proceeds faster than on acid treated, which may be supported by the observation that in acid activated samples adsorption mechanism is different than in raw material. CEC playing significant role in determining the amount adsorbed on raw vermiculite is replaced by new adsorption

centers located on developed surface area. Although, Fisher's test did not show significant differences in the experimental data between pseudo 1st and pseudo 2nd model, AIC and correlation coefficients indicate the pseudo 2nd order model as a better fit. Although in most natural materials a pseudo 2nd order kinetics is followed (Oliveira et al., 2009), it is still unclear which properties of the adsorption system make it better represented by one specific model. However, it is accepted that for most of the adsorption period the rate is controlled by various diffusion regimes, and therefore, the kinetic models are better considered as empirical equations that do not reflect the actual chemical and physical phenomena taking place, but are useful as simple equations to predict the kinetics of adsorption systems and design adsorption units (Hameed and El-Khaiary, 2008).

The results show that adsorption of AR seems to follow the Langmuir model, while MB follows Freundlich model. Although some studies report that it may correspond to monolayer theory according to the Langmuir's assumptions (Chen et al., 1999; Mouzdahir et al., 2007; Almeida et al., 2009), other reports suggest that adsorption of MB might fulfill the multilayer model (Weng and Pan, 2006), which is compatible with the results obtained. This might be due to the fact that, on certain surfaces, MB adsorption can be followed by the formation of dimmers and trimmers on the external surface of clay and then by disaggregation and migration of the dye in between layers (Neumann et al., 2002). This fact together with assumption that MB might not lie flat on the surface but take tilted position (Hähner et al., 1996) may explain the reason of the Freundlich model being a better fit in that case. Additionally, AR has bigger molecule and higher number of resonance structures equal 7 in comparison to MB having only 3 possible configurations, which may allow the molecule to attach to the surface with different geometrical coordination and better covering of the surface with monolayer.

In column experiments the Yan's model was the best fit. The experiments proved that the material is good as adsorbent for use in column operation. Such system configuration is preferable since filtration process in not required to separate adsorbent and regeneration can be easily performed without a loss of the material. The adsorption capacity estimated for MB on raw vermiculite based on the equilibrium isotherm for the concentration of 50 mg L^{-1} (the column inlet concentration) is coincident with the one estimated by the Yan's model (Table 2.5), which was expected because use in column systems the equilibrium is established with the inlet concentration. However, the adsorption capacities obtained for the other systems in column experiments (Table 2.5) are higher than those estimated from the respective equilibrium isotherms. The same temperature and pH conditions were used in all experiments. Moreover, these parameters were monitored during the experiments and no significant changes were

observed. Therefore, it could be concluded that observed divergence might be due to the heterogeneity of raw vermiculite as a natural material.

2.5 Conclusions

Treatment of vermiculite with nitric acid followed by washing with citric acid leads to a significant increase in the adsorption capacity of the material (100.8 ± 0.8 mg g^{-1}, for modified material and 54 ± 1 mg g^{-1} for raw for AR and 150 ± 4 mg g^{-1} and 55 ± 2 mg g^{-1} for MB respectively in column experiment). During the process interlayer cations are exchanged by protons, and metals from the layers are leached causing changes in the structure of the material (increased porosity and specific surface area, decreased CEC and appearance of amorphous phase) facilitating adsorption of dyestuff molecules. Citric acid causes further leaching from the layers, removes interlayer cations and chelates metals present in solution. Acid treatment results in delamination of the structure and weaker interaction between layers. The results obtained prove a successful application of acid treated vermiculite to cationic textile dyestuffs removal resulting in a high adsorption capacity and open new perspectives for the application of this material in wastewater treatment as adsorbent.

Clay-based adsorbent production doesn't require advanced technology, neither is energy consuming nor requires expensive facilities. The developed adsorbent is recyclable, reusable and capable of decreasing dye content in wastewater to acceptable levels at affordable cost making it economically and environmentally friendly.

2.6 References

Allen, S.J., McKay, G., Porter, J.F., 2004. Adsorption isotherm models for basic dye adsorption by peat in single and binary component systems. J. Colloid Interface Sci. 280, 322-333.

Almeida, C.A.P., Debacher, N.A., Downs, A.J., Cottet, L., Mello, C.A.D., 2009. Removal of methylene blue from colored effluents by adsorption on montmorillonite clay. J. Colloid Interface Sci. 332, 46-53.

Bailey, S.W., Chairman, 1980. Summary of recommendations of AIPEA nomenclature committee on clay minerals. Am. Mineral. 65, 1-7.

Bergaya, F., Lagaly, G., 2006. General introduction: clays, clay minerals, and clay science. in: Bergaya, F., Theng, B.K.G., Lagaly, G. (Eds.). Handbook of Clay Science. Elsevier Ltd.

Bhatnagar, A., Jain, A.K., 2005. A comparative adsorption study with different industrial wastes as adsorbents for the removal of cationic dyes from water. J. Colloid Interface Sci. 281, 49-55.

Cavas, L., Karabay, Z., Alyuruk, H., Doğan, H., Demir, G.K., 2011. Thomas and artificial neural network models for the fixed-bed adsorption of methylene blue by a beach waste Posidonia oceanica (L.) dead leaves. Chem. Eng. J. 171, 557-562.

Chen, G., Pan, J., Han, B., Yan, H., 1999. Adsorption of methylene blue on montmorillonite. J. Dispersion Sci. Technol. 20, 1179-1187.

Chmielarz, L., Kowalczyk, A., Michalik, M., Dudek, B., Piwowarska, Z., Matusiewicz, A., 2010. Acid-activated vermiculites and phlogophites as catalysts for the DeNOx process. Appl. Clay Sci. 49, 156-162.

Chmielarz, L., Kuśtrowski, P., Zbroja, M., Rafalska-Łasocha, A., Dudek, B., Dziembaj, R., 2003. SCR of NO by NH3 on alumina or titania-pillared montmorillonite various modified with Cu or Co: Part I. General characterization and catalysts screening. Applied Catalysis B: Environmental 45, 103-116.

Duman, O., Tunç, S., 2008. Electrokinetic Properties of Vermiculite and Expanded Vermiculite: Effects of pH, Clay Concentration and Mono- and Multivalent Electrolytes. Sep. Sci. Technol. 43, 3755-3776.

Duman, O., Tunç, S., Polat, T.G., 2015. Determination of adsorptive properties of expanded vermiculite for the removal of C. I. Basic Red 9 from aqueous solution: Kinetic, isotherm and thermodynamic studies. Appl. Clay Sci. 109–110, 22-32.

Fein, J.B., 1994. Porosity enhancement during clastic diagenesis as a result of aqueous metal-carboxylate complexation: Experimental studies. Chem. Geol. 115, 263-279.

Forgacs, E., Cserháti, T., Oros, G., 2004. Removal of synthetic dyes from wastewaters: a review. Environ. Int. 30, 953-971.

Freundlich, H.M.F., 1906. Über die adsorption in läsungen. Z. Phys. Chem. 57, 385-470.

Greluk, M., Hubicki, Z., 2010. Kinetics, isotherm and thermodynamic studies of Reactive Black 5 removal by acid acrylic resins. Chem. Eng. J. 162, 919-926.

Hähner, G., Marti, A., Spencer, N.D., Caseri, W.R., 1996. Orientation and electronic structure of methylene blue on mica: A near edge x-ray absorption fine structure spectroscopy study. J. Chem. Phys. 104, 7749-7757.

Hajjaji, M., El Arfaoui, H., 2009. Adsorption of methylene blue and zinc ions on raw and acid-activated bentonite from Morocco. Appl. Clay Sci. 46, 418-421.

Hameed, B.H., El-Khaiary, M.I., 2008. Sorption kinetics and isotherm studies of a cationic dye using agricultural waste: broad bean peels. J. Hazard. Mater. 154, 639-648.

Helmer, R., Hespanhol, I., 1997. Water pollution control: A guide to the use of water quality management principles. E & FN Spon, London, Great Britain.

Ho, Y.S., 2004. Citation review of Lagergren kinetic rate equation on adsorption reactions. Scientometrics 59, 171-177.

Ho, Y.S., McKay, G., 1999. Pseudo-second order model for sorption processes. Process Biochem. 34, 451-465.

Huang, W.-L., Longo, J.M., 1992. The effect of organics on feldspar dissolution and the development of secondary porosity. Chem. Geol. 98, 271-292.

Huang, W.H., Keller, W.D., 1971. Dissolution of clay minerals in dilute organic acids at room temperature. Am. Mineral. 56, 1082-1095.

Hue, N.V., Craddock, G.R., Adams, F., 1986. Effect of organic acids on aluminum txicity in subsoils. Soil Science Society of America 50, 28-34.

Komadel, P., Madejova, J., 2006. Acid Activation of Clay Minerals. in: Bergaya, F., Theng, B.K.G., Lagaly, G. (Eds.). Handbook of Clay Science. Elsevier Ltd.

Kubicki, J.D., Schroeter, L.M., Itoh, M.J., Nguyen, B.N., Apitz, S.E., 1999. Attenuated total reflectance Fourier-transform infrared spectroscopy of carboxylic acids adsorbed onto mineral surfaces. Geochim. Cosmochim. Acta 63, 2709-2725.

Lagergren, S., 1898. About theory of so-called adsorption of soluble substances. Kongl. Vetenskaps Academiens Handlingar 24, 1-39.

Langmuir, I., 1918. The adsorption of gases on plane surfaces of glass, mica and platinum. J. Am. Chem. Soc. 40, 1361-1403.

Lehr, J.H., Gass, T.E., Pettyjohn, A.W., DeMarre, J., 1980. Domestic Water Treatment. McGraw-Hill Book Company, New York.

Leitão, A., Serrão, R., 2005. Adsorption of phenolic compounds from water on activated carbon: prediction of multicomponent equilibrium isotherms using single-component data. Adsorption 11, 167-179.

Lodeiro, P., Barriada, J.L., Herrero, R., Sastre de Vicente, M.E., 2006. The marine macroalga Cystoseira baccata as biosorbent for cadmium(II) and lead(II) removal: kinetic and equilibrium studies. Environ. Pollut. 142, 264-273.

Mall, I.D., Srivastava, V.C., Agarwal, N.K., Mishra, I.M., 2005. Adsorptive removal of malachite green dye from aqueous solution by bagasse fly ash and activated carbon-kinetic study and equilibrium isotherm analyses. Colloids Surf. Physicochem. Eng. Aspects 264, 17-28.

Maqueda, C., Perez-Rodriguez, J.L., Šubrt, J., Murafa, N., 2009. Study of ground and unground leached vermiculite. Appl. Clay Sci. 44, 178-184.

Maqueda, C., Romero, A.S., Morillo, E., Pérez-Rodríguez, J.L., 2007. Effect of grinding on the preparation of porous materials by acid-leached vermiculite. J. Phys. Chem. Solids 68, 1220-1224.

Marczewski, A.W., 2010. Application of mixed order rate equations to adsorption of methylene blue on mesoporous carbons. Appl. Surf. Sci. 256, 5145-5152.

Molina, F.V., 2013. Soil Colloids: Properties and Ion Binding. CRC Press.

Mouzdahir, Y.E., Elmchaouri, A., Mahboub, R., Gil, A., Korili, S.A., 2007. Adsorption of methylene blue from aqueous solutions on a moroccan clay. J. Chem. Eng. Data 52, 1621-1625.

Muir, I.J., Nesbitt, H.W., 1991. Effects of aqueous cations on the dissolution of labradorite feldspar. Geochim. Cosmochim. Acta 55, 3181-3189.

Neumann, M.G., Gessner, F., Schmitt, C.C., Sartori, R., 2002. Influence of the layer charge and clay particle size on the interactions between the cationic dye methylene blue and clays in an aqueous suspension. J. Colloid Interface Sci. 255, 254-259.

Noroozi, B., Sorial, G.A., 2013. Applicable models for multi-component adsorption of dyes: A review. J Environ Sci 25, 419-429.

Oliveira, F.D., Paula, J.H., Freitas, O.M., Figueiredo, S.A., 2009. Copper and lead removal by peanut hulls: Equilibrium and kinetic studies. Desalination 248, 931-940.

Pan, B., Pan, B., Zhang, W., Lv, L., Zhang, Q., Zheng, S., 2009. Development of polymeric and polymer-based hybrid adsorbents for pollutants removal from waters. Chem. Eng. J. 151, 19-29.

Pentrák, M., Czímerová, A., Madejová, J., Komadel, P., 2012. Changes in layer charge of clay minerals upon acid treatment as obtained from their interactions with methylene blue. Appl. Clay Sci. 55, 100-107.

Polubesova, T., Zadaka, D., Groisman, L., Nir, S., 2006. Water remediation by micelle–clay system: Case study for tetracycline and sulfonamide antibiotics. Water Res. 40, 2369-2374.

Powell, A.K., Heath, S.L., 1996. X-ray structural analysis of biologically relevant aluminium(III) complexes. Coord. Chem. Rev. 149, 59-80.

Reife, A., Freeman, H.S., 1996. Environmental Chemistry of Dyes and Pigments. John Wiley & Sons, New York.

Rieder, M., Cavazzini, G., D'yakonov, Y.S., Frank-Kamenetskii, V.A., Gottardi, G., Guggenheim, S., Koval, P.V., Müller, G., Neiva, A.M.R., Radoslovich, E.W., Robert, J.-L., Sassi, F.P., Takeda, H., Weiss, Z., Wones, D.R., 1998. Nomenclature of micas. Clays Clay Miner. 46, 586-595.

Santos, S.S.G., Silva, H.R.M., de Souza, A.G., Alves, A.P.M., da Silva Filho, E.C., Fonseca, M.G., 2015. Acid-leached mixed vermiculites obtained by treatment with nitric acid. Appl. Clay Sci. 104, 286-294.

Schoonheydt, R.A., Johnston, C.T., 2006. Surface and interface chemistry of clay minerals. in: Bergaya, F., theng, B.K.G., Lagal, G. (Eds.). Handbook of Clay Science. Elsevier.

Silva, H.R.M., Fonseca, M.G., Espinola, J.G.P., Brito, H.F., Faustino, W.M., Teotonio, E.E.S., 2014. Luminescent Eu-III Complexes Immobilized on a Vermiculite Clay Surface. Eur. J. Inorg. Chem. 2014, 1914-1921.

Sparks, D.L., 2003. Environmental Soil Chemistry. Elsevier Science.

Steudel, A., 2008. Selection Strategy and Modification of Layer Silicates for Technical Applications. Univ.-Verlag Karlsruhe.

Steudel, A., Batenburg, L.F., Fischer, H.R., Weidler, P.G., Emmerich, K., 2009. Alteration of swelling clay minerals by acid activation. Appl. Clay Sci. 44, 105-115.

Stumm, W., Furrer, G., 1987. The dissolution of oxides and alumi-num silicates: Examples of surface-coordination-controlled kinetics. in: Stumm, W. (Ed.). Aquatic Surface Chemistry. Jonh Wiley and Sons, Canada, pp. 197–219.

Thomas, H.C., 1944. Heterogeneous ion exchange in a flowing system. J. Am. Chem. Soc. 66, 1664-1666.

Torn, M.S., Trumbore, S.E., Chadwick, O.A., Vitousek, P.M., Hendricks, D.M., 1997. Mineral control of soil organic carbon storage and turnover. Nature 389, 170-173.

Vinod, V.P., Anirudhan, T.S., 2003. Adsorption Behaviour of Basic Dyes on the Humic Acid Immobilized Pillared Clay. Water, Air, Soil Pollut. 150, 193-217.

Waite, T.D., 1986. Photoredox chemistry of metal oxides. in: Davis, J.A., Hayes, K.F. (Eds.). Geochemical Processes at Mineral Surfaces. ACS Symp. Ser, pp. 426 – 445.

Welch, S.A., Ullman, W.J., 1993. The effect of organic acids on plagioclase dissolution rates and stoichiometry. Geochim. Cosmochim. Acta 57, 2725-2736.

Weng, C.-H., Pan, Y.-F., 2006. Adsorption characteristics of methylene blue from aqueous solution by sludge ash. Colloids Surf. Physicochem. Eng. Aspects 274, 154-162.

Yan, G., Viraraghavan, T., Chen, M., 2001. A new model for heavy metal removal in a biosorption column. Adsorpt. Sci. Technol. 19, 25-43.

Yoon, Y.H., Nelson, J.H., 1984. Application of gas adsorption kinetics--II. A theoretical model for respirator cartridge service life and its practical applications. Am. Ind. Hyg. Assoc. J. 45, 517-524.

Zhao, M., Tang, Z., Liu, P., 2008. Removal of methylene blue from aqueous solution with silica nano-sheets derived from vermiculite. J. Hazard. Mater. 158, 43-51.

Zinder, B., Furrer, G., Stumm, W., 1986. The coordination chemistry of weathering: II. Dissolution of Fe(III) oxides. Geochim. Cosmochim. Acta 50, 1861-1869.

Appendix A.2

A.2.1 UV–vis-diffuse reflectance spectroscopy analysis

The UV–vis-diffuse reflectance spectroscopy is a suitable technique to study solids, particularly transition metal oxides and ions in constrained environment such as MCM structure, zeolites and clay materials (Rao and Mishra, 2005). Iron is a natural component of vermiculite, its coordination and agglomeration can be determined by UV-Vis spectroscopy (Węgrzyn et al., 2013). The position of the bands depends on coordination and agglomeration of iron species (Kumar et al., 2004; Pérez-Ramírez et al., 2004). The samples were diluted with SiO_2 before the measurements in order to lower the absorbancy and to obtain the measurable range (30 mg of the sample pounded with 270 mg of SiO_2 in an agate mortar). The coordination and aggregation of iron present in the samples was measured in the range of 190–900 nm with a resolution of 2 nm using an Evolution 600 (Thermo) spectrophotometer.

The bands in the region of 300–400 nm are characteristic for small oligonuclear Fe_xO_y clusters, particles of Fe_2O_3 give characteristic bands above 400 nm (Kumar et al., 2004). In the case of mononuclear Fe^{3+} ions, iron ions in tetrahedral (band below 250 nm) and octahedral (band at 250–300 nm) coordination can be distinguished (Kumar et al., 2004; Pérez-Ramírez et al., 2004). Peak at around 220 nm in the obtained spectra is attributed to mononuclear cations in tetrahedral coordination, this peak is more intensive than the one at around 250 nm related to octahedral coordination, which suggests that tetrahedral coordination of Fe^{3+} dominates in the material (Table A.2.1). It was also noticed that the peak at 250 nm becomes broader and a bit more intensive after the acid treatment. The band assigned to small Fe_xO_y cluster (at around 360 nm) and bands above 400 nm, for bulk Fe_2O_3, decreased after the treatment (Chmielarz et al., 2010; Chmielarz et al., 2012). The results suggest that iron is located mainly in tetrahedral and octahedral sheets, the small amount of iron oxide is located outside the clay layers. Acid treatment resulted in change of iron species distribution by removal of oligonuclear and bulk Fe_2O_3 components. No significant shift in band position was observed. All the spectra are shown in Fig. A.2.1.

Table A.2.1 UV-vis-DRS band assignment for starting and treated vermiculites.

W	WN1.8	WN1.8C10%	WN2.0C10%	Assignment
nm				
220	218	220	223	Tetrahedral Fe^{3+}
248	250	250	245	Octahedral Fe^{3+}
360	370	370	374	Fe_xO_y clusters
420	418	420	420	Bulk Fe_2O_3
470	480	480	476	Bulk Fe_2O_3

(Chmielarz et al., 2010; Chmielarz et al., 2012; Węgrzyn et al., 2013)

The Figs.A.2.1 to A.2.4 below are presented in Kubelka-Munk units. This format relates sample concentration to diffuse reflectance and applies a scattering factor (Sherman Hsu, 1997).

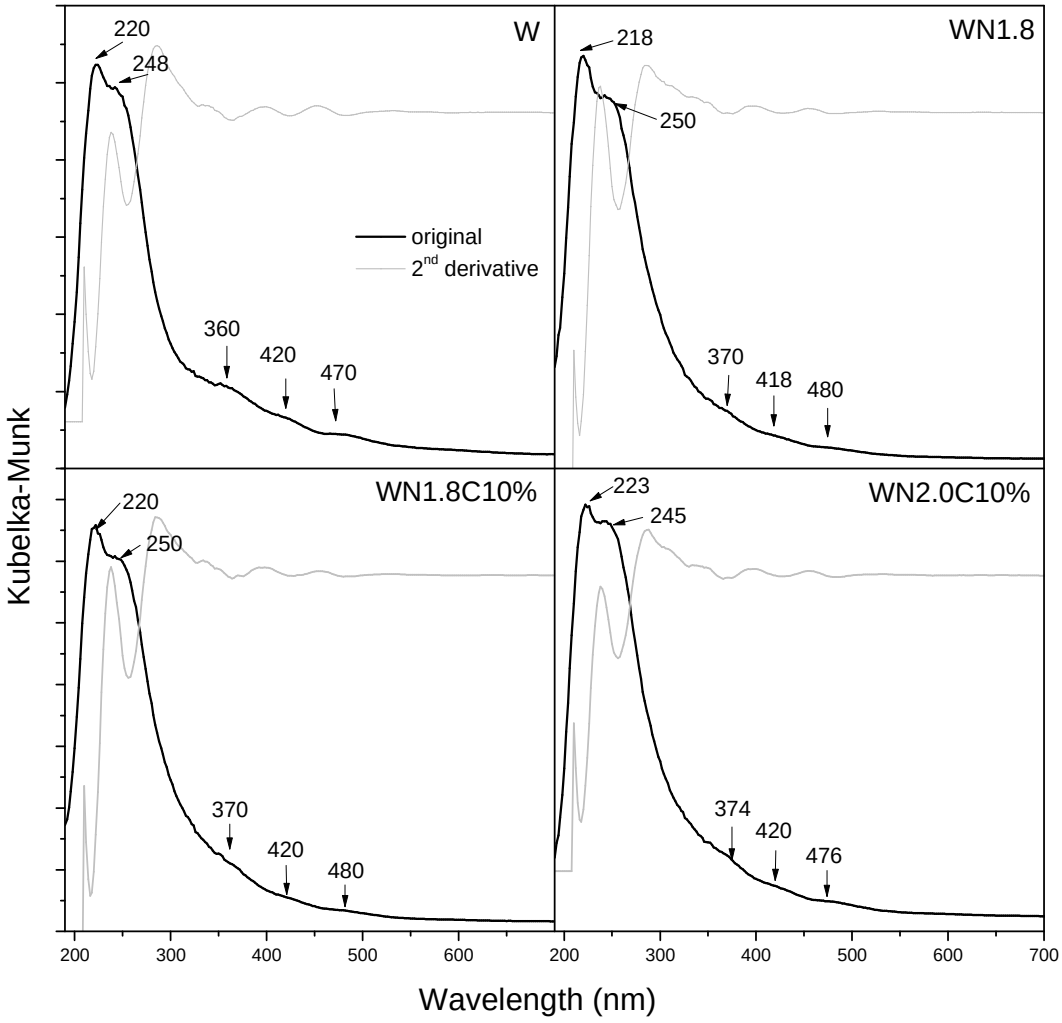

Figure A.2.1 The UV-vis-diffuse-reflectance spectra of the starting and acid treated material.

A.2.2 Diffuse reflectance infrared Fourier transform analysis

Infrared (IR) spectroscopy is a common method widely used in the analysis of clay minerals (Schroeder, 2002). The IR analysis can be done very quickly and non-destructively. One of the measurement techniques in IR is diffuse reflectance technique (DRIFT). Infrared spectra of the samples diluted with KBr in order to lower the absorbancy and to obtain the measurable range (4 mg of sample crushed with 96 mg of KBr in a mortar) were recorded using diffused reflectance technique (Nicolet 6700 FT-IR, Thermo Scientific). In both spectral techniques (UV-vis-DRS and DRIFT) second derivative of original spectra was used to distinguish several overlapping peaks.

One band at 3368 cm-1 dominates in the starting material (Table A.2.2) and upon acid treatment it becomes broader and shifts to 3411 cm-1, which together with appearance of two additional bands (3607 cm-1 and 3614 cm-1) suggests higher heterogeneity of –OH species (Węgrzyn et al., 2013). The band at 3368 cm-1 corresponding to OH stretching in weakly bonded water molecules (Chmielarz et al., 2012) becomes broader and shifts to 3400 cm-1. Bending deformation of adsorbed and interlayer water resulted in the formation of the bands between 1630 and 1640 cm-1.

Several other bands, which are ascribed to vibrations of aluminosilicate structure, appear. The dominant band for the raw material (990 cm^{-1}) is relatively narrow and becomes broad in the treated samples, the band of stretching of Si-O (1090 cm^{-1}) (Madejová and Komadel, 2001) disappears. Other bands attributed to vibrations of Si-O-Si in amorphous silica (1200-1225 cm^{-1}) appear in treated material, along with bands in the range of 1000-1024 cm^{-1}, ascribed to Si-O vibrations, which should indicate higher heterogeneity and amorphousness of the lattice structure (Ritz et al., 2014). Several studies (Komadel et al., 1996; Madejová et al., 1998; Steudel et al., 2009) postulated that changes in the Si-O stretching region are due to the partial transformation of the tetrahedral sublayers into a three dimensional framework of amorphous silica. Bands with lower intensity (915-770 cm^{-1}) result from bending and deformation vibrations in octahedral layer (e.g. Al-OH, Al-Mg-OH) (Liu et al., 2011). All the spectra are shown in Figs. A.2.2 and A.2.3.

Table A.2.2 Band assignment in DRIFT spectra in starting and treated vermiculites.

W	WN1.8	WN1.8C10%	WN2.0C10%	Assignment
		cm^{-1}		
3674	3666	3666	3675	Si-Mg_3OH
3623	3634	3638	3632	OH stretching of structural hydroxyl groups (terminal OH groups in Al≡OH)
-	-	3607	3614	OH stretching of structural hydroxyl groups
3555	3548	3548	3555	OH stretching of water coordinated to Al, Mg
3368	-	-	-	OH stretching in weakly bonded water molecules
3243	3243	3220	3240	shoulder of OH stretching of structural hydroxyl groups
1640	1633	1633	1632	Bending of water molecules in hydration layers of soil phyllosilicates
-	1385	1387	-	OH in water that is retained by the adsorbent
-	1224	1203	1223	Si-O-Si In amorphus silica
1090	-	-	-	Si-O stretching
-	1132	1144	1187	Si–O stretching vibration (out-of-plane)
1042	1047	1052	1054	Si–O stretching vibration (in-plane)
-	1024	1003	1008	Si–O stretching vibration (in-plane)
990	960	973	973	Si–O stretching vibration
915	902	901	904	AlAlOH bending
876	868	870	868	AlFeOH bending
808	817	814	817	Al-O-Si In amorphous silica
790	771	786	786	Si–O–Al vibration

(Vicente-Rodríguez et al., 1996; Madejová and Komadel, 2001; Spaccini et al., 2001; Madejova, 2003; Petit, 2006; Steudel et al., 2009; Chmielarz et al., 2010; Liu et al., 2011)

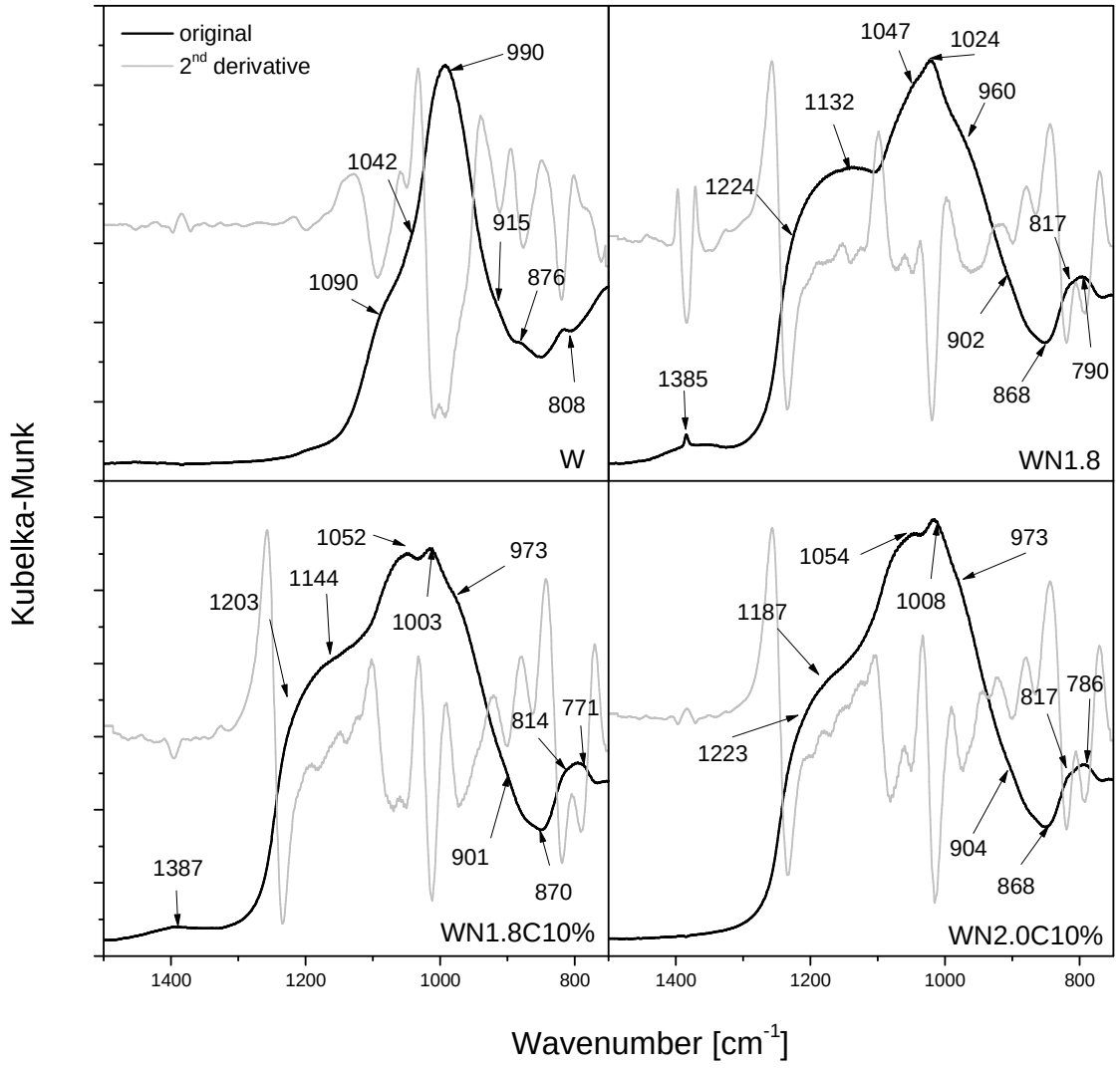

Figure A.2.2 Diffuse Reflectance Infrared Fourier Transform spectra of the starting and acid modified vermiculite.

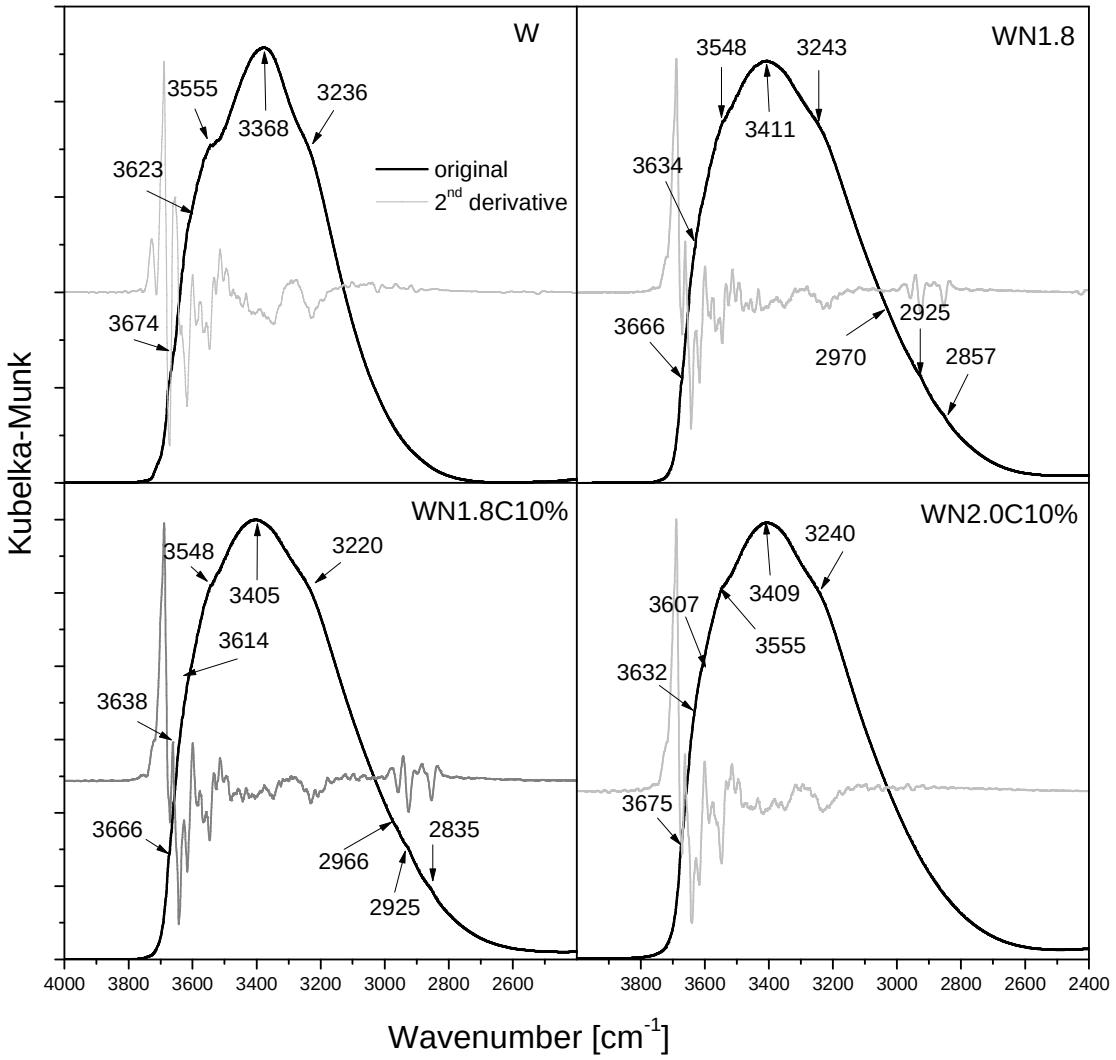

Figure A.2.3 Diffuse Reflectance Infrared Fourier Transform spectra of the starting and acid modified vermiculite.

A.2.3 X-ray diffraction analysis

X-ray powder diffraction (XRD) is an analytical technique used for phase identification of a crystalline material and it is useful in providing information on unit cell dimension and atomic structure of crystalline substances. The structure of the materials was studied with X-ray powder diffractometer (Bruker, D2 PHASER) equipped with CuKα radiation source. The samples were measured without any previous preparation.

In the diffractogram of the samples (Table A.2.3) several reflections were found at: 5.61 °2θ (d=1.58 nm), 6.22 °2θ (d_{002}=1.43 nm), 7.06 °2θ (d_{004}=1.25 nm), 9.45 °2θ (d=0.94 nm). The basal spacing of 1.43 nm is characteristic for magnesium in hydrated forms of vermiculite and the basal spacing around 1.25 nm might be attributed to partially dehydrated magnesium cations present in the interlayer space (Chmielarz et al., 2012). The reflection at 12.36 °2θ (0.72 nm) corresponds to the presence of interstratification between swelling and non-swelling forms (Walker, 1961) and reflection at 24.84 °2θ

(d=0.36 nm) might be attributed to quartz impurities in the sample (Chmielarz et al., 2012). No reflection at about 8.60 °2θ was noticed, what indicates the absence of potassium cation in the sample. The origin of the reflection in raw vermiculite at 5.61 °2θ (1.58 nm), 9.45 °2θ (0.94 nm) and 28.64 °2θ (0.31 nm) in all the samples remains unclear. All diffraction patterns are shown in the Fig.A.2.4.

Table A.2.3 Identification of peaks in XRD patterns of raw and treated vermiculites.

W		WN1.8 WN1.8C10 %		Assignment
°2θ	nm	°2θ	nm	
5.61	1.6	-	-	-
6.22 (002)	1.4	6.3	1.4	Hydrated Mg^{2+}
7.06	1.3	-	-	Presence of partially dehydrated magnesium interlayer cation
9.45	0.9	9.4	0.9	-
12.36	0.7	12.3	0.7	interstratification between contracting and non-contracting forms
18.57 (006)	0.5	18.6	0.5	Low amount of octahedral iron in interlayer space
24.84	0.4	24.9	0.4	Quartz impurities
28.64	0.3	28.6	0.3	-

(Walker, 1961; Marcos et al., 2009; Mouzdahir et al., 2009; Chmielarz et al., 2012; Węgrzyn et al., 2013; Santos et al., 2015)

Acid treatment significantly decreased the intensity of basal reflections of the samples. This is probably related to the partial transformation of the ordered structure of clay (parallel ordering of clay layers) into delaminated structure (non-parallel ordering of clay layers – “house of card” structure) due to deposition and redeposition of the components leached from the clay layers outside the layers. Formation of the delaminated structure is possible when cationic species of various sizes (e.g. clustered species, various metal cations) are deposited into the interlayer space of clay (Chmielarz et al., 2012). Fig. A.2.5 presents changes in interlayer distances for spent adsorbents. It may be concluded, that partial intercalation of dyes might occur for acid treated sample.

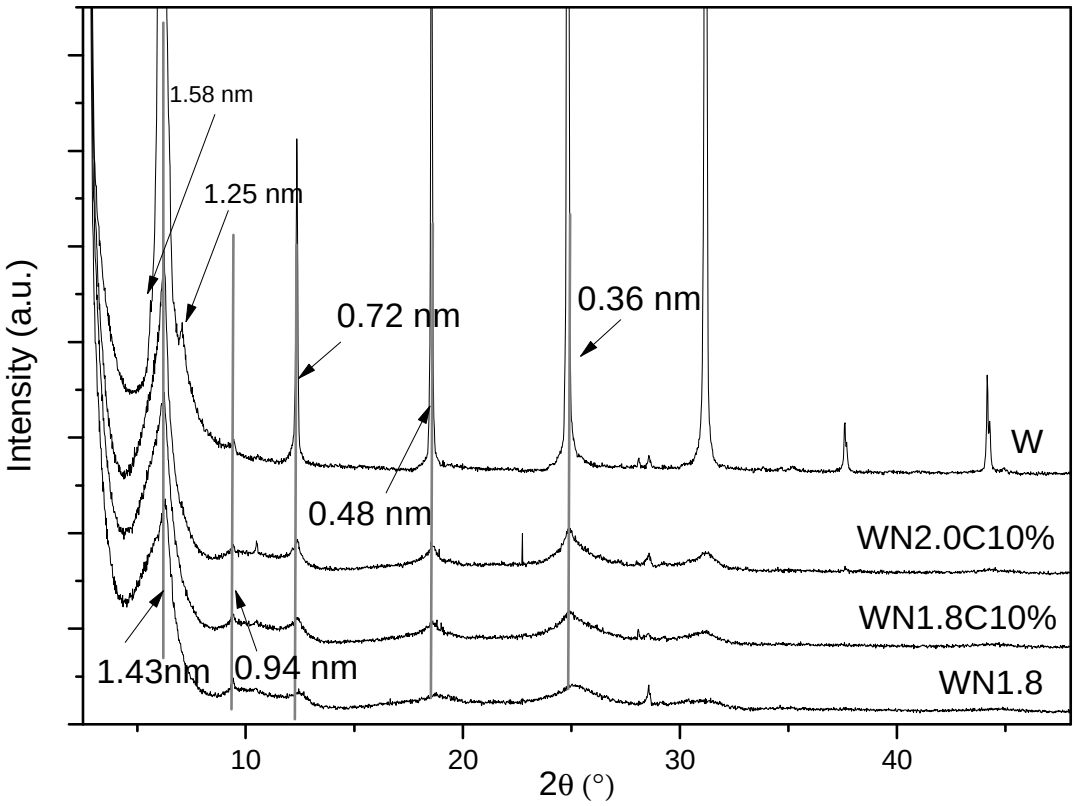

Figure A.2.4 Phase composition of raw and treated vermiculites.

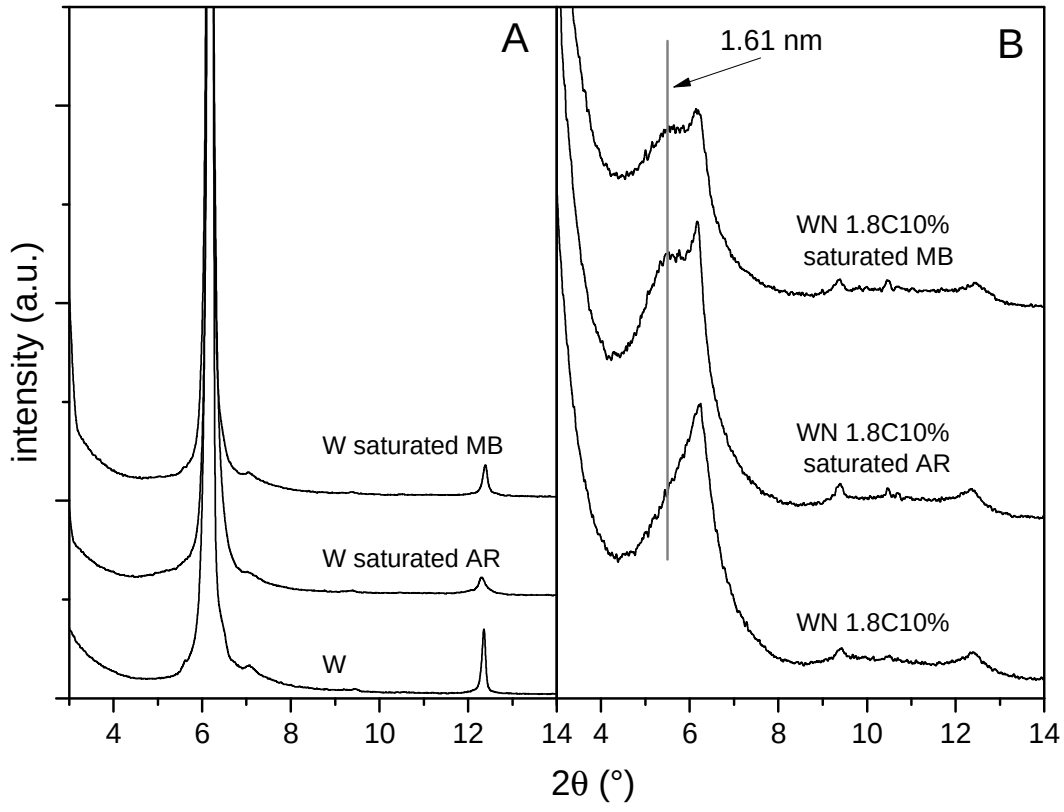

Figure A.2.5 Phase composition of raw (A) and acid activated vermiculite (B) saturated with MB and AR.

Table A.2.4 Codes of the samples and feed composition for the samples activation at 98 °C.

Sample	Starting vermiculite	treatment step 1		treatment step 2	
		solution	time [h]	solution	time [h]
W	raw	x	x	x	x
WN1.8		1.8 M HNO_3	2	10% (m/v) citric acid	2
WN1.8C10%					
WN2.0C10%		2.0 M HNO_3			
WC10%		10% (m/v) citric acid			
VeN0.8	expanded	0.8 M HNO_3		x	x
VeS0.4		0.4 H_2SO_4			
VeCl0.8		0.8 M HCl			
VeN2.5		2.5 M HNO_3			
VeN2.5C		2.5 M HNO_3		10% (m/v) citric acid	2
VeH_20		distilled water		x	x
VeN0.8 24h		0.8 M HNO_3	24		

Table A.2.5 Textural parameters of starting and acid modified vermiculites.

Sample	S_{BET}	S_{ext}	S_{meso}	S_{micro}	V_{total}
	[m^2g^{-1}]	[m^2g^{-1}]	[m^2g^{-1}]	[m^2g^{-1}]	[cm^3g^{-1}]
Ve	9	8	1	0	0.01
VeC1%	6	5	1	0	0.02
VeN1.2	146	11	108	27	0.12
W	21	12	5	4	0.02
WN1.5	318	20	248	50	0.21
WN1.5C10%	n.d.	n.d.	n.d.	n.d.	n.d.
WN1.8	333	23	268	42	0.21
WN1.8C10%	338	24	279	35	0.22
WN2.0	459	27	371	61	0.32
WN2.0C10%	449	24	369	56	0.3
WN3.2C10%	525	31	439	55	0.38

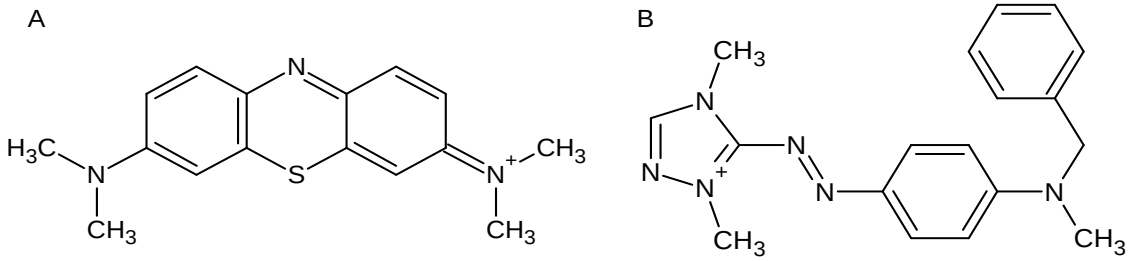

Figure A.2.6 Structural and molecular formulas of MB (A) and AR (B) cations.

A.2.4 References

Chmielarz, L., Kowalczyk, A., Michalik, M., Dudek, B., Piwowarska, Z., Matusiewicz, A., 2010. Acid-activated vermiculites and phlogophites as catalysts for the DeNOx process. Appl. Clay Sci. 49, 156-162.

Chmielarz, L., Wojciechowska, M., Rutkowska, M., Adamski, A., Węgrzyn, A., Kowalczyk, A., Dudek, B., Boroń, P., Michalik, M., Matusiewicz, A., 2012. Acid-activated vermiculites as catalysts of the DeNOx process. Catal. Today 191, 25-31.

Komadel, P., Madejová, J., Janek, M., Gates, W.P., Kirkpatrick, R.J., Stucki, J.W., 1996. Dissolution of hectorite in inorganic acids. Clays Clay Miner. 44, 228-236.

Kumar, M.S., Schwidder, M., Grünert, W., Brückner, A., 2004. On the nature of different iron sites and their catalytic role in Fe-ZSM-5 DeNOx catalysts: new insights by a combined EPR and UV/VIS spectroscopic approach. J. Catal. 227, 384-397.

Liu, D., Yuan, P., Liu, H., Cai, J., Qin, Z., Tan, D., Zhou, Q., He, H., Zhu, J., 2011. Influence of heating on the solid acidity of montmorillonite: A combined study by DRIFT and Hammett indicators. Appl. Clay Sci. 52, 358-363.

Madejova, J., 2003. FTIR techniques in clay mineral studies. Vib. Spectrosc. 31, 1-10.

Madejová, J., Bujdák, J., Janek, M., Komadel, P., 1998. Comparative FT-IR study of structural modifications during acid treatment of dioctahedral smectites and hectorite. Spectrochimica Acta Part A: Molecular and Biomolecular Spectroscopy 54, 1397-1406.

Madejová, J., Komadel, P., 2001. Baseline studies of the clay minerals society source clays: infrared methods. Clays Clay Miner. 49, 410-432.

Marcos, C., Arango, Y.C., Rodriguez, I., 2009. X-ray diffraction studies of the thermal behaviour of commercial vermiculites. Appl. Clay Sci. 42, 368-378.

Mouzdahir, Y.E., Elmchaouri, A., Mahboub, R., Gil, A., Korili, S.A., 2009. Synthesis of nano-layered vermiculite of low density by thermal treatment. Powder Technol. 189, 2-5.

Pérez-Ramírez, J., Santhosh Kumar, M., Brückner, A., 2004. Reduction of N2O with CO over FeMFI zeolites: influence of the preparation method on the iron species and catalytic behavior. J. Catal. 223, 13-27.

Petit, S., 2006. Fourier transform infrared spectroscopy. in: Bergaya, F., Theng, B.K.G., Lagaly, G. (Eds.). Handbook of Clay Science. Elsevier Ltd, pp. 909-918.

Rao, G.R., Mishra, B.G., 2005. A comparative UV–vis-diffuse reflectance study on the location and interaction of cerium ions in Al- and Zr-pillared montmorillonite clays. Mater. Chem. Phys. 89, 110-115.

Ritz, M., Zdrálková, J., Valášková, M., 2014. Vibrational spectroscopy of acid treated vermiculites. Vib. Spectrosc. 70, 63-69.

Santos, S.S.G., Silva, H.R.M., de Souza, A.G., Alves, A.P.M., da Silva Filho, E.C., Fonseca, M.G., 2015. Acid-leached mixed vermiculites obtained by treatment with nitric acid. Appl. Clay Sci. 104, 286-294.

Schroeder, P.A., 2002. Infrared Spectroscopy in clay science. Teaching Clay Science CMS Workshop Lectures, vol. 11. The Clay Mineral Society, Colorado, pp. 181-206.

Sherman Hsu, C.-P., 1997. Infrared Spectroscopy. in: Settle, F.A. (Ed.). Handbook of Instrumental Techniques for Analytical Chemistry. y Prentice Hall PTR (ECS Professional), Virginia, pp. 247-283.

Spaccini, R., Piccolo, A., Haberhauer, G., Stemmer, M., Gerzabek, M.H., 2001. Decomposition of maize straw in three European soils as revealed by DRIFT spectra of soil particle fractions. Geoderma 99, 245-260.

Steudel, A., Batenburg, L.F., Fischer, H.R., Weidler, P.G., Emmerich, K., 2009. Alteration of swelling clay minerals by acid activation. Appl. Clay Sci. 44, 105-115.

Vicente-Rodríguez, M.A., Suarez, M., Bañares-Muñoz, M.A., de Dios Lopez-Gonzalez, J., 1996. Comparative FT-IR study of the removal of octahedral cations and structural modifications during acid treatment of several silicates. Spectrochimica Acta Part A: Molecular and Biomolecular Spectroscopy 52, 1685-1694.

Walker, G.F., 1961. Vermiculite minerals. in: Brown, G. (Ed.). The X-ray Identification and Crystal Structures of Clay Minerals. Mineralogical Society of Great Britain Monograph, Great Britain, pp. 297-324.

Węgrzyn, A., Chmielarz, L., Zjeżdżałka, P., Jabłońska, M., Kowalczyk, A., Żelazny, A., Vázquez Sulleiro, M., Michalik, M., 2013. Vermiculite-based catalysts for oxidation of organic pollutants in water and wastewater. Acta, Geodyn. Geomater. 10, 341-352.

CHAPTER 3

Acid-base treatment of vermiculite

Chemosphere 173 (2017) 107–115

Contents lists available at ScienceDirect

Chemosphere

journal homepage: www.elsevier.com/locate/chemosphere

Acid-base treated vermiculite as high performance adsorbent: Insights into the mechanism of cationic dyes adsorption, regeneration, recyclability and stability studies

Wojciech Stawiński[a], Agnieszka Węgrzyn[b,*], Tomasz Dańko[b], Olga Freitas[a], Sónia Figueiredo[a], Lucjan Chmielarz[b]

[a] *REQUIMTE, LAQV, Instituto Superior de Engenharia do Porto, Instituto Politécnico do Porto, Rua Dr. António Bernardino de Almeida 431, 4200-072 Porto, Portugal*
stawor@gmail.com; omf@isep.ipp.pt; saf@isep.ipp.pt

[b] *Faculty of Chemistry, Jagiellonian University, ul. Ingardena 3, 30-060 Kraków, Poland*
wegrzyn@chemia.uj.edu.pl; tom_91@o2.pl; chmielar@chemia.uj.edu.pl

Abstract

Additional treatment with NaOH of acid activated vermiculite results in even higher increase in the adsorption capacity in comparison to samples modified only in acidic solution (first step of activation) with respect to raw material. Optimization of treatment conditions and adsorption capacity for two cationic dyes (methylene blue (MB) and astrazon red (AR)), also as binary mixture, was evaluated. The capacity, based on column studies, increased from 48 ± 2 to 203 ± 4 mg g^{-1} in the case of methylene blue and from 51 ± 1 to 127 ± 2 mg g^{-1} in the case of astrazon red on starting and acid-base treated material, respectively. It was shown that adsorption mechanism changes for both cationic dyes after NaOH treatment and it results in decrease of adsorption rate. In binary mixtures methylene blue is bound stronger by adsorbent and astrazon red may be removed in initial stage of adsorption. Extensive studies on desorption/regeneration process proved high efficiency in recyclable use of all materials. Although cation exchange capacity decreases due to acid treatment, after base treatment exchange properties are used more efficiently. On the other hand, increased specific surface area has less significant contribution into the adsorption potential of studied materials. Obtained adsorbents worked efficiently in 7 adsorption-regeneration cycles and loss of adsorption capacity was observed only in two first cycles.

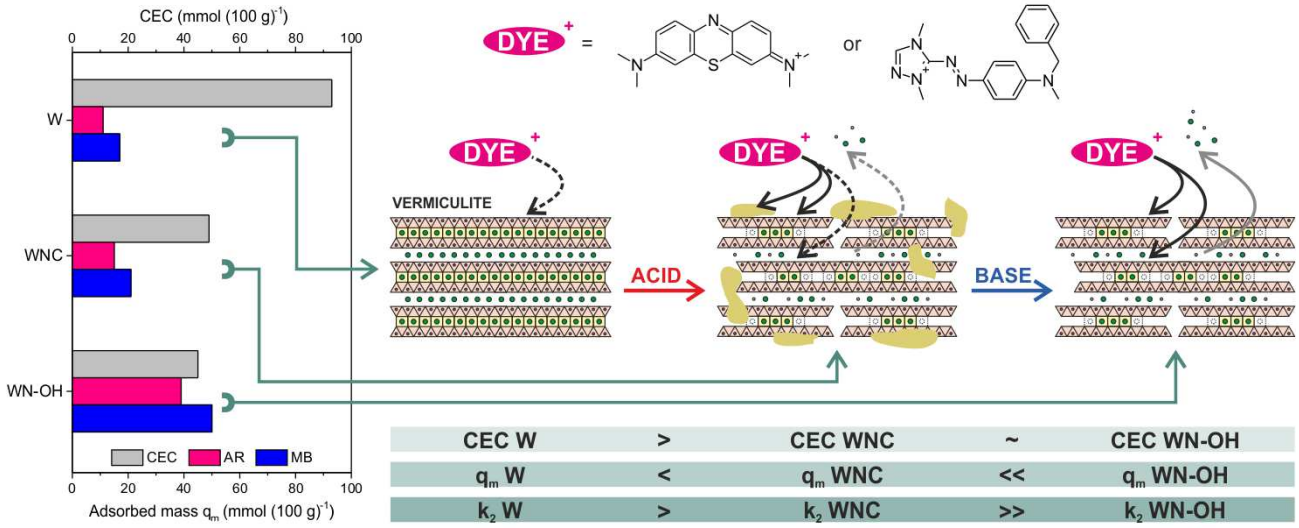

Keywords: acid treatment; base treatment; vermiculite; cationic dyes; adsorption; regeneration

3.1 Introduction

Developing industry and increasing human population contribute greatly to deterioration of water quality. The European Union took step in keeping water in good condition by adopting Water Framework Directive 2000/60/CE (with subsequent changes by 2455/2001/CE, 2006/11/CE, 2008/32/CE, 2008/105/CE, 2009/31/CE, 2013/39/UE and 2014/101/UE), and Industrial Emissions Directive (2010/75/EU). Those documents determined priority substances to be eliminated from wastewaters and defined the obligations to be met by industrial activities, to avoid pollution, take preventive measures against it, and reduce, recycle and dispose of waste in the manner that generates less pollution. Chemical methods need the use of excess chemicals. In chemical methods, some toxic byproducts may occur (Duman et al., 2015a).

Dyes are common in effluents discharged by various industries such as paper, plastics, food, cosmetics, and textile (Rozada et al., 2003; Angın et al., 2013). They usually have complex molecular structure, some of them may have toxic or carcinogenic effects on animals, they are hard to degrade biologically and change the light penetration in receiving waters disturbing natural biological processes. Moreover, they are one of the most problematic and difficult types of pollutant to be treated by conventional methods (Reife and Freeman, 1996; Forgacs et al., 2004; Bhatnagar and Jain, 2005).

Coagulation/flocculation methods are often applied to treat colored waters but their operation cost is high due to chemicals addition and sludge management (Mall et al., 2005). In the need of efficient and sustainable methods adsorption has been getting more interest in the application to wastewaters treatment (Leitão and Serrão, 2005). It is considered as one of the best wastewater treatment methods due to its universal nature, ease of operation, ability to remove soluble and insoluble organic pollutants, high removal capacity and possibility to recycle and reuse many of adsorbents (Pan et al., 2009; Ali et al., 2012). One of the most commonly used adsorbents is activated carbon, having granular, powder, fiber and cloth form, due to its high specific surface area and high adsorption capacity for pollutants (Duman and Ayranci, 2006; Ayranci and Duman, 2009; Duman and Ayranci, 2010). However it is relatively expensive what makes it unattractive for discoloration purposes (Rozada et al., 2003). It is necessary to use an adsorbent that is freely available, inexpensive and non-hazardous in nature (Ali et al., 2012). Clays show good perspectives in this field.

Clays are minerals that have layer structure based on a tetrahedral (T) and an octahedral (O) phyllosilicate sheets, that may condense in either a 1:1 or 2:1 proportion to form T-O or T-O-T layer (Bergaya and Lagaly, 2006). If a charge is present on the sheets it is balanced by an ion located in between the sheets. These charge-balancing

ions can be exchanged resulting in very good ion-exchange properties of the material (Chmielarz et al., 2003). Vermiculite is a clay mineral classified as 2:1 phyllosilicate (Bailey and Chairman, 1980; Rieder et al., 1998). Vermiculite is very abundant and much cheaper compared with other clays. Owing to its remarkable features, vermiculite is commonly used in agricultural, industrial and environmental applications (Duman and Tunç, 2008; Duman et al., 2015b). It can be a subject to modifications in order to enhance its efficiency for the removal of pollutants from wastewaters (Ali et al., 2012).

Mechanism of adsorption on a clay particle surface can take place via three mechanisms involving formation of complexes with charged surface functional groups: inner-sphere surface complexes (mostly ionic and covalent bonding), outer-sphere surface complexes and formation of diffuse-ion swarm, when the cation screens a delocalized surface charge. The last two mechanisms involve mostly electrostatic bonding. Ions adsorbed by outer-sphere complexes and diffuse-ion swarm are readily exchangeable and can be easily leached from the clay (Sposito, 2008). Hence, the mechanism of adsorption determinates also possibility for regeneration and recycling of an adsorbent.

Acid activation of vermiculite is a common method of treatment of this clay however, to the best of authors' knowledge, little is known about complex modifications of already treated materials. The aim of this research was to investigate if any additional step to acid activation of vermiculite might result in further increase in the maximum adsorption capacity of the material. As shown in this work, when that modification is followed by treatment with a base it results in even more significant increase in the adsorption capacity compared to only acid treatment. The base treatment enhances the physicochemical characteristics of the material. The extensive adsorption experiments in batch and continuous flow (fixed bed column), as well as regeneration studies demonstrate the high performance of these materials, which offer interesting possibilities for industrial application as economical and sustainable adsorbent.

3.2 Experimental section

3.2.1 Materials

Vermiculite from South Africa (raw vermiculite, W) and its expanded derivative (Ve, obtained by rapid heating up to 1000°C) were kindly supplied by ROMINCO POLSKA Sp. z o.o. Samples of acid activated vermiculite (WNC) were prepared by treating the raw material (W) for 2 h in 1.8 M nitric acid at 98 °C and then during 1 h in 10% citric acid solution at room temperature (24°C) following the procedure described in

previous study (Stawiński et al., 2016). Experiments were conducted in Erlenmeyer flasks with caps or a reflux condenser in case where elevated temperature was used.

The basic dyestuffs methylene blue (MB), CI 52015, supplied by Riedel de Haen and astrazon red FBL 200% (AR), CI 85496-37-3, supplied by Dystar, were used for adsorption experiments (Fig. A.3.1 in the Supplementary Material).

In the first step 1 g of WNC and W were mixed with 10 mL of 1 M NaOH and stirred for 2 h and 24 h, after that, samples were washed, centrifuged (5 cycles of 10 min at 4000 rpm, Sartorius, Sigma 2-16) and left to dry. In the next step, in order to obtain base treated samples (WN-OH), weighted portions of 1 g of WNC were mixed with 10 mL of NaOH solutions of different concentrations (0.5 M, 1 M, 1.5 M and 2 M, respectively), stirred during 2 h at room temperature, washed and left to dry. In the last step, four samples of 1 g of WNC were placed in flasks with 10 mL of 0.5 M NaOH and stirred during 2 h and 4 h at different temperatures (room temperature (24°C) and 98°C), a reflux condenser was used where elevated temperature was applied.

3.2.2 Methods

The structure of the materials was studied with X-ray powder diffractometer (Bruker, D2 PHASER) equipped with CuKα radiation source (measurement range: 2-70° 2θ, step size: 0.02° 2θ, counting time: 1 s per step, slit width: 0.6 mm). Infrared spectra of the samples diluted with KBr (4 mg of sample ground with 96 mg of KBr) were recorded in the range of 650-4000 cm^{-1} with resolution of 2 cm^{-1} (200 scans), using diffused reflectance technique (Nicolet 6700 FT-IR, Thermo Scientific, MCT/A detector). The textural parameters of the samples were determined by adsorption of N_2 at −196 °C using a Quantachrome surface area and pore size analyzer, model 2200 E, on outgassed samples (25 °C, 2 h, pressure 0.001 bar). MB area was calculated based on adsorption studies of methylene blue taking 130 $Å^2$ as the surface occupied by one molecule of the dye. Cation exchange capacity was determined using the ammonium acetate method (Steudel, 2008). Chemical composition of samples was determined using atomic absorption spectroscopy (AAS) (Analytic Jena High-Resolution Continuum Source Atomic Absorption Spectrometer, ContrAA 700) method. The results are presented only for the most abundant elements (>0.25 wt.%). Point of zero charge was determined using two different methods: according to procedures described by Mular (Mular and Roberts, 1966) and Riviera (Rivera-Utrilla et al., 2001) and given as an average of four pH values obtained in the experiment. The SEM/EDS analysis was performed using a High resolution (Schottky) Environmental Scanning Electron Microscope with X-Ray Microanalysis and Electron Backscattered Diffraction analysis:

Quanta 400 FEG ESEM/EDAX Genesis X4M. Samples were coated with an Au/Pd thin film by sputtering, using the SPI Module Sputter Coater equipment.

Adsorbate concentration in batch adsorption experiments was measured using UV-VIS spectrophotometer (Thermo Scientific, Evolution 300) at the maximum absorbance wavelength (665 nm for MB and 531 nm for AR).

Models were fitted to the experimental data gathered in the kinetics, equilibrium and column experiments using non-linear regression analysis. Variances and correlation coefficients were determined and compared using Fisher's, and Akaike's Information Criterion (AIC) tests.

The pseudo 1st order Lagergren's model (Lagergren, 1898) and the pseudo 2nd order Ho's model (Ho and McKay, 1999) were fitted for the kinetic data, the Langmuir's (Langmuir, 1918) and the Freundlich's (Freundlich, 1906) models were fitted to the adsorption isotherm data. In the column experiments Yan's model (Yan et al., 2001) was fitted to the experimental data in order to determine the maximum adsorption capacity of the materials and Yoon-Nelson's model (Yoon and Nelson, 1984) to obtain breakthrough times. Models equations and description are given in section 1 in the Supplementary Material.

Batch adsorption experiments were performed in Erlenmeyer flasks with caps and a magnetic stirrer (Velp, Multistirrer 15) at room temperature (24°C), without pH adjustment. Portions of 20 mg of each sample was placed in a flask and mixed with 50 mL of a 50 mg L^{-1} solution of AR or MB, stirred for 2 h, centrifuged (5 min in 4500 rpm, Sartorius, Sigma 2-16) and concentration of adsorbate in the supernatant determined.

Kinetic experiments were carried out at room temperature (24°C) using a magnetic stirrer (Velp, Multistirrer 15), without pH adjustment. A mass of 250 mg of the material was placed in a flask with 500 mL of dyestuff solution with an initial concentration of 100 mg L^{-1}. Samples were collected in selected time intervals using a micropipette and immediately centrifuged (1 min in 4500 rpm, Sartorius, Sigma 2-16) and concentration of the supernatant was determined.

Equilibrium studies were performed in 100 mL Erlenmeyer flasks with caps and 50 mL of dyes solutions of two concentrations (50 mg L^{-1} and 100 mg L^{-1}) and varying amount of material (from 10 mg to 250 mg). Suspensions were agitated on a stirrer (Velp, Multistirrer 15) for 2 h, samples were collected, centrifuged (Sartorius, Sigma 2-16) and concentration of supernatant was determined.

Colum experiments were performed using a glass column (Omnifit, 2.5 cm inside diameter, 15 cm height) and a peristaltic pump (Gilson, Miniplus 3). The studies were carried out with dyes concentration of 50 mg L^{-1}, at room temperature and a flow rate of 2.0 mL min^{-1}. Weighted portions of 0.5 g of W and of 0.1 g of WNC and NaOH treated

material (WN-OH), respectively, were mixed with 24 g of washed sand. In the next step, the column was washed with deionized water for 2 h and desorption proceeded using a solution of ethanol and sodium chloride, which was considered the best solvent according to the results in section 2.4, till the effluent showed no color. When the desorption process was finished, the column was washed with deionized water again and another cycle of adsorption performed (7 cycles on the raw material and 5 cycles on the modified materials). Three independent cycles of adsorption and desorption of MB and AR onto WN-OH were performed, during which changes of pH were monitored. In the last part of the studies co-adsorption of both dyestuffs was investigated on W, WNC and WN-OH. In each case the influent consisted of a mixture of both dyes in the proportion 50:50 to get final concentration of 50 mg of dyes per liter.

Desorption studies were performed by agitating 1 g of expanded (Ve) and acid activated vermiculite (WNC) in high concentration of AR for 2 h to prepare saturated material. Samples were washed with distilled water, centrifuged (5 cycles, 10 minutes at 4000 rpm) and left to dry. Desorption studies were carried out on saturated samples using different organic and inorganic eluents: cold water (COLD), hot water (HOT), hydrogen peroxide (Perox), 0.1 M hydrochloric acid (HCl), sodium chloride solutions (0.5 M; 1 M; 5 M respectively) (NaCl); acetone (Act), ethanol (EtOH), chloroform (Clfm), methanol (MeOH), carbon tetrachloride (CCl_4); mixture (50:50) of ethanol and 1 M aqueous sodium chloride solution (EtOH+NaCl) and mixture (50:50) of ethanol and 0.5 M nitric acid (EtOH+HNO_3). A mass of 100 mg of each saturated sample was put in a flask with a cap and mixed with 50 ml of eluent and stirred for 2 h or 24 h. After that time, the regenerated material was filtrated, washed and dried. In the next step, adsorption experiments on the recovered materials were performed by placing 50 mg of each sample in a flask and 100 mL of dyestuff of concentration of 100 mg L^{-1} and stirred for 2 h, after which concentrations of solutions were determined.

3.3 Results and discussion

Detailed analysis of the results of specific surface area measurements and cation exchange capacity are presented in the supporting information in section 2.1, point of zero charge determination in section 2.2, chemical composition in section 2.3, X-ray-diffraction analysis in section 2.4 and diffuse reflectance infrared Fourier transform analysis in section 2.5. Brief overview of obtained results is presented in Supplementary Material (Figures A.3.2 to A.3.6).

Particles morphology is visibly changing in each step of treatment. Crystals in starting material are characterized with relatively smooth edges, however between neighboring packets parallel stacking order is not always preserved. Upon acid treatment

small clusters of amorphous products were formed and deposited on the surface, moreover numerous fragments of broken platelets may be observed. Leaching in sodium hydroxide solution results in removal of irregular and rough particles. X-ray diffraction patterns indicate decrease of particle size as well as basal spacing. As expected, the highest decrease of cation exchange capacity was observed in first stage of treatment (acid lixiviation), while it was almost unaltered after contact with solution of base. Results of chemical analysis confirm that components of octahedral layer were dissolved in acid in large extent. Similarly silica content was significantly decreased upon leaching in basic solution. Formation of amorphous silica, also confirmed by infrared spectra analysis, was accompanied with large increase of specific surface area and consecutive decrease after its dissolution. Point of zero charge on the other hand at first decreased to rise again to higher values after the second stage of treatment.

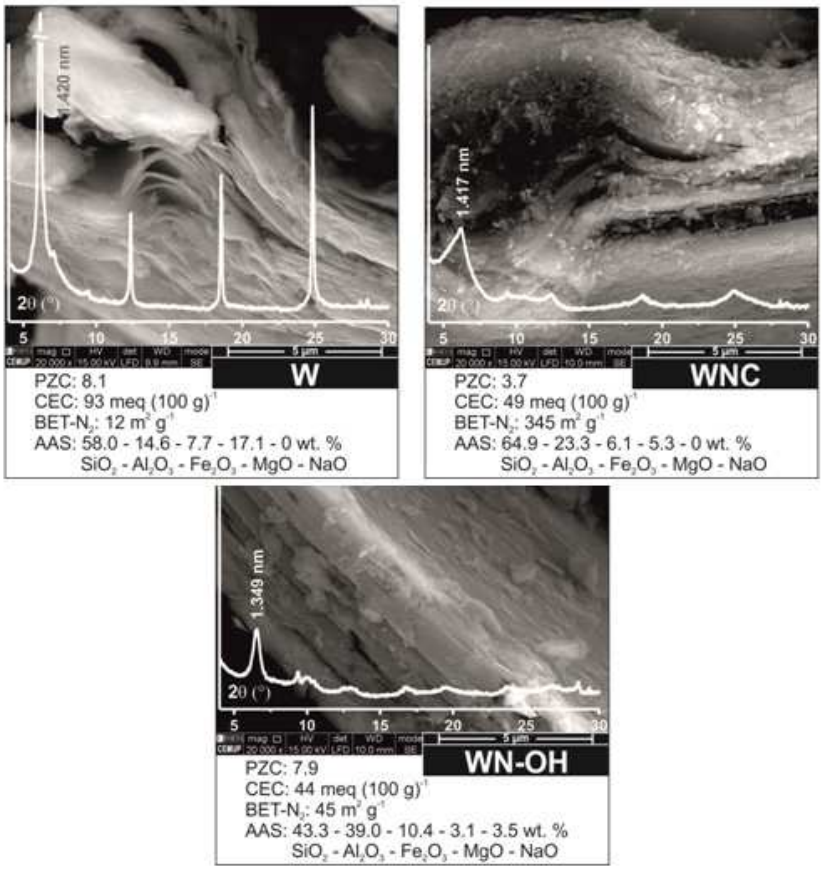

Figure 3.1 Results of physicochemical characterization of acid-base treated vermiculite: particles morphology, XRD pattern, chemical composition, values of PZC, BET-N_2 and CEC

3.3.1 NaOH treatment optimization

The raw material treated only with 1M NaOH did not show any significant increase in the adsorption capacity, which stayed at an average level of 48 ± 2 mg g^{-1} (48 ± 2, 45 ± 2 and 49 ± 5 mg g^{-1} for the raw (W), the raw treated for 2 h (W2h) and for 24 h (W24h), respectively. However, if the vermiculite is activated in acid (WNC) prior to

the NaOH treatment, a big increase in the adsorption capacity, which reached an average level of 140 ± 6 mg g^{-1} was noticed and additionally a slight decrease in the capacity was observed after longer treatment time of 24 h compared to 2h (86 ± 2 mg g^{-1} for the WNC and 144 ± 1 and 135 ± 1 mg g^{-1} for WNC treated with 1M NaOH for 2 h (WNC2h) and for 24 h (WNC 24h), respectively. Neither different concentrations of NaOH, nor time or temperature of the treatment resulted in statistically significant differences in the adsorption capacity of the material that was equal to an average level of 145 ± 7 mg g^{-1}.

3.3.2 Kinetic and equilibrium studies

Pseudo 2nd order model was the best fit according to AIC for both dyes. However, in the case of Fisher's test pseudo 2nd order model fits better for MB but no statistically significant difference between the models exists for AR. Adsorption rate decreases after each treatment step for both dyes. Adsorption of MB occurs faster than adsorption of AR in the case of W and WNC. That trend changes however for NaOH treated material on which AR exhibits higher adsorption rate (Table 3.1). The time needed to reach equilibrium on NaOH treated material was approximately 110 min and 50 min for MB and AR, respectively (Fig. A.3.7A in the Supplementary Material).

Adsorption of each dye followed different mechanism (Fig. A.3.7B in the Supplementary Material and Table 3.1). In the case of MB Langmuir's model fits better for the starting (W) and the acid treated material (WNC) and adsorption of AR on those materials fits better to Freundlich's model according to AIC test. Fisher's test however, showed no difference between the models except for adsorption of MB on WNC, where Freundlich's model was a better fit. For the material after the NaOH treatment, this situation reverses and Langmuir's model fits better for adsorption of MB and Freundlich's for adsorption of AR. The results revealed that NaOH treatment increased greatly the adsorption capacity of vermiculite in relation to the starting material. Based on Langmuir's model the adsorption capacity raised from 44 ± 1 to 155 ± 11 mg g^{-1} in the case of AR and from 53 ± 10 to 161 ± 5 mg g^{-1} for MB, for raw and NaOH treated material respectively (Table 3.1).

Table 3.1 Parameters of kinetic and equilibrium equations obtained for adsorption of MB and AR on starting vermiculite (W), acid treated (WNC) and NaOH treated (WN-OH) vermiculite.

Sample	Experiment	Model	Parameter	AR	MB
WN-OH	kinetics	pseudo 1st	q_e (mg g^{-1})	130 ± 7	127 ± 4
			k_1 (min^{-1})	0.06 ± 0.01	0.19 ± 0.02
			s^2	80.43	25.21
			R^2_{adj}	0.945	0.978
		pseudo 2nd	q_e (mg g^{-1})	147 ± 5	140 ± 4
			k_2 (g (mg $min)^{-1}$)	0.0005 ± 0.0001	0.0013 ± 0.0002
			s^2	16.96	12.97
			R^2_{adj}	0.988	0.989
		Models comparison	Fisher's Test	pseudo 2nd	no difference
			AIC	pseudo 2nd	pseudo 2nd
	equilibrium	Langmuir	q_m (mg g^{-1})	155 ± 11	161 ± 5
			K_L (L mg^{-1})	51 ± 48	0.8 ± 0.2
			s^2	297.12	7.36
			R^2_{adj}	0.513	0.998
		Freundlich	K_F ((mg g^{-1})(L $mg^{-1})^{1/n}$)	128 ± 2	116 ± 18
			n	15 ± 1	13 ± 8
			s^2	8.49	37.36
			R^2_{adj}	0.986	0.989
		Best fit	Fisher's test	Freundlich	Langmuir
			AIC	Freundlich	Langmuir
WNC*	kinetics	pseudo 2nd	q_e (mg g^{-1})	64 ± 4	63 ± 4
			k_2 (g (mg $min)^{-1}$)	0.004 ± 0.001	0.003 ± 0.001
	equilibrium	Langmuir	q_m (mg g^{-1})	60 ± 2	66 ± 3
		Freundlich	K_F ((mg g^{-1})(L $mg^{-1})^{1/n}$)	27 ± 2	42 ± 2
		Best fit	Fisher's test	no difference	Freundlich
			AIC	Langmuir	Freundlich
W*	kinetics	pseudo 2nd	q_e (mg g^{-1})	35 ± 2	45 ± 2
			k_2 (g (mg $min)^{-1}$)	0.007 ± 0.002	0.005 ± 0.002
	equilibrium	Langmuir	q_m (mg g^{-1})	44 ± 1	53 ± 10
		Freundlich	K_F ((mg g^{-1})(L $mg^{-1})^{1/n}$)	30 ± 2	33 ± 6
		Best fit	Fisher's test	no difference	no difference
			AIC	Langmuir	Freundlich

*(Stawiński et al., 2016)

3.3.3 Pre-selection of eluent for regeneration

Solutions of inorganic substances (Fig. 3.2) did not show good desorbing properties (Ve HCl, Ve Perox, Ve H_2O COLD, Ve H_2O HOT, Ve NaCl). Organic solvents (Fig. 3.2) seem better for that purpose (Ve EtOH, Ve MeOH, Ve Act), however, the best results were obtained when a solution containing both, organic and inorganic compounds, was used (Ve EtOH+NaCl, Ve EtOH+HNO_3). The results also showed that time plays an important role in regeneration process. Significant increase in the regeneration efficiency was observed after 24 h in comparison to 2 h.

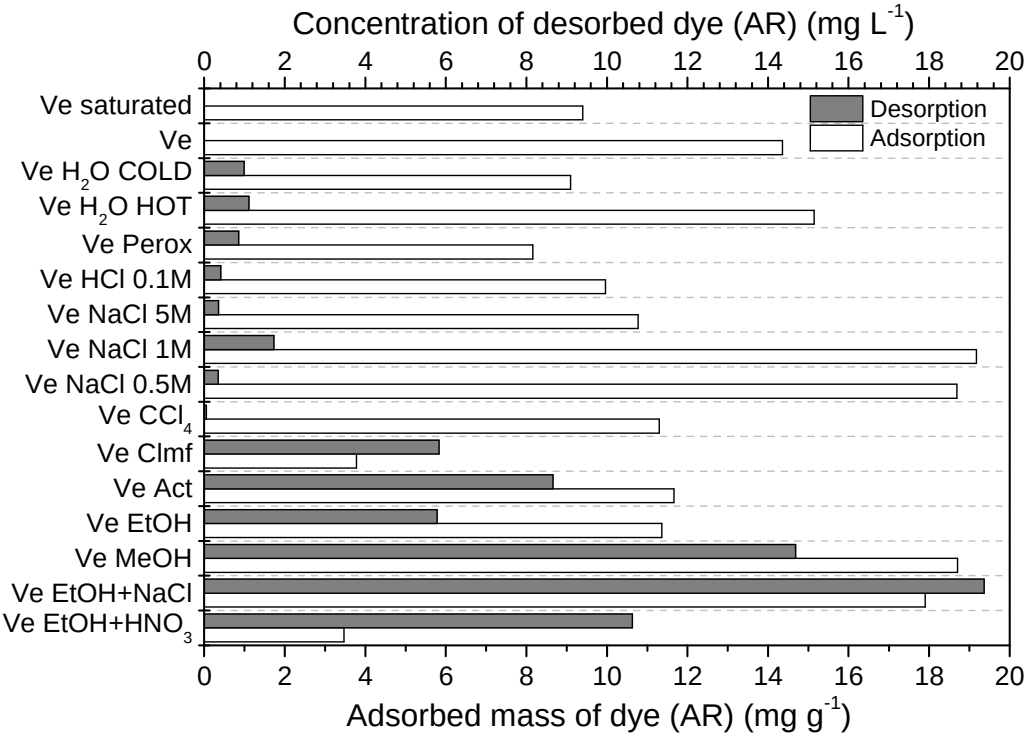

Figure 3.2 Desorption efficiency after 2h (bottom axis) from the expanded vermiculite (Ve) saturated with AR, and adsorption efficiency (top axis) on regenerated material (100 mL of 100 mg L^{-1} AR solution, 2 h at 24 °C).

It was observed that methanol (Ve MeOH) desorbs better than ethanol (Ve EtOH) and the methanol-regenerated material showed adsorption capacity higher than the raw one (Fig. 3.2). Mixture of ethanol and sodium chloride (WNC EtOH+NaCl and Ve EtOH+NaCl) resulted in good desorption, also adsorption on the regenerated material is on the level of the starting one (Fig. 3.3). It should be noted that none of these solvents, ethanol or sodium chloride solution, is as effective as their combination.

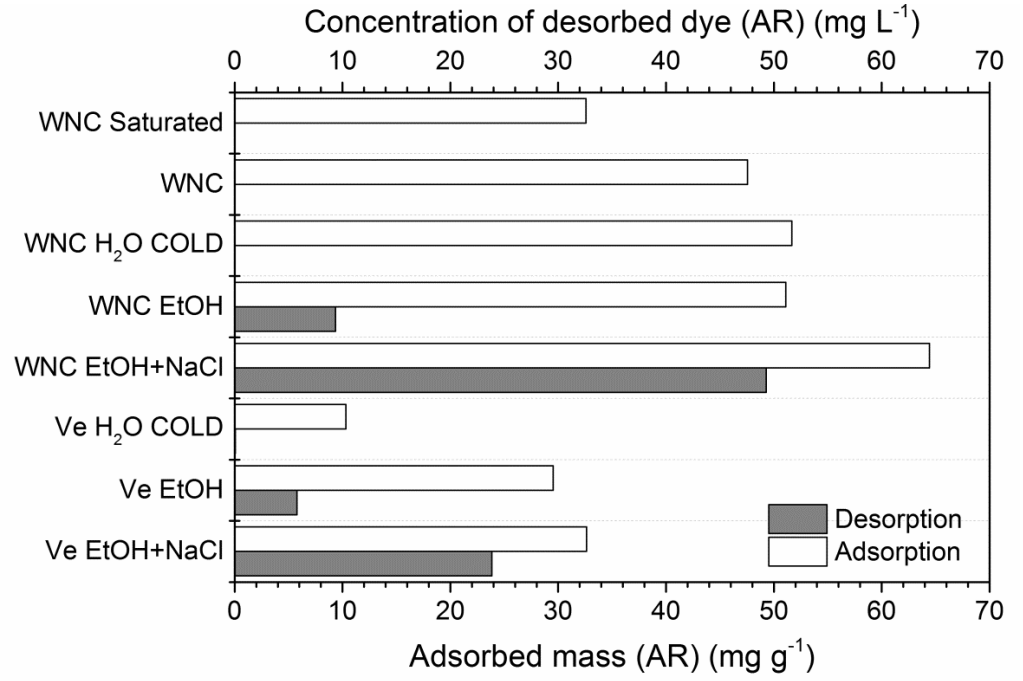

Figure 3.3 Desorption efficiency after 24 hours (bottom axis) from saturated materials (Ve and WNC) and adsorption efficiency (top axis) on regenerated material in selected conditions (100 mL of 100 mg L^{-1} AR solution, 2 h at 24 °C).

3.3.4 Column studies

Results from column studies were adjusted to Yan's and Yoon-Nelson's models (Tables A.3.1 and A.2 in the Supplementary Material). Experimental data with fitted Yan's model are shown in Fig. A.3.8 and Table A.3.1. The experiments confirmed an increase in the adsorption capacity of vermiculite on each step of the treatment. Higher adsorption capacities were obtained for MB on modified materials (WNC and WN-OH) with an exception for the starting vermiculite on which AR reached higher adsorption level compared to MB (Fig. 3.4A). After two cycles the breakthrough time stabilized at an average level of 144 ± 15 and 212 ± 27 min on the raw material, 114 ± 25 and 88 ± 13 min on acid treated material, and 123 ± 25 and 99 ± 8 min on NaOH treated material, respectively for MB and AR (Fig. 3.4B).

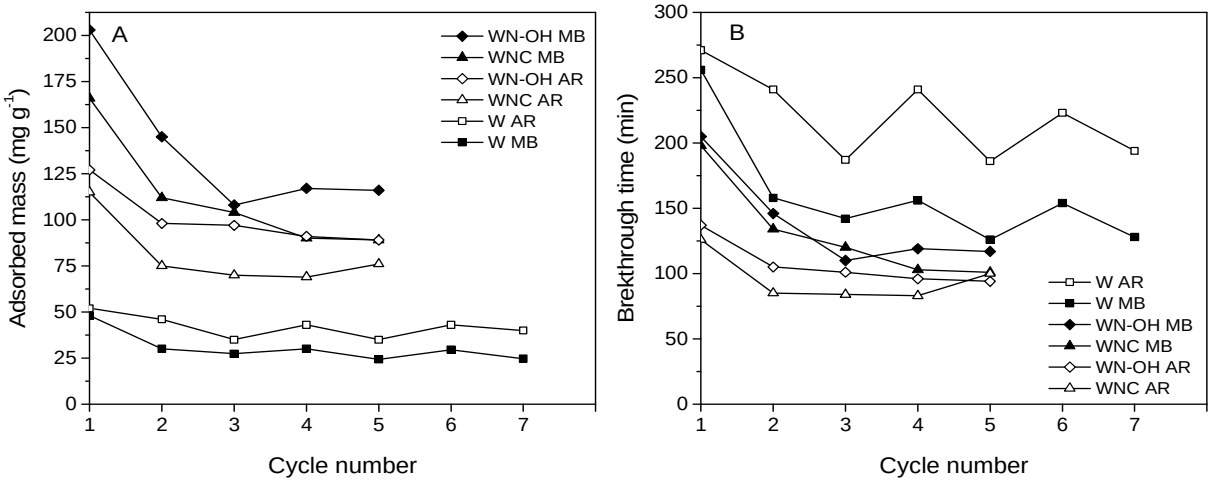

Figure 3.4 Changes of the adsorption capacity during adsorption/desorption cycles obtained from Yan's model fit (A) and changes in breakthrough times obtained from Yoon-Nelson's model fit (B); initial dyes concentrations: 50 mg L^{-1}, flow rate: 2.0 mL min^{-1}, temperature 24 °C.

Desorption studies showed that an average time of 100 min is enough to allow a satisfactory reuse of the column packing material (Fig. A.3.9 in the Supplementary Material). The experiments showed a general trend of changes in pH towards higher values in the case of AR and towards lower ones in the case of MB (Fig. A.3.10 and Fig. A.3.11 in the Supplementary Material). MB exhibited higher affinity to the material compared to AR which was being gradually desorbed from the column as adsorption of MB preceded (overshooting) when the column reached its maximum capacity. The values in that region were not considered during adjustments of the models. The materials showed higher adsorption capacity for MB compared to AR (Fig. 3.5). Table A.3.3 in the Supplementary Material contains full models' parameters.

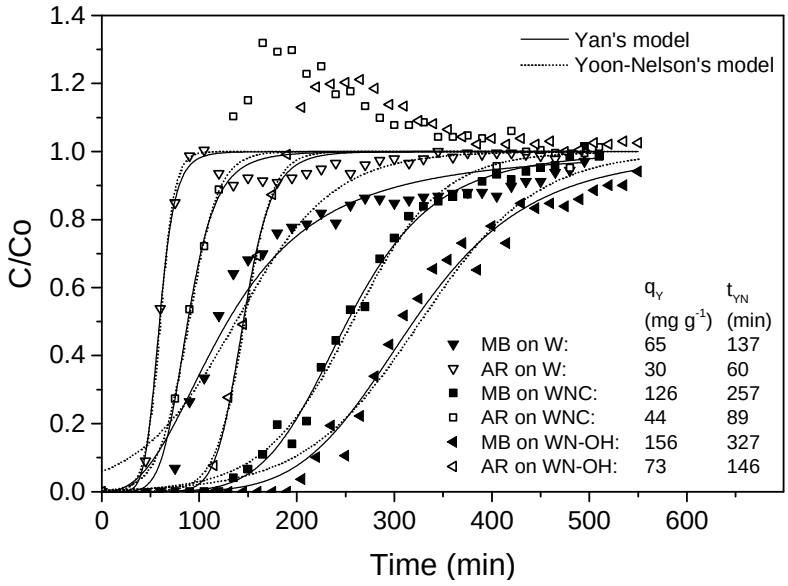

Figure 3.5 Adsorption curves with models fitted to the experimental data of co-adsorption of MB and AR on starting (W), acid treated (WNC) and NaOH treated (WN-OH) material in column system; initial dyes concentrations: 50 mg L^{-1}, flow rate: 2.0 mL min^{-1}, temperature 24 °C.

3.4 Discussion

Vermiculite being a natural mineral, used without any additional purification, shows significant variances in measured properties, thus two methods were used to determine the point of zero charge (PZC). Shift between the measured PZC values was observed in different electrolyte concentrations, with a tendency towards lower pH with an increase of the ionic strength. That indicates electrolyte adsorption causing a release of protons associated with cation exchange sites (Conklin, 2014). Particle charge was then neutralized not only by adsorption of H^+ and OH^- but also electrolyte ions.

The pH measured when the following charges are neutralized: the charge depending on adsorbent structure (structural charge) and resulting from adsorption and immobilization of ions into surface complexes in adsorbent (net particle charge or net adsorbed surface charge), thus, a state when there is no more charge to be neutralized by ions in the diffuse layer, is simply called point of zero charge and corresponds to neutralization of net total particle charge (Sposito, 2008). PZC of raw vermiculite was found at about 8.1, which is in agreement with previous studies (Fox and Malati, 1993; Abollino et al., 2008). After treatment it shifted to 3.8, subsequent treatment with NaOH shifted the PZC back to approximately initial value of 7.9. The final product of acid treatment of clays is partly dissolved material of increased surface area, porosity and surface acidity, the final solid product also contains amorphous three-dimensional cross-linked silica (Komadel and Madejova, 2006). Chemical decomposition of clays causes an evolution of the surface functional groups from the pre-eminence of the siloxane ditrigonal cavity to an increase in abundance of inorganic hydroxides, that are capable of being ionized in contact with water (Sposito, 1984; Molina, 2013). When the crystalline surface of phyllosilicates is distorted, unsaturated “broken bonds” occur at the edge surface, these may be compensated by formation of reactive OH groups leading to Brønsted acid sites such as Si-OH and coordinately unsaturated Al and Mg easily formed at the edges behave as Lewis acids (Komadel and Madejova, 2006). When OH group is coordinated to Al (III) they can form inner-sphere complexes with a proton or hydroxide anion depending on pH values, when coordinated to Si, they tend to complex only hydroxide anions. Such prepared clays are also riddled with defects (vacant Ion sites) that promote forming hollow spherule whose outer boundary contains many apertures through which small molecules or ions can enter (Sposito, 1984). Also the point of zero net charge (PZNC), thus PZC as well, for silica is relatively low (usually below 4) (Sposito, 2008). Those factors caused the shift of PZC in the treated material. The treatment with citric acid causes dissolution of metal hydroxides by complexing the multivalent ions with citrate. Presence of such hydroxides prevents optimal dispersion of

the clay causing coagulation and aggregation (Carrado et al., 2006). Citrate ions might also complex and remove the part of interlayer cations that had not been leached or exchanged during the mineral acid treatment and as well bulk metal oxides present on the layers surface. After the acid treatment deposits of amorphous silica, that act as a cementing agent impeding swelling and dispersion, are present in the material. During NaOH treatment that silica, as well as hydrous aluminosilicates (allophanes) formed during acid treatment, are dissolved (Carrado et al., 2006). This might clean the material and make the interlayer space more accessible for adsorption and removed degradation product responsible for lowering the PZC, as well as it was reported, the shift of PZC towards higher values is a normal phenomenon occurring in chemical weathering of clays provided that it involves removal of silica (Sposito, 2008).

The specific surface areas of the materials obtained by MB method are significantly higher than those from BET. This is due to the fact that specific surface area is an operational concept and obtained values may differ depending on an experimental method used, thus it precludes any interpretation of its numerical values in absolute geometric sense. Hence there is no one specific surface of a clay, but rather specific surfaces (Sposito, 1984). N_2 adsorption method creates limitations in samples containing layer-silicates (Aringhieri et al., 1992) due to the relatively large Van der Waals radius of the N_2 molecule that prevents it from interacting with surface functional group occluded in small void spaces and it is adsorbed only on the external surfaces of phyllosilicate quasicrystals (Sposito, 1984). The poor reactivity of non-polar molecule of N_2 to exposed surfaces might also contribute to lowering the values of specific surface area (Aringhieri et al., 1992). Methylene blue molecule, on the other hand, can penetrate the structure of the material, enter interlayer regions and the siloxane ditrigonal cavities. Another factor affecting the obtained specific surface area in MB experiment is the fact that the distribution of the dye cations on the surface of clays is influenced not only by electrostatic interactions, but also by dye–dye interactions (Lagaly et al., 2006). MB adsorption may follow the multilayer model (Weng and Pan, 2006) and on certain surfaces it can form dimmers or trimmers on the external surface of clay, which precedes the disaggregation and migration of the dyes in between the layers (Neumann et al., 2002). Decreasing particle size can increase the adsorption capacity since molecules don't penetrate the interlayer region but adsorb on the surface, smaller particles give larger surface areas. Also the inability to penetrate the micropores by large dyes molecules affects results obtained by dye adsorption (Gupta et al., 2003; Dizge et al., 2008). Although it seems there was a reduction of specific surface area (N_2 adsorption method) after the base treatment, before that stage the total area available to adsorption was not accessible to the dyestuffs (inner surface of micropores). On the other hand,

interlayers were not available to N_2 molecules after outgassing (Fig. A.3.2), while they can be penetrated by adsorbate molecules in the solution. Diffusion into interlayer galleries is possible due to base treatment and removal of silica clusters binding adjacent layers.

The DRIFT analysis showed that the acid treatment resulted in an increase in intensity and width of the peaks in mentioned range due increase in heterogeneity of OH species in the material (Węgrzyn et al., 2013). NaOH treatment decreased significantly that intensity, due to washing off hydroxyl group bearing species. After the NaOH modification hydrophilic cations of Na are present in the material strengthening the H-bonding of the polarized water. When the H-bonding is stronger, lower energy is required for an occurrence of OH-stretching vibration and thus the observed bands in NaOH treated vermiculite are shifter towards higher wavenumbers (Tomić et al., 2012). The bands in the spectrum of acid treated samples are broadened. This phenomenon may be due to decreasing crystallinity attributed to the weakening of H-bonds within the crystal and changes in Fe-O bonds associated with the tilting of octahedra rows within the structure (Parikh et al., 2014). Also it can be attributed to the partial transformation of the tetrahedral sublayers into a three dimensional framework of amorphous silica (Komadel et al., 1996; Madejová et al., 1998; Steudel et al., 2009). The shift of bands in the Si-O stretching region may correspond to progressive transformation of Si-O-Mg-O-Si bonds in the silicate to the more rigid Si-O-Si-O-Si bonds in amorphous silica when the octahedral cations were removed (Belver et al., 2002). Moreover, such shift in the band position of Si-O stretching region was reported as a result of reduction of Fe^{3+} and increasing amount of structural Fe^{2+} (Stucki, 2006).

The XRD analysis showed that upon the acid treatment some amorphous species of silica appear in the material (Maqueda et al., 2007) however, the vermiculite structure is preserved although the crystallinity significantly decreases. After the NaOH treatment the vermiculite structure changes, the material almost completely loses its crystallinity and some of the amorphous phase is leached from the material along with formation of another hydroxy phase.

Fisher's test showed no preference towards any model in the case of adsorption on the raw material and in the case of adsorption of AR on acid treated vermiculite. Adsorption of MB on acid treated material according to that test fits better to Freundlich's model, suggesting that it assumes multilayer adsorption on heterogeneous surface. AIC test however indicated Langmuir's model, which assumes monolayer adsorption on homogeneous surface, as a better fit in the case of adsorption of AR on the raw and acid treated material and Freundlich's in the case of adsorption of MB on those materials. The adsorption seems to change its mechanism after the material had been treated with

NaOH. The trend of adsorption of AR driven by Langmuir's model's assumptions changes to Freundlich's and the opposite happens in the case of MB, both tests indicated the same models as the best fits in each case. Cation can be adsorbed on clays directly to the surface by forming an outer-sphere complexes as well as in a form of an outer-sphere complexes where water molecules are located between the cation and the clay surface (Sposito, 1984). Astrazon red is a bigger molecule so it should have lower ionic potential, which is a ratio of charge and molecule radius, compared to methylene blue, and that is why it has less affinity to the material. Additionally the interactions between the dyes and the clay are weakened due to decreasing of layer charge occurring during the dissolution of the vermiculite during the treatment. Such process also renders the layer charge distribution more heterogeneous (Pentrák et al., 2012). Those facts may explain the change of adsorption mechanism of AR on NaOH treated material. Some of the molecules can migrate from the inner-sphere complexes and outer-sphere complexes forming multilayer, also AR is a more flexible molecule and has more resonance structures than MB, which may allow different geometric coordination of the molecule on the surface making the layer more heterogeneous. The fact of MB tending to form multilayers might be explained by its ability to form dimmers and trimmers on external surfaces of adsorbents as a first step followed by disaggregation and migration of dye molecules in between the layers (Neumann et al., 2002). Moreover after the acid treatment the sample contains amorphous material that may provide additional adsorption sites and as they occupy also micropores what impedes access to some internal structures rendering the surface more heterogeneous (Hajjaji and El Arfaoui, 2009). After the final step of treatment, during which the amorphous phase is leached, the material becomes more homogenous allowing MB to form more ordered layers on the surface and Langmuir's model becomes again the best fit. It has been reported (Pentrák et al., 2012) that MB tends to form monolayer on clays with reduced layer charge due to their decomposition. Decreasing particle size can increase the adsorption capacity, since the dyestuff molecules don't penetrate the interlayer region but adsorb on the external surface which may be significantly higher for small particles. It has to be mentioned that no matter how good the fit of a model is, it does not mean that an actual phenomenon the model expresses takes place. Most of the time, adsorption is controlled by various factors. Thus the adsorption isotherms equation, as well as rate laws should be rather considered as curve fitting models without actual mechanistic significance as they do not always reflect the actual phenomena taking place. However they are useful means with predictive capability of the adsorption to design adsorption units (Hameed and El-Khaiary, 2008; Sposito, 2008).

Desorption studies showed promising results in terms of regeneration the material. It is shown that contact time plays an important role in this process. Better desorption results of methanol compared to ethanol might be attributed to the fact that methanol being a smaller and more polar molecule than ethanol has easier access the interlayer space it displaces the adsorbed dyes molecules and interlayer water more efficiently. However, methanol due to its toxicity was no longer considered in this research. Adsorption capacity of the material regenerated that way is higher than of the raw sample. This phenomenon can be attributed to so called propping-open procedure. Ethanol and methanol molecules, previously adsorbed onto the material, are exchanged and facilitate intercalation of bigger organic molecules, which are not intercalated directly but in a stepwise process (Lagaly et al., 2006). Significant increase in the adsorption capacity of the material regenerated with a solution containing NaOH is due to changes in the structure of the material and its partial dissolution that causes significant loss of the sorbent mass. This is an undesired effect in this case of a material that is supposed to be used in continuous adsorption-desorption cycles. This process is discussed later in the article. Mixture of ethanol and sodium chloride and ethanol and sodium hydroxide give good desorption results, better than when the organic solvents are used isolated, due to enhanced adsorption of counter ions, in this case Na^+, that occurs in the presence of organic solvents in the solution (Lagaly, 2006), thus removal of the adsorbed dyes is enhanced. This phenomenon can be explained by the fact that when ethanol is added to water it decreases the dielectric constant of the solution, thus the columbic attraction between exchangeable cations and negative silicate surface increases. The higher adsorption capacity of the regenerated material can be attributed to exchange of remaining interlayer divalent metal cations to sodium. This results in better delamination of the clay (Lagaly, 2006) and better accessibility of the surface to dyes. Also the saturated material still showed some adsorption abilities.

By means of the column experiments it was shown that the material can be re-used in several adsorption-regeneration cycles. The maximum adsorption capacity decreased during the first two cycles to maintain a stable level in the case of treated materials but reminded unchanged in the case of the raw vermiculite. This phenomenon can be explained in terms of the changes occurring during the acid/base treatment. The material becomes more porous and its specific surface increases. Some of the adsorption sites might not be available to the solvent to penetrate (micropores, interlayer spaces) thus not all of the dyes molecules are able to be displaced and desorbed. It was also noticed that the total capacity in the case of co-adsorption was higher than in the case of systems with only one dye, it also proves that each dye might be adsorbed on different sites. Another factor contributing to lowering the capacity in adsorption-

regeneration cycles is that the eluent reaches the mentioned structures and occupies them not allowing the dyes to adsorb there in a following cycle. Also some of the dye or eluent molecules might adsorb on the materials with creation of chemical bonds permanently being attached to the surface. After the two cycles equilibrium is reached and adsorption takes place in more available sites. In the case of the raw material, that has crystalline structure and is more ordered, the diffusion of the solvent is easier rendering the desorption more efficient. The affinity of a dye seems to be a determinant factor in the removal of adsorbed molecules/ions. The molecule with the lowest affinity will always break through the column first, followed by other components of the feed having higher affinity. Concentration overshooting of one of the component occurs at the column outlet when an ion or molecule being less strongly adsorbed is pushed further in the column by more slowly moving, more strongly adsorbed species. That results in an increase in the solution concentration at the outlet of the column that can be higher that the initial one. Another factor causing overshooting may be the interference of ions or molecules displaced by ion exchange from the adsorbent surface, by that which have higher affinity to the adsorbent (Franca and Oliveira, 2010). The dye structure, molecular flexibility and differences in dimensions can influence the competition for the adsorption sites (Duta and Visa, 2015). MB molecule is more rigid (heterocyclic aromatic rings), thus is has slower diffusion rendering the adsorption slower, but it is able to give use to a larger amount of adsorption sites (e.g., inside micropores). AR however, being more flexible shows faster diffusion and adsorption process at the easily accessible sites.

3.5 Conclusions

Acid treatment of clays is a well-known procedure to increase their adsorption capacity. However, if such modification is followed by treatment with sodium hydroxide, which is reported in our work for the first time, it increases the adsorption properties even more. That treatment removes amorphous phase formed during the acid attack on the material, decreases its crystallinity and greatly increases its specific surface area (MB method). Adsorbent prepared by consecutive acid and base modification was successfully used in column recyclable system with a possibility of regeneration. The adsorption capacity of two cationic dyes in column studies, increased from 48 ± 2 to 203 ± 4 mg g^{-1} for methylene blue on starting material and from 51 ± 1 to 127 ± 2 mg g^{-1} for astrazon red on acid-base treated material. The loss of the adsorption capacity was observed only during the first two cycles, after that it maintained a stable level. Adsorption and regeneration was performed efficiently for 7 cycles. Acid-base treated vermiculite proved to be an economical, recyclable and high performance adsorbent.

3.6 References

Abollino, O., Giacomino, A., Malandrino, M., Mentasti, E., 2008. Interaction of metal ions with montmorillonite and vermiculite. Appl. Clay Sci. 38, 227-236.

Ali, I., Asim, M., Khan, T.A., 2012. Low cost adsorbents for the removal of organic pollutants from wastewater. J. Environ. Manage. 113, 170-183.

Angın, D., Köse, T.E., Selengil, U., 2013. Production and characterization of activated carbon prepared from safflower seed cake biochar and its ability to absorb reactive dyestuff. Appl. Surf. Sci. 280, 705-710.

Aringhieri, R., Pardini, G., Gispert, M., Sole, A., 1992. Testing a simple methylene blue method for surface area estimation in soils. Agrochimica 36, 224-232.

Ayranci, E., Duman, O., 2009. In-Situ UV-Visible Spectroscopic Study on the Adsorption of some Dyes onto Activated Carbon Cloth. Sep. Sci. Technol. 44, 3735-3752.

Bailey, S.W., Chairman, 1980. Summary of recommendations of AIPEA nomenclature committee on clay minerals. Am. Mineral. 65, 1-7.

Belver, C., Bañares Muñoz, M.A., Vicente, M.A., 2002. Chemical Activation of a Kaolinite under Acid and Alkaline Conditions. Chem. Mater. 14, 2033-2043.

Bergaya, F., Lagaly, G., 2006. General introduction: clays, clay minerals, and clay science. in: Bergaya, F., Theng, B.K.G., Lagaly, G. (Eds.). Handbook of Clay Science. Elsevier Ltd.

Bhatnagar, A., Jain, A.K., 2005. A comparative adsorption study with different industrial wastes as adsorbents for the removal of cationic dyes from water. J. Colloid Interface Sci. 281, 49-55.

Carrado, K.A., Decarreau, A., Petit, S., Bergaya, F., Lagaly, G., 2006. Synthetic clay minerals and purification of natural clays. in: Bergaya, F., Theng, B.K.G., Lagaly, G. (Eds.). Handbook of Clay Science. Elsevier Ltd.

Chmielarz, L., Kuśtrowski, P., Zbroja, M., Rafalska-Łasocha, A., Dudek, B., Dziembaj, R., 2003. SCR of NO by NH3 on alumina or titania-pillared montmorillonite various modified with Cu or Co: Part I. General characterization and catalysts screening. Applied Catalysis B: Environmental 45, 103-116.

Conklin, A.R., 2014. Introduction to Soil Chemistry: Analysis and Instrumentation, Second Edition. John Wiley & Sons, USA.

Dizge, N., Aydiner, C., Demirbas, E., Kobya, M., Kara, S., 2008. Adsorption of reactive dyes from aqueous solutions by fly ash: Kinetic and equilibrium studies. J. Hazard. Mater. 150, 737-746.

Duman, O., Ayranci, E., 2006. Adsorption Characteristics of Benzaldehyde, Sulphanilic acid, and p-Phenolsulfonate from Water, Acid, or Base Solutions onto Activated Carbon Cloth. Sep. Sci. Technol. 41, 3673-3692.

Duman, O., Ayranci, E., 2010. Adsorptive removal of cationic surfactants from aqueous solutions onto high-area activated carbon cloth monitored by in situ UV spectroscopy. J. Hazard. Mater. 174, 359-367.

Duman, O., Tunç, S., 2008. Electrokinetic Properties of Vermiculite and Expanded Vermiculite: Effects of pH, Clay Concentration and Mono- and Multivalent Electrolytes. Sep. Sci. Technol. 43, 3755-3776.

Duman, O., Tunç, S., Gürkan Polat, T., 2015a. Adsorptive removal of triarylmethane dye (Basic Red 9) from aqueous solution by sepiolite as effective and low-cost adsorbent. Microporous Mesoporous Mater. 210, 176-184.

Duman, O., Tunç, S., Polat, T.G., 2015b. Determination of adsorptive properties of expanded vermiculite for the removal of C. I. Basic Red 9 from aqueous solution: Kinetic, isotherm and thermodynamic studies. Appl. Clay Sci. 109–110, 22-32.

Duta, A., Visa, M., 2015. Simultaneous removal of two industrial dyes by adsorption and photocatalysis on a fly-ash–TiO2 composite. J. Photochem. Photobiol. A: Chem. 306, 21-30.

Forgacs, E., Cserháti, T., Oros, G., 2004. Removal of synthetic dyes from wastewaters: a review. Environ. Int. 30, 953-971.

Fox, I., Malati, M.A., 1993. An investigation of phosphate adsorption by Clays and its relation to the problems of eutrophication of the river stour, Kent. J. Chem. Technol. Biotechnol. 57, 97-107.

Franca, A.S., Oliveira, L.S., 2010. Fixed-bed adsorption studies. in: Crini, G., Badot, P.M. (Eds.). Sorption processes and pollution : conventional and non-conventional sorbents for pollutant removal from wastewaters. Besançon: Presses universitaires de Franche-Comté.

Freundlich, H.M.F., 1906. Über die adsorption in läsungen. Z. Phys. Chem. 57, 385-470.

Gupta, V.K., Ali, I., Suhas, Mohan, D., 2003. Equilibrium uptake and sorption dynamics for the removal of a basic dye (basic red) using low-cost adsorbents. J. Colloid Interface Sci. 265, 257-264.

Hajjaji, M., El Arfaoui, H., 2009. Adsorption of methylene blue and zinc ions on raw and acid-activated bentonite from Morocco. Appl. Clay Sci. 46, 418-421.

Hameed, B.H., El-Khaiary, M.I., 2008. Sorption kinetics and isotherm studies of a cationic dye using agricultural waste: broad bean peels. J. Hazard. Mater. 154, 639-648.

Ho, Y.S., McKay, G., 1999. Pseudo-second order model for sorption processes. Process Biochem. 34, 451-465.

Komadel, P., Madejova, J., 2006. Acid Activation of Clay Minerals. in: Bergaya, F., Theng, B.K.G., Lagaly, G. (Eds.). Handbook of Clay Science. Elsevier Ltd.

Komadel, P., Madejová, J., Janek, M., Gates, W.P., Kirkpatrick, R.J., Stucki, J.W., 1996. Dissolution of hectorite in inorganic acids. Clays Clay Miner. 44, 228-236.

Lagaly, G., 2006. Colloid Clay Science. in: Bergaya, F., Theng, B.K.G., Lagaly, G. (Eds.). Handbook of Clay Science. Elsevier Ltd.

Lagaly, G., Ogava, M., Dekany, I., 2006. Clay Mineral Organic Interactions. in: Bergaya, F., Theng, B.K.G., Lagaly, G. (Eds.). Handbook of Clay Science. Elsevier Ltd.

Lagergren, S., 1898. About theory of so-called adsorption of soluble substances. Kongl. Vetenskaps Academiens Handlingar 24, 1-39.

Langmuir, I., 1918. The adsorption of gases on plane surfaces of glass, mica and platinum. J. Am. Chem. Soc. 40, 1361-1403.

Leitão, A., Serrão, R., 2005. Adsorption of phenolic compounds from water on activated carbon: prediction of multicomponent equilibrium isotherms using single-component data. Adsorption 11, 167-179.

Madejová, J., Bujdák, J., Janek, M., Komadel, P., 1998. Comparative FT-IR study of structural modifications during acid treatment of dioctahedral smectites and hectorite. Spectrochimica Acta Part A: Molecular and Biomolecular Spectroscopy 54, 1397-1406.

Mall, I.D., Srivastava, V.C., Agarwal, N.K., Mishra, I.M., 2005. Adsorptive removal of malachite green dye from aqueous solution by bagasse fly ash and activated carbon-kinetic study and equilibrium isotherm analyses. Colloids Surf. Physicochem. Eng. Aspects 264, 17-28.

Maqueda, C., Romero, A.S., Morillo, E., Pérez-Rodríguez, J.L., 2007. Effect of grinding on the preparation of porous materials by acid-leached vermiculite. J. Phys. Chem. Solids 68, 1220-1224.

Molina, F.V., 2013. Soil Colloids: Properties and Ion Binding. CRC Press.

Mular, A.L., Roberts, R.B., 1966. A simplified method to determine isoelectric points of oxides. Transactions of the Canadian Institute of Mining, Metallurgy and Petroleum 69, 438-439.

Neumann, M.G., Gessner, F., Schmitt, C.C., Sartori, R., 2002. Influence of the layer charge and clay particle size on the interactions between the cationic dye methylene blue and clays in an aqueous suspension. J. Colloid Interface Sci. 255, 254-259.

Pan, B., Pan, B., Zhang, W., Lv, L., Zhang, Q., Zheng, S., 2009. Development of polymeric and polymer-based hybrid adsorbents for pollutants removal from waters. Chem. Eng. J. 151, 19-29.

Parikh, S.J., Goyne, K.W., Margenot, A.J., Mukome, F.N.D., Calderón, F.J., 2014. Chapter One - Soil Chemical Insights Provided through Vibrational Spectroscopy. in: Donald, L.S. (Ed.). Advances in Agronomy. Academic Press, pp. 1-148.

Pentrák, M., Czímerová, A., Madejová, J., Komadel, P., 2012. Changes in layer charge of clay minerals upon acid treatment as obtained from their interactions with methylene blue. Appl. Clay Sci. 55, 100-107.

Reife, A., Freeman, H.S., 1996. Environmental Chemistry of Dyes and Pigments. John Wiley & Sons, New York.

Rieder, M., Cavazzini, G., D'yakonov, Y.S., Frank-Kamenetskii, V.A., Gottardi, G., Guggenheim, S., Koval, P.V., Müller, G., Neiva, A.M.R., Radoslovich, E.W., Robert, J.-L., Sassi, F.P., Takeda, H., Weiss, Z., Wones, D.R., 1998. Nomenclature of micas. Clays Clay Miner. 46, 586-595.

Rivera-Utrilla, J., Bautista-Toledo, I., Ferro-García, M.A., Moreno-Castilla, C., 2001. Activated carbon surface modifications by adsorption of bacteria and their effect on aqueous lead adsorption. J. Chem. Technol. Biotechnol. 76, 1209-1215.

Rozada, F., Calvo, L.F., García, A.I., Martín-Villacorta, J., Otero, M., 2003. Dye adsorption by sewage sludge-based activated carbons in batch and fixed-bed systems. Bioresour. Technol. 87, 221-230.

Sposito, G., 1984. The surface chemistry of soils. Oxford University Press.

Sposito, G., 2008. The Chemistry of Soils. Oxford University Press, New York.

Stawiński, W., Freitas, O., Chmielarz, L., Węgrzyn, A., Komędera, K., Błachowski, A., Figueiredo, S., 2016. The influence of acid treatments over vermiculite based material as adsorbent for cationic textile dyestuffs. Chemosphere 153, 115-129.

Steudel, A., 2008. Selection Strategy and Modification of Layer Silicates for Technical Applications. Univ.-Verlag Karlsruhe.

Steudel, A., Batenburg, L.F., Fischer, H.R., Weidler, P.G., Emmerich, K., 2009. Alteration of swelling clay minerals by acid activation. Appl. Clay Sci. 44, 105-115.

Stucki, J.W., 2006. Properties and behaviour of iron in clay minerals. in: Bergaya, F., Theng, B.K.G., Lagaly, G. (Eds.). Handbook of Clay Minerals. Elsevier.

Tomić, Z.P., Ašanin, D., Antić-Mladenović, S., Poharc-Logar, V., Makreski, P., 2012. NIR and MIR spectroscopic characteristics of hydrophilic and hydrophobic bentonite treated with sulphuric acid. Vib. Spectrosc. 58, 95-103

Weng, C.-H., Pan, Y.-F., 2006. Adsorption characteristics of methylene blue from aqueous solution by sludge ash. Colloids Surf. Physicochem. Eng. Aspects 274, 154-162.

Węgrzyn, A., Chmielarz, L., Zjeżdżałka, P., Jabłońska, M., Kowalczyk, A., Żelazny, A., Vázquez Sulleiro, M., Michalik, M., 2013. Vermiculite-based catalysts for oxidation of organic pollutants in water and wastewater. Acta, Geodyn. Geomater. 10, 341-352.

Yan, G., Viraraghavan, T., Chen, M., 2001. A new model for heavy metal removal in a biosorption column. Adsorpt. Sci. Technol. 19, 25-43.

Yoon, Y.H., Nelson, J.H., 1984. Application of gas adsorption kinetics--II. A theoretical model for respirator cartridge service life and its practical applications. Am. Ind. Hyg. Assoc. J. 45, 517-524.

Supplementary Material S.3

S.3.1 Dyestuffs

A

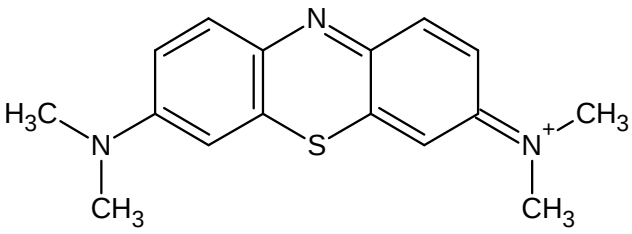

Molecular Formula: $C_{16}H_{18}N_3S^+$
Molar mass (Cl^- as counterion): 319.85 g mol^{-1}

B

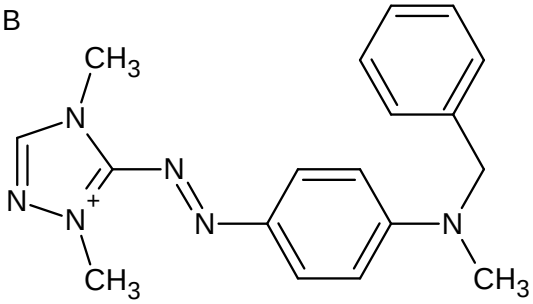

Molecular Formula: $C_{18}H_{21}N_6^+$
Molar mass (Br^- as counterion): 401.3 g mol^{-1}

Figure. A.3.1 Structural and molecular formulas of methylene blue (A) and astrazon red (B)

S.3.2 Models

Adsorption capacities of the materials were calculated according to Eq. A.1:

$$q_{m=}\frac{(C_0-C_{eq})V}{m} \qquad (A.1)$$

where q_m is adsorption capacity (mg g^{-1}), C_0 and C_{eq} initial and final concentrations (mg L^{-1}) respectively, V volume of adsorbate (mL), m adsorbent mass (mg).

S.3.2.1 Kinetics

The pseudo 1st order Lagergren's model (Lagergren, 1898) describes diffusion dependent kinetics following the Langmuir's model but it can be also applied to adsorption on energetically heterogeneous surfaces (Marczewski, 2010). The model is expressed by the Eq. A.2 (Ho, 2004):

$$q_t = q_e\left(1 - e^{-k_1 t}\right) \qquad (A.2)$$

where, q_e and q_t (mg g^{-1}) are adsorption capacities at equilibrium and at time t (min), respectively, and k_1 is the pseudo 1st order kinetic rate constant of the model (min^{-1}).

The pseudo 2nd order Ho's model (Ho and McKay, 1999) is used for systems where heterogeneity of various origins exists and a change of concentration during the experiment is significant. This model is expressed by Eq. A.3 (Ho and McKay, 1999):

$$q_t = \frac{q_e^2 k_2 t}{1+q_e k_2 t} \qquad (A.3)$$

where k_2 is the pseudo 2nd order kinetic rate constant (g mg^{-1} min^{-1}).

S.3.2.2 Equilibrium

The Langmuir's (Langmuir, 1918) model assumes that adsorbent's adsorption sites are homogenous and only one molecule of adsorbate can occupy one adsorption site within the adsorbent (Greluk and Hubicki, 2010). This model is expressed by Eq. A.4.

$$q = \frac{q_m K_L C_e}{1+K_L C_e} \qquad \text{(A.4)}$$

The Freundlich's (Freundlich, 1906) model assumes heterogeneity of the adsorbent active sites, and possible interactions between the adsorbed molecules leading to multilayer adsorption (Greluk and Hubicki, 2010). This model is expressed by Eq. A.5.

$$q = K_F C_e^{\frac{1}{n}} \qquad \text{(A.5)}$$

The parameters used in the models are: q (mg g^{-1}) the amount of dyestuff adsorbed per unit weight of adsorbent, C_e (mg L^{-1}) the equilibrium concentration, q_m (mg g^{-1}) and K_L (L mg^{-1}) are the Langmuir's constants related to the maximum adsorption capacity considering monolayer coverage, and energy of adsorption, respectively; n and K_F ((mg g^{-1})(L $mg^{-1})^{1/n}$) are the Freundlich's constants related to adsorption intensity and adsorption capacity, respectively.

S.3.2.3 Column

Yan's model (Yan et al., 2001) is expressed by Eq. A.6.

$$\frac{C}{C_0} = 1 - \frac{1}{1+\left(\frac{F^2 t}{k_Y q_Y m}\right)^{a_y}} \qquad \text{(A.6)}$$

where, a_y is the Yan's model constant (L min^{-1} mg^{-1}), q_Y is the maximum adsorption capacity (mg g^{-1}), m is the adsorbent mass (mg).

Yoon-Nelson model (Yoon and Nelson, 1984) is expressed by Eq. A.7.

$$\frac{C}{C_0 - C} = \exp\left(k_{YN} t - \tau k_{YN}\right) \qquad \text{(A.7)}$$

Where, k_{YN} is the Yoon-Nelson's model constant (min^{-1}),τ is the time required for 50% adsorbate removal (min) and t is the time (min).

S.3.3 Characterization of the materials

S.3.3.1 Specific surface area

The acid activation of vermiculite resulted in significant changes in its specific surface area that increased from 12 to 345 m^2 g^{-1}. Also the specific surface area determined by the methylene blue method showed an increase from 130 to 360 m^2 g^{-1}. However, method based on N_2 adsorption revealed a decrease in the specific surface area after the NaOH treatment (45 m^2 g^{-1}). As it is shown in Fig. A.3.2, prior to N_2 adsorption vacuum was applied in order to remove volatile molecules such as H_2O and hydroxyl groups. This may result in a collapse of the structure of starting material and the sample treated with basic solution. The methylene blue method, on the contrary, showed a further increase of the specific surface area of such treated vermiculite that reached level of 490 m^2 g^{-1}. Each step of the treatment caused a decrease of cation exchange capacity (CEC) of the material which changed from 93 meq $(100g)^{-1}$ to 49 meq $(100g)^{-1}$ after the acid activation and further decreased to 44 meq $(100g)^{-1}$ after the NaOH treatment.

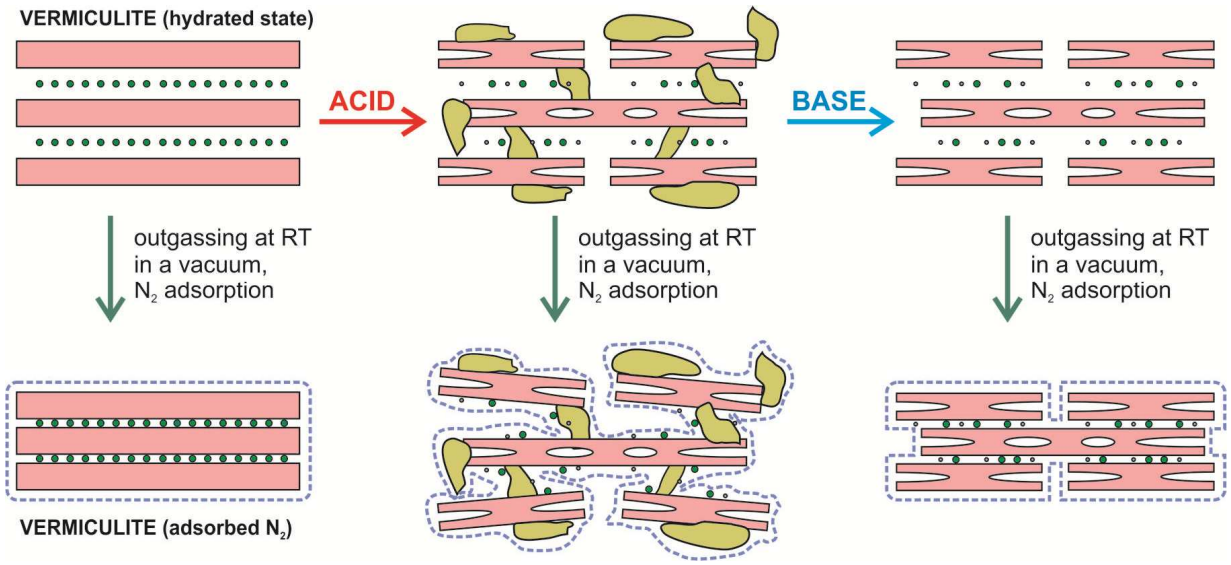

Figure. A.3.2 The influence of vacuum on the specific surface area determination results obtained using N_2 adsorption.

S.3.3.2 Chemical composition

The results showed a loss of particular elements from the materials composition along with the treatment procedure. After the first step significant amount of Mg which is mainly the interlayer cation, Fe and Al located in the layers are leached from the material. The content of Si, which is not removed by acid activation, relatively increased its abundance in the sample due to removal of other components. The treatment with NaOH caused further leaching of Al and removal of Si from the sample. However Fe is not leached and its relative content increased, also Na appears in the sample (Fig. A.3.3).

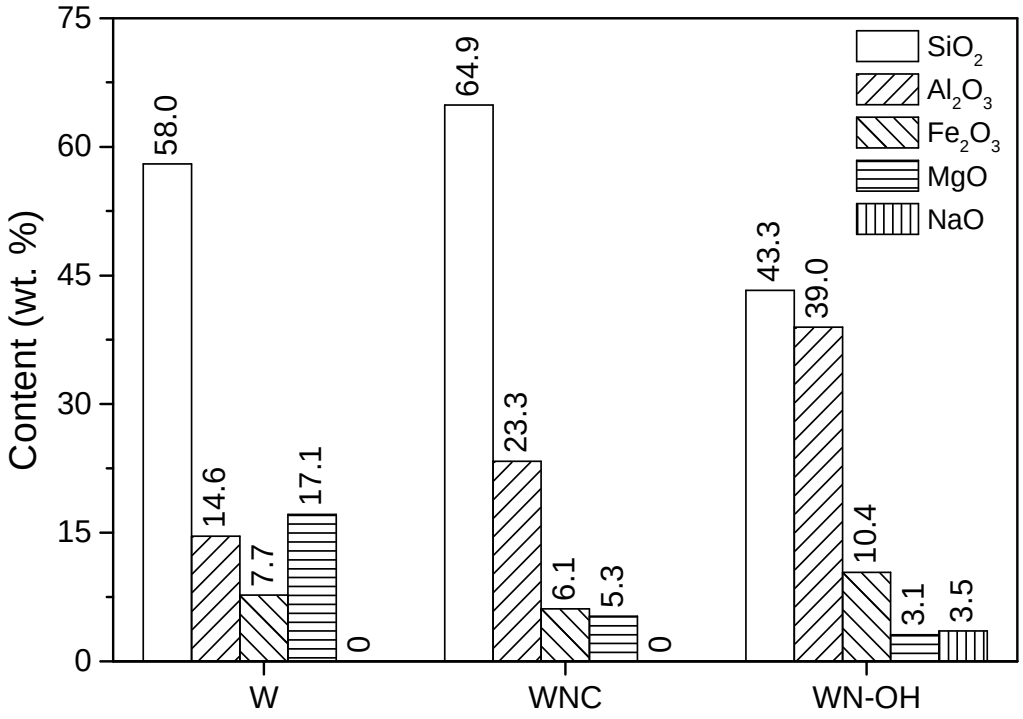

Figure. A.3.3 Chemical composition of the starting (W), acid activated (WNC) and NaOH treated (WN-OH) vermiculite.

S.3.3.3 Point of zero charge

The starting material reached PZC in pH 8.1 ± 0.4, the acid activated in pH 3.7 ± 0.4 and the NaOH treated in pH 7.9 ± 0.4 (Fig. A.3.4).

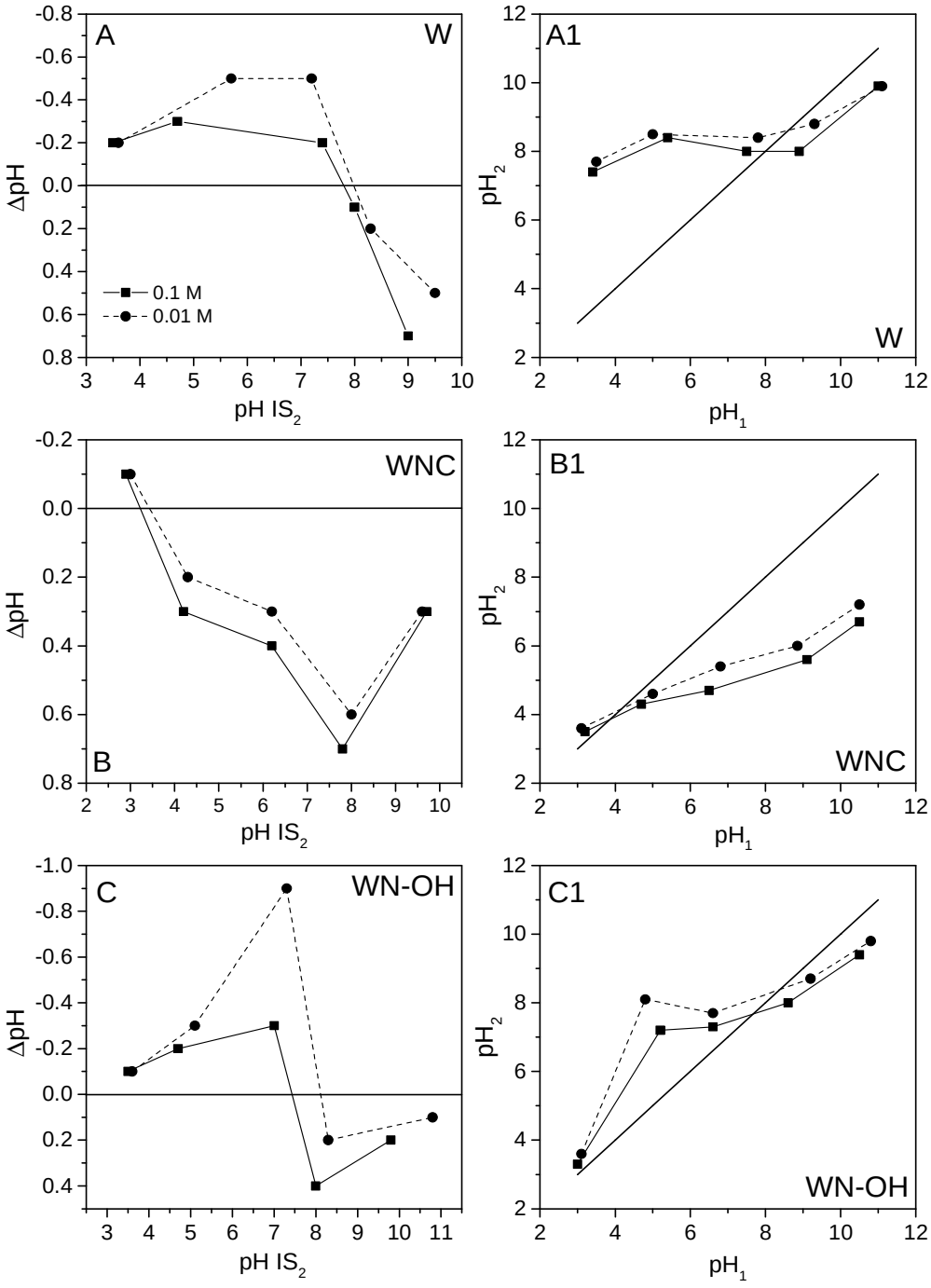

Figure. A.3.4 Determination of PZC for W, WNC and WN-OH samples with Rivera-Utrillo's method (graphs A, B, C, respectively) and with Mullar's method (graphics A1, B1, C1, respectively).

S.3.3.4 XRD

Diffractograms of investigated materials are presented in Fig. A.3.5. The raw material showed typical reflections of vermiculite at 6.2° (d=14.2 Å, 002), 12.3° (d=7.2 Å, 004), 18.5° (d=4.8 Å, 006), 24.8° (d=3.6 Å, 008), 31.2° (d=2.9 Å, 0010), 37.5° (d=2.4 Å, 0012), 44.1° (d=2.05 Å, 0014) what is in agreement with JCPDS card nos. 01-076-0847 and 00-016-0613 (Santos et al., 2015). The reflection at 9.45° (d=9.36 Å) is attributed to phlogopite (Steudel, 2008) and at 28.58° (d_{120}=3.12 Å) to boehmite (Oberlin and Couty, 1970)

The reflection at 6.2° is consistent with a vermiculite phase with two, slightly incomplete, water bilayers (Muiambo et al., 2010) indicating presence of hydrated cations like Mg (El Mouzdahir et al., 2009). Peak at 7° (d=12.6 Å) may be attributed to one layer of water on partially dehydrated interlayer magnesium cation (Chmielarz et al., 2012; Santos et al., 2015) or hydrophlogopite-like layers interstratification originated probably from two- and one-sheet hydrates, or interstratification between contracting and non-contraction phases (Harraz and Hamdy, 2010). Upon the acid treatment vermiculite peaks still remain in the material (except for the reflection at 2.4 Å) and are accompanied by a broad peak at around 26° attributed to amorphous silica (Maqueda et al., 2007). After the NaOH treatment the intensity of most of the reflections is significantly lower and new peaks appeared suggesting a creation of new phases. The reflections at 6.55^{o} (d=13.49 Å) with its secondary reflections at 13° (d=6.8 Å), 19.4° (d=4.57 Å) and 26.8° (d=3.33 Å) might be to attributed to a new phase, saturated with Mg (Sakharov et al., 1999), composed of smectite-like layers and hydroxy-intercalated vermiculite (HIV) formed due to migration of metal ions from the active dissolution sites into the interlayer space (Kalinowski and Schweda, 2007; Mareschal et al., 2009). Peaks at 10° (d=8.8 Å), 16.79° (d=0.52 Å), 23.7° (d=3.75 Å) and 30.51° (d=2.93 Å) remain unidentified. Broad peak in the background decreased after that treatment due to leaching of amorphous material (Carrado et al., 2006).

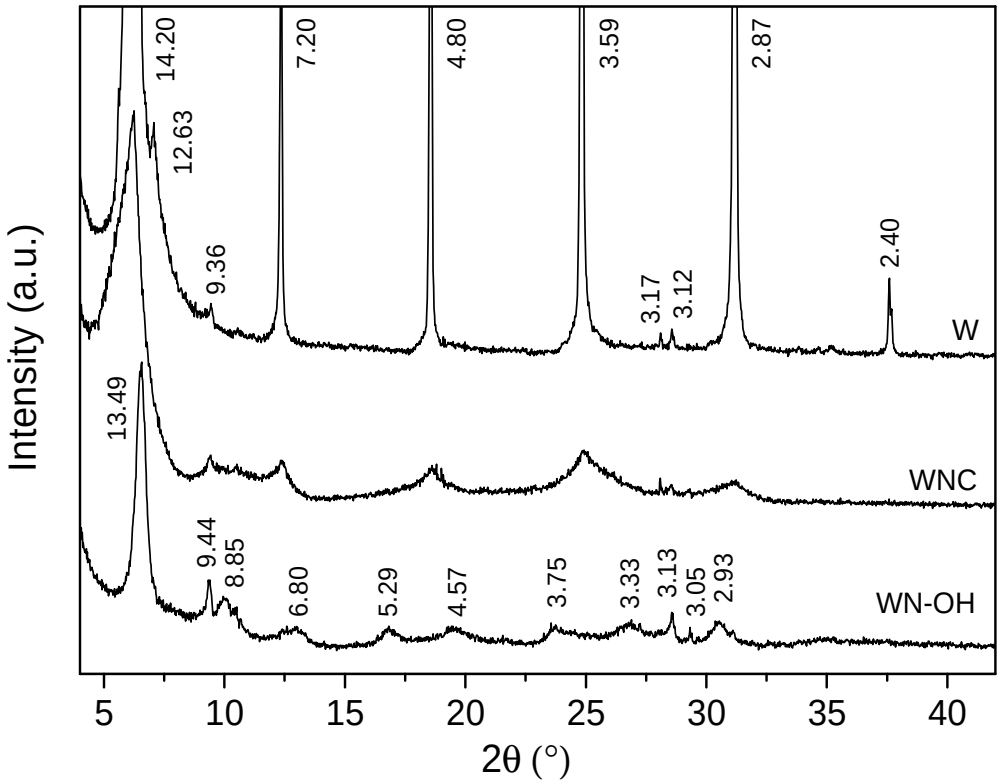

Figure. A.3.5 Phase composition of raw (W), acid treated (WNC) and NaOH treated (WN-OH) vermiculite.

S.3.3.5 DRIFT

The analysis showed multiple peaks in the range between 3700 and 3100 cm^{-1} that is attributed to stretching vibrations of proton against oxygen in bound hydroxyl groups (Stubičan and Roy, 1961; Pansou and Gautheyrou, 2006; Chukanov, 2014). The range between 1200 and 800 cm^{-1} corresponds to vibrations in the silicate anion and vibrations of silica-oxygen bonds (Pansou and Gautheyrou, 2006). Some of these bands correspond to Si-O-Si linkages at the surface of the clay layers, other to Si-O bond directed towards the octahedrally coordinated aluminum ions at the center of the layer (Cole, 2008). The bands in the lover range correspond to high-force-strength octahedral cations like Fe^{3+} and Al^{3+} with charge >2 (Chukanov, 2014), bending and deformation vibrations in octahedral layer (e.g. Al-OH, Al-Mg-OH) (Liu et al., 2011). Also a band at around 1635 cm^{-1} is attributed to HOH bending vibrations (Chukanov, 2014) appears in all spectra.

In the spectrum of the raw material a dominant peak at 3377 cm^{-1}, OH-stretching in weakly bonded water molecules (Chmielarz et al., 2012), became broader and shifted to 3400 cm^{-1} after acid activation, after NaOH treatment its intensity decreased and it shifted to 3447 cm^{-1}.

In the spectrum of the raw and the acid activated vermiculite a peak corresponding to vibration in Fe_2OH or AlFeOH (Besson and Drits, 1997; Parikh et al., 2014) was found at around 3555 cm^{-1} and a peak assigned to stretching vibration in Al_2OH (Madejová and Komadel, 2001) at 3227 cm^{-1}. A shift towards higher wavenumbers of these peaks was observed after NaOH treatment (Fig. A.3.6). A band associated with vibrations in Mg_3OH (Parikh et al., 2014) is present at 3675 cm^{-1} in each sample without significant changes in its intensity. After the NaOH treatment heterogeneity of the species giving vibrations in the lower wavenumbers range decreased and only bands attributed to AlFeOH (Madejová and Komadel, 2001) at 866 cm^{-1}, tetrahedral Al–O out-of-plane and Al–O–Si in-plane vibrations (Madejová and Komadel, 2001) remained at 817 cm^{-1} and 758 cm^{1}, respectively.

In the spectra of the materials sharp peaks at 992, 1015, and 1010 cm^{-1} corresponding to stretching vibrations of Si-O (Stubičan and Roy, 1961; Ritz et al., 2014) were observed with a shoulder at 1075 cm^{-1} due to amorphous silica (Ritz et al., 2014). Other peaks ascribed to amorphous silica are well visible in the acid activated vermiculite: 1180, 1050, 995 and 815 cm^{-1} (Chmielarz et al., 2012; Barabaszová and Valášková, 2013). The band at 795 cm^{-1} in the acid treated material can be attributed to free silica (Belver et al., 2002). The peak at 671 cm^{-1} appeared in all spectra and is attributed to asymmetric bending of SiO_4 tetrahedron (Chukanov, 2014). The band present in the raw and the acid treated material at 664 cm^{-1} attributed to Si-O bending (Stubičan and Roy, 1961) disappears after the NaOH treatment. Spectra are presented in Fig. A.3.6.

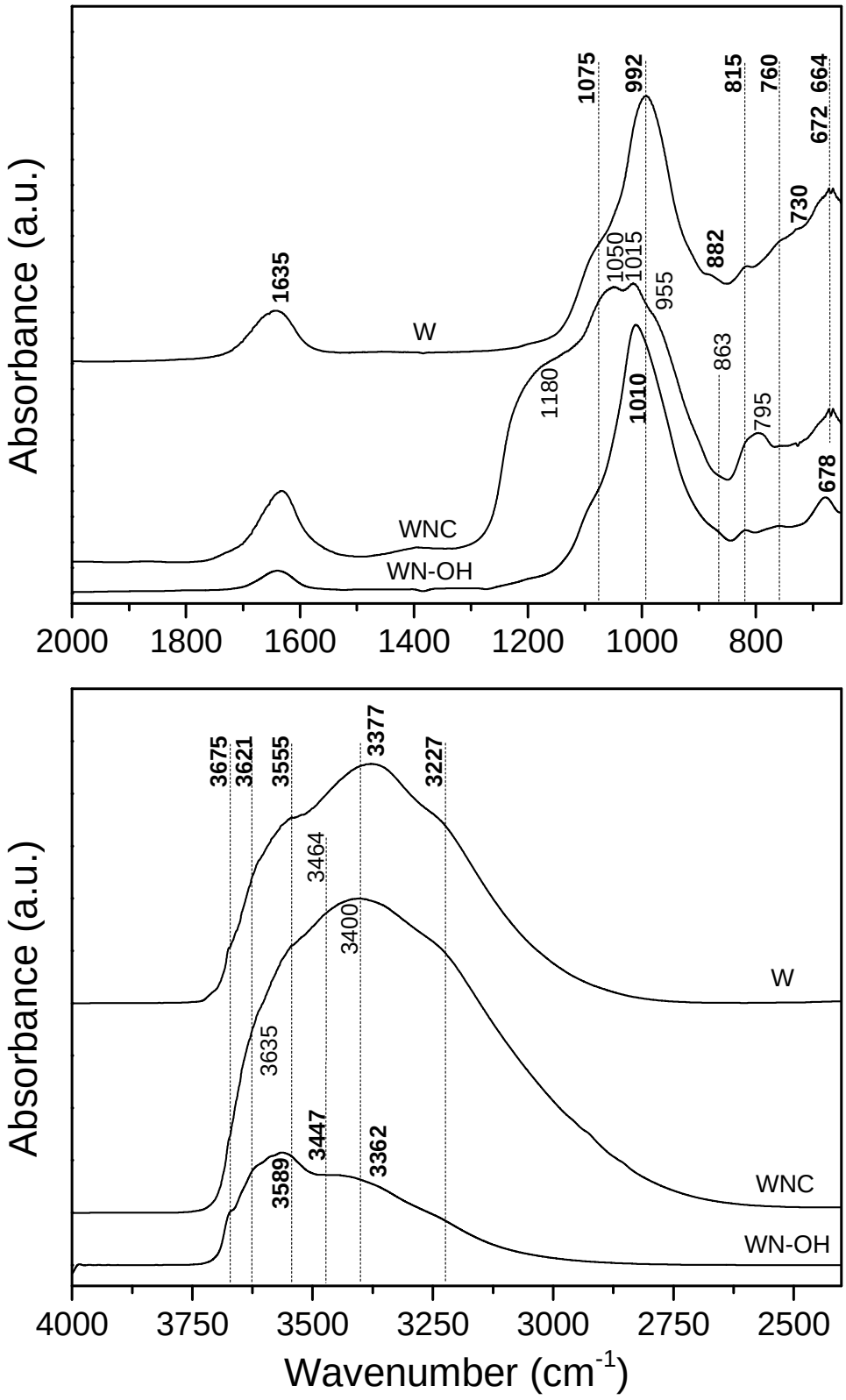

Figure. A.3.6 DRIFT spectra of the starting (W), acid treated (WNC) and NaOH treated (WN-OH) materials.

S.3.4 Kinetic and equilibrium experiments

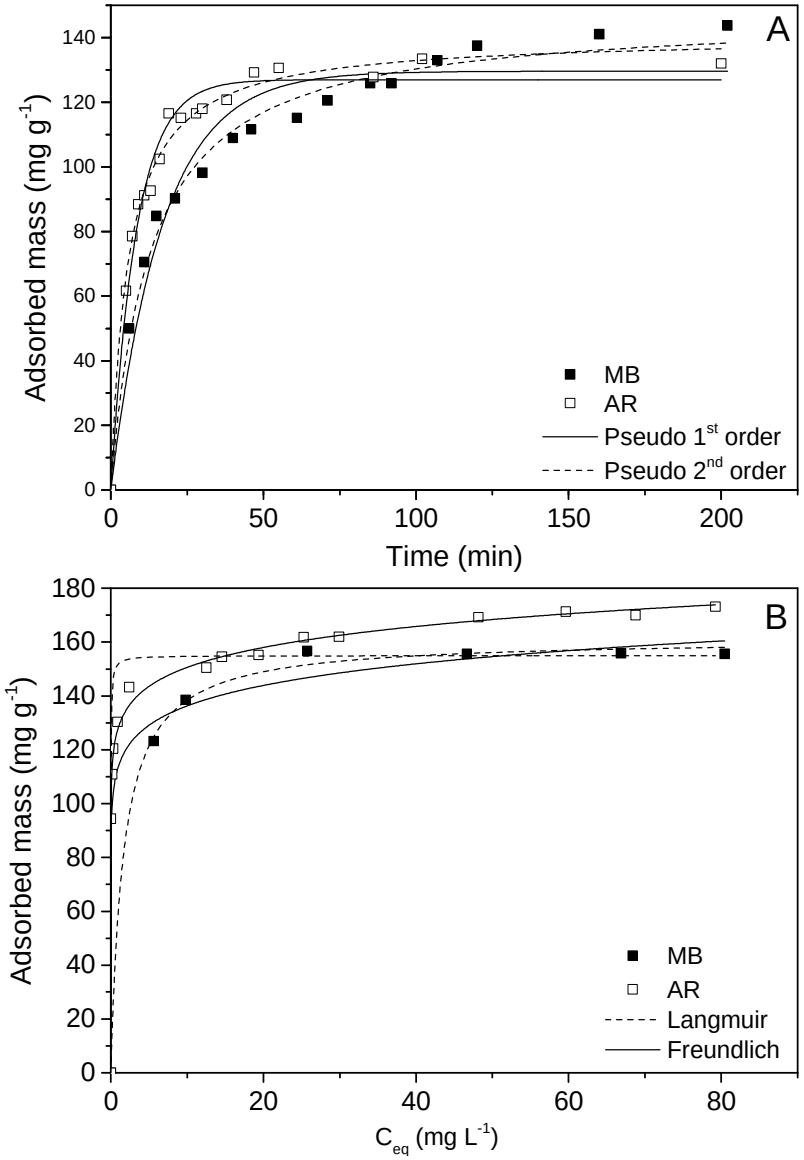

Figure. A.3.7 Kinetic model fitted to the experimental data (250 mg of vermiculite, 500 mL of 100 mg L^{-1} dye solution, no pH adjustment, temperature 24 °C) (A), and equilibrium model fitted to the experimental data (10 – 250 mg of vermiculite, 50 mL of 50 and 100 mg L^{-1} dye solution, no pH adjustment, 2 h at temperature 24 °C)
(B) for adsorption of MB and AR over NaOH treated vermiculite.

S.3.5 Column experiments

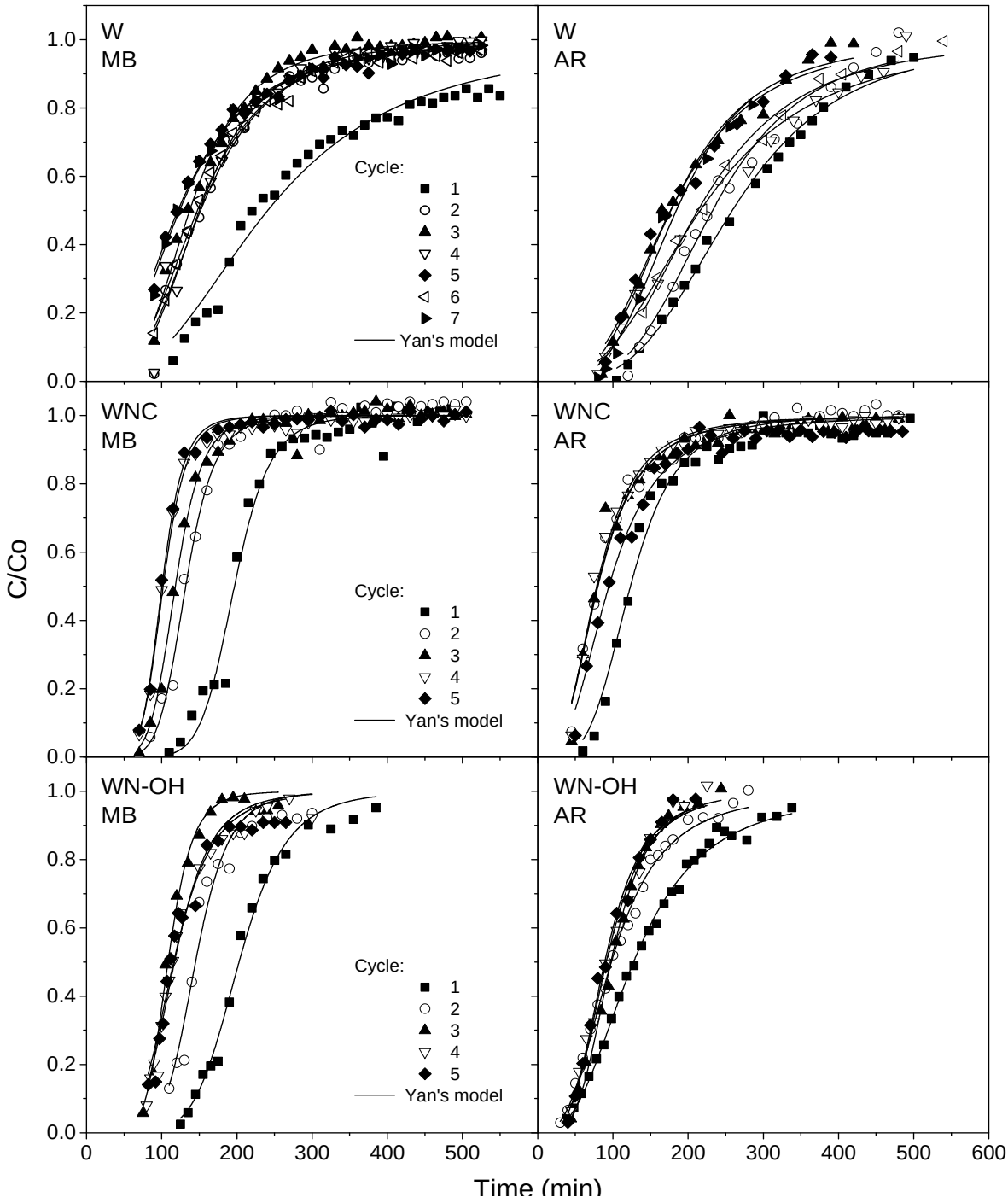

Figure. A.3.8 Yan's model fitted to the experimental data of adsorption cycles for MB and AR on starting (W), acid activated (WNC) and NaOH treated vermiculite (WN-OH).

Table A.3.1 Yan's model parameters for adsorption cycles of AR and MB over starting (W), acid treated (WNC) and NaOH treated material (WN-OH).

Material	Dye	Parameter	Cycle number I	II	III	IV	V	VI	VII
W	MB	q_Y (mg g^{-1})	48 ± 2	30 ± 1	27.4 ± 0.6	30.0 ± 0.8	24.3 ± 0.6	29.5 ± 0. 6	24.7 ± 0.6
		a_Y	2.6 ± 0.2	3.2 ± 0.2	3.6 ± 0.2	3.5 ± 0.4	2.5 ± 0.2	3.1 ± 0.2	2.6 ± 0.2
		s^2	0.00166	0.00109	0.000517	0.00118	0.000327	0.000388	0.000292
		R^2_{adj}	0.977	0.986	0.993	0.986	0.994	0.995	0.995
	AR	q_Y (mg g^{-1})	52 ± 1	46 ± 2	35 ± 1	43 ± 2	35 ± 1	43 ± 1	40 ± 2
		a_Y	3.6 ± 0.2	3.7 ± 0.4	3.3 ± 0.4	2.8 ± 0.4	3.1 ± 0.5	3.2 ± 0.5	3.6 ± 0.7
		s^2	0.000568	0.0018	0.00152	0.00169	0.00119	0.00076	0.00159
		R^2_{adj}	0.995	0.984	0.987	0.987	0.988	0.993	0.986
WNC	MB	q_Y (mg g^{-1})	166 ± 4	112 ± 2	104 ± 2	90 ± 2	89 ± 2	-	-
		a_Y	8.4 ± 1	7 ± 1	6.7 ± 0.8	6.7 ± 0.8	7.0 ± 0.6		
		s^2	0.0027	0.00118	0.000868	0.000586	0.000429		
		R^2_{adj}	0.981	0.99	0.991	0.992	0.994		
	AR	q_Y (mg g^{-1})	115 ± 4	75 ± 2	70 ± 4	69 ± 2	76 ± 4	-	-
		a_Y	4.1 ± 0.6	2.9 ± 0.2	2.9 ± 0.4	3.0 ± 0.2	2.8 ± 0.2		
		s^2	0.00184	0.000851	0.00151	0.00072	0.00113		
		R^2_{adj}	0.981	0.988	0.979	0.99	0.985		
WN-OH	MB	q_Y (mg g^{-1})	203 ± 4	145 ± 7	108 ± 2	117 ± 4	116 ± 4	-	-
		a_Y	6.4 ± 0.9	7 ± 2	7 ± 1	4.9 ± 0.6	4.5 ± 0.8		
		s^2	0.00151	0.00458	0.00132	0.00202	0.00337		
		R^2_{adj}	0.988	0.949	0.987	0.979	0.955		
	AR	q_Y (mg g^{-1})	127 ± 2	98 ± 2	97 ± 2	91 ± 4	89 ± 2	-	-
		a_Y	2.7 ± 0.2	2.9 ± 0.2	3.9 ± 0.2	3.5 ± 0.4	3.5 ± 0.4		
		s^2	0.00032	0.000583	0.00054	0.00116	0.000906		
		R^2_{adj}	0.997	0.995	0.996	0.991	0.993		

Table A.3.2 Yoon-Nelson's model parameters for adsorption cycles over starting (W), acid treated (WNC) and NaOH treated material (WN-OH).

Material	Dye	Parameter	Cycle number						
			I	II	III	IV	V	VI	VII
W	MB	k_{YN} (min^{-1})	0.010 ± 0.002	0.019 ± 0.004	0.022 ± 0.002	0.020 ± 0.002	0.016 ± 0.002	0.0180 ± 0.00	0.016 ± 0.002
		τ_{YN} (min)	256 ± 16	158 ± 8	142 ± 4	156 ± 6	126 ± 10	154 ± 6	1 28 ± 8
		s^2	0.00562	0.00307	0.00094	0.0022	0.00219	0.00197	0.00188
		R^2_{adj}	0.921	0.961	0.989	0.974	0.959	0.973	0.967
	AR	k_{YN} (min^{-1})	0.014 ± 0.002	0.015 ± 0.002	0.017 ± 0.004	0.012 ± 0.002	0.016 ± 0.002	0.013 ± 0.002	0.021 ± 0.006
		τ_{YN} (min)	271 ± 6	241 ± 11	187 ± 11	241 ± 15	186 ± 11	223 ± 9	194 ± 19
		s^2	0.00116	0.00334	0.00364	0.00225	0.0026	0.000974	0.00493
		R^2_{adj}	0.989	0.969	0.969	0.989	0.974	0.99	0.959
WNC	MB	k_{YN} (min^{-1})	0.043 ± 0.008	0.052 ± 0.008	0.058 ± 0.008	0.068 ± 0.001	0.071 ± 0.008		
		τ_{YN} (min)	198 ± 4	134 ± 2	120 ± 2	103 ± 2	101 ± 2	-	-
		s^2	0.0027	0.00129	0.00129	0.000949	0.0006785		
		R^2_{adj}	0.981	0.989	0.987	0.988	0.991		
	AR	k_{YN} (min^{-1})	0.035 ± 0.008	0.032 ± 0.006	0.034 ± 0.008	0.036 ± 0.006	0.028 ± 0.006		
		τ_{YN} (min)	126 ± 6	85 ± 6	84 ± 6	83 ± 6	100 ± 6	-	-
		s^2	0.00371	0.00264	0.00375	0.00252	0.0029		
		R^2_{adj}	0.962	0.964	0.947	0.964	0.961		
WN-OH	MB	k_{YN} (min^{-1})	0.033 ± 0.006	0.05 ± 0.02	0.06 ± 0.02	0.04 ± 0.02	0.04 ± 0.01		
		τ_{YN} (min)	205 ± 6	146 ± 7	110 ± 4	119 ± 4	117 ± 6	-	-
		s^2	0.00269	0.0063	0.00232	0.00408	0.00572		
		R^2_{adj}	0.978	0.929	0.977	0.958	0.924		
	AR	k_{YN} (min^{-1})	0.020 ± 0.002	0.028 ± 0.002	0.039 ± 0.002	0.036 ± 0.004	0.038 ± 0.007		
		τ_{YN} (min)	137 ± 5	105 ± 5	101 ± 2	96 ± 4	94 ± 4	-	-
		s^2	0.00177	0.00153	0.000502	0.00113	0.0021		
		R^2_{adj}	0.981	0.986	0.999	0.991	0.984		

Table A.3.3 Parameters of Yan's and Yoon-Nelson's models fitted to the experimental data for co-adsorption of MB and AR over starting (W), acid treated (WNC) and NaOH treated vermiculite (WN-OH) in column system.

Model		Yan's Model		Yoon-Nelson's Model		
Material/Dye	Parameter	MB	AR	MB		AR
W	q_y	65 ± 4 mg g^{-1}	30 ± 1 mg g^{-1}	τ_{YN} (min)	137 ± 14	60 ± 3
		0.20 ± 0.01 mmol g^{-1}	0.075 ± 0.003 mmol g			
	a	2.5 ± 0.4	8 ± 2	k_{YN} (min^{-1})	0.020 ± 0.005	0.13 ± 0.04
	R^2_{adj}	0.961	0.965	R^2_{adj}	0.892	0.962
	s^2	0.00359	0.0021	s^2	0.01001	0.00224
WNC	q_y	126 ± 2 mg g^{-1}	44 ± 1 mg g^{-1}	τ_{YN} (min)	257 ± 5	89 ± 3
		0.395 ± 0.006 mmol g^{-1}	0.110 ± 0.003 mmol g			
	a	5.6 ± 0.4	6 ± 1	k_{YN} (min^{-1})	0.022 ± 0.002	0.07 ± 0.01
	R^2_{adj}	0.995	0.99	R^2_{adj}	0.992	0.99
	s^2	0.0007	0.000978	s^2	0.00126	0.00097
WN-OH	q_y	156 ± 4 mg g^{-1}	73 ± 1 mg g^{-1}	τ_{YN} (min)	327 ± 10	146 ± 2
		0.50 ± 0.01 mmol g^{-1}	0.183 ± 0.003 mmol g			
	a	5.3 ± 0.6	10 ± 2	k_{YN} (min^{-1})	0.019 ± 0.003	0.07 ± 0.01
	R^2_{adj}	0.984	0.991	R^2_{adj}	0.968	0.992
	s^2	0.0021	0.00101	s^2	0.00427	0.00095

S.3.6 Desorption experiments

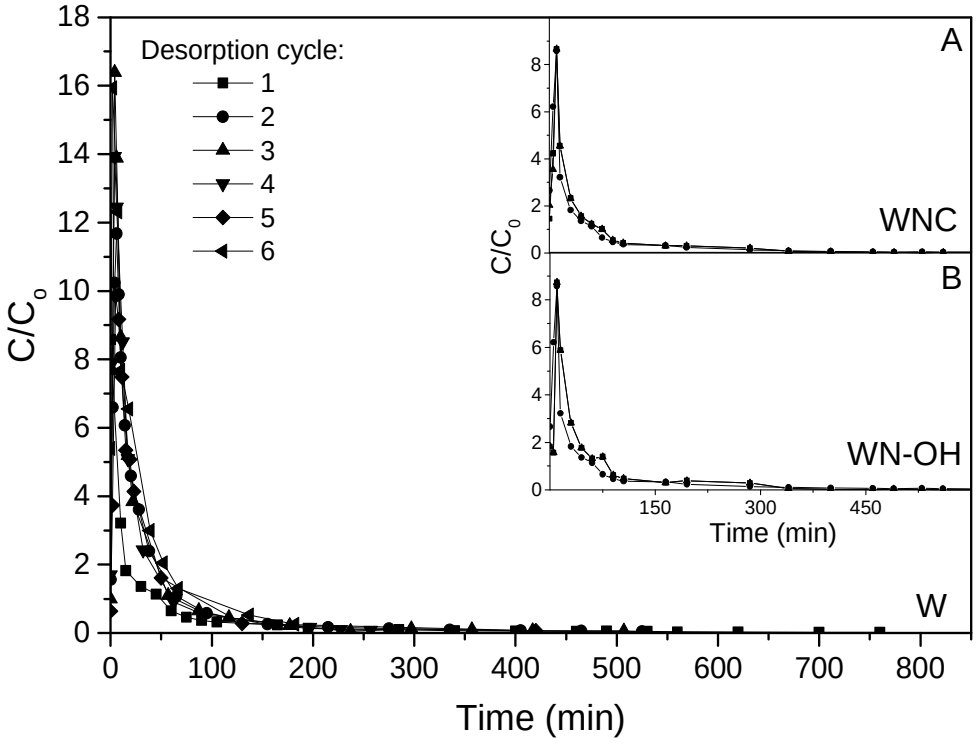

Figure A.3.9 Desorption curves of AR from raw material; Insertion A – desorption from WNC, Insertion B – desorption from WN-OH.

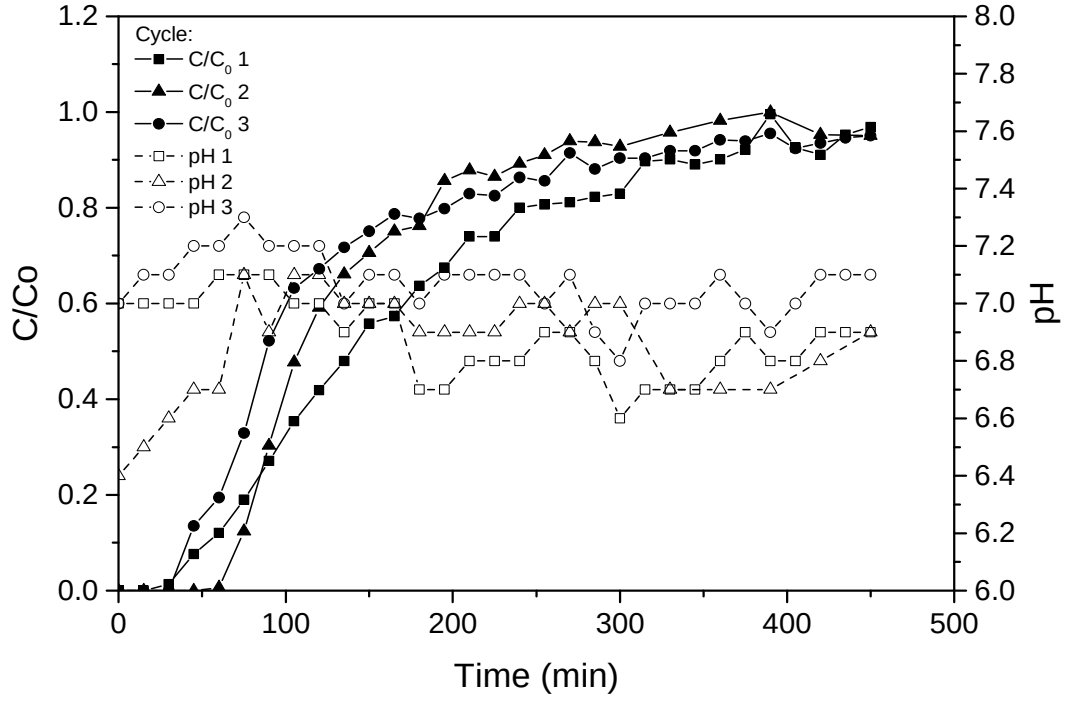

Figure A.3.10 Changes of adsorbate concentration and pH of the effluent during adsorption cycles of AR over NaOH treated vermiculite (WN-OH).

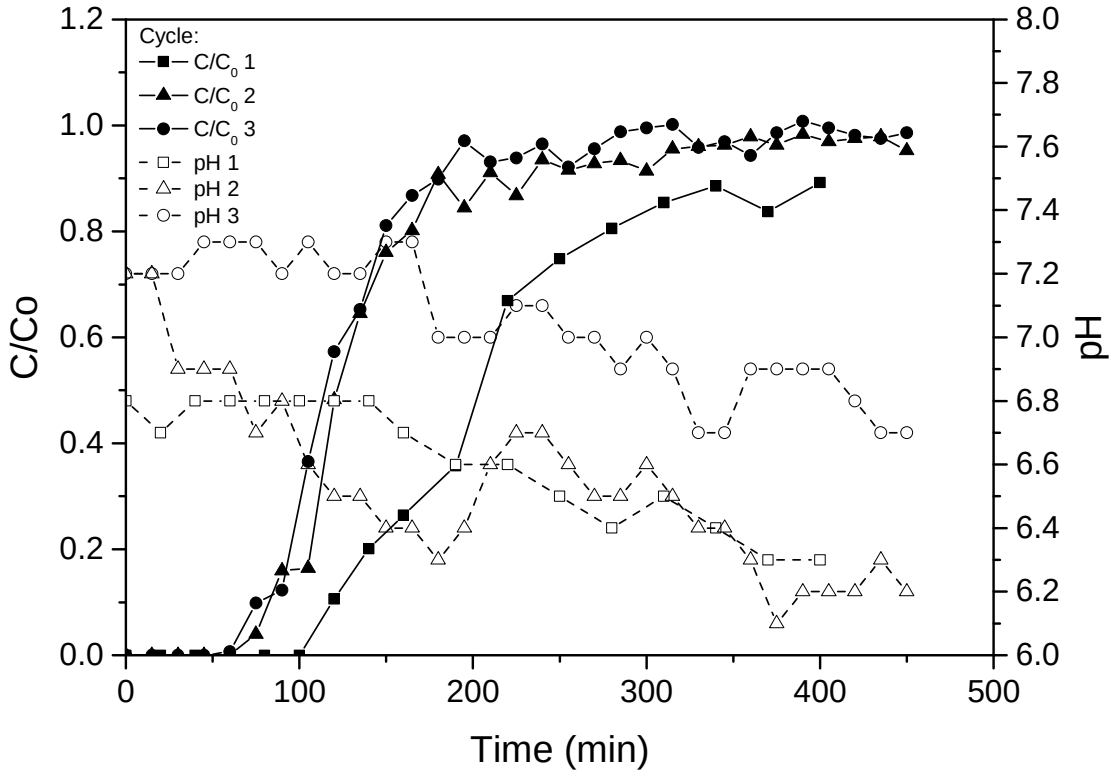

Figure A.3.11 Changes of adsorbate concentration and pH of the effluent during adsorption cycles of MB over NaOH treated vermiculite (WN-OH).

S.3.6 References

Barabaszová, K.Č., Valášková, M., 2013. Characterization of vermiculite particles after different milling techniques. Powder Technol. 239, 277-283.

Belver, C., Bañares Muñoz, M.A., Vicente, M.A., 2002. Chemical Activation of a Kaolinite under Acid and Alkaline Conditions. Chem. Mater. 14, 2033-2043.

Besson, G., Drits, V.A., 1997. Refined relationships between chemical composition of dioctahedral fine-grained mica minerals and their infrared spectra within the oh stretching region. Part I: identification of the oh stretching bands. Clay and Clay Minerals 45, 158-169.

Carrado, K.A., Decarreau, A., Petit, S., Bergaya, F., Lagaly, G., 2006. Synthetic clay minerals and purification of natural clays. in: Bergaya, F., Theng, B.K.G., Lagaly, G. (Eds.). Handbook of Clay Science. Elsevier Ltd.

Chmielarz, L., Wojciechowska, M., Rutkowska, M., Adamski, A., Węgrzyn, A., Kowalczyk, A., Dudek, B., Boroń, P., Michalik, M., Matusiewicz, A., 2012. Acid-activated vermiculites as catalysts of the DeNOx process. Catal. Today 191, 25-31.

Chukanov, N.V., 2014. Infrared spectra of mineral species. Extended library.

Cole, K.C., 2008. Use of Infrared Spectroscopy To Characterize Clay Intercalation and Exfoliation in Polymer Nanocomposites. Macromolecules 41, 834-843.

El Mouzdahir, Y., Elmchaouri, A., Mahboub, R., Gil, A., Korili, S.A., 2009. Synthesis of nano-layered vermiculite of low density by thermal treatment. Powder Technol. 189, 2-5.

Freundlich, H.M.F., 1906. Über die adsorption in läsungen. Z. Phys. Chem. 57, 385-470.

Greluk, M., Hubicki, Z., 2010. Kinetics, isotherm and thermodynamic studies of Reactive Black 5 removal by acid acrylic resins. Chem. Eng. J. 162, 919-926.

Harraz, H.Z., Hamdy, M.M., 2010. Interstratified vermiculite–mica in the gneiss–metapelite–serpentinite rocks at Hafafit area, Southern Eastern Desert, Egypt: From metasomatism to weathering. Journal of African Earth Sciences 58, 305-320.

Ho, Y.S., 2004. Citation review of Lagergren kinetic rate equation on adsorption reactions. Scientometrics 59, 171-177.

Ho, Y.S., McKay, G., 1999. Pseudo-second order model for sorption processes. Process Biochem. 34, 451-465.

Kalinowski, B.E., Schweda, P., 2007. Rates and nonstoichiometry of vermiculite dissolution at 22°C. Geoderma 142, 197-209.

Lagergren, S., 1898. About theory of so-called adsorption of soluble substances. Kongl. Vetenskaps Academiens Handlingar 24, 1-39.

Langmuir, I., 1918. The adsorption of gases on plane surfaces of glass, mica and platinum. J. Am. Chem. Soc. 40, 1361-1403.

Liu, D., Yuan, P., Liu, H., Cai, J., Qin, Z., Tan, D., Zhou, Q., He, H., Zhu, J., 2011. Influence of heating on the solid acidity of montmorillonite: A combined study by DRIFT and Hammett indicators. Appl. Clay Sci. 52, 358-363.

Madejová, J., Komadel, P., 2001. Baseline studies of the clay minerals society source clays: infrared methods. Clays Clay Miner. 49, 410-432.

Maqueda, C., Romero, A.S., Morillo, E., Pérez-Rodríguez, J.L., 2007. Effect of grinding on the preparation of porous materials by acid-leached vermiculite. J. Phys. Chem. Solids 68, 1220-1224.

Marczewski, A.W., 2010. Application of mixed order rate equations to adsorption of methylene blue on mesoporous carbons. Appl. Surf. Sci. 256, 5145-5152.

Mareschal, L., Ranger, J., Turpault, M.P., 2009. Stoichiometry of a dissolution reaction of a trioctahedral vermiculite at pH 2.7. Geochim. Cosmochim. Acta 73, 307-319.

Muiambo, H.F., Focke, W.W., Atanasova, M., der Westhuizen, I.v., Tiedt, L.R., 2010. Thermal properties of sodium-exchanged palabora vermiculite. Appl. Clay Sci. 50, 51-57.

Oberlin, A., Couty, R., 1970. Conditions of kaolinite formation during alternation of smoe silicates by water at 200 °C. Clays nad Clay Minerals 19, 47-356.

Pansou, M., Gautheyrou, J., 2006. Handbook of Soil Analysis. Mineralogical, Organic and Inorganic Methods. Springer.

Parikh, S.J., Goyne, K.W., Margenot, A.J., Mukome, F.N.D., Calderón, F.J., 2014. Chapter One - Soil Chemical Insights Provided through Vibrational Spectroscopy. in: Donald, L.S. (Ed.). Advances in Agronomy. Academic Press, pp. 1-148.

Ritz, M., Zdrálková, J., Valášková, M., 2014. Vibrational spectroscopy of acid treated vermiculites. Vib. Spectrosc. 70, 63-69.

Sakharov, B.A., Lindgreen, H., Salyn, A.L., Drits, V.a., 1999. Mixed-layer kaolinite-illite-vermiculite in North Sea shales. Clay Miner. 34, 333-334.

Santos, S.S.G., Silva, H.R.M., de Souza, A.G., Alves, A.P.M., da Silva Filho, E.C., Fonseca, M.G., 2015. Acid-leached mixed vermiculites obtained by treatment with nitric acid. Appl. Clay Sci. 104, 286-294.

Steudel, A., 2008. Selection Strategy and Modification of Layer Silicates for Technical Applications. Univ.-Verlag Karlsruhe.

Stubičan, V., Roy, R., 1961. Infrared Spectra of Layer-Structure Silicates. J. Am. Ceram. Soc. 44, 625-627.

Yan, G., Viraraghavan, T., Chen, M., 2001. A new model for heavy metal removal in a biosorption column. Adsorpt. Sci. Technol. 19, 25-43.

Yoon, Y.H., Nelson, J.H., 1984. Application of gas adsorption kinetics--II. A theoretical model for respirator cartridge service life and its practical applications. Am. Ind. Hyg. Assoc. J. 45, 517-524.

CHAPTER 4

Base treatment of vermiculite

Science of the Total Environment 576 (2017) 398–408

Contents lists available at ScienceDirect

Science of the Total Environment

journal homepage: www.elsevier.com/locate/scitotenv

Simultaneous removal of dyes and metal cations using an acid, acid-base and base modified vermiculite as a sustainable and recyclable adsorbent

Wojciech Stawiński[a], Agnieszka Węgrzyn[b*], Olga Freitas[a], Lucjan Chmielarz[b], Grzegorz Mordarski[c] , Sónia Figueiredo[a]

[a] *REQUIMTE, LAQV, Instituto Superior de Engenharia do Porto, Instituto Politécnico do Porto, Rua Dr. António Bernardino de Almeida 431, 4200-072 Porto, Portugal*
stawor@gmail.com; omf@isep.ipp.pt; saf@isep.ipp.pt

[b] *Faculty of Chemistry, Jagiellonian University, ul. Ingardena 3, 30-060 Kraków, Poland*
wegrzyn@chemia.uj.edu.pl; chmielar@chemia.uj.edu.pl

[c] *Jerzy Haber Institute of Catalysis and Surface Chemistry Polish Academy of Sciences ul. Niezapominajek 8, 30-239 Kraków, Poland*
nbmordar@cyf-kr.edu.pl

Abstract

The aim of this work was the modification of vermiculite in order to produce a low cost, efficient and sustainable adsorbent for dyes and metals. Three activation methods consisting of acid, base and combined acid/base treatment were applied to improve the of vermiculite's adsorption properties. Adsorbents were tested in single, bi- and tricomponent solutions containing cationic dyes and Cu^{2+} cations. The raw material showed low adsorption capacity for dyes and metal. The acid/base treated vermiculite had very good adsorption capacity toward dyes whilst the maximum adsorption capacity for Cu^{2+} did not change comparing to the starting material. The alkaline treated vermiculite was a good adsorbent for metals, while still being able to remove dyes on the level of the not treated material. Moreover, it was shown that the materials may be regenerated and used in several adsorption-desorption cycles. Furthermore, it was possible to separate adsorbed dyes from metals that were desorbed, using as eluents ethanol/NaCl and 0.05M HNO_3, respectively. This opens a possibility for sustainable disposal and neutralization of both of the pollutants or for their further applications in other processes.

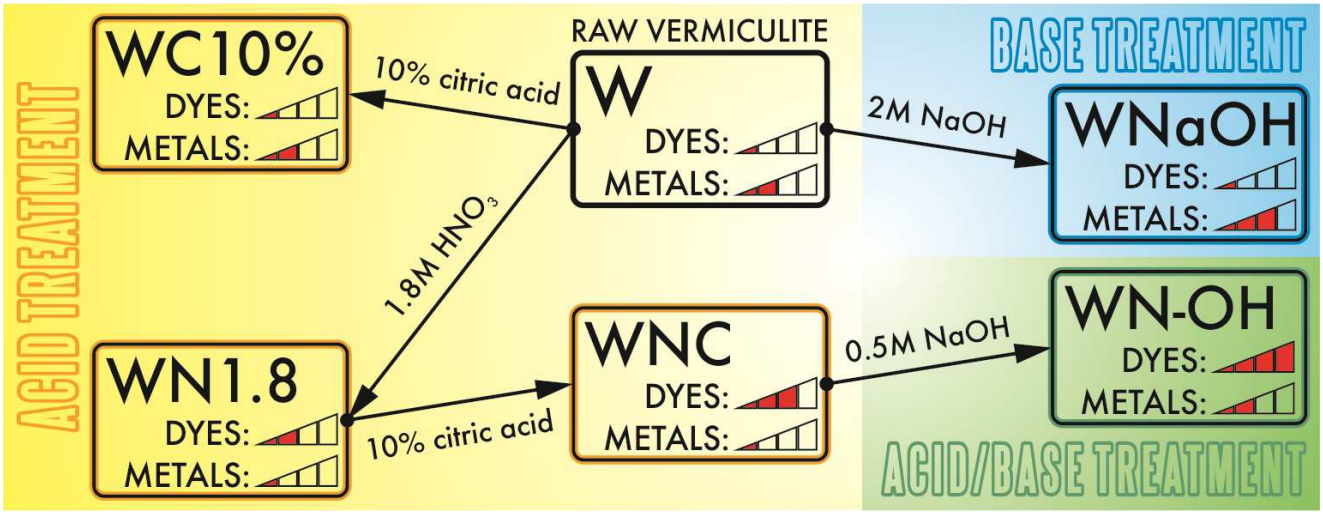

Keywords: waste prevention; dyes and metals removal; adsorption; activation of clays; adsorbent regeneration

4.1 Introduction

Although water is wide spread all over the world, it is not always available in sufficient quantity and with the necessary quality. Therefore this scarce good should be preserved and protected from the effects of pollution. Dyes are common pollutants in effluents discharged by various industries such as paper, plastics, food, cosmetics, and textile (Rozada et al., 2003; Angın et al., 2013). They usually have complex molecular structure, being refractory to biological treatments. Their presence in the aquatic environment reduces the penetration of light and consequently reduces photosynthetic activity of primary producers and some of them may be toxic or carcinogenic (Reife and Freeman, 1996; Forgacs et al., 2004; Bhatnagar and Jain, 2005). Heavy metals have been reported to affect cellular organelles and components, and some enzymes involved in metabolism, detoxification and damage repair (Wang and Shi, 2001). Moreover, they have bioaccumulative nature in biotic systems and pose a threat to human beings and animals even at low concentrations (Gautam et al., 2015). They are found among the most common pollutants and often accompany dyes in wastewaters (Pereira and Alves, 2011). Since wastewater treatment is often expensive, United Nation studies show that high-income developed nations treat about 70 % of their wastewaters, while only 8 % receives treatment in low-income developing nations (Monsalvo, 2016). Coagulation/flocculation methods are often applied to remove metals and dyes from wastewaters. However, the application of chemicals and the generation of hazardous sludge contribute to high operation cost (Mall et al., 2005). The application of adsorption to wastewaters treatment has been increasing (Leitão and Serrão, 2005) as it is considered one of the best wastewater treatment methods due to its universal nature, insensibility to toxicants, easy operation, high removal efficiency and possibility to recycle and reuse many adsorbents (Pan et al., 2009; Ali et al., 2012). It is desirable to use an adsorbent that is easy available in nature, inexpensive and non-hazardous (Ali et al., 2012). The development of materials derived from sustainable and renewable resource has been encouraged (Ummartyotin et al., 2016).

Clays, being a natural mineral and low cost material, show good perspectives in this field. The interest in clays and their modification has been increasing due to their outstanding properties, high thermal and chemical resistance, as well as high porosity (Ummartyotin et al., 2016). They are minerals with layered structure build of phyllosilicate sheets that may carry a charge. If a charge is present it is balanced by a counter ion located between the layers. These charge balancing ions can be exchanged giving clays good ion-exchange properties (Bergaya and Lagaly, 2006). Vermiculite is a clay build of an octahedral sheet sandwiched between two tetrahedral sheets, classified as 2:1

phyllosilicate (Bailey and Chairman, 1980; Rieder et al., 1998) and due to possibility of various modification in order to enhance its adsorption efficiency, it is a good precursor for sustainable adsorbents production to be used in water and wastewater treatment (Liu et al., 2010; Ali et al., 2012).

So far not much is known about the interactions between dyes and metals in binary systems, even less about interactions in multi-component solutions (Česuniene et al., 2013) and the literature on adsorption process is mainly related to mono-component solutions. The presence of several pollutants in the same solution may significantly affect the removal performance of the adsorbent (Hernandez-Eudave et al., 2016). The interaction between dyes and adsorbents may vary in the presence of heavy metals as well as the presence of dyes may change the behavior of heavy metals toward adsorbent. Some multicomponent studies have been performed with metals and dyestuffs, namely with methylene blue (MB), Cd^{2+}, Cu^{2+} and Ni^{2+} on fly ash modified with NaOH (Duta and Visa, 2015), MB and Cu^{2+} on wheat straw (Wu et al., 2009) showing high removal efficiencies despite the competitive behavior.

Competitive adsorption of Congo Red (CR) and Cu^{2+} by chitosan hydrogel in a binary adsorption studies revealed that the addition of the metal reduced adsorption capacity for CR by 25% while adsorption of Cu^{2+} was increased in the presence of CR (Teng et al., 2009). Synergic effect on the adsorption of Acid Blue 25 (AB25) and Cd^{2+} and Zn^{2+} was observed in adsorption from binary solution on physically activated bituminous carbon and a phosphoric activated carbon from wood (Tovar-Gómez et al., 2012). Coadsorption studies of Cu^{2+} and Lanasyn Navy M-DNL dye on activated carbon revealed different behavior along with time (Česuniene et al., 2013). The removal of three basic dyes by adsorption onto bentonite has shown competitive behavior (Turabık and Gozmen, 2013). Adsorption of dye AB25 and Ni^{2+} and Zn^{2+} was investigated in packed bed column system and revealed strong synergic adsorption of heavy metals on activated carbon caused by the presence of the dye (Hernandez-Eudave et al., 2016).

One of the most common methods of clays treatment is acid activation. It was shown that silica nano-sheets derived from vermiculite via acid leaching process are efficient for MB removal (Zhao et al., 2008). As shown in previous studies (Stawiński et al., 2016), such modifications with nitric acid followed by washing in citric acid resulted in an increase in adsorption capacity of the material. Also, as reported in another study (Stawiński et al., 2014), it was found out that if acid activated vermiculite is additionally treated with a base at the end of modification process, the increase in the adsorption capacity is even bigger. Both activated materials were tested for adsorption of dyes. However, the problem of heavy metals was not raised.

The present research was focused on modifications in order to increase vermiculite's adsorption capacity simultaneously for organic (dyestuffs) and inorganic (metals) compounds, which are commonly found in industrial wastewaters. The materials were tested in single-, bi- and tri-component solutions, containing two cationic dyes and copper cations, using batch and column systems. Also intensive and thorough studies were conducted on desorption of the adsorbates and regeneration of the adsorbent.

4.2 Experimental Section

4.2.1 Adsorbate

Two basic dyestuffs methylene blue (MB), CI 52015, supplied by Riedel de Haen and astrazon red FBL 200% (AR), CI 85496-37-3, supplied by Dystar, were used for adsorption experiments. The molecular structures of the dyes are illustrated in Fig. S.4.1 in the Supporting Material. Analytical grade salt, $CuCl_2$, obtained from Sigma-Aldrich was employed for preparation of Cu^{2+} solutions. Adsorbate concentration was measured using UV-VIS spectrophotometer (Thermo Scientific, Evolution 300) at the maximum absorbance wavelength (665 nm for MB and 531 nm for AR) in the case of dyes and using atomic absorption spectroscopy (AAS) (Analytic Jena High-Resolution Continuum Source Atomic Absorption Spectrometer, ContrAA 700) in the case of Cu^{2+}.

4.2.2 Adsorbents preparation

Vermiculite from South Africa (raw vermiculite, W) was kindly supplied by ROMINCO POLSKA Sp. z o.o. and was used as starting material for adsorbents preparation. A simplified scheme for all treatments carried out in the research is presented in Fig.4.1.

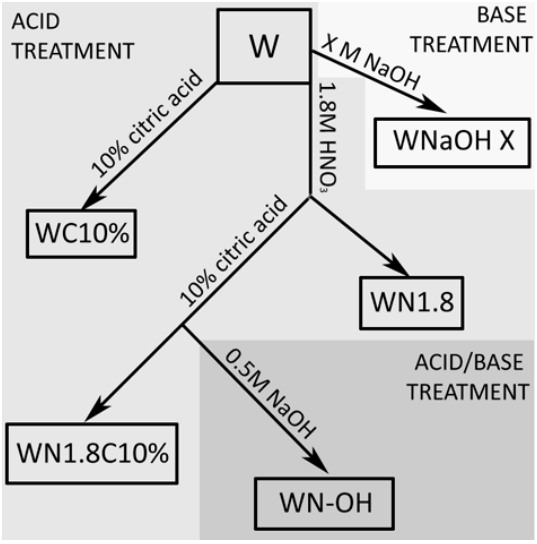

Figure 4.1. Scheme of preparation of the acid, acid/base and base treated vermiculites.

4.2.2.1 Base treatment

Weighted portions of 5 g of W were placed in Erlenmeyer flasks with caps and mixed with 50 mL of NaOH solution, with different concentrations varying from 0.005 to 6 M, at room temperature (24 °C). After 2 h stirring, they were centrifuged, washed in deionized water in cycles (5 cycles, 4500 rpm 5 min each) of repeated centrifugation (Sartorius, Sigma 2-16) and left to dry, originating the following materials: WNaOH0.005, WNaOH0.01, WNaOH0.05, WNaOH0.1, WNaOH0.5, WNaOH1, WNaOH1.5, WNaOH2, WNaOH3, WNaOH4, WNaOH5 and WNaOH6. Additionally the experiment was repeated for NaOH concentrations of 2 and 6 M, then samples were stirred for 1, 2, 4, 24 and 72 h, in order to produce the following materials: WNaOH2-H1, WNaOH2-H2, WNaOH2-H4, WNaOH2-H24, WNaOH2-H72, WNaOH6-H1, WNaOH6-H2, WNaOH6-H4, WNaOH6-H24 and WNaOH6-H72.

4.2.2.2 Acid and acid/base treatment

The preparation of acid and acid/base activated materials included different steps. i) Portions of 10 g of W were placed in Erlenmeyer flasks (with a condenser) then 100 mL of 1.8 M nitric acid solution was added and left in constant stirring at 98 °C for 2 h. Then materials were washed as described in the section 2.1.1. One portion of this material was put away and left to dry for 24 h at 50 °C (sample WN1.8). ii) The remaining portion was mixed with 100 mL of 10% citric acid solution and stirred for 2 h after which the washing procedure was repeated (as in the step i) and another material was obtained after drying (WN1.8C10%). iii) A portion of the material obtained in step ii) was transferred into 100 mL of 0.5 M NaOH solution, stirred for 1 h, washed (as described in step i) and left to dry (sample WN-OH). iv) Another material (WC10%) was prepared by only washing a portion of 5 g of W in 50 mL 10% solution of citric acid for 2 h, after which the sample was centrifuged, washed and dried.

4.2.3 Adsorbent characterization

The structure of the materials was studied by analysis of XRD patterns recorded using a X-ray powder diffractometer (Bruker, D2 PHASER) equipped with CuKα radiation source. Infrared spectra of the samples diluted with KBr (4 wt. %) were recorded using attenuated total reflectance technique (Nicolet 6700 FT-IR, Thermo Scientific). The textural parameters of the samples were determined by adsorption of N_2 at −196 °C using a 3Flex (Micromeritics) surface characterization analyzer on outgassed samples. Cation exchange capacity was determined using the ammonium acetate method

(Steudel, 2008). X-ray fluorescence (XRF) analysis was performed using Skayray Instrument EDX 3600H - Alloy Analyzer.

4.2.4 Adsorption experiments

Whenever a solution containing more than one component was used in adsorption experiments the element, for which a result is presented, is denoted first and is followed (after hyphen) by other component or components that was or were present in the solution.

4.2.4.1 Batch preliminary screening: the influence of pH

In order to find the optimum pH for adsorption experiments of Cu^{2+}, weighted masses of 20 mg of the raw material were placed in Erlenmeyer flasks with caps and mixed with 25 mL of a Cu^{2+} solution with pH previously adjusted between 3.0 and 6.0. Samples were stirred for 2 h, centrifuged (5 min, 4500 rpm) and content of Cu^{2+} in the supernatant was determined.

4.2.4.2 Desorption studies

For desorption studies a mass of 1 g of W was saturated in a concentrated solution of MB, AR and Cu^{2+}. Samples were centrifuged, washed with deionized water and left to dry at 50 °C for 24 h. In the following step the material was divided in 5 parts and each of them was placed in an Erlenmeyer flask (with cap) with one of the following solutions: water (H_2O), ethanol (Et-OH), 0.05 M nitric acid (HNO_3), a mixture of ethanol and 0.05 M nitric acid (Et-OH+HNO_3) and a mixture of ethanol and sodium chloride (Et-OH+NaCl). Solutions were stirred for 2 h, centrifuged and concentration of desorbed dyes and Cu^{2+} determined. After washing samples they were dried at 50 °C for 24 h. Samples of each material (25 mg) were placed in Erlenmeyer flasks and mixed with 25 mL of a solution containing 50 mg L^{-1} MB, 50 mg L^{-1} AR and 25 mg L^{-1} Cu^{2+}. The pH has been adjusted to 5.0. After 2 h of stirring, samples were centrifuged and concentration of dyes and Cu^{2+} in the solution was determined. Both experiments were made in duplicate.

In order to determine maximum HNO_3 concentration that could be used in desorption and does not affect material's layers, a portion of 1 g of W was mixed in Erlenmeyer flasks, equipped with condensers, with 10 mL solution of HNO_3 (concentrations varying from 0.001 to 2.0 M) were stirred for 2 h at 50 °C, centrifuged, washed and left to dry at 50 °C for 24 h, originating the following materials: WN0.001-T50-H2, WN0.005-T50-H2, WN0.01-T50-H2, WN0.05-T50-H2, WN0.1-T50-H2, WN0.5-T50-H2, WN1-T50-H2, WN1.5-T50-H2, WN1.8-T50-H2 and WN2.0-T50-H2. Additional set of samples were treated in 0.05 M HNO_3 solutions for 2 h at 25 °C (WN0.05-T25-H2)

and 98 °C (WN0.05-T98-H2), and at 50 °C for different periods of time: 8 h (WN0.05-T50-H8), 14 h (WN0.05-T50-H14) and 24 h (WN0.05-T50-H24).

4.2.4.3 Batch experiments: kinetics, equilibrium

For kinetic studies, masses of 200 mg of W, WN-OH, and WNaOH2 were placed in beakers and mixed with 200 mL of the following solutions: 1) 50 mg L^{-1} AR, 2) 50 mg L^{-1} MB, 3) 25 mg L^{-1} Cu^{2+}, 4) 50 mg L^{-1} AR and 25 mg L^{-1} Cu^{2+}, 5) 50 mg L^{-1} MB and 25 mg L^{-1} Cu^{2+}, 6) 25 mg L^{-1} AR, 25 mg L^{-1} MB and 25 mg L^{-1} Cu^{2+}. The pH of each solution was adjusted to 5.0. Experiments were conducted at room temperature (24 °C) at constant stirring (300 rpm). Samples were collected at selected time intervals, immediately centrifuged (2 min, 4500 rpm) and concentration of the adsorbate was determined.

Isotherms were performed for each system of material/adsorbates studied. A volume of 25 mL of each solution (1 to 6) was mixed in Erlenmeyer flasks with different amounts of the material (from 20 mg to 100 mg). Solutions were stirred for 2 h, then centrifuged and final concentration of adsorbates was determined.

4.2.4.4 Column experiments

Experiments were performed using a glass column (Omnifit), with 2.5 cm inside diameter and 15 cm height, and a peristaltic pump (Gilson, Minipuls 3) at room temperature (24 °C). Masses of 250 mg of W and 100 mg of WN-OH and WNaOH2 were mixed with 24 g of washed sand (fraction 0.25-0.30 mm) and placed in the column. Solution with pH adjusted to 5.0, containing 25 mg L^{-1} of MB, 25 mg L^{-1} of AR and 25 mg L^{-1} of Cu^{2+} was pumped upflow with a flow rate of 2 mL min^{-1}. Samples were collected at selected time intervals and concentration of each component determined. After each cycle of adsorption, the column was washed with water during 1 h and desorbing solutions (previously selected) were pumped through. Firstly 0.05 M HNO_3 to remove the metal and then Et-OH + 1M NaCl to desorb the dyes, the column was washed with deionized water in-between the solutions. Concentration of dyes and metal in the effluent was determined.

4.2.5 Data analysis

Adsorption capacities of the materials were calculated according to Eq. 1: q=((C_0-C)V)\m where q is adsorption capacity (mg g^{-1}), C_0 and C are initial concentration and concentration at determined time (mg L^{-1}) respectively, V is the volume of adsorbate (L) and m is adsorbent mass (g).

The pseudo 1st order Lagergren's model (Lagergren, 1898) and the pseudo 2nd order Ho's model (Ho and McKay, 1999) were fitted for the kinetic data. Weber-Morris (Weber and Morris, 1963) was used to examine if intra-particular diffusion is the only rate limiting step. The Langmuir's (Langmuir, 1918) and the Freundlich's (Freundlich, 1906) models were fitted to the equilibrium experiments data. In the column experiments Yan's model (Yan et al., 2001) was fitted to the experimental data in order to determine the maximum adsorption capacity of the materials and Yoon-Nelson's model (Yoon and Nelson, 1984) to obtain breakthrough times.

All models were fitted to the experimental data using non-linear regression. The parameters of models are presented with the respective confidence intervals at 95% confidence level. Variances and correlation coefficients were determined and compared using Fisher's, Akaike Information Criterion (AIC), and Bayesian Information Criterion (BIC) tests.

4.3 Results and Discussion

4.3.1 Adsorbent characterization

The ATR analysis revealed that upon the treatment Mg^{2+} cations from the interlayer space were exchanged to Na^{+}. Similar position of other peaks in the range of vibrations of structural hydroxyls reminded unchanged. The XRD study showed that with the increase of treatment time hydroxy-intercalated vermiculite (HIV) became the dominant phase in the material, which was manifested in shift of the 002 reflection towards higher angles. In the sample treated in the optimal conditions Mg-vermiculite coexisted with the HIV phase, as well as with Na-vermiculite that gave reflections in the range of higher angles. The specific surface area of the material did not significantly change and remained of an average level of 17 $m^2\ g^{-1}$, however, a slight increase in the cation exchange capacity from approximately 92 to 97 mmol 100 g^{-1} was observed upon the treatment. The XRF analysis showed that the composition of the material subjected to the NaOH treatment did not change compared to the starting one, what suggests no leaching of the components but their deposition in situ after the modifications. Detailed results of the characterization of the materials and spent adsorbents are presented in the Supporting Material in sections 1 to 4. Observations considering structural alternations responsible for changes in adsorption properties have been also included in the following chapters.

4.3.2 Selection of treatment regime

Optimal pH was determined for adsorption of Cu^{2+}. The pH optimization experiment showed that the best conditions were achieved for an initial pH of 5.0 at which adsorption capacity increased from 0.4 ± 0.2 to 12.0 ± 0.5 mg g^{-1}, keeping this capacity at pH 6.0, 12.3 ± 0.2 mg g^{-1}. To avoid possible precipitation of Cu^{2+} pH 5.0 was chosen for further experiments.

Basic activation of raw vermiculite resulted in an increase in its adsorption capacity toward Cu^{2+}.

A one-way between subjects ANOVA was conducted to compare the effect of NaOH concentration and treatment time on the maximum adsorption capacity of vermiculite. There was a significant effect of NaOH concentration and treatment time on maximum adsorption capacity of the material for Cu^{2+} cations at the $p < 0.05$ level [$F(12, 39) = 54.08$, $p = 0.000$], and $p < 0.05$ [$F(4, 5) = 10.81$, $p = 0.0112$] for the 13 concentrations and 5 treatment times, respectively. Post hoc comparison using the Tukey HDS test indicated that the mean score for the 2.0 M NaOH concentration was significantly different than the mean scores of the conditions below that concentration (0.005 - 1.5 M) and the raw material. However, the mean score of conditions higher than 2 M (3.0 - 6.0 M) did not significantly differ from the concentration of 2.0 M. In the case of treatment time optimization for 2 M NaOH concentration, the mean score for 4 h contact time was significantly different than for the conditions of 1 and 2 h, however, no difference was found between 4, 24 and 72 h. Taken together, these results suggest that 2.0 M NaOH (Fig.4.2A) and treatment time of 4 h (Fig.4.2B, sample WNaOH2-H4) improved the maximum adsorption capacity of the material and application of higher concentrations or longer treatment times did not result in further increase in the capacity.

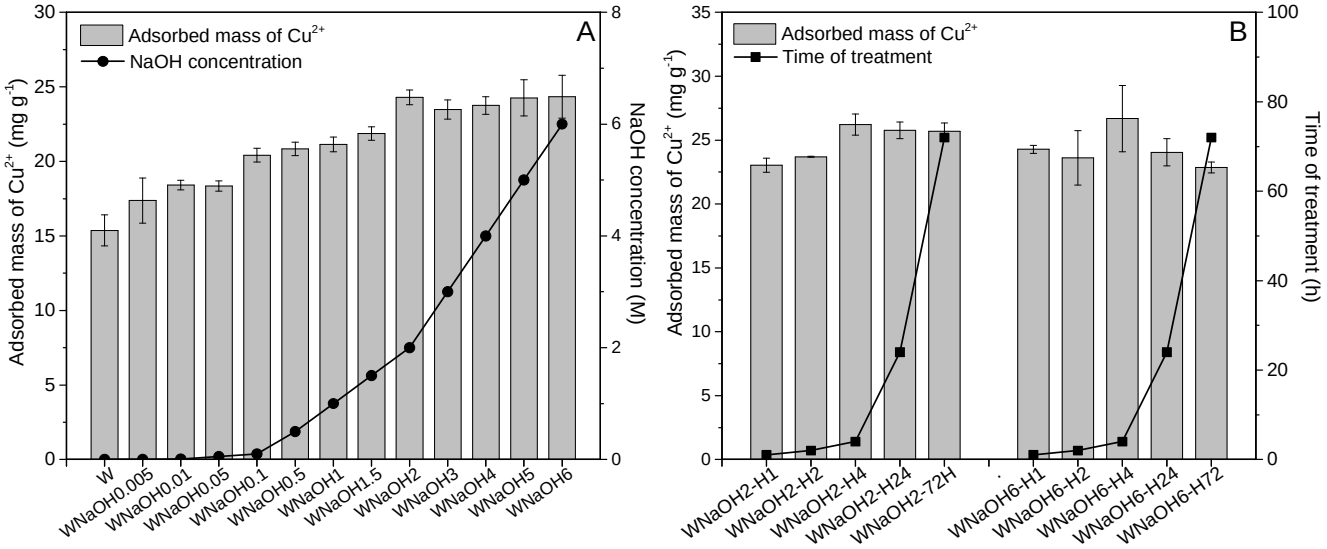

Figure 4.2 Optimization of NaOH concentration (A) and treatment time (B) of raw vermiculite.

Samples prepared by acid activation showed a significant deterioration in their adsorption capacity towards Cu^{2+} that decreased from 15 ± 1 to 3.6 ± 0.6 mg g^{-1} for the raw (W) and the material treated in 1.8 M HNO_3 respectively. A slight increase to 5.28 ± 0.09 mg g^{-1} was observed when such treatment was finished with the sample being washed in citric acid (WN1.8C10%). However, if the step of treatment with 0.5 NaOH was added at the end (WN-OH), the capacity returned approximately to the level of the raw material and reached 13.8 ± 0.3 mg g^{-1}. When only citric acid was applied (WC10%) no changes in adsorption capacity were observed compared to W. Only the sample treated with base without prior acid activation, exhibited enhanced adsorption capacity toward Cu^{2+} equal to 24.8 ± 0.8 mg g^{-1}.

Vermiculites are characterized by high layer charge, thus strong interaction between layers and interlayer cations results in limited diffusion of ions between layers which makes the ion exchange more difficult to proceed. Acid treatment caused leaching of octahedral layers (Fig.S.4.8B in the Supplementary Materials) and it decreased layer charge of the material, facilitating ion exchange (Schoonheydt and Johnston, 2006). Also such treatment resulted in creation of amorphous silica that acts as a cementing agent impeding swelling and dispersion (Carrado et al., 2006). Basic treatment of acid activated sample caused dissolution of that amorphous phase leaving a material with decreased layer charge and interlayer space available for adsorbates. At the same time a new phase of hydroxy-intercalated vermiculite (HIV) was formed due to migration of metal ions from the active dissolution sites into the interlayer space (Kalinowski and Schweda, 2007; Mareschal et al., 2009) and acted as new adsorption centers for metals. Dissolution of the outer silica sheets of clay mineral lattices by alkali, which is visible in the ATR spectra (Fig.S.4.2 in the Supporting Materials), leaves aluminum hydroxides layers and produces alkali insoluble iron hydroxides (Jozefaciuk et al., 2002) as well as magnesium hydroxide and sodium aluminum silicate hydrate and sodium aluminum carbonate silicate (Aldabsheh et al., 2015). The XRF analysis (Fig.S.4.8A in the Supplementary Materials) showed no change in the chemical composition of the base treated material, which might indicate that upon dissolution of the layers the elements are redeposited as hydroxides. Hydroxides of Fe, Al, and Mg may exist as coating or as interlayers between clay mineral surfaces, in addition part of the OH species might be adsorbed by broken-edge sites. All of these configurations might be present at the same time. The reactivity of such phases might be considerably higher than the reactivity of free hydroxides, especially with respect to metal adsorption. Thus, on alkali activated clay three groups of adsorption sites are present: siloxane surface of the clay with a permanent charge, singly coordinated hydroxide groups at the clay edges and sites originated from the newly formed hydroxide species. The structure of such prepared

systems strongly depends on the experimental conditions and preparation procedures (Keizer and Bruggenwert, 1991). Adsorption on those sites is the result of either specific adsorption by complexation by singly coordinated OH groups, or adsorption of hydrolyzed metal ions at the siloxane surface. Specifically adsorbed ions can generally be desorbed by a decrease in pH. Non-specific adsorption takes place at the siloxane surface as a result of regular cation exchange. The adsorbed ions are unhydrolyzed and readily exchangeable by neutral salt solution. On the other hand, on regular clay adsorption of metals is mainly an ion exchange process and the adsorption capacity is usually small (Keizer and Bruggenwert, 1991). Adsorption on pure hydroxide systems is specific and involves separation of a proton from the surface hydroxyls groups and coordination of the metal cation with the negatively charged site (Mustafa et al., 1992). However, the nature of hydroxide species does not need to be the same in systems containing clay. The presence of clay may promote the polymerization and inhibit the crystallization of hydroxides. Therefore, adsorption of metal ions by the hydroxide phase is also likely to be affected by the presence of clay (Keizer and Bruggenwert, 1991). Material treated in chosen optimal condition exhibited the maximum cation exchange capacity (CEC) equal 96.88 mmol 100 g^{-1} that decreased when higher concentrations of NaOH were applied which is normal when hydroxide layers are created on the material (Keizer and Bruggenwert, 1991). The raw material was characterized with CEC on the level of 92.6 mmol 100 g^{-1}, whereas the CEC of acid/base treated sample, as previous study denoted was 44.89 mmol 100 g^{-1} (Stawiński et al., 2014). The specific surface area of base treated sample slightly decreased from 21 to 16 m^2 g^{-1} however, such small change could be attributed to the method's error (Fig.S.4.7B in The Supporting Materials).

4.3.3 Batch desorption studies

Solution of 0.05 M HNO_3 was found to be safe to be applied as desorbing agent without destroying the material's structure and lowering its adsorption capacity. Neither temperature nor treatment time in such concentration affected the material's adsorption properties (Fig.4.3). Concentrations higher than 0.1 M, on the other hand, caused changes in the material: an increase in its specific surface area, formation of amorphous silica followed by a decrease in its crystallinity and cation exchange capacity, leaching of metals from the layers, and lowering cation exchange capacity. (Fig.S.4.5A and B and Fig.S.4.7A in the Supporting Material). All that changes were reflected in lowered maximum adsorption capacity of the material.

Although the treatment with 0.1 M HNO_3 did not altered the structure, the adsorption capacity of such treated sample decreased (Fig.4.3). That might be explained by protonation of active sites of the adsorbent that might impede adsorption of Cu^{2+}.

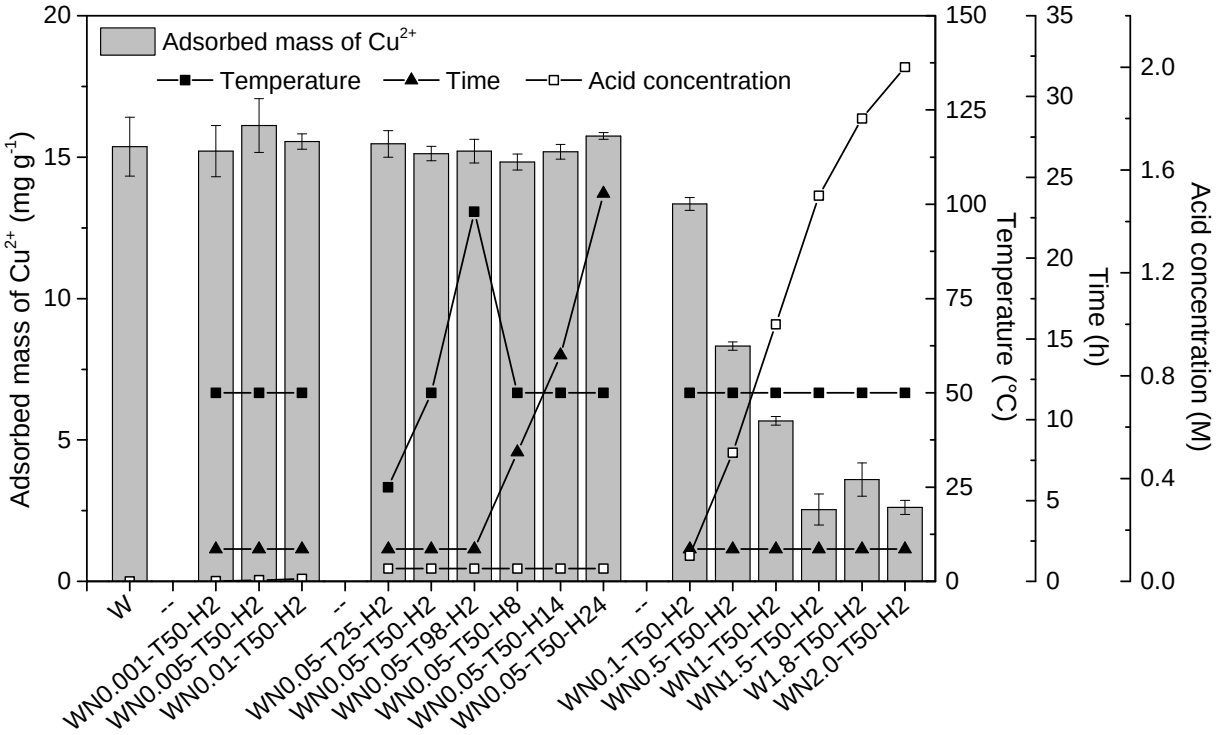

Figure 4.3 Adsorption capacity of Cu^{2+} on nitric acid modified vermiculite, time and temperature optimization.

The experiment showed that upon applying different desorbing solutions, separation of metals from dyes from saturated material became feasible. A solution of 0.05 HNO_3 exhibited good efficiency in desorbing Cu^{2+} from spent adsorbent, whereas a solution of ethanol and sodium chloride (Et-OH + 1M NaCl) desorbed dyes well, while not removing much Cu^{2+}. Good desorbing properties of the latter might be due to enhanced adsorption of counter ions, in this case Na^+, that occurs in the presence of organic solvents in the solution (Lagaly, 2006) and thus removal of the adsorbed dyes is more efficient. Desorption with a solution of ethanol and nitric acid (Et-OH + 0.05M HNO_3) resulted in moderate removal of both adsorbates, whereas neither water, nor ethanol showed any significant desorbing properties when used alone (Fig.4.4).

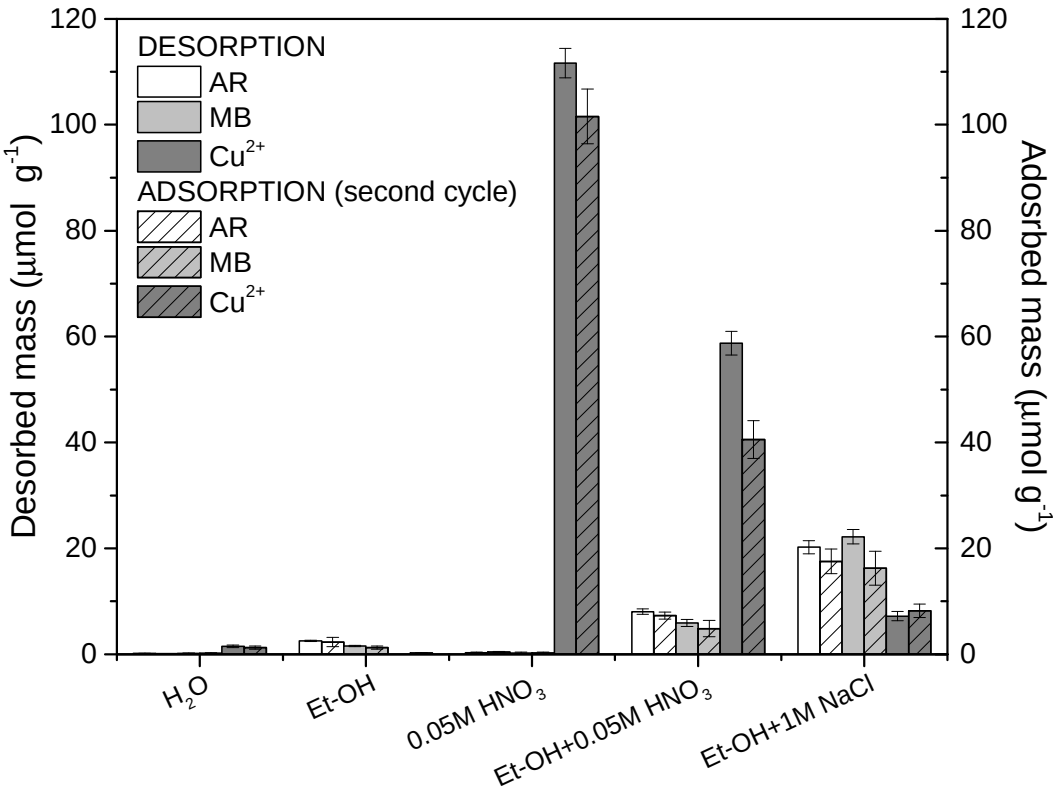

Figure 4.4 Desorption with different solutions from the raw material saturated with AR, MB and Cu^{2+} and adsorption of AR, MB and Cu^{2+} on regenerated material.

Adsorption on regenerated material revealed just a slight deterioration in the adsorption capacity towards each component after desorption (Fig.4.4). In the column system rapid desorption of dyes occurred during the first 60 min with an increase in Na^+ concentration in the effluent (Fig.A.4.2A). After that time the concentration of Na^+ remained constant and desorption was completed in 300 min (Fig.A.4.2 B, D and F). Desorption of Cu^{2+} was the most intense in the first 30 min and was completed in approximately 100 min (Fig.A.4.2 A, C and E). Similar desorption times of dyes and Cu^{2+} were observed in the case of all tested materials.

4.3.4 Kinetic experiments

In general adsorption kinetics in each case in the experiment followed the pseudo 2nd model. Table A.4.1 in the Appendix shows models comparison and their parameters.

The adsorption of AR and MB from single solutions on the raw vermiculite (W) showed moderate rate because the material still had a high layer charge and adsorption by ion exchange with the interlayer cation (Mg^{2+}) was more difficult and timely due to high polarization power of the interlayer ion. On only base treated vermiculite (WNaOH) the adsorption rate was the highest what might be due to the fact that dyes adsorbed on the surface of the hydroxyl coated clay and by ion exchange with Na^+ which is easier to

exchange with Mg^{2+} due to lower polarization power of Na^{+}. However, the exchange was incomplete and Na^{+} saturated phase was still present in the sample (Fig.S.4.6C in the Supporting Material). The lowest adsorption rate was observed on the acid\base treated material (WN-OH) where the dyes were intensively intercalated between the layers causing an increase in the interlayer spacing (Fig.S.4.6B in the Supporting Material). Such process is slow and requires more time to reach equilibrium. No statistically significant difference between the models was noticed for dyes, except for WN-OH where MB adsorption exhibited lower rate than for AR (curves AR and MB Fig.4.5).

In binary solutions, where Cu^{2+} and a dye were present, the adsorption rate for dyes increased by an order of magnitude for W and WN-OH, still being higher on the latter material, whereas the rate did not change for WNaOH in case or AR but decreased for MB. This proved that the synergic effect of coadsorption of dyes and metal might, in some cases, help to overcome some mass transfer resistances (curves AR-Cu and MB-Cu, Fig.4.5).

In the case of adsorption of Cu^{2+} from single component solutions the highest adsorption rate was on WN-OH, moderate on WNaOH and the lowest on W (curves Cu Fig.4.5). The first material has good access to the interlayer space and is cleaned from amorphous phases and its layer charge is decreased, thus ions can easily penetrate between them. Also no increase of interlayer space of the material was noticed, that why adsorption occurs fast. The difference in the rates between WNaOH and W might be explained by easier exchange of Na^{+} ions than Mg^{2+} due to reasons mentioned before. It was also observed that the adsorption rates of Cu^{2+} decreased when dyes were present in the solution, with higher decrease of that parameter for MB than for AR in the case of each material (curves Cu-AR and Cu-MB Fig.4.5).

According to the Weber-Morris model, the results gathered during the kinetic experiments indicate that in investigated systems intra-particle diffusion was not the only rate limiting step (Fig.S.4.9 in the Supporting Material).

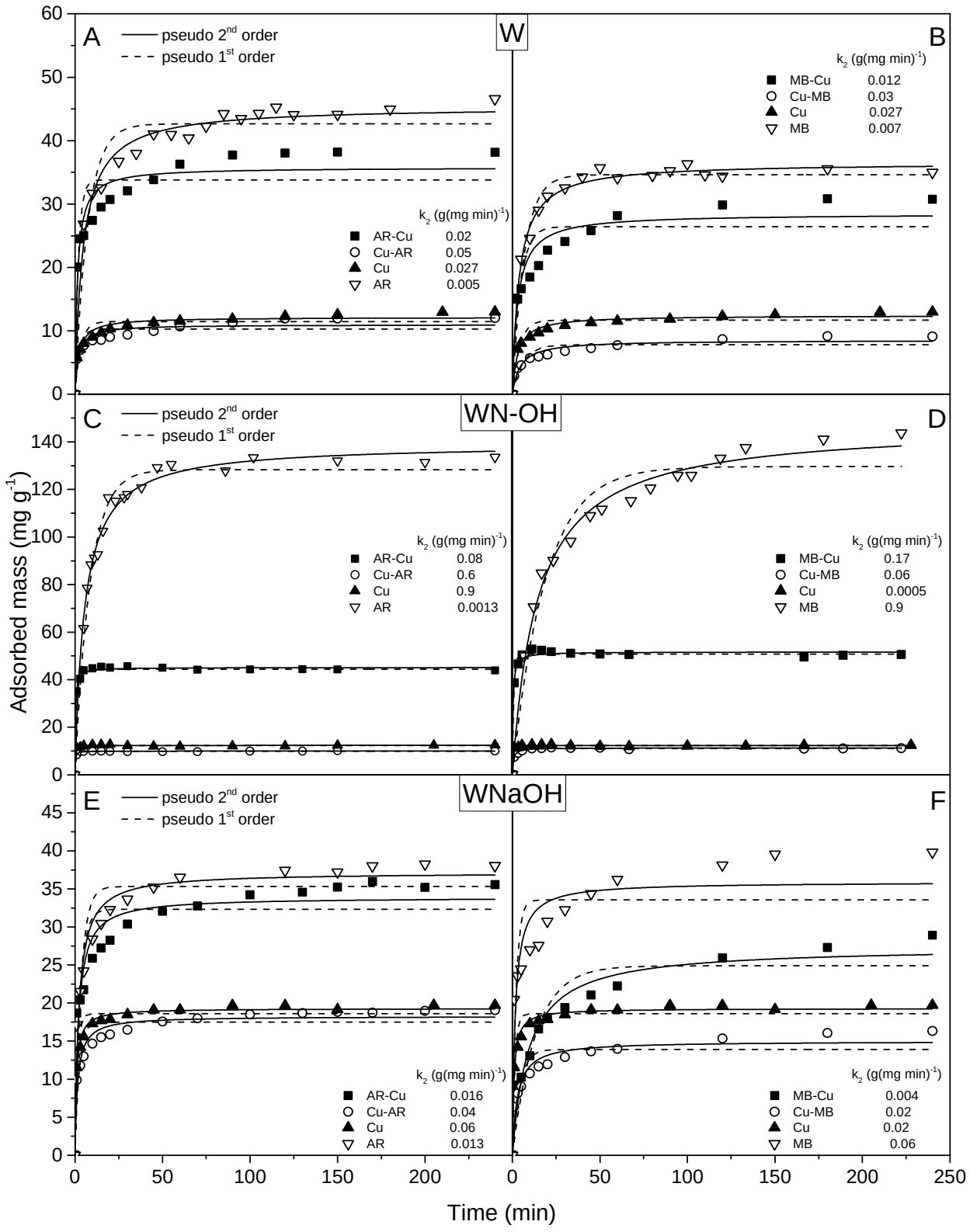

Figure 4.5 Kinetic experiments' results data for single component solutions adsorption of Cu^{2+}, AR and MB (Cu, AR, MB, respectively) and for multi component solution adsorption of Cu^{2+} (Cu-MB and Cu-AR), of AR (AR-Cu) and of MB (MB-Cu) with fitted models and kinetics parameter of pseudo 2nd order model given, for the raw (W) (A and B), acid/base treated (WN-OH) (C and D) and base treated (WNaOH) (E and F) vermiculite.

4.3.5 Isotherms

Models' parameters related to maximum adsorption capacity are presented in Fig.4.6. Table A.4.2 in the Appendix presents details of models' parameters. Experimental data with fitted models are presented in Fig.4.7. To facilitate comparison of the material the maximum adsorption capacities will be discussed according to results obtained from the Langmuir's model. On the raw material (W) the adsorption of Cu^{2+} and AR followed the Freundlich's and Langmuir's model, respectively, both in single and binary solutions. Adsorption of MB, on the other hand, in a single component solution followed the Freundlich's model and Langmuir's in bi-component system. The material had the maximum adsorption capacity for MB on the level of 53 ± 3 mg g^{-1} which exhausted approximately 18 ± 1% of the cation exchange capacity (CEC) of the material. When Cu^{2+} ions were present in the solution the capacity decreased to 39 ± 4 mg g^{-1} (13 ± 1% of the CEC), however the capacity for Cu^{2+} did not change for single and bi-component solution and remained on the level of 20 ± 3 mg g^{-1} (39 ± 5% of the CEC). No competition between AR and Cu^{2+} was noticed on that material. The maximum adsorption capacity for the dye reached 44 ± 2 and 50 ± 3 mg g^{-1} corresponding to 12 ± 1% of the CEC in a single and a binary solution, respectively. No statistically significant difference in the maximum adsorption capacity of Cu^{2+} in the presence of AR was observed.

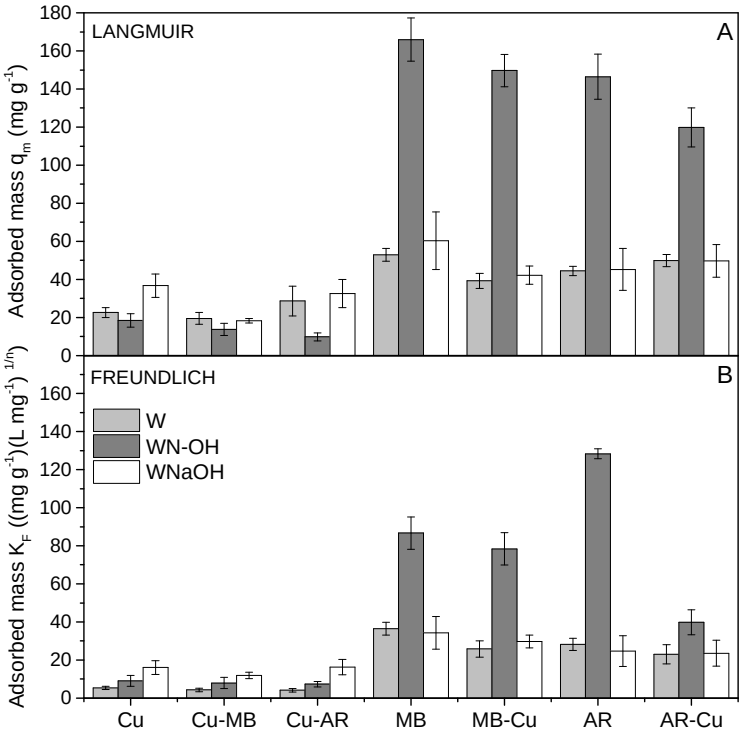

Figure 4.6 Maximum adsorption capacities based on Langmuir's (A) and Freundlich's (B) models of the raw (W), acid/base (WN-OH) and base (WNaOH) treated vermiculites in single (Cu, MB, AR) and binary solutions (Cu-MB, Cu-AR, MB-Cu, AR-Cu).

On acid/base treated material (WN-OH) the adsorption mechanism of MB changed to Langmuir's model and of AR to Freundlich's in the case of single component solutions. The mechanisms of adsorption of Cu^{2+} from single and binary solutions, and also of AR from single component solution, remained unchanged however, the shape of the isotherm of Cu^{2+} adsorption in the presence of MB changed to the Langmuir's model. In this case MB most probably was adsorbed as dimmers and trimmers, and formed multilayers on the surface (Neumann et al., 2002) reaching higher adsorption capacity on the level of 166 ± 11 mg g^{-1} which is 116 ± 8% of the CEC. Cu^{2+} used approximately 63 ± 11% of the CEC and the maximum adsorption capacity was equal 18 ± 3 mg g^{-1}. On this material no competition between MB and Cu^{2+} was noticed. On the other hand, AR exhibited a decrease in the maximum adsorption capacity when Cu^{2+} was present in the solution. The capacity changed from 145 ± 12 mg g^{-1} (80 ± 7% of the CEC) to 120 ± 10 mg g^{-1} (67 ± 6% of the CEC) at the same time a decrease to 10 ± 2 mg g^{-1} in the capacity for Cu^{2+} (35 ± 7% of the CEC) was observed.

In the case of base treated vermiculite adsorption of all components followed the Freundlich's model except for adsorption of Cu^{2+} in bi-component solution with MB, where the Langmuir's model was a better fit. On this material, adsorption of MB was favored over adsorption of Cu^{2+} in bi-component solution. The maximum adsorption capacity for MB in a single component solution reached 60 ± 15 mg g^{-1} (19 ± 5% of the CEC) and did not change significantly in the presence of Cu^{2+} reaching 42 ± 5 mg g^{-1} (14 ± 2% of the CEC). However, a decrease in the capacity for Cu^{2+} occurred in binary solution with MB and changed from 37 ± 6 mg g^{-1} (60 ± 10% of the CEC) to 18 ± 1 mg g^{-1} (29 ± 2% of the CEC). The capacity for AR remained on a similar level of 45 ± 11 (12 ± 3% of the CEC) and 50 ± 9 mg g^{-1} (13 ± 2% of the CEC) in single and bi-component systems, respectively. The adsorption capacity for Cu^{2+} also did not change and stayed on the level of 33 ± 7 mg g^{-1} (54 ± 11% of the CEC) with AR present in the solution.

Most of the time, adsorption is controlled by various factors. Thus the adsorption isotherms equation, as well as rate laws should be rather considered as curve fitting models without actual mechanistic significance as they do not always reflect the actual phenomena taking place. However, they are useful means with predictive capability of the adsorption to design adsorption units (Hameed and El-Khaiary, 2008; Sposito, 2008).

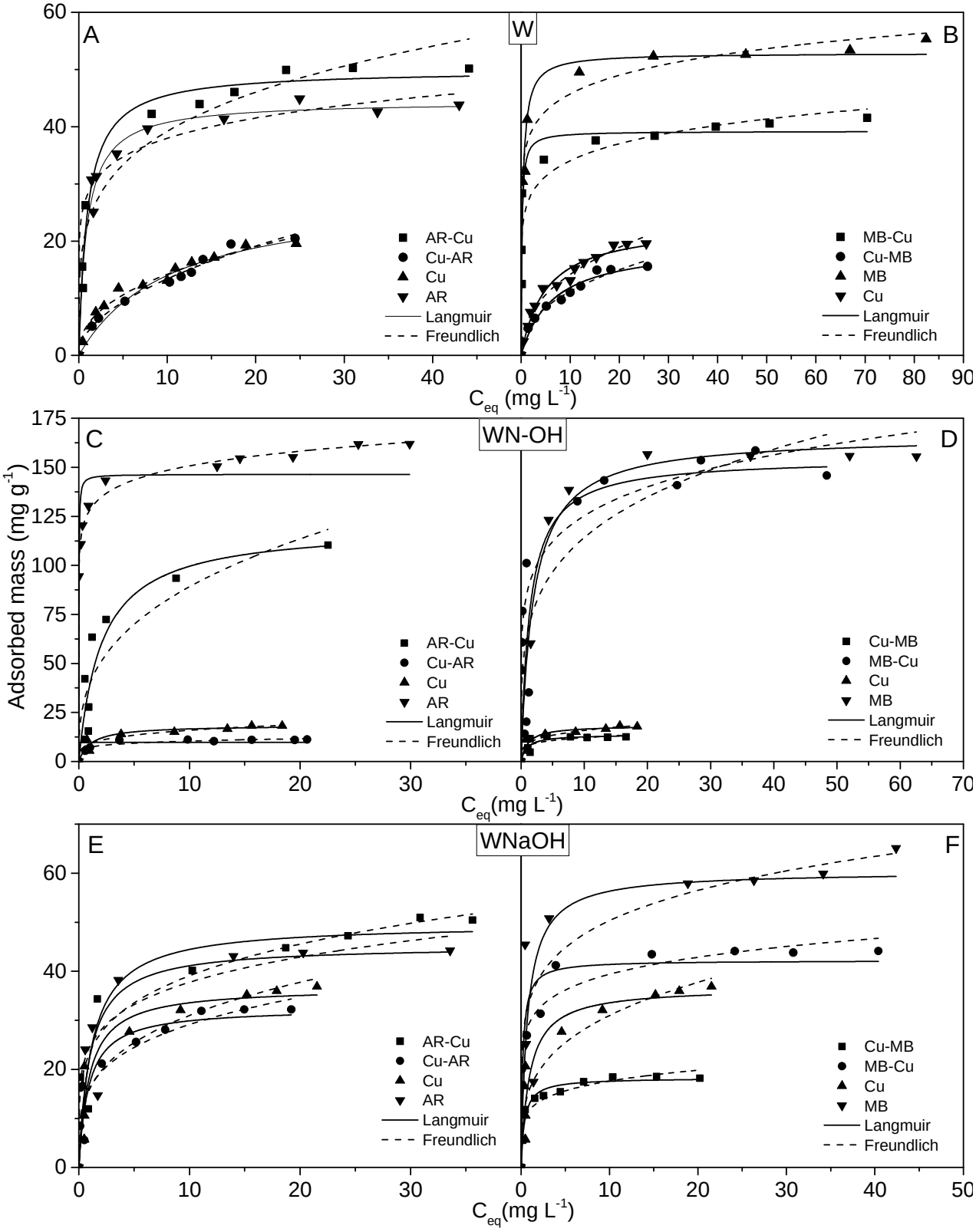

Figure 4.7 Equilibrium experiments data for single component solutions adsorption of Cu^{2+}, AR and MB (Cu, AR, MB, respectively) and for multi component solution adsorption of Cu^{2+} (Cu-MB and Cu-AR), of AR (AR-Cu) and of MB (MB-Cu) with fitted models, for the raw (W) (A and B), acid/base treated (WN-OH) (C and D) and base treated (WNaOH) (E and F) vermiculite.

4.3.6 Column studies

Detailed models' parameters are presented in Table.A.4.3 in the Appendix.

The materials exhibited different behavior in column system with ternary mixtures. The raw material exhibited stable adsorption capacity during the two first cycles on average level of 16.4 ± 0.1, 15.4 ± 0.5 and 25.5 ± 0.7 mg g^{-1} that decreased in the third cycle to 12.9 ± 0.7, 14 ± 0.3 and 22 ± 1 mg g^{-1} for Cu^{2+}, AR and MB, respectively (Fig.4.8. A, C and E). However, the maximum adsorption capacity was decreased in comparison to the batch experiments. It was observed that adsorption curve for AR changed its shape becoming steeper in each cycle (Fig.A.4.1 A to C in the Appendix). The cation exchange capacity (CEC) of that material was exhausted in approximately 40% with Cu^{2+} taking 28% of it while only 4 and 8% were used by AR and MB in the first cycle, respectively. AR was the first adsorbate to reach breakthrough time, followed by MB and Cu^{2+}. In the following cycles the adsorption curves for MB and Cu^{2+} were similar while adsorption curve for AR became steeper suggesting faster adsorption of that dye. The batch experiments revealed no competition between AR and Cu^{2+} on this material, thus the faster adsorption might be due to exchange of interlayer Mg^{2+} cations with Na^{+} during regeneration of the adsorbent making the adsorption of the dye is easier. No overshooting was observed suggesting that there is no competition between the dyes for adsorption sites, or the competition is not strong enough to cause desorption of either of the dyes. This results is in agreement with previous study (Stawiński et al., 2014).

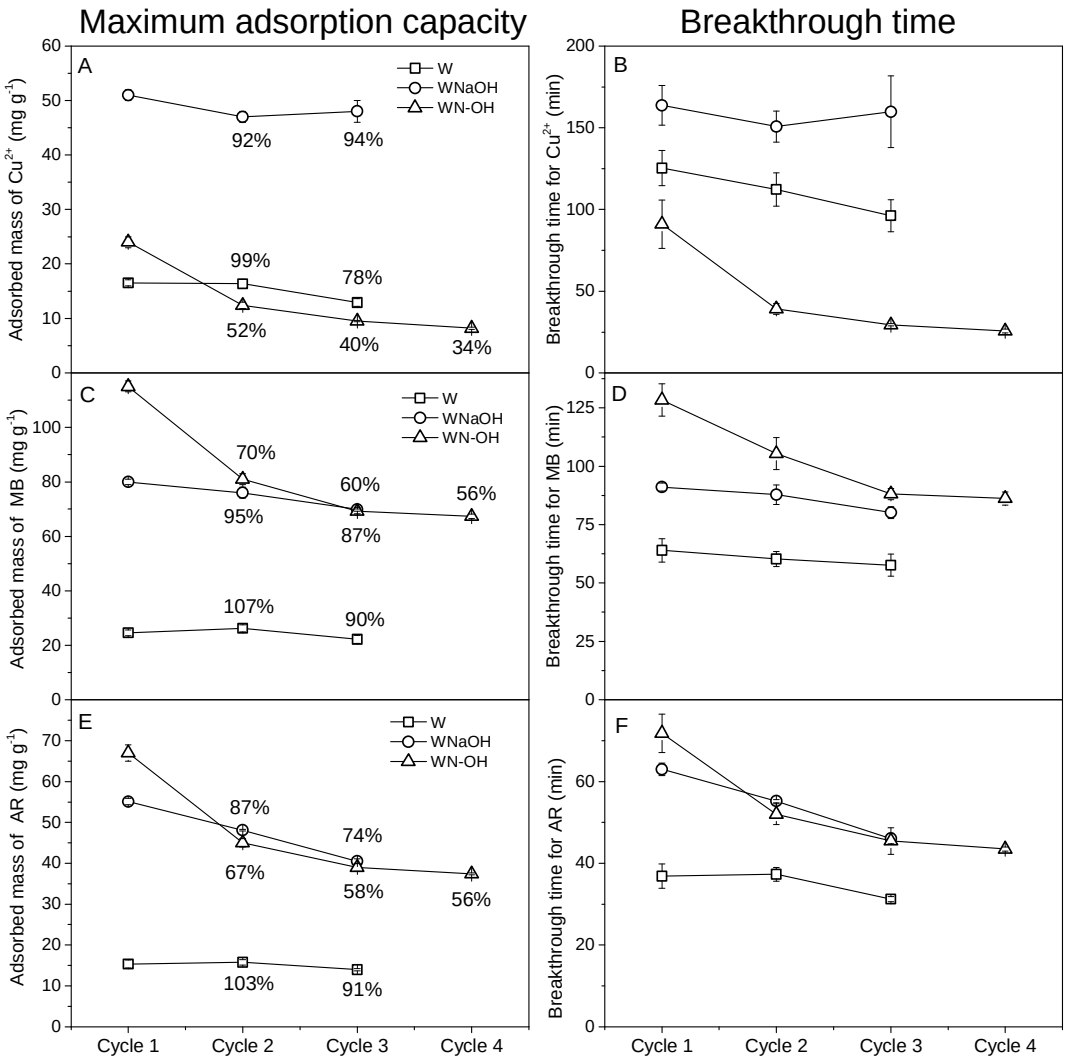

Figure 4.8 Maximum adsorption capacities with regeneration efficiency (%), and breakthrough times obtained by fitting Yan's and Yoon-Nelson's models to the experimental data for adsorption of Cu^{2+}, AR and MB on W, WNaOH and WN-OH.

Acid/base treated vermiculite reached high adsorption capacity on the level of 67 ± 2 and 115 ± 2 mg g^{-1} for AR and MB, respectively, and 24 ± 1 mg g^{-1} for Cu^{2+}. However, a significant decrease, to around 52, 70% and 67% of the indicial capacity, was noticed after the first cycle for Cu^{2+}, MB and AR, respectively. In the following cycles the decrease was smaller and the capacity reached an average level of 8.9 ± 0.9 (34%) 68 ± 1 (56%) and 38 ± 1 (56%) mg g^{-1} for Cu^{2+}, MB, AR and respectively (Fig.4.8. A, C and E). This result is with agreement with previous study (Stawiński et al., 2014). After the first cycle an increasing overshooting of AR was observed in the following cycles (Fig.A.4.1 D to G in the Appendix). Here, MB seemed not to show competitive adsorption with Cu^{2+}, however competition existed between Cu^{2+} and AR. Cu^{2+} and MB used 84% and 80% of the CEC, respectively, while AR contributes only with 37%. In the case of that material an expansion of the interlayer distance upon adsorption was clearly

noticeable (Fig.S.4.6B in the Supporting Material). This and the fact that the CEC was exceeded almost two times might suggest that there is a strong synergic effect on adsorption of Cu^{2+} and MB. Although the material has lowered cation exchange capacity compared to the starting vermiculite, it might be compensated by an easier access to its interlayer space as a result of the treatment, and by a decrease in the layer charge adsorbates can more freely penetrate between the layers. Also, as mentioned above, MB tends to form dimmers and trimmers in multilayers on the surface of an adsorbent. In the first cycle the breakthrough times and the curves for Cu^{2+} and AR are quite similar, however since approximately 80 min concentration of Cu^{2+} remained almost constant while adsorption of AR still proceeded. Breakthrough times in the following cycles were shorter and Cu^{2+} reached it quicker than AR. The material showed a decrease in adsorption capacity for both dyes and an increase in the capacity for Cu^{2+} compared to batch studies. That fact and also the phenomenon of overshooting became noticeable, which might be attributed to competition between MB and AR.

Base treated material showed high adsorption capacity towards Cu^{2+} on the level of 49 ± 2 mg g^{-1} and did not change significantly in subsequent cycles, however adsorption capacity for dyes decreased from 55.1 ± 0.8 and 80 ± 1 mg g^{-1} to 40.5 ± 0.6 and 69.9 ± 0.7 mg g^{-1} that corresponds to 74% and 87% of the initial capacity, after 3 cycles, for AR and MB, respectively (Fig.4.8. A, B and C). In this case the adsorption curve for AR became steeper with increasing overshooting in each cycle (Fig.A.4.1 H to J in the Appendix). The decrease in adsorption capacity was accompanied by decreasing breakthrough time for each material (Fig.4.8. A, C and E). In batch experiments adsorption of AR on base treated vermiculite did not exhibit competition with Cu^{2+}. Although it was not expected, the increasing overshooting of that dye in following cycles could be attributed to competitive adsorption of AR with MB. However, MB should compete with Cu^{2+} and the competition seems to be in favor of the dye. This relationship is not that clearly expressed in column system where adsorption capacity for Cu^{2+} on this material is somewhat increased compared to the batch experiments more efficiently exhausting the CEC i.e. in 80%, and remains unchanged in cycles. The maximum adsorption capacity for MB that exhausted approximately 26% of the CEC of the material in the first cycle and slightly decreased in following cycles, however it was higher when compared to batch system. The capacity also decreased slightly after desorption cycles for AR, which used 14% of the CEC but it was in agreement with the results obtained in the batch experiment. Thus, it can be concluded that some synergic effect of adsorption of Cu^{2+} and MB occurred leading to an increase in the adoption capacity for both adsorbates while adsorption of AR remained unaffected.

Desorption studies revealed that a mixture of ethanol with NaCl successfully removed adsorbed dyes from the adsorbent bed in column in approximately 300 min. The removal of dyes was correlated with increasing concentration of Na^+ in the effluent (Fig.A.4.2A in the Appendix). An efficient eluent for desorbing metals was 0.05 M HNO_3 that desorbed Cu^{2+} from the material within approximately 100 min (Fig.A.4.2B in the Appendix)

It should also be taken into consideration that many of the differences in adsorption described above might have originated from different structure of each adsorbate. AR is a larger molecule than MB thus it has lower ionic potential (ratio of charge and molecule radius) and consequently it has lower affinity to the material. On the other hand, Cu^{2+} has the highest ionic potential of all adsorbates present in the solutions giving it the highest affinity to the material. AR is also a more flexible molecule that has more resonance structures than MB, which may allow different geometric coordination of the molecule while attaching to the surface with different geometrical coordination and better covering of the surface. Cations can be adsorbed on clays directly to the surface by forming an outer-sphere complexes as well as in a form of an outer-sphere complexes where water molecules are located between the cation and the clay surface or simply cumulate in the swarm near the solid surface without complex formation (Sposito, 1984). Some of the molecules can migrate from the inner-sphere complexes and outer-sphere complexes forming multilayer. The fact of MB being able to form dimmers and trimmers on external surfaces of adsorbents as a first step followed by disaggregation and migration of dye molecules in between the layers may also play an important role during adsorption (Neumann et al., 2002).

4.4 Conclusions

Three modifications of vermiculite, based on acid and alkaline, treatment resulted in formation of adsorbents characterized by different properties in adsorption of dyes: astrazon red (AR) and methylene blue (MB), and metal cations (Cu^{2+}). Based on the results obtained in the column experiments in the first adsorption cycle, the raw material showed low adsorption capacity on the level of 16.5 ± 0.5, 15 ± 1 and 25 ± 1 mg g^{-1} for Cu^{2+}, AR and MB, respectively. The acid/base treated vermiculite had very good adsorption capacity toward dyes on the level of 67 ± 3 and 115 ± 2 mg g^{-1} for AR and MB, respectively, and the maximum adsorption capacity for Cu^{2+} did not deteriorate remaining on the level of the starting material. The alkaline treated vermiculite was a good adsorbent for metals, reaching the maximum adsorption capacity of 51 ± 1 mg g^{-1} for Cu^{2+}, and it was also still able to adsorb dyes on the level of the starting material. Moreover, it was shown that the materials may be regenerated and used in several

adsorption-desorption cycles. Furthermore, it was possible to separate adsorbed dyes from metals by using a solution of ethanol and NaCl to desorb the dyes and 0.05M HNO_3 for desorption of Cu^{2+}. This opens a possibility for sustainable disposal and neutralization of both of the pollutants or for their further applications in other processes.

The adsorbents were prepared in a sustainable way. Their production does not require concentrated chemicals, high temperatures and it is not energy or time consuming. Additionally, it is based on simple procedures that do not need advanced technology, highly trained staff or complicated infrastructure and above all, it is not expensive. What is more, a research is being carried out on utilization of byproducts of the treatments (wastewater after acid and base activation) in order to create hybrid vermiculite-hydrotalcite adsorbents, turning the whole process more environment friendly. All that features make the technology readily available for applications not only in developed countries that have already advanced solutions, but also in countries that are still developing where water pollution and a lack of advanced facilities is still a major problem.

4.5 References

Aldabsheh, I., Khoury, H., Wastiels, J., Rahier, H., 2015. Dissolution behavior of Jordanian clay-rich materials in alkaline solutions for alkali activation purpose. Part I. Appl. Clay Sci. 115, 238-247.

Ali, I., Asim, M., Khan, T.A., 2012. Low cost adsorbents for the removal of organic pollutants from wastewater. J. Environ. Manage. 113, 170-183.

Angın, D., Köse, T.E., Selengil, U., 2013. Production and characterization of activated carbon prepared from safflower seed cake biochar and its ability to absorb reactive dyestuff. Appl. Surf. Sci. 280, 705-710.

Bailey, S.W., Chairman, 1980. Summary of recommendations of AIPEA nomenclature committee on clay minerals. Am. Mineral. 65, 1-7.

Bergaya, F., Lagaly, G., 2006. General introduction: clays, clay minerals, and clay science. in: Bergaya, F., Theng, B.K.G., Lagaly, G. (Eds.). Handbook of Clay Science. Elsevier Ltd.

Bhatnagar, A., Jain, A.K., 2005. A comparative adsorption study with different industrial wastes as adsorbents for the removal of cationic dyes from water. J. Colloid Interface Sci. 281, 49-55.

Carrado, K.A., Decarreau, A., Petit, S., Bergaya, F., Lagaly, G., 2006. Synthetic clay minerals and purification of natural clays. in: Bergaya, F., Theng, B.K.G., Lagaly, G. (Eds.). Handbook of Clay Science. Elsevier Ltd.

Česuniene, R., Gefeniene, A., Kaušpediene, D., Selskiene, A., 2013. Kinetics of copper(II) and metal complex dye adsorption on activated carbon in the single and binary systems. Chemija 24, 88-96.

Duta, A., Visa, M., 2015. Simultaneous removal of two industrial dyes by adsorption and photocatalysis on a fly-ash–TiO2 composite. J. Photochem. Photobiol. A: Chem. 306, 21-30.

Forgacs, E., Cserháti, T., Oros, G., 2004. Removal of synthetic dyes from wastewaters: a review. Environ. Int. 30, 953-971.

Freundlich, H.M.F., 1906. Über die adsorption in läsungen. Z. Phys. Chem. 57, 385-470.

Gautam, R.K., Sharma, S.K., Mahiya, S., Chattopadhyaya, M.C., 2015. Contamination of heavy metals in aquatic media: transport, toxixity and technologies for remediation. in: Sharma, S.K. (Ed.). Heavy metals in water. Presence, removal and safety. The Royal Society of Chemistry, Cambridge.

Hameed, B.H., El-Khaiary, M.I., 2008. Sorption kinetics and isotherm studies of a cationic dye using agricultural waste: broad bean peels. J. Hazard. Mater. 154, 639-648.

Hernandez-Eudave, M.T., Bonilla-Petriciolet, A., Moreno-Virgen, M.R., Rojas-Mayorga, C.K., Tovar-Gómez, R., 2016. Design analysis of fixed-bed synergic adsorption of heavy metals and acid blue 25 on activated carbon. Desalination and Water Treatment 57, 9824-9836.

Ho, Y.S., McKay, G., 1999. Pseudo-second order model for sorption processes. Process Biochem. 34, 451-465.

Jozefaciuk, G., Muranyi, A., Alekseeva, T., 2002. Effect of extreme acid and alkali treatment on soil variable charge. Geoderma 109, 225-243.

Kalinowski, B.E., Schweda, P., 2007. Rates and nonstoichiometry of vermiculite dissolution at 22°C. Geoderma 142, 197-209.

Keizer, P., Bruggenwert, M.G.M., 1991. Adsorption of heavy metals by clay-aluminium hydroxide complexes. in: Bolt G. H., De Boodt M. F, Hayes M. H. B., McBride M. B., De Strooper E. B. A. (Eds.). Interaction at the soil colloid - soil solution interface. Springer-Science+ Buisness Media, B.V.

Lagaly, G., 2006. Colloid Clay Science. in: Bergaya, F., Theng, B.K.G., Lagaly, G. (Eds.). Handbook of Clay Science. Elsevier Ltd.

Lagergren, S., 1898. About theory of so-called adsorption of soluble substances. Kongl. Vetenskaps Academiens Handlingar 24, 1-39.

Langmuir, I., 1918. The adsorption of gases on plane surfaces of glass, mica and platinum. J. Am. Chem. Soc. 40, 1361-1403.

Leitão, A., Serrão, R., 2005. Adsorption of phenolic compounds from water on activated carbon: prediction of multicomponent equilibrium isotherms using single-component data. Adsorption 11, 167-179.

Liu, Y., Zheng, Y., Wang, A., 2010. Enhanced adsorption of Methylene Blue from aqueous solution by chitosan-g-poly (acrylic acid)/vermiculite hydrogel composites. J Environ Sci 22, 486-493.

Mall, I.D., Srivastava, V.C., Agarwal, N.K., Mishra, I.M., 2005. Adsorptive removal of malachite green dye from aqueous solution by bagasse fly ash and activated carbon-kinetic study and equilibrium isotherm analyses. Colloids Surf. Physicochem. Eng. Aspects 264, 17-28.

Mareschal, L., Ranger, J., Turpault, M.P., 2009. Stoichiometry of a dissolution reaction of a trioctahedral vermiculite at pH 2.7. Geochim. Cosmochim. Acta 73, 307-319.

Monsalvo, V.M., 2016. Introduction. in: Monsalvo, V.M. (Ed.). Water treatment in developed and developing nations. An international perspective. CRC Proess, Apple academic Proess.

Mustafa, S., Safdar, M., Samad, Y., Naeem, K., 1992. Adsorption of heavy metal ions form aqueous electrolite solution on a-aluminium hydroxide. PCCP 12, 63-76.

Neumann, M.G., Gessner, F., Schmitt, C.C., Sartori, R., 2002. Influence of the layer charge and clay particle size on the interactions between the cationic dye methylene blue and clays in an aqueous suspension. J. Colloid Interface Sci. 255, 254-259.

Pan, B., Pan, B., Zhang, W., Lv, L., Zhang, Q., Zheng, S., 2009. Development of polymeric and polymer-based hybrid adsorbents for pollutants removal from waters. Chem. Eng. J. 151, 19-29.

Pereira, L., Alves, M., 2011. Dyes-Environmental Impact and Remediation. in: Malik, A., Grohmann, E. (Eds.). Environmental Protection Strategies for Sustainable Development. Springer Science & Business Media.

Reife, A., Freeman, H.S., 1996. Environmental Chemistry of Dyes and Pigments. John Wiley & Sons, New York.

Rieder, M., Cavazzini, G., D'yakonov, Y.S., Frank-Kamenetskii, V.A., Gottardi, G., Guggenheim, S., Koval, P.V., Müller, G., Neiva, A.M.R., Radoslovich, E.W., Robert, J.-L., Sassi, F.P., Takeda, H., Weiss, Z., Wones, D.R., 1998. Nomenclature of micas. Clays Clay Miner. 46, 586-595.

Rozada, F., Calvo, L.F., García, A.I., Martín-Villacorta, J., Otero, M., 2003. Dye adsorption by sewage sludge-based activated carbons in batch and fixed-bed systems. Bioresour. Technol. 87, 221-230.

Schoonheydt, R.A., Johnston, C.T., 2006. Surface and interface chemistry of clay minerals. in: Bergaya, F., theng, B.K.G., Lagal, G. (Eds.). Handbook of Clay Science. Elsevier.

Sposito, G., 1984. The surface chemistry of soils. Oxford University Press.

Sposito, G., 2008. The Chemistry of Soils. Oxford University Press, New York.

Stawiński, W., Figueiredo, S.A., Freitas, O.M., Węgrzyn, A., 2014. Application of acid-base treated vermiculite for sorption of textile dyestuffs wastewaters in: Portalegre, I.P.d. (Ed.). International Congress on Water, Waste and Energy Management, Porto, Portugal, pp. 88-89.

Stawiński, W., Freitas, O., Chmielarz, L., Węgrzyn, A., Komędera, K., Błachowski, A., Figueiredo, S., 2016. The influence of acid treatments over vermiculite based material as adsorbent for cationic textile dyestuffs. Chemosphere 153, 115-129.

Steudel, A., 2008. Selection Strategy and Modification of Layer Silicates for Technical Applications. Univ.-Verlag Karlsruhe.

Teng, S.-X., Wang, S.-G., Liu, X.-W., Gong, W.-X., Sun, X.-F., Cui, J.-J., Gao, B.-Y., 2009. Interaction between congo red and copper in a binary adsorption system: Spectroscopic and kinetic studies. Colloids Surf. Physicochem. Eng. Aspects 340, 86-92.

Tovar-Gómez, R., Rivera-Ramírez, D.A., Hernández-Montoya, V., Bonilla-Petriciolet, A., Durán-Valle, C.J., Montes-Morán, M.A., 2012. Synergic adsorption in the simultaneous removal of acid blue 25 and heavy metals from water using a Ca(PO3)2-modified carbon. J. Hazard. Mater. 199–200, 290-300.

Turabık, M., Gozmen, B., 2013. Removal of Basic Textile Dyes in Single and Multi-Dye Solutions by Adsorption: Statistical Optimization and Equilibrium Isotherm Studies. CLEAN – Soil, Air, Water 41, 1080-1092.

Ummartyotin, S., Bunnak, N., Manuspiya, H., 2016. A comprehensive review on modified clay based composite for energy based materials. Renewable and Sustainable Energy Reviews 61, 466-472.

Wang, S., Shi, X., 2001. Molecular mechanisms of metal toxicity and carcinogenesis. Mol. Cell. Biochem. 222, 3-9.

Weber, W.J., Morris, J.C., 1963. Kinetics of Adsorption on Carbon from Solution. Journal of the Sanitary Engineering Division 89, 31-60.

Wu, Y., Zhang, L., Gao, C., Ma, J., Ma, X., Han, R., 2009. Adsorption of Copper Ions and Methylene Blue in a Single and Binary System on Wheat Straw. J. Chem. Eng. Data 54, 3229-3234.

Yan, G., Viraraghavan, T., Chen, M., 2001. A new model for heavy metal removal in a biosorption column. Adsorpt. Sci. Technol. 19, 25-43.

Yoon, Y.H., Nelson, J.H., 1984. Application of gas adsorption kinetics--II. A theoretical model for respirator cartridge service life and its practical applications. Am. Ind. Hyg. Assoc. J. 45, 517-524.

Zhao, M., Tang, Z., Liu, P., 2008. Removal of methylene blue from aqueous solution with silica nano-sheets derived from vermiculite. J. Hazard. Mater. 158, 43-51.

Appendix A.4

Table A.4.1 kinetic models' parameters for the raw (W), acid/base treated (WN-OH) and base treated (WNaOH) vermiculites.

Sample	Model	Parameter	Adsorbate						
			AR	**AR-Cu**	**MB**	**MB-Cu**	**Cu**	**Cu-AR**	**Cu-MB**
W	pseudo 1st	q_e (mg g^{-1})	43 ± 2	34 ± 3	34.6 ± 0.9	26 ± 4	11.7 ± 0.7	10 ± 1	7.8 ± 0 .9
		k_1 (min^{-1})	0.14 ± 0.04	0.5 ± 0.3	0.14 ± 0.02	0.2 ± .0.2	0.22 ± 0.0 8	0.4 ± 0.2	0.16 ± 0.09
		s^2	0.87539	0.47775	2.06367	20.53538	1.10677	10.72839	1.17572
		R^2_{adj}	0.99	0.932	0.975	0.724	0.905	0.856	0.832
	pseudo 2nd	q_e (mg g^{-1})	45 ± 1	36 ± 2	36.5 ± 0.8	8.5 ± 0.8	12.4 ± 0.5	11.0 ± 0.8	28 ± 3
		k_2 (g (mg min)$^{-1}$)	0.005 ± 0.001	0.02 ± 0.01	0.007 ± 0.001	0.03 ± 0.01	0.0 27 ± 0.008	0.05 ± 0.03	0.012 ± 0.009
		s^2	2.30327	8.55641	0.87539	10.72839	0.28477	0.94914	0.47775
		R^2_{adj}	0.981	0.919	0.99	0.856	0.976	0.908	0.932
	Model compariso	Fisher Test	pseudo 2nd	pseudo 2nd	no difference	no difference	pseudo 2nd	pseudo 2nd	no difference
		AIC	pseudo 2nd						
		BIC							
WN-OH	pseudo 1st	q_e (mg g^{-1})	128 ± 4	44.4 ± 0.8	130 ± 7	50.7 ± 0.9	12.3 ± 0.2	9.89 ± 0.08	11.0 ± 0.4
		k_1 (min^{-1})	0.12 ± 0.01	1.5 ± 0.3	0.06 ± 0.01	1.4 ± 0.2	2.6 ± 0.2	1. 9 ± 0.2	1.0 ± 0.3
		s^2	0.09321	0.01555	0.09431	1.9304	80.42519	1.42869	1.9304
		R^2_{adj}	0.991	0.998	0.991	0.99	0.945	0.99	0.99
	pseudo 2nd	q_e (mg g^{-1})	139 ± 3	45.4 ± 0.6	147 ± 5	52 ± 1	12.3 ± 0.2	10.0 ± 0.1	1 1.3 ± 0.3
		k_2 (g (mg min)$^{-1}$)	0.0013 ± 0.0002	0.08 ± 0.02	0.0005 ± 0.0001	0.06 ± 0.0 2	0.9 ± 0.6	0.6 ± 0.2	0.17 ± 0.05
		s^2	12.67754	0.03082	0.08118	1.99899	17.02521	0.7637	0.10288
		R^2_{adj}	0.988	0.996	0.992	0.99	0.988	0.995	0.99
	Model compariso	Fisher Test	pseudo 2nd	no difference	no difference	no difference	pseudo 2nd	no difference	pseudo 2nd
		AIC	pseudo 2nd						
		BIC							
WNaOH	pseudo 1st	q_e (mg g^{-1})	35 ± 2	32 ± 3	34 ± 4	25 ± 3	18.6 ± 0.9	17 ± 1	14 ± 1
		k_1 (min^{-1})	0.3 ± 0.1	0.3 ± 0.2	0.5 ± 0.3	0.08 ± 0.04	0.7 ± 0.3	0.4 ± 0.2	0.2 ± 0.1
		s^2	12.69965	16.5867	26.2201	10.8596	1.84179	3.2823	3.35595
		R^2_{adj}	0.887	0.812	0.771	0.848	0.931	0.857	0.837
	pseudo 2nd	q_e (mg g^{-1})	37 ± 2	34 ± 2	36 ± 3	27 ± 3	19.3 ± 0.4	18.3 ± 0.8	15 ± 1
		k_2 (g (mg min)$^{-1}$)	0.013 ± 0.004	0.016 ± 0.08	0.02 ± 0.01	0.004 ± 0.002	0. 06 ± 0.01	0.04 ± 0.01	0.02 ± 0.01
		s^2	3.86432	1.13408	13.0282	5.54252	0.37624	7.13213	1.36035
		R^2_{adj}	0.965	0.954	0.886	0.922	0.986	0.919	0.934
	Model compariso	Fisher Test	pseudo 2nd	pseudo 2nd	no difference	no difference	pseudo 2nd	no difference	no difference
		AIC	pseudo 2nd						
		BIC							

Table A.4.2 Equilibrium models' parameters for the raw (W), acid/base treated (WN-OH) and base treated (WNaOH) vermiculites.

Sample	Model	Parameter	Adsorbate						
			AR	**AR-Cu**	**MB**	**MB-Cu**	**Cu**	**Cu-AR**	**Cu-MB**
W	Langmuir	q_m (mg g^{-1})	44 ± 2	50 ± 3	53 ± 3	39 ± 4	23 ± 3	29 ± 8	20 ± 3
		K_L (L mg^{-1})	1.1 ± 0.4	1.0 ± 0.4	3 ± 1	6 ± 4	0.21 ± 0.07	0.10 ± 0.06	0 .16 ± 0.07
		s^2	3.86022	7.78006	9.52531	16.13978	0.99736	1.53117	0.74422
		R^2_{adj}	0.979	0.978	0.97	0.92	0.975	0.965	0.971
	Freundlich	K_F ((mg g^{-1})(L mg^{-1}) $^{1/n}$)	28 ± 3	23 ± 5	36 ± 3	26 ± 4	5.4 ± 0.9	4.1 ± 0.9	4.3 ± 0.9
		n	8 ± 3	4 ± 1	10 ± 3	8 ± 3	2.4 ± 0.4	1.9 ± 0.3	2.4 ± 0.4
		s^2	6.07661	18.18369	7.17517	17.41732	0.89801	0.73306	0.52895
		R^2_{adj}	0.966	0.948	0.978	0.914	0.977	0.983	0.979
	Model comparison	Fisher Test	no difference						
		AIC	Langmuir	Langmuir	Freundlich	Langmuir	Freundlich	Freundlich	Freundlich
		BIC	Langmuir	Langmuir	Freundlich	Inconclusive	Inconclusive	Freundlich	Freundlich
WN-OH	Langmuir	q_m (mg g^{-1})	145 ± 12	120 ± 10	166 ± 11	150 ± 9	18 ± 3	10 ± 2	14 ± 3
		K_L (L mg^{-1})	69 ± 66	0.5 ± 0.4	0.5 ± 0.2	2 ± 2	0.9 ± 0.9	1.0 ± 0.2	1 ± 1
		s^2	220.66847	196.5586	252.0213	962.297	4.40553	4.98789	3.86874
		R^2_{adj}	0.901	0.868	0.925	0.715	0.897	0.668	0.818
	Freundlich	K_F ((mg g^{-1})(L mg^{-1}) $^{1/n}$)	128 ± 3	40 ± 7	87 ± 9	78 ± 9	9 ± 3	7 ± 1	8 ± 3
		n	14 ± 2	3 ± 1	6 ± 4	5 ± 2	4 ± 2	6 ± 3	5 ± 5
		s^2	10.44326	290.125	344.4944	549.3615	3.61909	0.97868	4.75621
		R^2_{adj}	0.995	0.806	0.897	0.835	0.915	0.935	0.776
	Model comparison	Fisher Test	Freundlich	no difference	no difference	no difference	no difference	Freundlich	no difference
		AIC	Freundlich	Langmuir	Langmuir	Freundlich	Freundlich	Freundlich	Langmuir
		BIC	Freundlich	Langmuir	Langmuir	Freundlich	Inconclusive	Freundlich	Inconclusive
WNaOH	Langmuir	q_m (mg g^{-1})	45 ± 11	50 ± 9	60 ± 15	42 ± 5	37 ± 6	33 ± 7	18 ± 1
		K_L (L mg^{-1})	1 ± 1	0.8 ± 0.9	1 ± 2	5 ± 5	1.1 ± 0.7	1 ± 1	3 ± 1
		s^2	44.96316	43.60653	145.8726	21.03966	24.24723	26.27256	1.05414
		R^2_{adj}	0.825	0.874	0.717	0.909	0.853	0.817	0.972
	Freundlich	K_F ((mg g^{-1})(L mg^{-1}) $^{1/n}$)	25 ± 8	24 ± 7	34 ± 9	30 ± 3	16 ± 4	16 ± 4	12 ± 2
		n	5 ± 4	5 ± 2	6 ± 4	8 ± 3	4 ± 1	4 ± 2	6 ± 2
		s^2	39.37857	27.34547	102.8979	8.32725	21.40007	14.66838	2.56476
		R^2_{adj}	0.847	0.921	0.8	0.964	0.871	0.898	0.933
	Model comparison	Fisher Test	no difference						
		AIC	Freundlich	Freundlich	Freundlich	Freundlich	Freundlich	Freundlich	Langmuir
		BIC	Inconclusive	Freundlich	Freundlich	Freundlich	Inconclusive	Freundlich	Langmuir

Table A.4.3 Yan's and Yoon-Nelson's models' parameters fitted to the experimental data gathered in column experiments for simultaneous adsorption of Cu^{2+}, AR and MB on starting (W), acid/base treated (WN-OH) and base treated (WNaOH) vermiculite.

Material	Model	Cycle	Cu				AR				MB			
		Parameter	I	II	III	IV	I	II	III	IV	I	II	III	IV
W	Yan	q_Y (mg g^{-1})	16.5 ± 0.5	16.3 ± 0.8	12.9 ± 0.7		15 ± 1	15.7 ± 0.6	14.0 ± 0.3		25 ± 1	26 ± 1	22 ± 1	
		a_Y	1.61 ± 0.08	2.3 ± 0.2	1.9 ± 0.2	-	2.6 ± 0.3	6 ± 1	21 ± 8	-	2. 1 ± 0.1	1.9 ± 0.3	2.7 ± 0.4	-
		R^2_{adj}	0.986	0.975	0.982		0.985	0.976	0.985		0.968	0.984	0.977	
		s^2	0.000214	0.00247	0.00201		0.00574	0.00025	0.00182		0.00147	0.00584	0.00268	
	Yoon-Nelson	k_{YN} (min^{-1})	0.013 ± 0.002	0.023 ± 0.0048	0.026 ± 0.006		0.09 ± 0.02	0.16 ± 0.04	0.6 ± 0.2		0.037 ± 0.006	0.032 ± 0.009	0.06 ± 0.02	
		τ_{YN} (min)	125 ± 11	112 ± 10	96 ± 10	-	37 ± 3	37 ± 2	31.2 ± 0.6	-	64 ± 5	60 ± 1	58 ± 5	-
		R^2_{adj}	0.884	0.916	0.908		0.927	0.982	0.985		0.925	0.862	0.951	
		s^2	0.00904	0.00937	0.01056		0.00482	0.00181	0.0018		0.00594	0.0133	0.00619	
WNaOH	Yan	q_Y (mg g^{-1})	51 ± 1	47 ± 1	48 ± 2		55.1 ± 0.8	48.1 ± 0.2	40.5 ± 0.6		80 ± 1	76 ± 2	69.9 ± 0.7	
		a_Y	2.9 ± 0.2	3.9 ± 0.4	2.3 ± 0.2	-	9 ± 1	29 ± 4	16 ± 3	-	5.9 ± 0 .3	5.2 ± 0.5	6.2 ± 0.3	-
		R^2_{adj}	0.969	0.973	0.927		0.984	0.997	0.983		0.994	0.983	0.994	
		s^2	0.003018	0.00356	0.00726		0.00355	0.000491	0.00431		0.00087	0.000276	0.000117	
	Yoon-Nelson	k_{YN} (min^{-1})	0.022 ± 0.005	0.032 ± 0.009	0.019 ± 0.006		0.13 ± 0.02	0 .5 ± 0.1	0.3 ± 0.1		0.072 ± 0.008	0.07 ± 0.02	0.083 ± 0. 01	
		τ_{YN} (min)	164 ± 12	151 ± 10	160 ± 23	-	63 ± 2	55 ± 1	46 ± 1	-	91 ± 2	88 ± 4	80 ± 3	-
		R^2_{adj}	0.913	0.95	0.993		0.991	0.997	0.985		0.991	0.971	0.985	
		s^2	0.085	0.00728	0.00214		0.00196	0.000496	0.00148		0.0014	0.00436	0.00325	
WN-OH	Yan	q_Y (mg g^{-1})	24 ± 1	12.4 ± 0.6	9.5 ± 0.1	8.2 ± 0.2	67 ± 2	45 ± 1	39 ± 1	37.4 ± 0.2	115 ± 2	81 ± 2	69.2 ± 0.9	67.3 ± 0.8
		a_Y	1.7 ± 0.1	3.7 ± 0.6	11 ± 1	7 ± 1	3.6 ± 0.3	5.5 ± 0.8	12 ± 5	9.2 ± 0.5	3.0 ± 0.1	3.2 ± 0.2	6.5 ± 0.5	4.8 ± 0.2
		R^2_{adj}	0.924	0.931	0.985	0.966	0.964	0.965	0.906	0.997	0.99	0.978	0.994	0.994
		s^2	0.007	0.00869	0.00156	0.00288	0.0044	0.0033	0.0202	0.000425	0.00139	0.0034	0.0014	0.000918
	Yoon-Nelson	k_{YN} (min^{-1})	0.020 ± 0.006	0.12 ± 0.04	0.38 ± 0.09	0.30 ± 0.09	0.06 ± 0.02	0.12 ± 0.04	0.20 ± 0.02	0.22 ± 0.02	0.028 ± 0.00 5	0.039 ± 0.009	0.08 ± 0.01	0.062 ± 0.009
		τ_{YN} (min)	91 ± 15	39 ± 3	29.4 ± 0.7	26 ± 1	75 ± 5	52 ± 3	45 ± 3	43.5 ± 0.5	128 ± 7	105 ± 7	88 ± 2	86 ± 3
		R^2_{adj}	0.787	0.922	0.985	0.964	0.945	0.98	0.907	0.997	0.959	0.952	0.992	0.988
		s^2	0.01905	0.00971	0.00163	0.00308	0.0065	0.00356	0.01998	0.000418	0.00553	0.0075	0.00177	0.00206

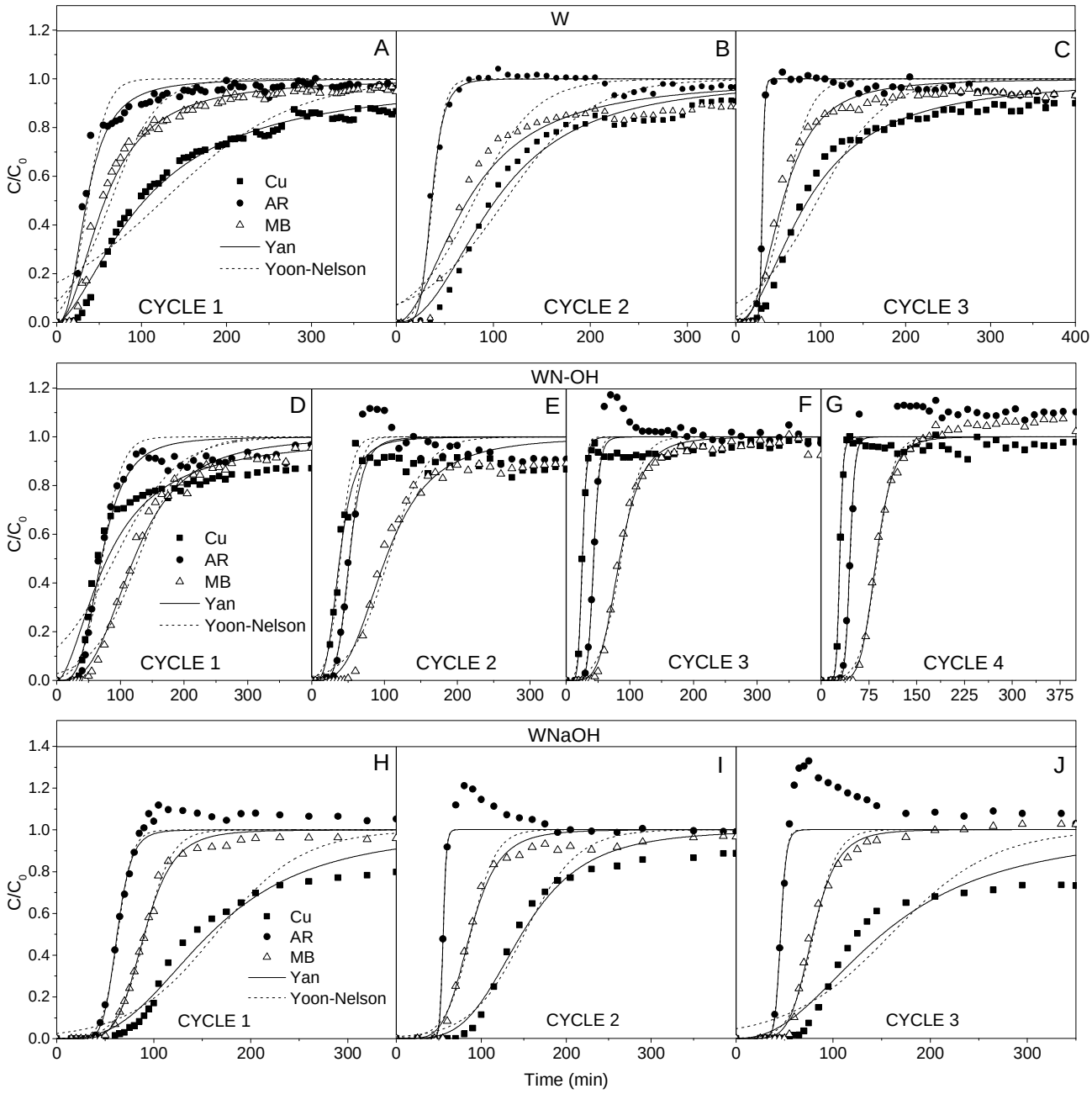

Figure A.4.1 Adsorption curves for Cu^{2+}, AR and MB in simultaneous adsorption, with fitted Yan's and Yoon-Nelson's model on starting (W), acid/base treated (WN-OH) and base treated (WNaOH) vermiculite in subsequent adsorption/desorption cycles.

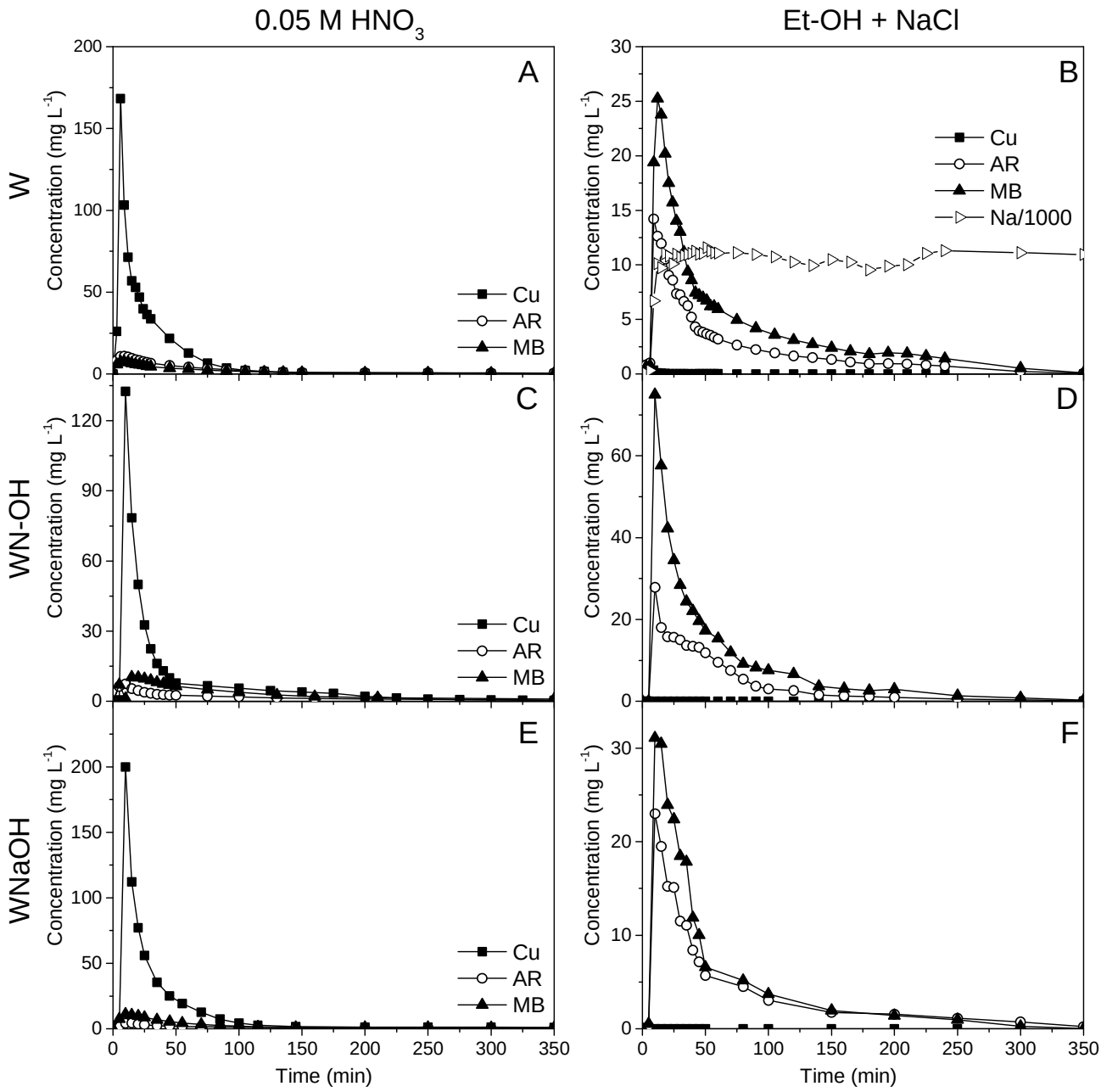

Figure A.4.2 Desorption curves from raw vermiculite (W), acid/base treated vermiculite (WN-OH), and base treated vermiculite (WNaOH): (A,C,E) desorption of Cu^{2+} with 0.05 M, (B,D,F) HNO_3 desorption of dyes with Et-OH + 1 M NaCl.

Supporting material S.4

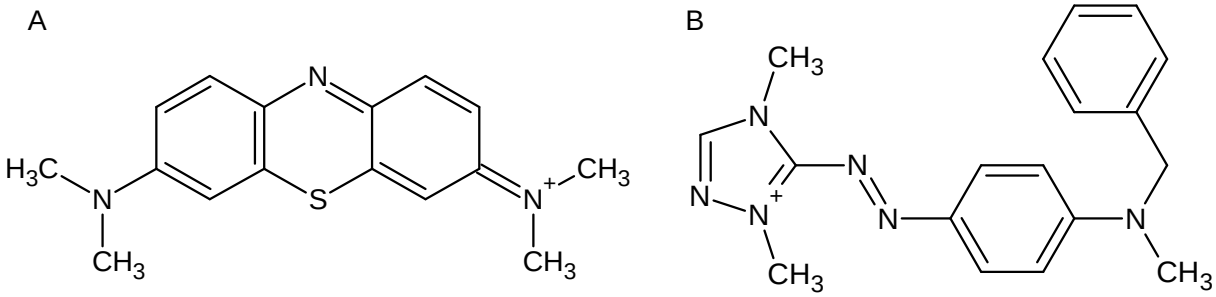

Figure S.4.1 Structural and molecular formulas of methylene blue (A) and astrazon red (B).

S.4.1 Attenuated total reflectance (ATR)

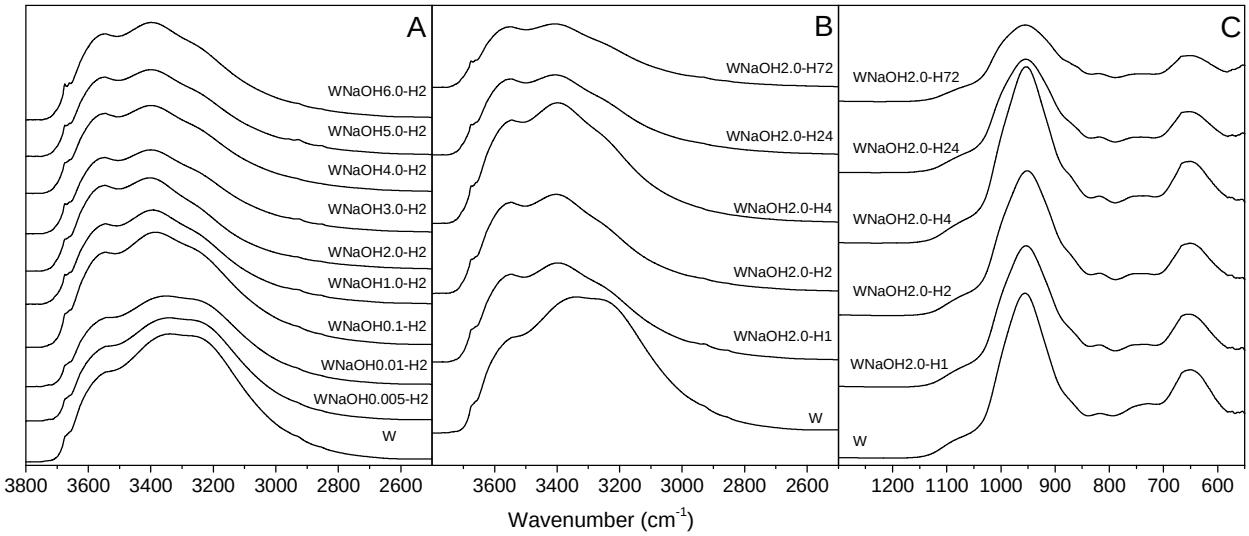

Figure S.4.2 ATR spectra of vermiculite treated in different NaOH concentrations (A) and different treatment time (B and C).

In the spectra of the NaOH treated material two peaks at 3672 cm^{-1} and 3555 cm^{-1} can be seen and associated to stretching vibrations of structural hydroxyls (Chukanov, 2014): Mg_3OH (Číčel and Komadel, 1997; Parikh et al., 2014) and AlFeOH (Besson and Drits, 1997; Parikh et al., 2014), respectively. Similar position of the peaks in the spectra after modifications proves minor effect of interlayer cation on such adsorption properties. However, position of the peak attributed to stretching vibrations of H-O-H at 3348 cm^{-1} (Farmer, 1974) in the raw material shifted towards higher wavenumbers and the peak attributed to stretching vibrations of OH (Chukanov, 2014) at 3230 cm^{-1} lowered its intensity. The process is completed after 2 h treatment in 2.0 M NaOH (Fig.S.4.2A and B). Such change is consistent with exchange of the interlayer cation from Mg^{2+} to Na^+ that has lower polarizing power (charge/radius) (Madejova, 2003). Interlayer cation is also determinative for how much water is adsorbed into the

interlayer region of clays which is reflected in decreased intensity of water bands in the NaOH treated material. Spectra of the material in the range of lower wavelengths do not change up to treatment time equal 24 h where the peak at around 960 cm^{-1} assigned to Si-O stretching (Stubičan and Roy, 1961; Ritz et al., 2014) decreases (Fig.S.4.2C).

In the spectra of acid treated material the peaks at 3672 cm^{-1} and at 3230 cm^{-1} decrease their intensity with increasing acid concentration beginning from 0.1 M (Fig.S.3A). Also peak at around 960 cm^{-1} assigned to Si-O stretching (Stubičan and Roy, 1961; Ritz et al., 2014) together with peaks associated with bending and deformation vibrations in octahedral layer (Liu et al., 2011) at 866 cm^{-1} assigned to AlFeOH (Madejová and Komadel, 2001) 815 cm^{-1} and 765 cm^{-1} corresponding to tetrahedral Al–O out-of-plane and Al–O–Si in-plane vibrations (Madejová and Komadel, 2001) respectively, decrease intensity and disappear with increasing acid concentration. Peaks at 1075 cm^{-1} and 995 associated with amorphous silica become sharper in the spectra and peaks at 815 cm^{-1} also assign to amorphous silica (Chmielarz et al., 2012; Barabaszová and Valášková, 2013) broadens after acid treatment (Fig.S.4.3B)

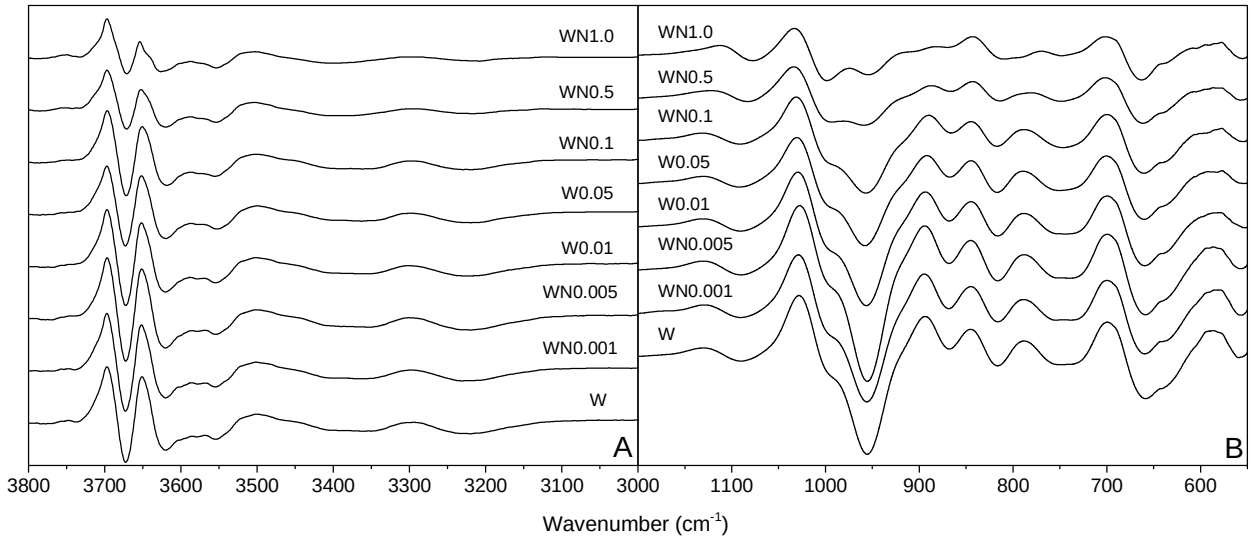

Figure S.4.3. Second derivative (d^2A/dv^2) of ATR spectra of acid treated vermiculite in desorption studies.

S.4.2 X-ray diffraction (XRD)

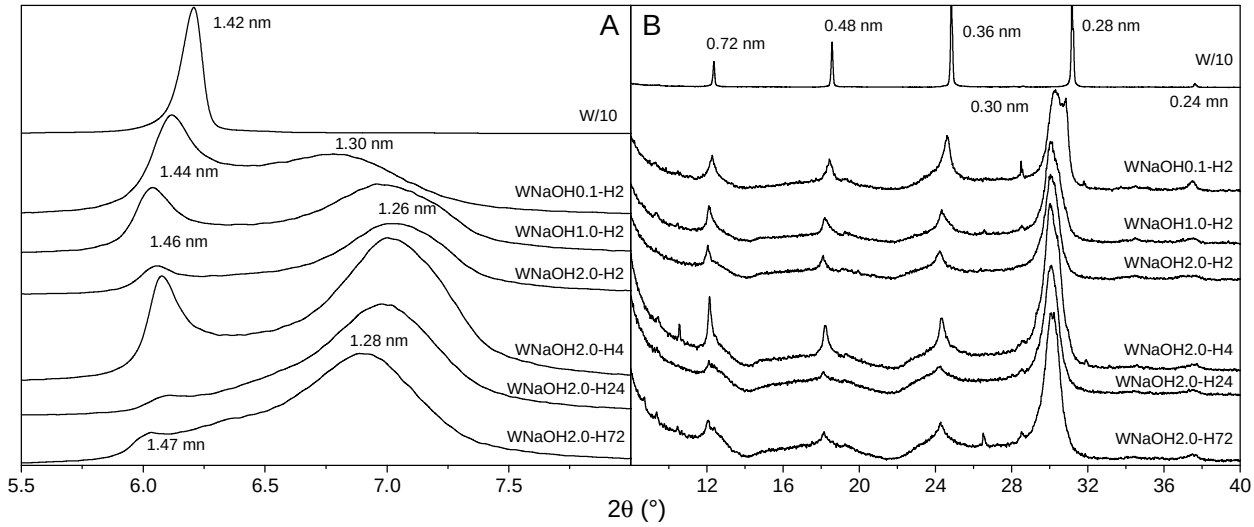

Figure S.4.4 XRD phase composition of raw (W) and NaOH treated vermiculite in different times and concentrations.

The raw material showed typical reflections of vermiculite at 6.2° (d=1.42 nm, 002), 12.3° (d=0.72 nm, 004), 18.5° (d=0.48 nm, 006), 24.8° (d=0.36 nm, 008), 31.2° (d=0.28 Å, 0010), 37.5° (d=0.24 nm, 0012), what is in agreement with JCPDS card nos. 01-076-0847 and 00-016-0613 (Santos et al., 2015). The reflection at 6.2° is consistent with a vermiculite phase with two, slightly incomplete, water bilayers (Muiambo et al., 2010) indicating presence of hydrated cations like Mg (El Mouzdahir et al., 2009). This reflection loses intensity and shifts slightly towards lower angles after the treatment. Position of that reflection may slightly vary without changing the hydration state depending on the number of interlayer water molecules (Ferrage et al., 2005). The reflection present in the pattern of base treated materials between 6.80° to 7.02° (Fig.S.4.4A) may be attributed to a phase originated from two- (Mg-vermiculite) and one-sheet (Na-vermiculite (Huo et al., 2012)) layers of water (Collins et al., 1992; Ruiz-Conde et al., 1996; Marcos et al., 2003) and interstratification between contracting and non-contracting phases (Walker, 1961). Also the peak at 30.30° (Fig.S.4.4B) is attributed to Na-vermiculite (Huo et al., 2012).

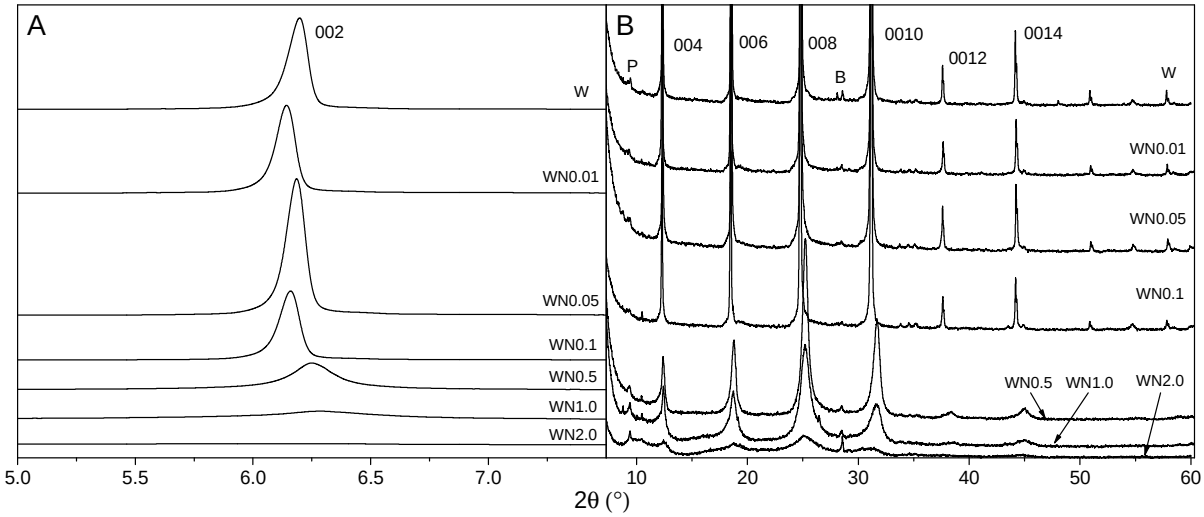

Figure S.4.5 XRD patterns of HNO_3 treated vermiculite.

The 002 reflection of vermiculite decrease its intensity after treating in 0.1 M HNO_3, when higher concentrations were used the peak became broader and shifted towards higher angles and finally disappeared. That suggests leaching of interlayer cations and dissolution of clay lattices (Komadel and Madejova, 2006). The peak of the sample treated in 0.05 M acid however, exhibited increased intensity compared to the starting material (Fig.S.4.5A). In the range of higher angles reflection between 50° and 60° completely disappeared in concentration higher than 0.1 M and other reflections became less intense and broader (Fig.S.4.5B). Impurities of boehmite (Oberlin and Couty, 1970) (B) present in the raw material were gradually washed off upon acid treatment (Fig.S.4.5B) while phlogopite (Steudel, 2008) (P) still may be identified. The results suggest that 0.05 M concentration of HNO_3 is optimal for desorption since it is strong enough to leach adsorbed species from the material and reactivate sample without damaging the structure of material.

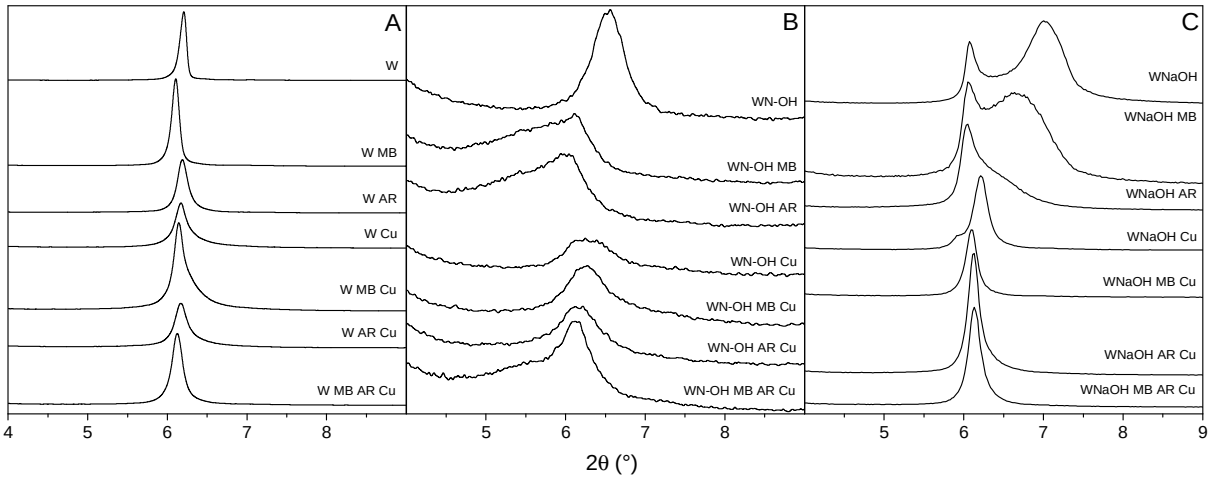

Figure S.4.6 XRD patterns of phase composition of spent adsorbents.

The diffractogram of spent raw vermiculite (Fig.S.4.6A) showed reflection at around 6.20° that corresponds to double layer of water around interlayer cation, no intercalation of adsorbate in-between the layers was noticed. The patterns of acid/base treated sample (Fig.S.4.6B) showed reflection at 6.55° attributed to a phase saturated with Mg (Sakharov et al., 1999), composed of smectite-like layers and hydroxy-intercalated vermiculite (HIV) formed due to migration of metal ions from the active dissolution sites into the interlayer space (Kalinowski and Schweda, 2007; Mareschal et al., 2009). After adsorption the peak shifts to 6.20° and additional peak appeared at 5.40° in case of adsorption of AR and MB from single component solution. In the patterns of alkali modified samples the peak at around 7° disappears after adsorption from solutions where Cu^{2+} was present. The peak shifts slightly towards lower angles in case of MB and after adsorption of AR is present as a shoulder on the main reflection at 6.20° (Fig.S.4.6C).

S.4.3 Cation exchange capacity (CEC) and specific surface area (BET)

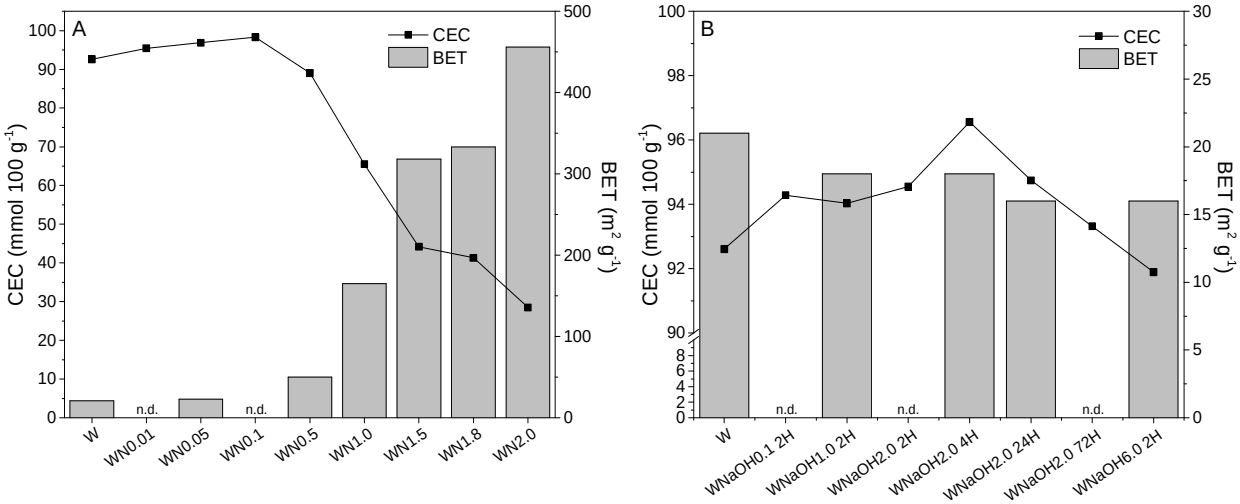

Figure S.4.7 Cation exchange capacity (CEC) and specific surface area (BET) for acid (A) and base (B) treated vermiculites.

The cation exchange capacity (CEC) slightly increased upon acid treatment with low concentrations however, beginning from 0.5 M the CEC rapidly decreased. Also treatment in such conditions caused a significant increase in specific surface of the material (Fig.S.4.7A). Alkali treatment resulted in an increase in the CEC of the material with an optimum after treating for 4 h in 2.0 M NaOH, beyond that concentration and during longer treatment the CEC decreased. No significant changes in specific surface area were noticed (Fig.S.4.7B).

S.4.4 X-ray fluorescence analysis (XRF)

The analysis showed that the starting material was composed of SiO_2 in approximately 52%, MgO in 24%, Al_2O_3 in 12%, Fe_2O_3 in 11% and of K_2O and CaO in 1%. Upon base treatment the chemical composition of the samples did not change significantly (Fig.S.4.8A). On the other hand, a significant leaching of elements was observed in case of acid activation. Application of concentrations up till 0.5 M removed only the metals occurring as trace additives, however concentrations higher than 0.5 M resulted in gradual leaching of Mg, Al and Fe from the material (Fig.S.4.8B).

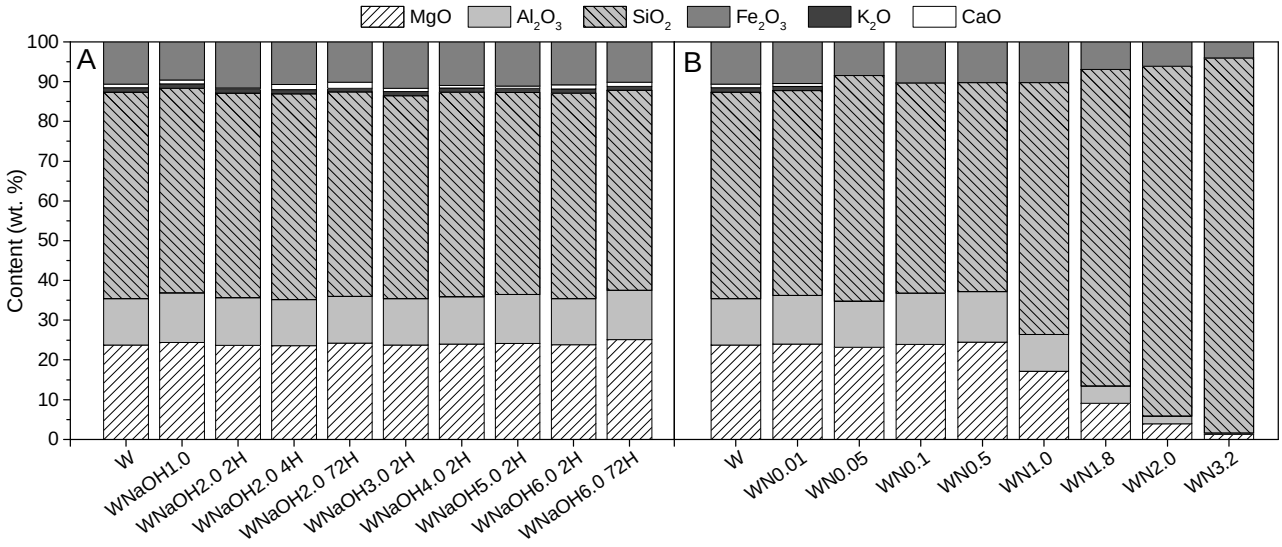

Figure S.4.8 X-ray fluorescence analysis of samples treated with base (A) and with acid (B).

S.4.5 Weber-Morris model

The plot of uptake, q_t, versus the square root of time ($t^{1/2}$) should be linear if intra-particle diffusion is involved in the adsorption process (Fig.S.4.9). Moreover, if these lines pass through the origin then intra-particle diffusion is the rate-controlling step (Arami et al., 2008). However, if the data exhibit multi-linear plots, then two or more steps influence the sorption process indicating that some degree of boundary layer controls the rate which shows that the intra-particle diffusion is not the only rate-limiting step, but also other kinetic models may control the rate of adsorption, e.g. film or external diffusion, pore diffusion, surface diffusion and adsorption on the pore surface, or a combination of more than one step operating simultaneously (Fierro et al., 2008).

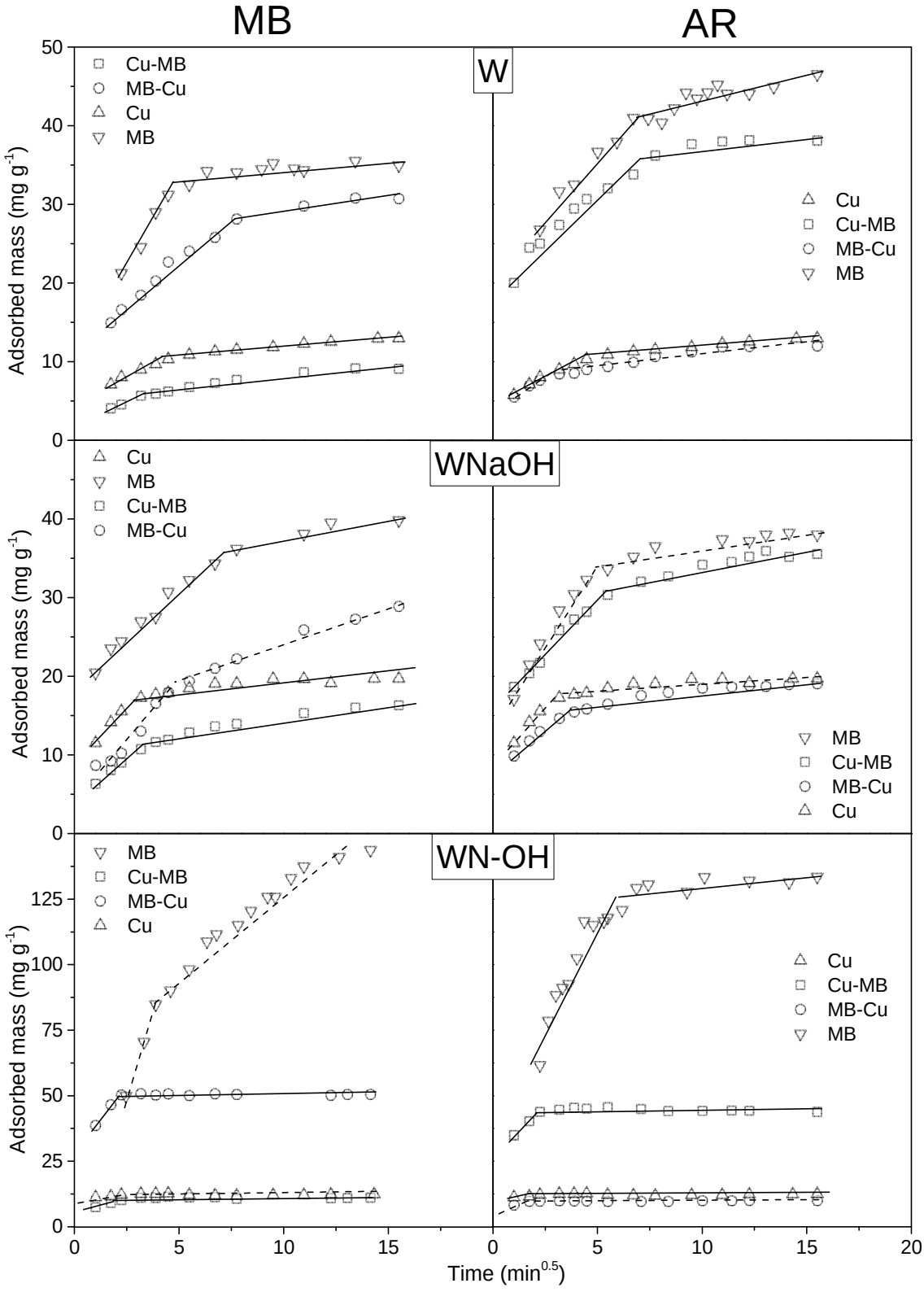

Figure S.4.9 Kinetic experimental data with Weber-Morris model fitted.

S.4.6 References

Arami, M., Limaee, N.Y., Mahmoodi, N.M., 2008. Evaluation of the adsorption kinetics and equilibrium for the potential removal of acid dyes using a biosorbent. Chem. Eng. J. 139, 2-10.

Barabaszová, K.Č., Valášková, M., 2013. Characterization of vermiculite particles after different milling techniques. Powder Technol. 239, 277-283.

Besson, G., Drits, V.A., 1997. Refined relationships between chemical composition of dioctahedral fine-grained mica minerals and their infrared spectra within the oh stretching region. Part I: identification of the oh stretching bands. Clay and Clay Minerals 45, 158-169.

Chmielarz, L., Wojciechowska, M., Rutkowska, M., Adamski, A., Węgrzyn, A., Kowalczyk, A., Dudek, B., Boroń, P., Michalik, M., Matusiewicz, A., 2012. Acid-activated vermiculites as catalysts of the DeNOx process. Catal. Today 191, 25-31.

Chukanov, N.V., 2014. Infrared spectra of mineral species. Extended library.

Čícel, B., Komadel, P., 1997. Structural formulae of layer silicates. in: Amonette, J.E., Zelazny, L.W. (Eds.). Quantitative Methods in Soil Mineralogy. SSSA.

Collins, D.R., Fitch, A.N., Catlow, C.R.A., 1992. Dehydration of vermiculites and montmorillonites: a time-resolved powder neutron diffraction study. J. Mater. Chem. 2, 865-873.

El Mouzdahir, Y., Elmchaouri, A., Mahboub, R., Gil, A., Korili, S.A., 2009. Synthesis of nano-layered vermiculite of low density by thermal treatment. Powder Technol. 189, 2-5.

Farmer, V.C., 1974. The Infrared spectra of minerals. Mineralogical Society.

Ferrage, E., Lanson, B., Malikova, N., Plançon, A., Sakharov, B.A., Drits, V.A., 2005. New Insights on the Distribution of Interlayer Water in Bi-Hydrated Smectite from X-ray Diffraction Profile Modeling of 00l Reflections. Chem. Mater. 17, 3499-3512.

Fierro, V., Torné-Fernández, V., Montané, D., Celzard, A., 2008. Adsorption of phenol onto activated carbons having different textural and surface properties. Microporous Mesoporous Mater. 111, 276-284.

Huo, X., Wu, L., Liao, L., Xia, Z., Wang, L., 2012. The effect of interlayer cations on the expansion of vermiculite. Powder Technol. 224, 241-246.

Kalinowski, B.E., Schweda, P., 2007. Rates and nonstoichiometry of vermiculite dissolution at 22°C. Geoderma 142, 197-209.

Komadel, P., Madejova, J., 2006. Acid Activation of Clay Minerals. in: Bergaya, F., Theng, B.K.G., Lagaly, G. (Eds.). Handbook of Clay Science. Elsevier Ltd.

Liu, D., Yuan, P., Liu, H., Cai, J., Qin, Z., Tan, D., Zhou, Q., He, H., Zhu, J., 2011. Influence of heating on the solid acidity of montmorillonite: A combined study by DRIFT and Hammett indicators. Appl. Clay Sci. 52, 358-363.

Madejova, J., 2003. FTIR techniques in clay mineral studies. Vib. Spectrosc. 31, 1-10.

Madejová, J., Komadel, P., 2001. Baseline studies of the clay minerals society source clays: infrared methods. Clays Clay Miner. 49, 410-432.

Marcos, C., Argüelles, A., Ruíz-Conde, A., Sánchez-Soto, P.J., Blanco, J.A., 2003. Study of the dehydration process of vermiculites by applying a vacuum pressure: formation of interstratified phases. Mineral. Mag. 67, 1253-1268.

Mareschal, L., Ranger, J., Turpault, M.P., 2009. Stoichiometry of a dissolution reaction of a trioctahedral vermiculite at pH 2.7. Geochim. Cosmochim. Acta 73, 307-319.

Muiambo, H.F., Focke, W.W., Atanasova, M., der Westhuizen, I.v., Tiedt, L.R., 2010. Thermal properties of sodium-exchanged palabora vermiculite. Appl. Clay Sci. 50, 51-57.

Oberlin, A., Couty, R., 1970. Conditions of kaolinite formation during alternation of smoe silicates by water at 200 °C. Clays nad Clay Minerals 19, 47-356.

Parikh, S.J., Goyne, K.W., Margenot, A.J., Mukome, F.N.D., Calderón, F.J., 2014. Chapter One - Soil Chemical Insights Provided through Vibrational Spectroscopy. in: Donald, L.S. (Ed.). Advances in Agronomy. Academic Press, pp. 1-148.

Ritz, M., Zdrálková, J., Valášková, M., 2014. Vibrational spectroscopy of acid treated vermiculites. Vib. Spectrosc. 70, 63-69.

Ruiz-Conde, A., Ruiz-Amil, A., Perez-Rodriguez, J.L., Sanchez-Soto, P.J., 1996. Dehydration-rehydration in magnesium vermiculite: conversion from two-one and one-two water layer hydration states through the formation of interstratified phases. J. Mater. Chem. 6, 1557-1566.

Sakharov, B.A., Lindgreen, H., Salyn, A.L., Drits, V.a., 1999. Mixed-layer kaolinite-illite-vermiculite in North Sea shales. Clay Miner. 34, 333-334.

Santos, S.S.G., Silva, H.R.M., de Souza, A.G., Alves, A.P.M., da Silva Filho, E.C., Fonseca, M.G., 2015. Acid-leached mixed vermiculites obtained by treatment with nitric acid. Appl. Clay Sci. 104, 286-294.

Steudel, A., 2008. Selection Strategy and Modification of Layer Silicates for Technical Applications. Univ.-Verlag Karlsruhe.

Stubičan, V., Roy, R., 1961. Infrared Spectra of Layer-Structure Silicates. J. Am. Ceram. Soc. 44, 625-627.

Walker, G.F., 1961. Vermiculite minerals. in: Brown, G. (Ed.). The X-ray Identification and Crystal Structures of Clay Minerals. Mineralogical Society of Great Britain Monograph, Great Britain, pp. 297-324.

CHAPTER 5

Hydrotalcite

Dual-function hydrotalcite-derived adsorbents with sulfur storage properties: dyes and hydrotalcite fate in adsorption-regeneration cycles

Wojciech Stawiński[a], Agnieszka Węgrzyn[b,*], Olga Freitas[a], Lucjan Chmielarz[b], Sónia Figueiredo[a]

[a] *REQUIMTE, LAQV, Instituto Superior de Engenharia do Porto, Instituto Politécnico do Porto, Rua Dr. António Bernardino de Almeida 431, 4200-072 Porto, Portugal*
stawor@gmail.com; omf@isep.ipp.pt; saf@isep.ipp.pt

[b] *Faculty of Chemistry, Jagiellonian University, ul. Ingardena 3, 30-060 Kraków, Poland*
wegrzyn@chemia.uj.edu.pl; chmielar@chemia.uj.edu.pl

Abstract

Thermal treatment of hydrotalcite at increasing temperatures resulted in formation of mixed oxides that exhibited different adsorption behavior toward anionic and cationic industrial dyes. The material annealed at 450 °C was characterized by the highest maximum adsorption capacity for both types of dyes. The adsorption was strongly pH dependent and for the anionic dye abatement low pH was favored whilst higher pH was more preferable for removal of the cationic dye. According to the equilibrium experiments, the maximum adsorption capacity increased from 179 ± 5 to 291 ± 8 mg g^{-1} in case of the anionic dye at pH 3.5 and from 6 ± 2 to 48 ± 2 mg g^{-1} in case of the cationic dye at pH 8.0, on starting and thermally treated material at 450 °C, respectively. Detailed characteristics of spent adsorbent and its reconstructed form revealed that after each cycle of adsorption and thermal regeneration the maximum adsorption capacity of the material decreased due to changes in the structure and accumulation of sulfur compounds. Evolution of specific surface area and porosity was correlated with annealing temperatures and behavior of dye's residues.

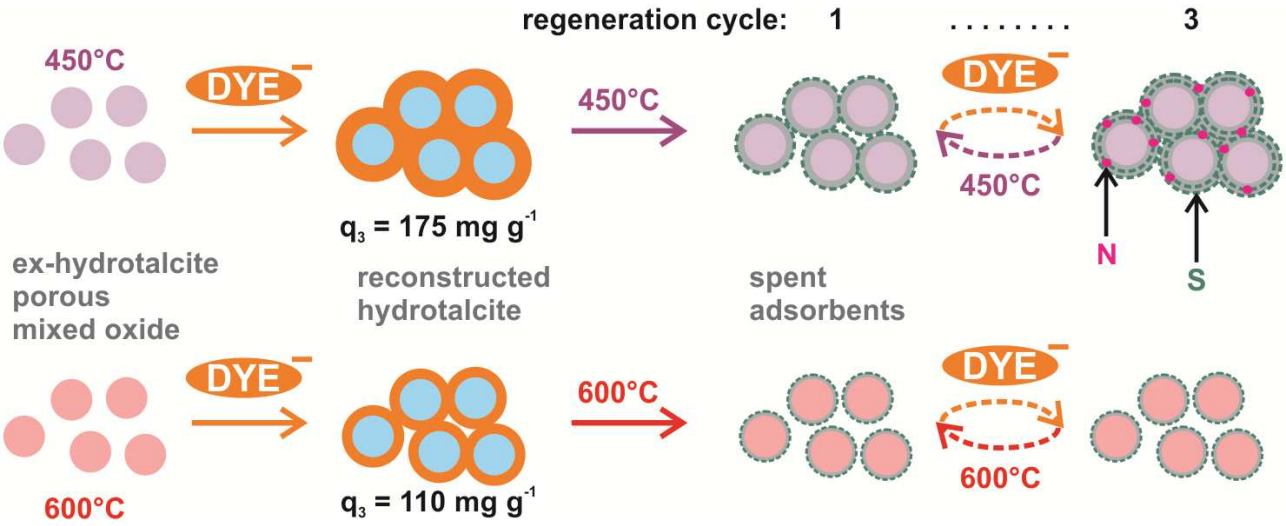

Keywords: hydrotalcite, thermal treatment, removal of dyes, spent adsorbent, sulfur accumulation

5.1 Introduction

Colored wastewater is created as a result of the production of the dye and as well as a direct consequence of its use in the textile and related industries. Consumption of colored textiles, which is one of the basic technologies in human civilization, is steadily increasing worldwide, following the growth of world population (Leube, 2007). The textile dyeing and finishing industry, being one of the most chemically intensive industries on earth has created major environmental problems and is the second greatest polluter of clean water, right after agriculture. Many of chemicals present in wastewaters are cause of significant environmental degradation and human diseases (Kant, 2012). Dyes can exhibit acute toxicity, sensitization, chronic effects after repeated application, mutagenic and carcinogenic effects on human. Dyestuffs, being intensely colored, are usually the first contaminant to be recognized in wastewaters and present special problems because even a small amount is highly visible. They can exhibit ecotoxicity and affect transparency and gas solubility of water bodies. By absorbing the sunlight entering water they alter growth of the aquatic species and hinder photosynthesis upsetting natural ecosystems. Synthetic dyes are in general not readily biodegradable and chemically stable thus traditional wastewater treatment techniques are ineffective. It is also important to handle the residues and byproducts obtained after decolorization process because many of them have negative influence on environment (Mondal and Chauhan, 2012) The development of efficient, economic and environmentally friendly technologies to remove color and detoxify the wastewaters to acceptable levels and decrease their environmental impact at affordable cost is the first and major concern of the utmost importance (Sevekow, 2003; Pereira and Alves, 2011). Among many other techniques adsorption is considered as one of the best wastewater treatment methods due to its universal nature, ease of operation, ability to remove soluble and insoluble organic pollutants, high removal capacity and possibility to recycle and reuse many of adsorbents (Pan et al., 2009; Ali et al., 2012). Activated carbon is the most widely used adsorbent however, its preparation is generally energy-consuming and commercially available product are relatively expensive, which may hamper its application (Rozada et al., 2003; Pereira and Alves, 2011). This has triggered a growing interest in production of low-cost adsorbents.

Hydrotalcite-like (HTL) materials, layered double hydroxides (LDH) or anionic clays are the common names given to a wide family of layered materials with both divalent and trivalent metallic cations in the main, positively charged layers and an interlayer anionic species balancing the layers charge. The interlayer anion can be almost freely exchanged for a wide possible selection of anionic compounds present in

liquid phase. The principal areas of interest, among others, include their application as adsorbents. A unique property of such materials is that after thermal treatment under mild conditions, they are able to reconstruct the layered structure which opens a possibility for regeneration of a spent adsorbent (de Roy et al., 2006; Rives, 2006).

5.2 Experimental

5.2.1 Materials

5.2.1.1 Adsorbent preparation and characterization

Hydrotalcite (HT) with formula $[Mg_{0.67}Al_{0.33}(OH)_2](CO_3)_{0.165}\cdot 2H_2O$, was prepared by co-precipitation method. A solution of 0.667 M $MgCl_2$ and 0.333 M $Al(NO_3)_2\cdot 9H_2O$ was added drop-wise from one dropping funnel and a solution of 2 M NaOH was added from another dropping funnel to a 0.160 M solution Na_2CO_3 while keeping it at pH 10, temperature 60 °C under constant stirring. Prepared HT was washed four times in hot water (70 °C), filtered, left to dry for 24 h at 100 °C and ground with a mortar.

Hydrotalcite-derived mixed oxides (HTox) were prepared by calcinating of HT in a muffle furnace at different temperatures 300, 450, 600 and 750 °C (originating HToxC300, HToxC450, HToxC600 and HToxC750 respectively) according to the following procedure: heating rate of 2 °C min^{-1} followed by 6 h of calcination at given temperature.

The structure of the materials was studied with X-ray powder diffractometer (Bruker, D2 PHASER) equipped with CuKα radiation source. Infrared spectra of the samples were recorded using attenuated total reflectance technique (Nicolet 6700 FT-IR, Thermo Scientific). UV–Vis-diffuse reflectance spectra were recorded using an Evolution 600 (Thermo) spectrophotometer. Samples were diluted before measurements with Al_2O_3 to lower the absorbance in order to obtain the measurable range (30 mg of the sample ground with 270 mg of Al_2O_3 in a mortar). The textural parameters of the samples were determined by adsorption of N_2 at −196 °C using a 3Flex (Micromeritics) surface characterization analyzer on outgassed samples. The elemental organic analysis was performed using Vario Micro Cube elemental analyzer with electronic microbalance.

5.2.1.2 Adsorbate

Two dyestuffs, kindly supplied by DyStar, were used in the pH optimization, kinetics, equilibrium and adsorbent regeneration experiments: a cationic dye, Astrazon Red FBL 200% (AR), CI 85496-37-3 and an anionic dye, Levafix Amber CA gran (AMB), which formula was not revealed by the manufacturer however, it is known to have a fluorotriazinedivinylsulphone structure.

Additionally, in order to better understand interactions of the dyes with adsorbent AMB and three other dyes, Reactive Red 184 (R), Congo Red (CR) and Methyl Orange (MO), were used to saturate adsorbent calcined at 450 °C with excess of concentrated solutions (5 g L^{-1}). Suspensions were stirred for 24 h, centrifuged (5 min at 4500 rpm), washed repeatedly with distilled water and left to dry at room temperature.
The structure of these dyes is presented in the Appendix (Fig. A.5.1).

5.3 Methods

5.3.1 Determination of dyestuff concentration

The dyestuff concentration was measured using UV-Vis spectrometer (Thermo Scientific, Evolution 300) at the maximum absorbance wavelength of each dyestuff (230 nm for AMB and 531 nm for AR).

5.3.2 pH optimization in adsorption studies

A portion of 20 mg of each material was placed in Erlenmeyer flasks with 30 mL of 100 mg L^{-1} dye solution (AMB and AR). Each flask was adjusted to a different pH value, 3.5, 4.5, 5.0, 7.0, 8.0 and 9.0. Flasks were shaken for 2 h at room temperature, centrifuged (1 min at 4500 rpm, Sartorius, Sigma 2-16) and the dye concentration was determined.

5.3.3 Kinetic experiments

Kinetic experiments were conducted using a magnetic stirrer, at room temperature, and at 400 rpm. The experiment was conducted at pH 3.5 for every sample and additionally at pH 8.0 only for HToxC450. Masses of 100 mg of each material were placed in round-bottom flasks and 200 mL of 200 mg L^{-1} the dyes solution (AMB and AR). Samples were collected in selected time intervals, immediately centrifuged and then concentration of the dye was determined.

5.3.4 Equilibrium experiments

Adsorption isotherms were obtained at room temperature, at pH adjusted to 3.5 for all samples and additionally at pH 8.0 only for HToxC450. Weighted portions of 20 mg of each material were placed in Erlenmeyer flasks with caps and mixed with 30 mL of dyes solutions (AMB and AR) of varying concentrations (10 mg L^{-1} to 300 mg L^{-1}). Flasks were shaken for 4 h, then solutions were centrifuged and concentration of the dye determined in each flask.

5.3.5 Regeneration of the spent adsorbent

Weighted portions of each sample were saturated in concentrated solution of AMB during 2 h in Erlenmeyer flasks with pH adjusted to 3.5 and another series was made without pH adjustment. In the latter case the final pH was equal to 6.0. Samples were centrifuged (5 minutes at 4500 rpm) and left to dry at 40 °C for 12 h. After that each of the samples was calcined at the same temperature used in their preparation (300, 400, 600, 750 °C) and another batch adsorption cycle was performed with the same dyestuff. Experiment was repeated 3 times and at the end of each cycle small portions of samples were collected and analyzed (BET, XRD, UV-Vis and OEA).

5.3.6 Data analysis

Adsorption capacities of the materials were then calculated according to Eq. 1.

$$q_{=}\frac{(C_0-C_{eq})V}{m} \qquad (1)$$

where q is adsorption capacity (mg g^{-1}), C_0 and C_{eq} initial and equilibrium concentrations (mg L^{-1}) respectively, V, volume of adsorbate (L) and m, adsorbent mass (g).

To describe the adsorption kinetics two models were adjusted to the experimental data. The pseudo 1st order model (Lagergren, 1898) and the pseudo 2nd order model (Ho and McKay, 1999). Two models were fitted to the data obtained in equilibrium studies. The Langmuir's model (Langmuir, 1918) model and the Freundlich's model (Freundlich, 1906). All models were fitted to the experimental data using non-linear regression. The parameters of models are presented with the respective confidence intervals at 95% confidence level. Variances and correlation coefficients were determined and compared using Fisher's, Akaike Information Criterion (AIC), and Bayesian Information Criterion (BIC) tests. Detailed models' description is given in the Supporting Materials

5.4 Results

5.4.1 Optimization of pH in adsorption studies

The results obtained (Fig. 5.1) revealed differences in the maximum adsorption capacities depending on the temperature used during calcination and pH of the solution. The best treatment conditions were achieved at 450 °C and the optimal pH condition for adsorption was 3.5 for AMB (Fig. 5.1A) and pH 8.0 for adsorption of AR (Fig. 5.1B). The samples treated that way exhibited good adsorption capacity towards the anionic dye (AMB) as well as satisfactory towards the cationic one (AR). It was observed that the adsorption capacity decreased with increasing pH in the first case, however in case of the cationic dye the lowest capacities are observed for pH values of 7.0 and 8.0, except for HToxC450.

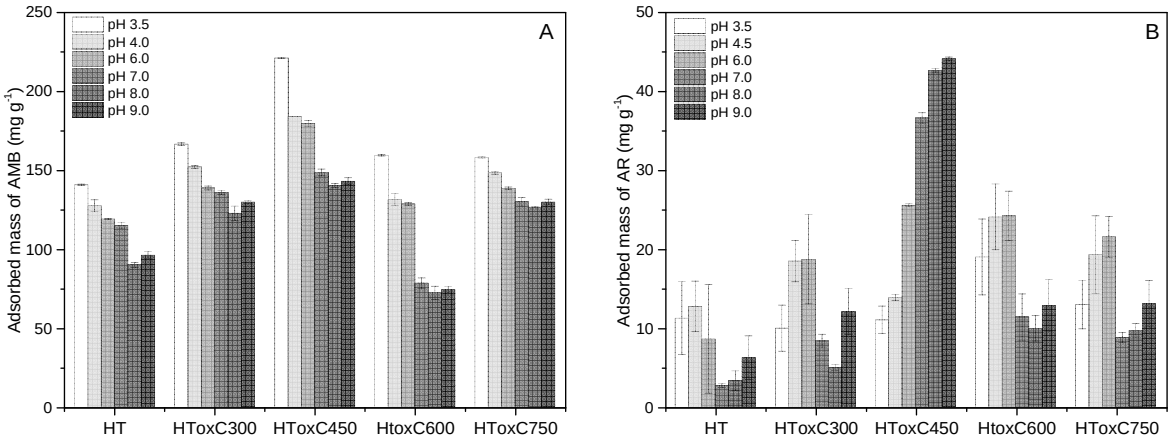

Figure 5.1 Adsorption capacity of AMB (A) and AR (B) for different pH and thermal treatment conditions of hydrotalcite.

5.4.2 Kinetics and equilibrium

Adsorption studies were performed for kinetics and equilibrium for all systems at pH 3.5, which is the optimal pH for AMB (Table A.5.1). Experimental values and the respective model fits are represented in Fig. 5.2.

Similar experiments were performed for HToxC450, which was the material that presented higher capacities in section 3.1, at pH 8.0 that is the optimal for adsorption of AR (Table A.5.2). Kinetic and equilibrium experimental values and their model fits are shown in Fig. 5.3.

There was no difference in goodness of fit between the models at pH 3.5 and 8.0 according to Fisher's test, however AIC and BIC tests revealed that pseudo 2nd order model fitted better at pH 3.5 and pseudo 1st order model at pH 8.0, for both dyes (Table A.5.1). Adsorption of AMB at pH 3.5 occurred at lower rate than adsorption of AR according to the pseudo 2nd order kinetic constant (Fig. 5.2A and 5.2B). At pH 8.0, where

pseudo 1st order model was the best fit, the rate for AMB was higher than for AR (Fig. 5.3A). In the experiment conducted at pH 3.5 the sample treated at 450 °C was the one with the lowest rate for both dyes and needed approximately 120 min to reach the equilibrium for AMB and 50 min for AR. In other cases equilibrium was reached in approximately 60 and 30 min (Fig. 5.2A and 5.2B). At pH 8.0 the adsorption equilibrium of AMB was reached approximately after 120 min and around 150 min was necessary for the equilibrium in case of AR (Fig. 5.3A).

Adsorption equilibrium studies of AMB and AR at pH 3.5, according to Fisher's AIC and BIC tests, followed the Langmuir's model. However at pH 8.0 Freundlich's model was a better fit for adsorption of AMB whereas adsorption of AR kept following the Langmuir's model. All parameters of the models are presented in Table A.5.1 for pH 3.5 and in Table A.5.2 for pH 8.0 in the Appendix.

Equilibrium experiments showed that the thermal treatment of the material resulted in an increase in its maximum adsorption capacity for both dyes. The highest adsorption capacity was reached for the sample treated at 450 °C (Fig. 5.2C and 5.2D). Above 450 °C the capacity decreased. The pH was the major factor affecting adsorption. At pH 3.5 an increase from 179 ± 5 to 291 ± 8 mg g^{-1} was noticed for AMB and from 4.8 ± 0.3 to 31 ± 5 mg g^{-1} for AR. At pH 8.0 the capacity for AR increased to 48 ± 2 mg g^{-1} however, the material exhibited lower capacity for AMB, which reached 178 ± 17 mg g^{-1} according to the Langmuir model (Fig. 5.3B).

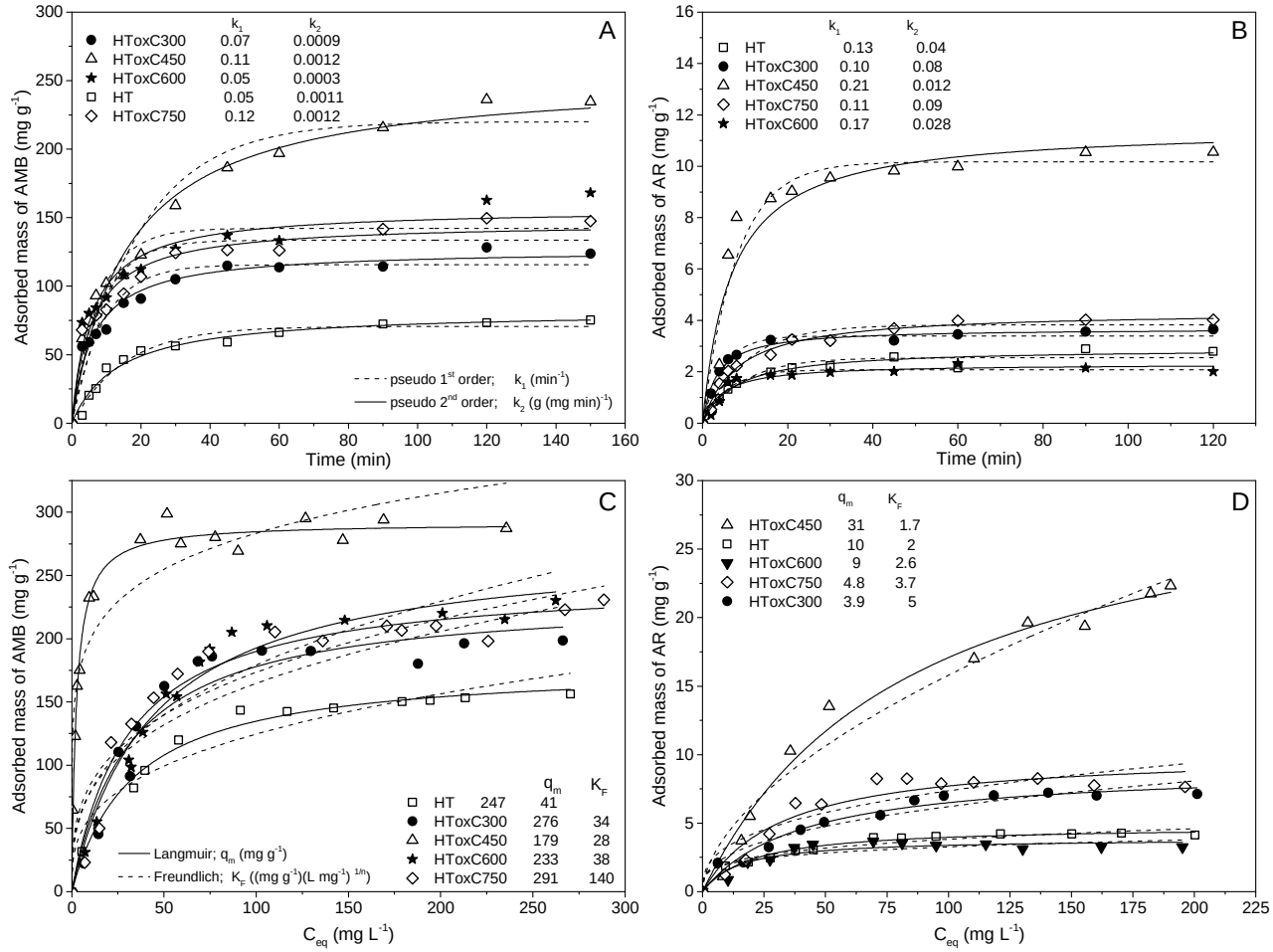

Figure 5.2 Kinetic models and kinetic rate constants obtained for adsorption of AMB (A) and AR (B) and equilibrium models with respective parameters related to adsorption capacity of AMB (C) and AR (D) at pH 3.5 for hydrotalcite and hydrotalcite-derived oxides.

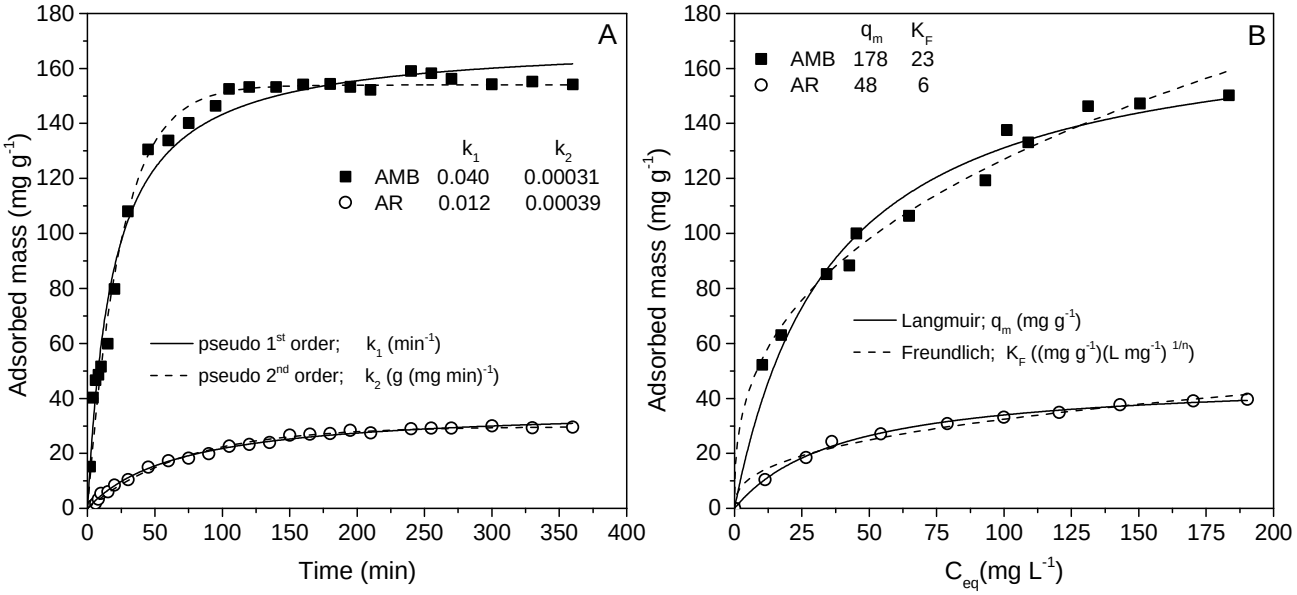

Figure 5.3 Kinetic models with kinetic rate constants (A) and equilibrium models with respective parameters related to adsorption capacity (B) obtained for adsorption of AMB and AR on HToxC450 at pH 8.0.

5.4.3 Regeneration of the spent adsorbents

The regeneration of the spent adsorbents studies carried out with AMB showed that generally the adsorbent loses some of its adsorption capacity after each cycle of regeneration with the loss being greater at lower pH (Fig. 5.4). The highest deterioration was in case of the sample calcineted at 300 °C where the capacity decreased finally, after 3 cycles, by 53 % (88 mg g^{-1}) at pH 3.5 and by 44 % (61 mg g^{-1}) at pH 6.0. The samples treated at 450 and 600 °C exhibited a loss of the adsorption capacity by 21 % (47 mg g^{-1}) and by 31 % (49 mg g^{-1}) at pH 3.5 and by 15 % (28 mg g^{-1}) and 22 % (28 mg g^{-1}) at pH 6.0. The sample regenerated at 750 °C showed only a decrease after the first cycle by 35 % (56 mg g^{-1}) at pH 3.5 and 34% (48 mg g^{-1}) at pH 6.0 and then the capacity remained on a stable level at both pH values (Fig. 5.4).

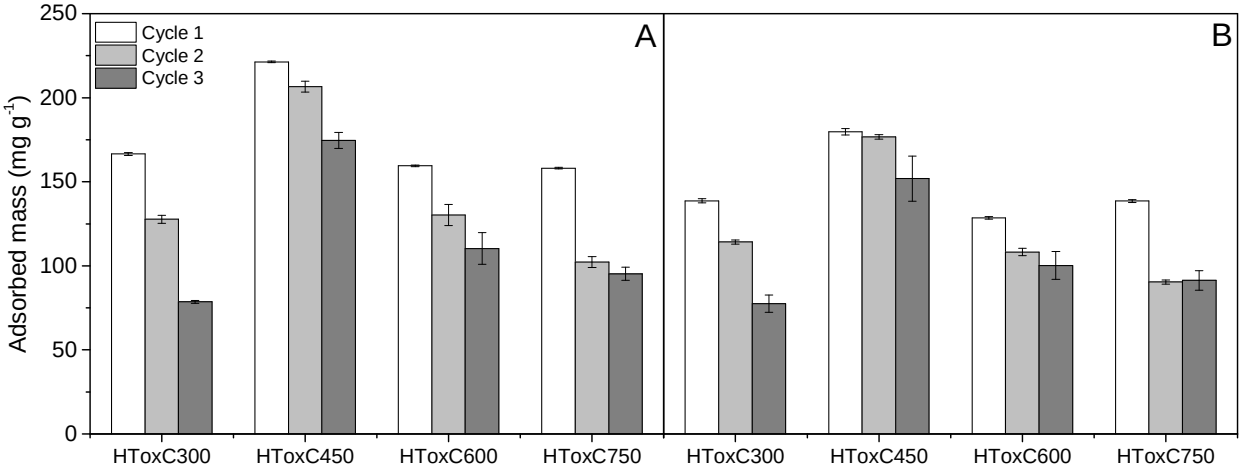

Figure 5.4 Adsorption capacities of the materials in subsequent cycles of adsorption and regeneration in pH 3.5 (A) and pH 6.0 (B).

5.4.4 Material characterization

5.4.4.1 UV-Vis-diffuse reflectance spectroscopy (DRS)

The dye in its solid state showed two peaks in the spectrum at around 380 and 555 nm. The second peak shifted hypsochromatically to around 515 nm in case of hydrotalcite with adsorbed dye and the sample recalcined at 300 °C. Further shift to around 535 nm was observed in samples treated at higher temperatures (Fig. 5.5E to 5.5I). This phenomenon known as metachromacy is ascribed to the formation of dye aggregates upon adsorption (Zollinger, 2003; Valandro et al., 2015) and to stacking interaction between the aggregated dyes in which dye's electron cloud can be attracted toward a polar group on the material's surface. This interaction lowers the energy of highest occupied molecular orbital (HOMO) while empty and lowest unoccupied molecular orbital (LUMO) remains unaffected creating a higher energy difference

between the orbitals and the transition occurs at higher energy thus at shorter wave length (Dobrogowska et al., 1991; Samuels et al., 2013).

The spectra of the samples calcined at 300 and 450 °C after adsorption showed 3 peaks at 315, 360 and 400 nm that increased their intensity after each cycle of regeneration suggesting accumulation of partially decomposed dyes (Fig. 5.5A and 5.5B). In the sample calcined at 600 °C only after the third calcination a small peak appeared (Fig. 5.5C). No signs of the dye were detected at 750 °C (Fig. 5.5D).

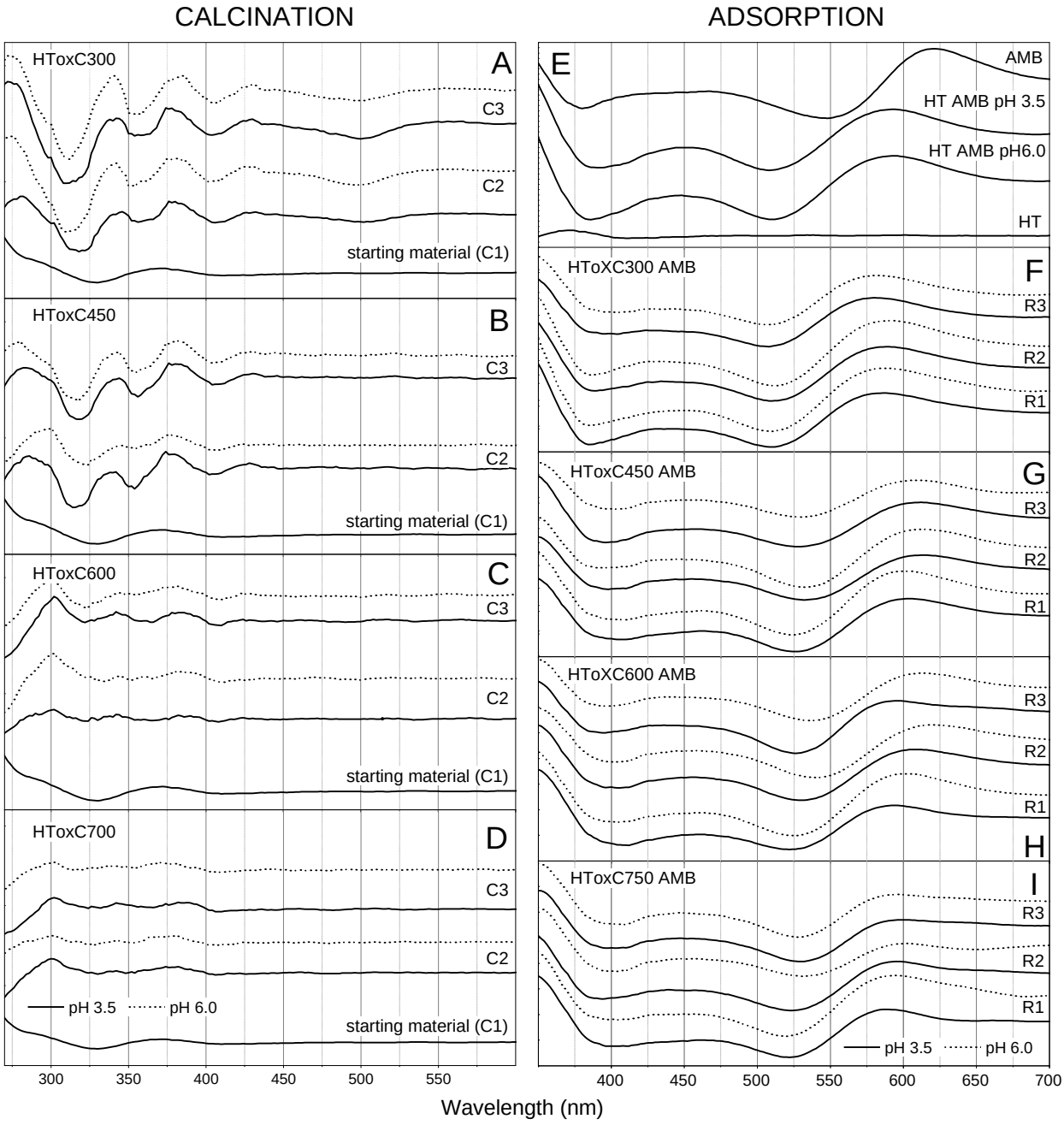

Figure 5.5 Second derivative of UV-Vis spectra of the samples after calcination at different temperatures (A-D) and adsorption at different pHs (E-I)

5.4.4.2 Attenuated total reflectance infrared spectroscopy (ATR)

In the spectra of the saturated materials several peaks that can be ascribed to vibrations of sulfonate groups (Fig. 5.6E) were found at 1224, 1182, 1126, 1083 and 1035 cm^{-1} (Guo et al., 2005; Bouraada et al., 2008). Those bands became more intense after each cycle of adsorption, especially the one located at 1030 cm^{-1}. At the same time the band at around 1355 cm^{-1} with a shoulder at 1400 cm^{-1} and the peak at 860 cm^{-1} attributed to interlayer carbonate (Kloprogge et al., 2004; Kloprogge and Frost, 2006) became less intensive. The spectra of the samples regenerated at 450 °C and higher temperature lost the band at around 775 cm^{-1} associated with lattice vibrations with metal hydroxide sheets (Costa et al., 2008) (Fig. 5.6E to 5.6I).

In the spectra of the samples regenerated at 300 °C the peaks from the vibrations of sulfonate groups range still appear (Fig. 5.6A), however when a higher temperature was used for the regeneration the peaks in that range become broad, overlapped with a dominant peak at 1088 cm^{-1}. The band at 1350 cm^{-1} disappeared together with appearance of the band at 1530 cm^{-1}, which might be attributed to bicarbonates formed upon dehydratation due to proton transfer from the hydroxide sheets to carbonate ion (Kloprogge and Frost, 2006). The peak at around 1400 cm^{-1} remained but was overlapped by a band at 1420 cm^{-1} assigned to sulfate (Xu et al., 2015). Similar phenomenon was observed in both investigated pH values, 3.5 and 8.0 (Fig. 5.6B to 5.6D).

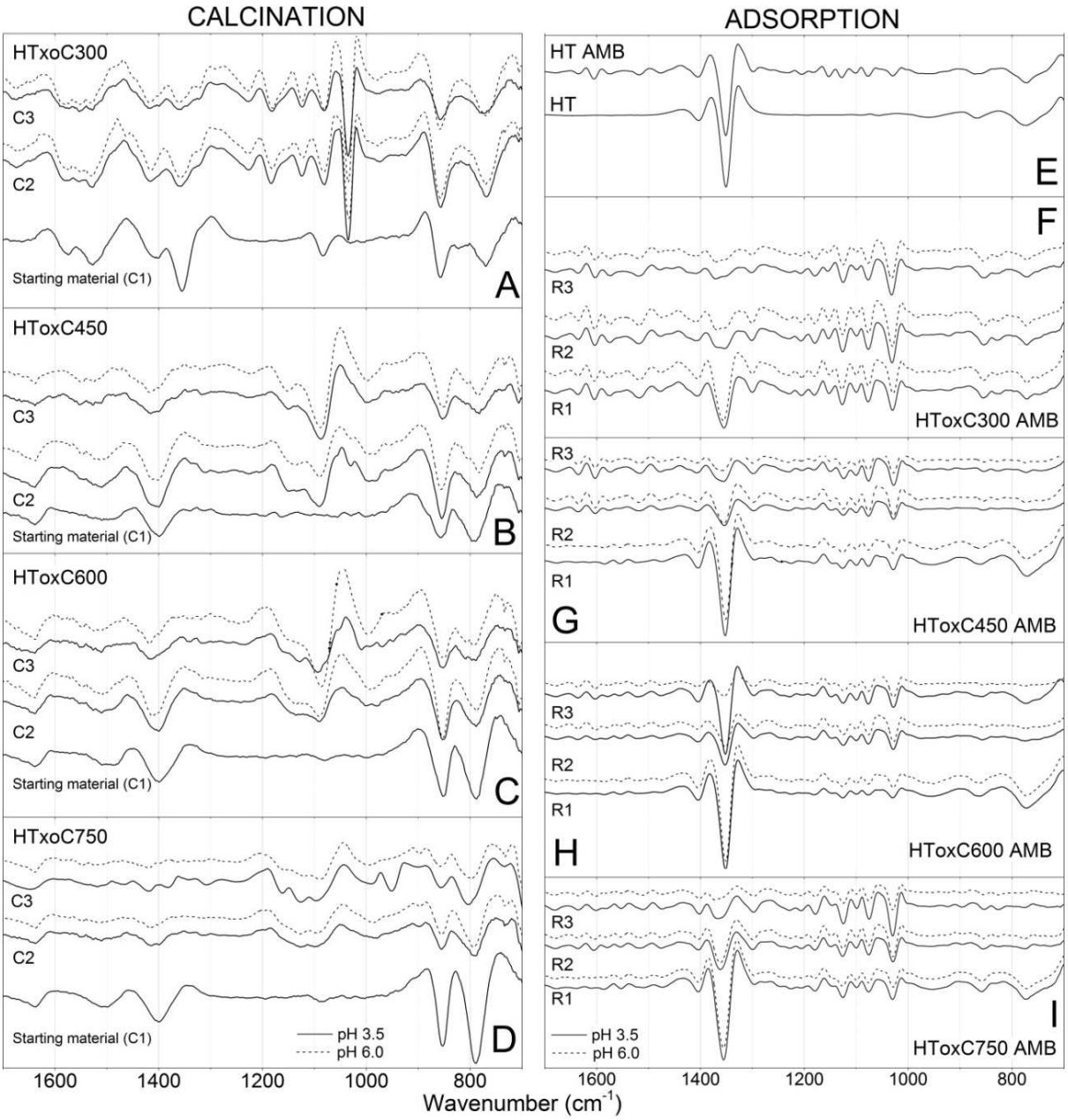

Figure 5.6 Second derivative of ATR spectra recorded for the regenerated samples (A-D) and for samples after adsorption (E-I) in following cycles.

5.4.4.3 X-ray powder diffraction (XRD)

Hydrotalcite showed typical reflections at 11.71° (d_{003}= 7.55 Å), 23.31° (d_{006}= 3.82 Å), 34.8° ($d_{009+012}$= 2.57 Å), 39.40° (d_{015}= 2.29 Å), 47.00° (d_{018}= 1.93 Å), 60.90° (d_{110}= 1.52 Å) and 62.19° (d_{112}= 1.49 Å) (de Roy et al., 2006) (Fig. 5.6E).

After adsorption, hydrotalcite successfully reconstructed its structure, however the reflections became less intensive after each cycle (Fig. 5.6F to 5.6I). In the samples after adsorption at pH 3.5 the cell parameter *a*, corresponding to the distance between two metal citations (de Roy et al., 2006), was smaller which can be attributed to the selective leaching of Mg^{2+} from the layers (Drits and Booking, 2006). Also the parameter *c*, related to the thickness of the brucite-like layers, decreased at pH 3.5 what can be correlated with increasing *x* value, which is the ratio between M^{2+} and M^{3+} in $[M^{2+}_{1-x}M^{3+}_{x}(OH)_2]^{x+}$ (Besson and Drits, 1997). Also an average crystallite dimension *Da* and *Dc*, average crystallite size parallel to a crystallographic length unit *a* and *c*, calculated using Sherrer equation, decreased upon each cycle and additionally it increases with calcination temperature rise (Fig. A.5.3A to A.5.3D). At the same time the peaks after adsorption at pH 3.5 were sharper than those at pH 6.0 in case of samples regenerated at 600 and 750 °C (Fig. 5.6H and 5.6I). Those changes could suggest dissolution of the poor crystalline material of small crystallite diameter and leaching of Mg^{2+} from the layers at lower pH. Additionally, in the sample calcined at 600 °C MgO phase was present after the second and third cycle of adsorption (Fig. 5.6H). At pH 6.0 the MgO phase was quite uniform however, in case of lower pH the cell parameter *a* had a broader range and an increase in mean crystallite diameter was observed after each cycle and with increasing calcination temperature (Fig. A.5.3E and A.5.3F). In case of calcination at 750 °C together with MgO phase, spinel phase was present and gave reflection at 65° after the first cycle and another sharper peaks at 19°, 36.62° and 44.6° in the following cycles (Fig. 5.6I). In this case the parameter *a* was similar for both pH values however, it decreased after each cycle and crystallite size increased (Fig. A.5.3G and A.3H) suggesting incomplete regeneration of hydrotalcite structure.

After heating at 300 °C the hydrotalcite phase was still present in the sample and showed reflections at 12.5° (d_{003}=7.08 Å), 25.2° (d_{006}= 3.53 Å), 34.50° (d_{009}= 2.60 Å) and 60.82° (d_{110}= 1.52 Å) (Fig. 5.6A and A.1A to A.1D). The 003 reflection shifted towards higher degrees. This shift together with the appearance of reflections at 36.00° (d_{111}= 2.49 Å) and 43.30° (d_{200}= 2.09 Å) suggest the creation of an intermediate dehydrated layered phase related to dehydratation of the material by gradual removal of interlayer water indicating a disorder in the stacking of the layers compared to the starting material (Pérez-Ramírez et al., 2007). After calcination at 450 and 600 °C only MgO phase was

detected in the samples giving reflections at 35.20° (d_{111}= 2.55 Å), 43.30° (d_{200}= 2.09 Å) and 62.50° (d_{220}= 1.48 Å) (Fig. 5.6B and 5.6C). The MgO crystallite size remains stable in the range of lower temperatures and it increased at higher temperatures. This behavior is due to substitution of Al into the MgO lattice that occurs in a range of lower temperature which inhibits growth of the crystals (Cavani et al., 1991). Also due to the substitution the parameter *a* increased (Al^{3+} has smaller cationic radius than Mg^{2+}) (Fig. A.5.2E and A.5.2F). Moreover, the parameter *a* is lower than in a pure MgO phase (*a*= 4.200 Å), what also suggests that such substitution produces a solid solution (Sánchez-Cantú et al., 2016). The sample prepared at 600 °C exhibited more intensive and sharper peaks suggesting better crystallinity of the sample. After calcination at 750 °C a dominant phase was $MgAl_2O_4$ spinel giving reflections at 19.00° (d_{111}= 4.67 Å), 31.00° (d_{220}= 2.89 Å), 36.62° (d_{311}= 2.45 Å), 44.60° (d_{400}= 2.03 Å) 59.12° (d_{511}= 1.56 Å) and 65.00° (d_{440}= 1.43 Å) accompanied by MgO with reflections at 43.10° (d_{200}= 2.10 Å) and 62.62° (d_{220}= 1.48 Å)(Schreyeck et al., 2001) (Fig. 5.6D). The parameter *a* of spinel phase decreases in each cycle and with increasing temperature, crystallite size increased in the process (Fig. A.5.2G and A.5.2H). When hydrotalcite is calcined in not too high temperature along with the elimination of hydroxyl and carbonate ions a non-stoichiometric spinel-like phase might be formed with divalent ions trapped inside. At higher calcination temperatures excess of two-valent ions can migrate out of the spinel-like phase giving rise to formation of M(II)O and stechiometric spinel with lowering of the parameter *a* and simultaneous increase in crystallite size of the spinel (Cavani et al., 1991). The results of structural characterization of samples saturated with R, AMB, CR, MO are shown in Fig. 5.8. It was observed that intercalation proceeds differently for all studied dyes. In the case of both industrial dyes (R and AMB) and Congo Red obtained materials are characterized with significant loss of crystallinity resulting from poor stacking order and random organization of interlayer anions. On the other hand, well resolved peaks were identified for Methyl Orange intercalated hydrotalcite.

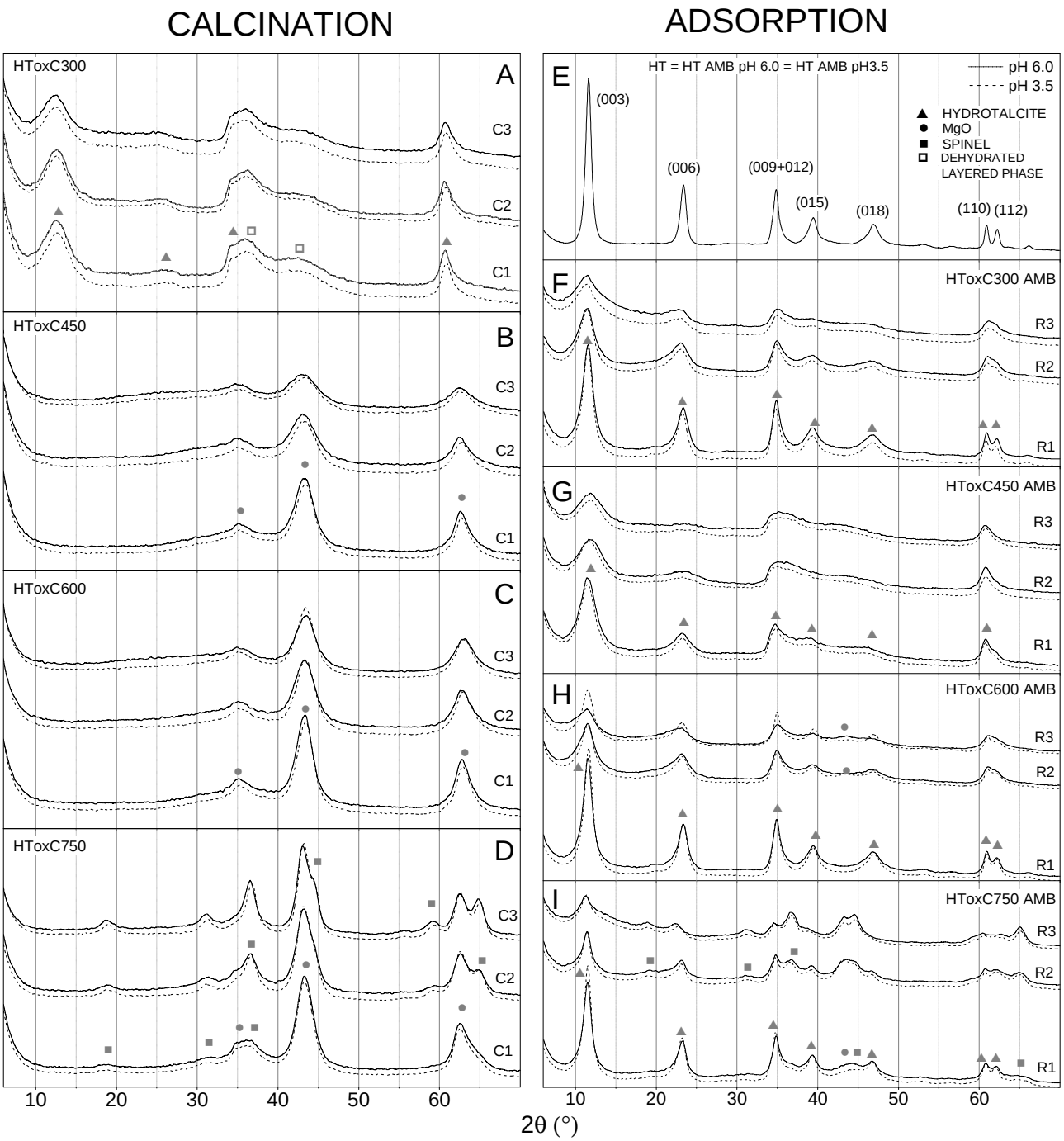

Figure 5.7 Phase composition of hydrotalcite and hydrotalcite-derived oxides after regeneration and adsorption cycles.

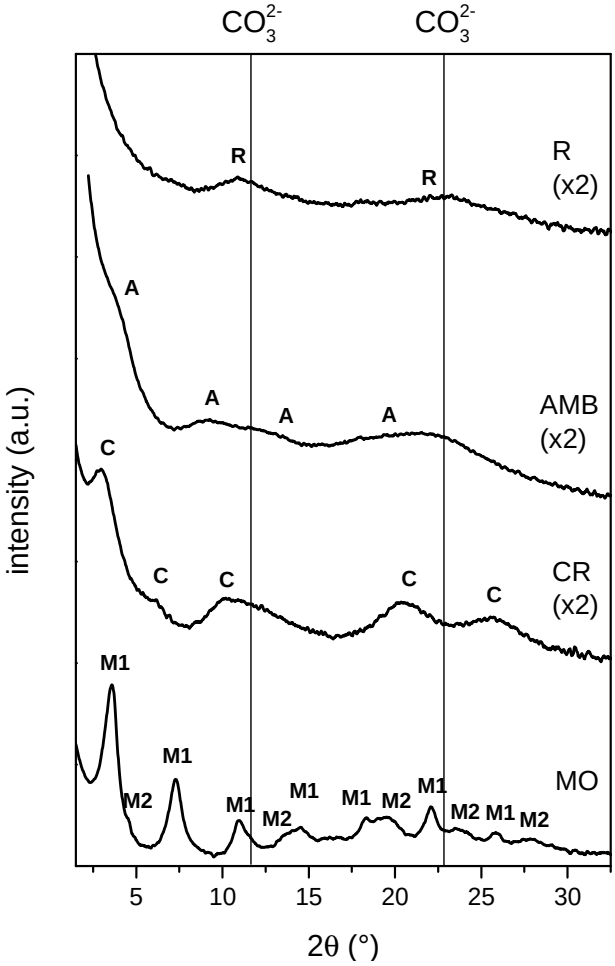

Figure 5.8 XRD patterns of hydrotalcites saturated with Reactive Red 184 (R), Levafix (AMB), Congo Red (CR) and Methyl Orange (MO)

5.4.4.4 BET surface area

The materials upon annealing in different temperatures exhibited diversity in their specific surface area. Generally up to 600 °C the specific surface area increased and for higher temperatures it decreased due to the creation of a spinel phase in the material (Fig. 5.9A). A slight but not such significant decrease in total pores' volume of the samples followed the same trend and reached their maximum value at 600 °C (Fig. 5.9B). Upon the following regeneration cycles the materials became less porous and their specific surface area generally decreased. It needs to be noticed that the samples annealed at 450 °C were characterized by the highest decrease in its specific surface area.

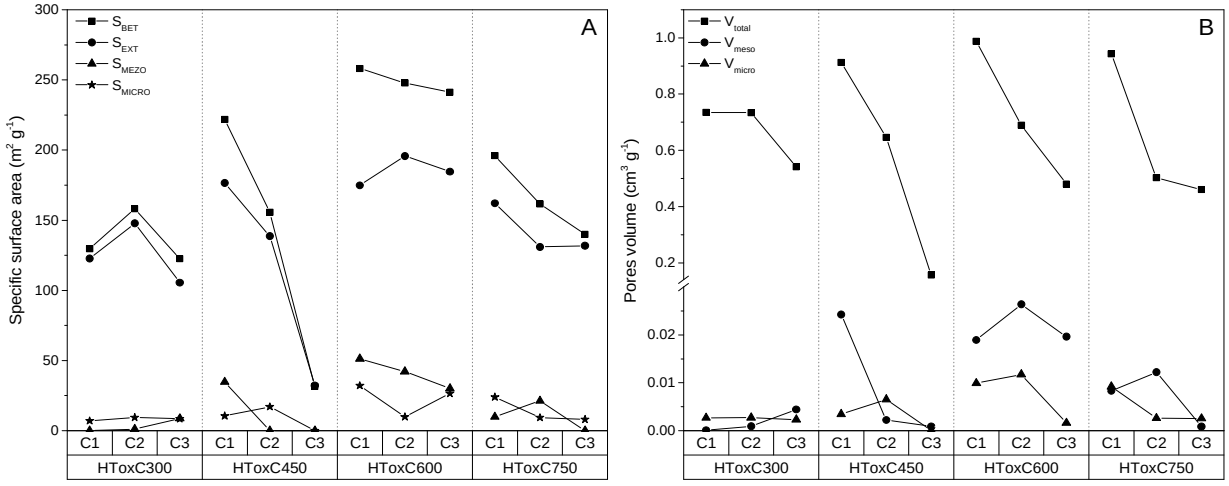

Figure 5.9 Changes of pores' volume (A) and specific surface area (B) of hydrotalcites calcined in different temperatures and following cycles of adsorption and regeneration.

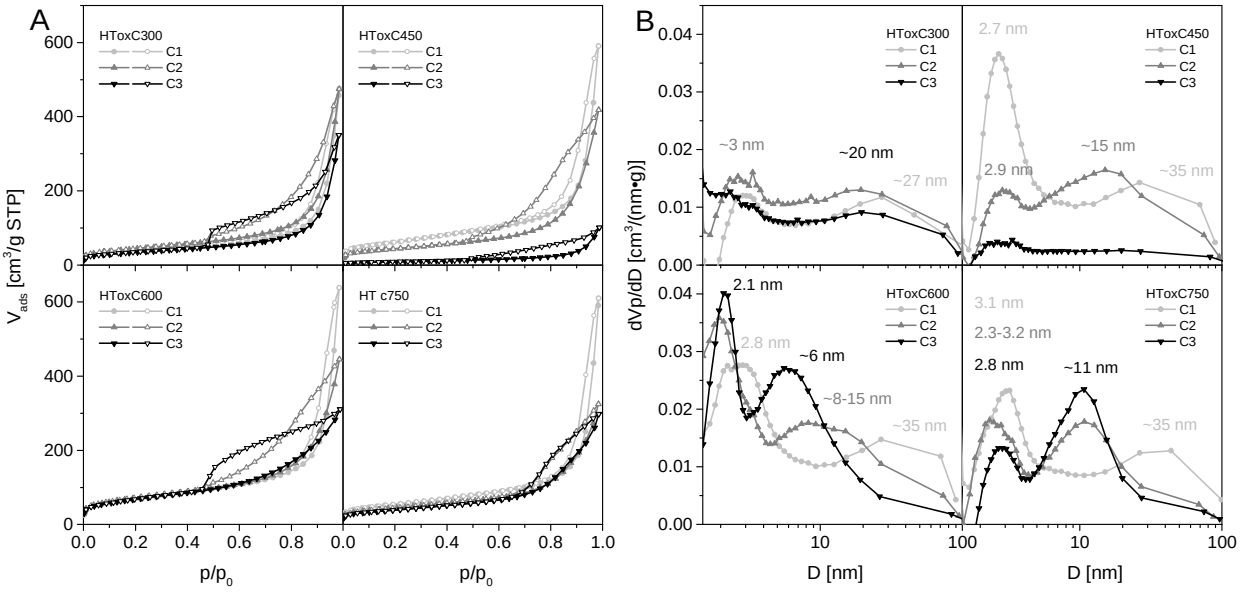

Figure 5.10 N_2 adsorption-desorption isotherms measured in calcination-regeneration cycles (A), BJH distribution of mesopores for calcined hydrotalcites after adsorption of AMB at pH 3.5 (B).

In measured isotherms (Fig. 5.10A) adsorption branch resembles type II isotherm, which is characteristic for nonporous or macroporous materials (Thommes et al., 2015), however in all samples hysteresis loops also appear. In starting materials after first calcination (C1), regardless the temperature, hysteresis loop is narrow and the thickness of the adsorbed N_2 multilayer increases at p/p_0 values close to 1. This phenomenon corresponds to adsorption at external surface, which in the case of studied materials makes a large contribution (Fig. 5.9). After second and third cycle (C2, C3) of regeneration hysteresis loop becomes broader, however, all shapes should be classified as type H3 or mixture of types H3 and H2. First type (H3) usually is observed for non-rigid aggregates of plate-like particles and also if network of macropores is formed and

not filled completely with condensate or other pore network effects play important role (H2). In the pore size distribution, calculated using BJH model, two distinctive peaks corresponding to small and large mesopores are observed (Fig. 5.10B) as well as micropores (Fig. 5.9B). It was noticed that mesopore range is not affected significantly by low temperature of calcination (300 °C). At higher temperature (450 °C) successive decrease of pore volume takes place and pores sintering (600-750 °C).

5.4.4.5 Organic elemental analysis (OEA)

The results showed that sulfur (S) and nitrogen (N) were accumulated in the samples. After the third cycle of regeneration the sample treated at 450 °C exhibited the highest level of sulfur while the sample regenerated at 300 °C was characterized by the highest content of nitrogen. At temperatures higher than 450 °C no traces of nitrogen were found upon regeneration whilst sulfur was still present (Fig. 5.11A). The sample treated at the optimal temperature, 450 °C, exhibited gradual accumulation of sulfur and nitrogen in following cycles of adsorption (R1-R3). The nitrogen was successfully eliminated upon regeneration and only traces were detected after the third cycle, however the content of sulfur significantly increased (Fig. 5.11B). The samples regenerated at 450 and 600 °C showed the highest difference in contents of S and N, depending on the pH at which adsorption had been carried out.

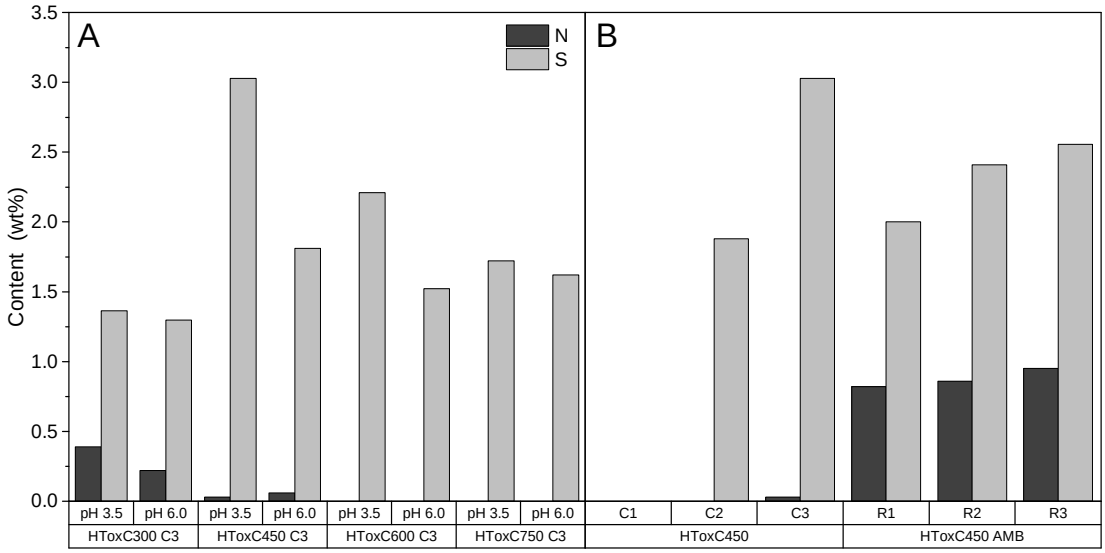

Figure 5.11 Accumulation of N and S in the samples obtained after the third cycle of regeneration at different temperatures (A) and accumulation of the elements in subsequent cycles of regeneration (C2 – C3) and after adsorption of AMB (R1-R3) onto the sample treated at 450 °C (B).

5.5 Discussion

Each sample exhibited different adsorption behavior toward cationic and anionic dyes that was strongly influenced by the pH of the solutions. Two different groups of adsorption sites are present in the material: sites within the interlayer corresponding to the structural anion exchange capacity and adsorption sites on the external surface, and the chemical properties of those two are different (Ulibarri and Hermosin, 2006). The presence of two isolated electron pairs and a dissociable hydrogen on a surface hydroxyl group, indicates that these groups are potential ampholytes (Schindler and Stumm, 1987). At low pH adsorption sites should be protonated what creates new sites for adsorption of anionic molecules thus adsorption of the anionic dye was promoted. In such conditions anions are adsorbed mainly by ligand exchange involving one or two surface hydroxyl groups (Schindler and Sposito, 1991). Also migration in the interlayer space should be easier since carbonates present in it should be eliminated at lower pH. At higher pH the situation reverses and adsorption of cationic molecules is privileged since the external adsorption sites are deprotonated and negatively charged. In such conditions cations are adsorbed by competitive complex formation involving one or two surface hydroxyl groups (Schindler and Sposito, 1991). Migration in-between the layers in the case of the cationic dye is unlikely and adsorption takes place only in the outer surface, this could explain relatively low adsorption capacity for the cationic dye. It still needs to be noticed that despite unfavorable pH some quantity of AMB adsorbed at high pH and some AR was adsorbed at low pH. This phenomenon can be explained by formation of type A or type B ternary surface complexes. The first is created when cation is adsorbed between the surface and a ligand (AMB) acquired from the solution phase (adsorption of AR at low pH). The second is formed when an anion is adsorbed between the metal and the cation (adsorption of AMB at high pH). Aside from the fact that the dye is incorporated in-between the layers while the hydrotalcite structure is reconstructed from the mixed oxide it also should be noticed that at high pH some of the interlayer carbonates that are the most important limiting factor for the anion exchange reaction (Ulibarri and Hermosin, 2006) might be exchanged with OH, which subsequently are exchanged by an AMB anions.

Thermal treatment of hydrotalcite resulted in formation of mixed oxides of different phase composition depending on the temperature used. After annealing at 300 °C hydrotalcite phase however, of decreased crystallinity, was still present in the sample together with dehydrated layered phase. Treatment at 450 and 600 °C totally transformed hydrotalcite phase into mixed oxides and at 750 °C it was additionally created a spinel phase in the product. After adsorption hydrotalcite was successfully

regenerated in all samples but it was the less crystalline in case of the sample treated at 450 °C. The sample treated at 750 °C after adsorption still exhibited presence of a spinel and a mixed oxide phase (Fig. 5.7). The temperature of 450 °C was found to be the optimal in terms of adsorption capacity and ability of adsorbing both types of dyes (Fig. 5.1). The best adsorption properties of the sample prepared at 450 °C might be attributed to its specific composition. The surface of dry oxides is characterized by the presence of metal ions that are not fully coordinated which gives rise to Lewis acidity. The presence of water leads in the first step to coordination of water molecules, dissociative chemisorption and formation of surface hydroxyl groups. Due to various feasible coordinative environments of metal ions in hydrated surfaces hydroxyl groups might not be chemically equivalent what in turn reflects in major differences in their chemical properties. Moreover it is very likely that a given oxide carries different types of surface hydroxyls (Schindler and Sposito, 1991) thus this contributes to different adsorption properties of the materials. Moreover, specific surface area of that sample greatly increased compared to the sample treated at 300 °C however it was not as high as for the sample treated at 600 °C, but it showed similar total pores volume nevertheless with bigger contribution of mesopores (Fig. 5.9). If adsorption should take place aside from interlayer space, i.e. on the outer surface of the material, such should be enhanced due to formation of mesopores that may be more accessible to bulk molecules like dyes than microspores.

The individual shape of hysteresis loop depends on processes taking place at a given temperature. In the case of the samples calcined at 300 °C, it should be expected that hydrotalcite platelets are preserved and incomplete dehydration takes place after calcination. Steep decrease of volume adsorbed close to p/p0 = 0.45 could be explained by cavitation-induced evaporation taking place in metastable fluid present in slit-like pores (type H2(a))(Thommes, 2010). N_2 isotherms for the samples after second cycle of regeneration and calcination at temperature range 450-600 °C, are characterized with not so sharp desorption branch, located at higher p/p_0 values. This temperature range is sufficient to transform hydrotalcite into mixed metal oxide and spinel, and additionally, as it was shown in chapter 4.4.5, accumulation of decomposition products occurs. It should be expected that complex network of pores is formed, and observed shape of hysteresis loop, which could be assigned as H2(b), is results of pore blocking. Moreover, pore size distribution of pore necks is wider than in the case of the sample obtained at 300 °C. Both samples obtained after third cycle of calcination at 450 and 600 °C contain mixture of pores and effects described above, however, due to much higher clogging by decomposition products at 450 °C, the isotherm is located at lower adsorption values. As it was shown in chapter 4.4.4, at temperature 600-750 °C, mesopores are still present,

however their size is reduced, especially large pores. Unlike low temperatures, that are not enough to decompose completely hydrotalcite (300 °C) or remove adsorbate (450 °C).. The adsorption kinetics at pH 3.5 followed the pseudo 2nd order model in case of both dyes. For AMB the adsorption rate on all materials that were characterized by relatively low adsorption capacity is statistically the same, however in case of the samples treated at 450 °C it is lower by an order of magnitude. That might confirm creation of additional adsorption sites and specific porous structure of the sample that rendered the adsorption slower but higher. At the same time the adsorption rate of AR at this pH was faster than adsorption of AMB and no statistically significant differences between the rates were observed for the starting material and sample treated at 300 and 600 °C. However, for the sample treated at 450 °C the rate was again the lowest and a decrease was noticed on sample treated at 750 °C. It is to be noticed that at higher pH the mechanisms changed and pseudo 1st order model fits better in both cases, with adsorption rate of AMB being higher than of AR. This can be explained by better access to the sites (Table A.5.1 and A.5.2). AMB should encounter competition with OH^- ions present in the solution and the exchange with interlayer anion should be imparted however, AR as it is a cation can adsorb on available deprotonated surface groups.

The equilibrium experiment indicated Langmuir's model as the best fit for adsorption of both dyes at pH 3.5. Adsorption of AR at pH 8.0 also followed Langmuir's model however, for AMB at this pH the Freundlich's model was a better fit (Table A.5.1 and A.5.2). This model assumes adsorption on heterogeneous surfaces, oppositely to Langmuir's model. While at low pH all the adsorption sites are protonated rendering the surface quite homogenous, at pH equal 8.0 the sites should be mostly deprotonated but some of them might still be protonated making the surface heterogeneous. Moreover there must be a competition between AMB and OH^- anions for adsorption sites that makes homogeneous coverage of the surface by AMB less likely.

The regeneration studies of the spent adsorbent revealed that after each cycle adsorption/regeneration a loss of adsorption capacity of the material was noticed (Fig. 5.4 A and B). This phenomenon is related to changes occurring in the samples after each cycle of adsorption and regeneration. The hydrotalcite reconstructed from calcined sample became less crystalline after each cycle since various kinds of disorders might be incorporated during crystallization of hydrotalcite. They lead to stacking faults that give rise to broad asymmetric reflections acquiring a "saw tooth" or "shark's fin" line shape in the XRD patterns (Evans and Slade, 2005) (Fig. 5.6). The loss in maximum adsorption capacity was correlated with temperature used during regeneration. The highest deterioration was noticed in the sample treated at 300 °C and the lowest at 600 °C. When 750 °C temperature was applied during treatment the adsorption capacity of

the material deteriorated more. The application of higher temperatures caused formation of additional phases in the material e.g. spinel in case of 750 °C and MgO in case of 600 °C that were not able to fully recreate hydrotalcite in adsorption cycle and caused loss of some of the adsorption capacity. Another important cause of changes in the adsorption capacity was accumulation of products of decomposition of the dye. It was observed that at 300 °C some nitrogen and sulfur compounds were still present in the sample. With rising regeneration temperature the amount of nitrogen detected in the samples decreased and disappeared when 600 °C or higher temperatures were used (Fig. 5.6 and 11) however, sulfur was present regardless the temperature. Also UV-Vis analysis confirmed that those temperatures were able to remove the decomposition products more efficiently and peaks from colored compounds disappeared (Fig. 5.5).

The accumulation of sulfates, although it contributes to the decrease in the maximum adsorption capacity, is actually a desired phenomenon. It prevents such compounds that have negative effect on the environment and human health (WHO/SDE/PHE/OEH/06.02; Ayres, 1998; Winterdahl et al., 2014) from being released in large amounts into the environment in the course of regeneration process. As they are adsorbed on the adsorbent they may be desorbed after several cycles of utilization of the material and giving concentrated solution that may be safely disposed of. However, this feature requires further research.

Thermal decomposition of hydrotalcite led to the formation of high surface area products. The highest specific surface area was achieved after calcination at 600 °C. The total pore volume was similar in samples treated at 450 °C and higher, however, the sample treated at 600 °C had better developed microporosity than the sample treated at 450 °C. Hydrotalcite-like compounds during thermal modification undergo textural modification attributed to a topotactic transformation where the interparticle porosity increases due to their reorganization during calcination. Also a part of the porosity is attributed to so called cratering effect due to expulsion of interlayer anion and water during the process of thermal treatment (Reichle et al., 1986). The sample annealed at 750 °C was characterized by lower specific surface area which might be attributed to formation of the spinel phase (Fig. 5.10). In following cycles of regeneration/adsorption both the porosity and specific surface area decreased in all samples. It is most likely the sulfur remaining in the samples after the calcination blocks up the pores and causes the decrease (Kuśtrowski et al., 2004). Sulfates can also show a tendency toward grafting with brucite-like layers rendering the internal surface of the material inaccessible (Constantino and Pinnavaia, 1995). The most significant decrease in the specific surface area was noticed for the samples annealed at 450 °C. This sample had the highest adsorption capacity thus it should have the highest amount of products of the

decomposition of the dye. When the samples are regenerated the obtained mixed oxides must be somehow clogged and cemented by the dyes residues. N_2 adsorption method creates limitations due to the relatively large van der Waals radius of the N_2 molecule that prevents it from interacting with surface functional group occluded in small void spaces inaccessible due to the presence of sulfates and it is adsorbed only on the most accessible surfaces (Aringhieri et al., 1992). However, the structure of the clusters may be broken in the solution, the hydrotalcite is regenerated and adsorption can proceed.

The analysis of the spent adsorbents saturated with excess with four dyes gave insight on the orientation of adsorbed dye. Usually dyes are large organic molecules and it is expected that in the interlayer space they occupy a larger area than the one associated with one layer charge. In the case of the adsorbent used for presented studies this area is equal 0.24 nm^2 and it is significantly smaller than dimensions (cross sections) of studied molecules (Table A.5.3). In such case rearrangement of anions occur from flat-lying to tilt-lying or orientation perpendicular to the brucite-like layer (Ruiz-Hitzky et al., 2004; Ulibarri and Hermosin, 2006; Węgrzyn et al., 2010). It was shown that, in specific conditions of high adsorbate excess, cell parameters increased due to described phenomenon for all dyes but one – Reactive Red 184. Because detailed information about molecular design of industrial dyes is not always available, we may predict on the basis of obtained XRD patterns, behavior of studied adsorbates. There is no large increase of cell parameter in the case of R intercalated hydrotalcite, probably as a result of low affinity toward adsorbent and for this dye it should be expected only limited removal degree. For AMB an expansion of interlayer space occurs, giving rise to interlayer distance similar to MO. Therefore we may conclude that AMB is not a very large molecule. However, much larger broadening of XRD peaks indicates that there are no such strong interactions between dye molecules, as in the case of MO via π-π interactions of phenyl groups (Costantino et al., 1999). Dimensions of both dyes (CR and MO) correspond very well with the height of interlayer gallery, but in the case of Congo Red anions they are most probably tilted.

5.6 Conclusions

Thermal treatment of hydrotalcite resulted in formation of mixed oxides characterized by high adsorption capacity and high specific surface area. Annealing at 450 °C gave the best material in terms of adsorption capacity toward both anionic and cationic dyes. The capacity increased from 179 ± 5 to 291 ± 8 mg g^{-1} in case of the anionic dye at pH 3.5 and from 6 ± 2 to 48 ± 2 mg g^{-1} in case of the cationic dye at pH 8.0, on starting and thermally treated material at 450 °C, respectively according to the equilibrium experiments. Adsorption exhibited strong pH dependence. The anionic dye was more efficiently removed at lower pH equal 3.5 whilst the adsorption of the cationic dye was favored at higher pH values, 8.0. Such adsorbent was successfully thermally regenerated with a slight loss in its adsorption capacity. One of the reasons of the decrease was accumulation of decomposition products of the dye i.e. sulfuric compound, however such behavior should be seen as additional advantage since it prevents emission of toxic sulfates into the environment after each regeneration cycle of spent adsorbent.

5.7 References

Ali, I., Asim, M., Khan, T.A., 2012. Low cost adsorbents for the removal of organic pollutants from wastewater. J. Environ. Manage. 113, 170-183.

Aringhieri, R., Pardini, G., Gispert, M., Sole, A., 1992. Testing a simple methylene blue method for surface area estimation in soils. Agrochimica 36, 224-232.

Ayres, J., G.,, 1998. Health effects of gaseous air pollutants. in: Hester, R., E.,, Harrison, R., M., (Eds.). Air pollution and health. Royal Society of Chemistry, Cambridge.

Besson, G., Drits, V.A., 1997. Refined relationships between chemical composition of dioctahedral fine-grained mica minerals and their infrared spectra within the oh stretching region. Part I: identification of the oh stretching bands. Clay and Clay Minerals 45, 158-169.

Bouraada, M., Lafjah, M., Ouali, M.S., de Menorval, L.C., 2008. Basic dye removal from aqueous solutions by dodecylsulfate- and dodecyl benzene sulfonate-intercalated hydrotalcite. J. Hazard. Mater. 153, 911-918.

Cavani, F., Trifirò, F., Vaccari, A., 1991. Hydrotalcite-type anionic clays: Preparation, properties and applications. Catal. Today 11, 173-301.

Constantino, V.R.L., Pinnavaia, T.J., 1995. Basic Properties of Mg2+1-xAl3+x Layered Double Hydroxides Intercalated by Carbonate, Hydroxide, Chloride, and Sulfate Anions. Inorg. Chem. 34, 883-892.

Costa, F.R., Leuteritz, A., Wagenknecht, U., Jehnichen, D., Häußler, L., Heinrich, G., 2008. Intercalation of Mg–Al layered double hydroxide by anionic surfactants: Preparation and characterization. Appl. Clay Sci. 38, 153-164.

Costantino, U., Coletti, N., Nocchetti, M., Aloisi, G.G., Elisei, F., 1999. Anion Exchange of Methyl Orange into Zn−Al Synthetic Hydrotalcite and Photophysical Characterization of the Intercalates Obtained. Langmuir 15, 4454-4460.

de Roy, A., ,, Forano, C., Besse, J.P., 2006. Layered double hydroxides: synthesis and post-synthesis modification. in: Rives, V. (Ed.). Layered Double Hydroxides: Present and Future Nova Science Publishers, Inc., New York.

Dobrogowska, C., Hepler, L.G., Ghosh, D.K., Yariv, S., 1991. Metachromasy in clay mineral systems - Spectrophotometric and calorimetric study of the adsorption of crystal-violet and ethyl violet by Na-montmorillonit and by Na-kaolinite. J. Therm. Anal. 37, 1347-1356.

Drits, V.A., Booking, A.S., 2006. Cristal structure and X-ray identification of layered double hydroxides. in: Rives, V. (Ed.). Layered Double Hydroxides: Present and Future. Nova Science Publishers.

Evans, D.G., Slade, R.C.T., 2005. Structural aspects of layered double hydroxides. in: Duan, X., Evans, D.G. (Eds.). Layered Double Hydroxides. Springer.

Freundlich, H.M.F., 1906. Über die adsorption in läsungen. Z. Phys. Chem. 57, 385-470.

Guo, Y., Zhang, H., Zhao, L., Li, G.-D., Chen, J.-S., Xu, L., 2005. Synthesis and characterization of Cd–Cr and Zn–Cd–Cr layered double hydroxides intercalated with dodecyl sulfate. J. Solid State Chem. 178, 1830-1836.

Ho, Y.S., McKay, G., 1999. Pseudo-second order model for sorption processes. Process Biochem. 34, 451-465.

Kant, R., 2012. Textile dyeing industry an environmental hazard. Natural Science 4, 22-26.

Kloprogge, J.T., Frost, R.L., 2006. Infrrared and Raman Spectorscopic Studies of Layered Double Hydroxides (LDHs). in: Rives, V. (Ed.). Layered Double Hydroxides: Present and Furure. Nova Science Publishers, pp. 153-215.

Kloprogge, J.T., Hickey, L., Frost, R.L., 2004. FT-Raman and FT-IR spectroscopic study of synthetic Mg/Zn/Al-hydrotalcites. J. Raman Spectrosc. 35.

Kuśtrowski, P., Chmielarz, L., Bożek, E., Sawalha, M., Roessner, F., 2004. Acidity and basicity of hydrotalcite derived mixed Mg–Al oxides studied by test reaction of MBOH conversion and temperature programmed desorption of NH3 and CO2. Mater. Res. Bull. 39, 263-281.

Lagergren, S., 1898. About theory of so-called adsorption of soluble substances. Kongl. Vetenskaps Academiens Handlingar 24, 1-39.

Langmuir, I., 1918. The adsorption of gases on plane surfaces of glass, mica and platinum. J. Am. Chem. Soc. 40, 1361-1403.

Leube, H., 2007. Textile Dyeing. in: Hunger, K. (Ed.). Industrial Dyes: Chemistry, Properties, Applications. Wiley, Germany.

Mondal, P.K., Chauhan, B., 2012. Biodegradation of azo dyes from wastewater. in: Lichtfouse, E., Schwarzbauer, J., Robert, D. (Eds.). Environmental Chemistry for a Sustainable World. Springer.

Pan, B., Pan, B., Zhang, W., Lv, L., Zhang, Q., Zheng, S., 2009. Development of polymeric and polymer-based hybrid adsorbents for pollutants removal from waters. Chem. Eng. J. 151, 19-29.

Pereira, L., Alves, M., 2011. Dyes-Environmental Impact and Remediation. in: Malik, A., Grohmann, E. (Eds.). Environmental Protection Strategies for Sustainable Development. Springer Science & Business Media.

Pérez-Ramírez, J., Abelló, S., Van Der Pers, N.M., 2007. Influence of the divalent cation on the thermal activation and reconstruction of hydrotalcite-like compounds. J. Phys. Chem. C 111, 3642-3650.

Reichle, W.T., Kang, S.Y., Everhardt, D.S., 1986. The nature of the thermal decomposition of a catalytically active anionic clay mineral. J. Catal. 101, 352-359.

Rives, V., 2006. Preface. in: Rives, V. (Ed.). Layered Double Hydroxides: Present and Future. Nova Science Publishers, Inc., New York.

Rozada, F., Calvo, L.F., García, A.I., Martín-Villacorta, J., Otero, M., 2003. Dye adsorption by sewage sludge-based activated carbons in batch and fixed-bed systems. Bioresour. Technol. 87, 221-230.

Ruiz-Hitzky, E., Aranda, P., Saerratosa, J.M., 2004. Clay-organic interactions: organoclay complexes and polymer-clay nanocomposites. in: Auerbach, S.M., Carrado, K.A., Dutta, P.K. (Eds.). Handbook of layered materials. Marcal Dekker, New York.

Samuels, M., Mor, O., Rytwo, G., 2013. Metachromasy as an indicator of photostabilization of methylene blue adsorbed to clays and minerals. J. Photochem. Photobiol. B: Biol. 121, 23-26.

Sánchez-Cantú, M., Galicia-Aguilar, J.A., Santamaría-Juárez, D., Hernández-Moreno, L.E., 2016. Evaluation of the mixed oxides produced from hydrotalcite-like compound's thermal treatment in arsenic uptake. Appl. Clay Sci. 121–122, 146-153.

Schindler, P.W., Sposito, G., 1991. Surface complexation at (hydr)oxide surfaces. in: Bolt, G.H., De Boodt, M.F., Hayes, M.H.B., McBride, M.B. (Eds.). Interactions at the soil colloid - soil solution interface. Springer-Science+Business MEdai, B.V.,.

Schindler, P.W., Stumm, W., 1987. The surface chemistry of oxides, hydroxides and oxide minerals. in: Stumm, W. (Ed.). Aquatic surface chamistry. Wiley, New York.

Schreyeck, L., Wlosik, A., Fuzellier, H., 2001. Influence of the synthesis route on MgAl2O4 spinel properties. J. Mater. Chem. 11, 483-486.

Sevekow, U., 2003. Health and safety aspects. in: Hunger, K. (Ed.). Indystrial Dyes. Chemistry, Properties, Applications. Wiley-Vch, Weinheim.

Tang, G., C.,C.,, 2007. Roles of Background Compound Molecular Size and Adsorbent Pore Size Distribution in Competitive Adsorption on Activated Carbon. University of Illinois at Urbana-Champaign.

Thommes, M., 2010. Physical Adsorption Characterization of Nanoporous Materials. Chem. Ing. Tech. 82, 1059-1073.

Thommes, M., Kaneko, K., Neimark, A., V.,, Olivier, P., Rodriguez-Reinoso, F., Rouquerol, J., Sing, K., S.,W.,, 2015. Physisorption of gases, with special reference to the evaluation of surface area and pore size distribution (IUPAC Technical Report). Pure Appl. Chem. 87, 1051-1069.

Ulibarri, M.A., Hermosin, M.C., 2006. Layered double hydroxides in water decontamination. in: Rives, V. (Ed.). Layered double hyeroxides: present and future. Nova Science Publishers, New York.

Valandro, S.R., Poli, A.L., Neumann, M.G., Schmitt, C.C., 2015. Photophysics of Auramine O adsorbed on solid clays. J. Lumin. 161, 209-213.

Węgrzyn, A., Rafalska-Łasocha, A., Majda, D., Dziembaj, R., Papp, H., 2010. The influence of mixed anionic composition of Mg–Al hydrotalcites on the thermal decomposition mechanism based on in situ study. J. Therm. Anal. Calorim. 99, 443-457.

WHO/SDE/PHE/OEH/06.02, WHO Air Quality Guidelines for Particulate Matter, Ozone, Nitrogen Dioxide and Sulfur Dioxide. Global Update 2005. World Health Organization.

Winterdahl, M., Bishop, K., Erlandsson, M., 2014. Acidification, dissolved organic carbon (DOC) and climate change. in: Freedman, B. (Ed.). Global environmnet change. Springer.

Xu, S., Liao, M.-C., Zeng, H.-Y., Liu, X.-J., Du, J.-Z., Ding, P.-X., Zhang, W., 2015. Surface modification and dissolution behavior of Mg–Al hydrotalcite particles. J. Taiwan Inst. Chem. Eng. 56, 174-180.

Zollinger, H., 2003. Color Chemistry: Syntheses, Properties, and Applications of Organic Dyes and Pigments. Wiley.

Appendix A.5

Table A.5.1 Parameters of equilibrium and kinetics models fitted to the experimental data for adsorption of AMB and AR on hydrotalcite and hydrotalcite-derived oxides in pH 3.5.

	Model		Parameter	Sample				
				HT	HToxC300	HToxC450	HToxC600	HToxC750
AMB	Kinetics	pseudo 1st	q_e (mg g^{-1})	71 ± 5	116 ± 10	220 ± 22	142 ± 15	133 ± 13
			k_1 (min^{-1})	0.07 ± 0.01	0.11 ± 0.04	0.05 ± 0.02	0.05 ± 0.01	0.12 ± 0.05
			s^2	20	107	350	267	204
			R^2_{adj}	0.97	0.918	0.935	0.866	0.883
		pseudo 2nd	q_e (mg g^{-1})	82 ± 6	127 ± 8	254 ± 22	156 ± 12	146 ± 10
			k_2 (g (mg min)$^{-1}$)	0.0009 ± 0.0003	0.0012 ± 0.0004	0.00025 ± 0.00009	0.0011 ± 0.0005	0.0012 ± 0.0005
			s^2	15	41	155	113	79
			R^2_{adj}	0.977	0.968	0.971	0.943	0.954
		Model comparison	Fisher	no difference				
			AIC	pseudo 2nd				
			BIC	inconclusive	pseudo 2nd			
	Equilibrium	Langmuir	q_m (mg g^{-1})	179 ± 5	233 ± 15	291 ± 8	276 ± 12	247 ± 9
			K_L (L mg^{-1})	0.030 ± 0.006	0.03 ± 0.01	0.41 ± 0.7	0.023 ± 0.006	0.03 ± 0.1
			s^2	31	314	101	157	200
			R^2_{adj}	0.989	0.935	0.989	0.971	0.963
		Freundlich	K_F ((mg g^{-1})(L mg^{-1}) 1/n)	28 ± 12	38 ± 23	140 ± 28	34 ± 17	41 ± 20
			n	3.0 ± 0.8	3 ± 1	7 ± 2	2.7 ± 0.8	3 ± 1
			s^2	167	845	861	599	634
			R^2_{adj}	0.941	0.825	0.897	0.888	0.883
		Model comparison	Fisher					
			AIC	Langmuir				
			BIC					
AR	Kinetics	pseudo 1st	q_e (mg g^{-1})	2.6 ± 0.2	3.4 ± 0.1	10 ± 1	2.1 ± 0.2	3.8 ± 0.2
			k_1 (min^{-1})	0.11 ± 0.03	0.21 ± 0.03	0.13 ± 0.05	0.17 ± 0.06	0.1 ± 0.03
			s^2	1.052	0.0667	0.019	0.033	0.042
			R^2_{adj}	0.932	0.964	0.914	0.942	0.945
		pseudo 2nd	q_e (mg g^{-1})	2.9 ± 0.2	3.7 ± 0.2	12 ± 2	2.3 ± 0.3	4.4 ± 0.3
			k_2 (g (mg min)$^{-1}$)	0.04 ± 0.02	0.08 ± 0.02	0.012 ± 0.002	0.09 ± 0.06	0.028 ± 0.008
			s^2	0.026	0.968	1.365	0.045	0.0257
			R^2_{adj}	0.969	0.984	0.952	0.971	0.984
		Best fit	Fisher	no difference				
			AIC	pseudo 2nd				
			BIC					
	Equilibrium	Langmuir	q_m (mg g^{-1})	4.8 ± 0.3	9 ± 1	31 ± 5	3.9 ± 0.6	10 ± 2
			K_L (L mg^{-1})	0.05 ± 0.1	0.023 ± 0.008	0.012 ± 0.05	0.07 ± 0.05	0.03 ± 0.02
			s^2	0.041	0.131	1.14	0.156	0.72
			R^2_{adj}	0.975	0.976	0.984	0.879	0.917
		Freundlich	K_F ((mg g^{-1})(L mg^{-1}) 1/n)	3.7 ± 0.9	2.6 ± 0.9	1.7 ± 0.4	5 ± 3	2 ± 1
			n	1.1 ± 0.3	1.1 ± 0.9	1.1 ± 0.7	1.2 ± 0.8	3 ± 1
			s^2	0.077	0.402	2.586	0.304	1.595
			R^2_{adj}	0.825	0.856	0.902	0.762	0.814
		Model comparison	Fisher	no difference				
			AIC	Langmuir				
			BIC					

Table A.5.2 Parameters of equilibrium and kinetics models fitted to the experimental data for adsorption of AMB and AR on HToxC450 in pH 8.0.

			Sample HToxC450			
Dye	Kinetics			Equilibrium		
	model	parameter		model	parameter	
AMB	pseudo 1st	q_e (mg g^{-1})	153 ± 3	Langmuir	q_m (mg g^{-1})	178 ± 17
		k_1 (min^{-1})	0.040 ± 0.004		K_L (L mg^{-1})	0.028 ± 0.008
		s^2	34		s^2	45
		R^2_{adj}	0.988		R^2_{adj}	0.977
	pseudo 2nd	q_e (mg g^{-1})	170 ± 5	Freundlich	K_F ((mg g^{-1})(L mg^{-1}) $^{1/n}$)	23 ± 5
		k_2 (g (mg $min)^{-1}$)	0.00031 ± 0.00005		n	2.7 ± 0.3
		s^2	40		s^2	28
		R^2_{adj}	0.976		R^2_{adj}	0.986
	Best fit	Fisher	no difference		no difference	
		AIC	pseudo 1st		Freundlich	
		BIC				
AR	pseudo 1st	q_e (mg g^{-1})	29.8 ± 0.7	Langmuir	q_m (mg g^{-1})	48 ± 2
		k_1 (min^{-1})	0.012 ± 0.001		K_L (L mg^{-1})	0.025 ± 0.004
		s^2	0.6		s^2	0.6
		R^2_{adj}	0.998		R^2_{adj}	0.996
	pseudo 2nd	q_e (mg g^{-1})	37 ± 1	Freundlich	K_F ((mg g^{-1})(L mg^{-1}) $^{1/n}$)	6 ± 2
		k_2 (g (mg $min)^{-1}$)	0.00039 ± 0.00006		n	2.6 ± 0.5
		s^2	0.6		s^2	3
		R^2_{adj}	0.991		R^2_{adj}	0.98
	Best fit	Fisher	no difference		Langmuir	
		AIC	pseudo 1st			
		BIC				

Table A.5.3 Comparison of dyes dimensions with cell parameters and intercalated phase properties.

intercalated dye	**dye dimensions [nm]***			**anions orientation, type of intercalated**	**cell parameter c [nm]**	**interlayer height [nm]**	**contamination with CO_3^{2-}**
R	0.5	0.9	2.38	(R) possibly flat lying; limited swelling, low crystalline phase	2.4	0.3	highly probable
AMB	n.a.			(A) tilted, non-uniform arrangement; strong swelling, low crystalline phase	6.8 - 7.4	1.8 - 2.0	probable
CR	0.56	1	2.6	(C) tilted, non-uniform arrangement; strong swelling, low crystalline phase	7.6 - 8.9	2.1 - 2.5	probable
MO	0.49	0.7	1.68	coexistence of two phases: uniform (M1) - anions lying perpendicular to the layers, crystalline; non-uniform (M2) - with tilt-lying anions and possible swelling, low crystalline	5.8 , 7.3	1.5, 2.0	limited

*(Costantino et al., 1999; Tang, 2007)

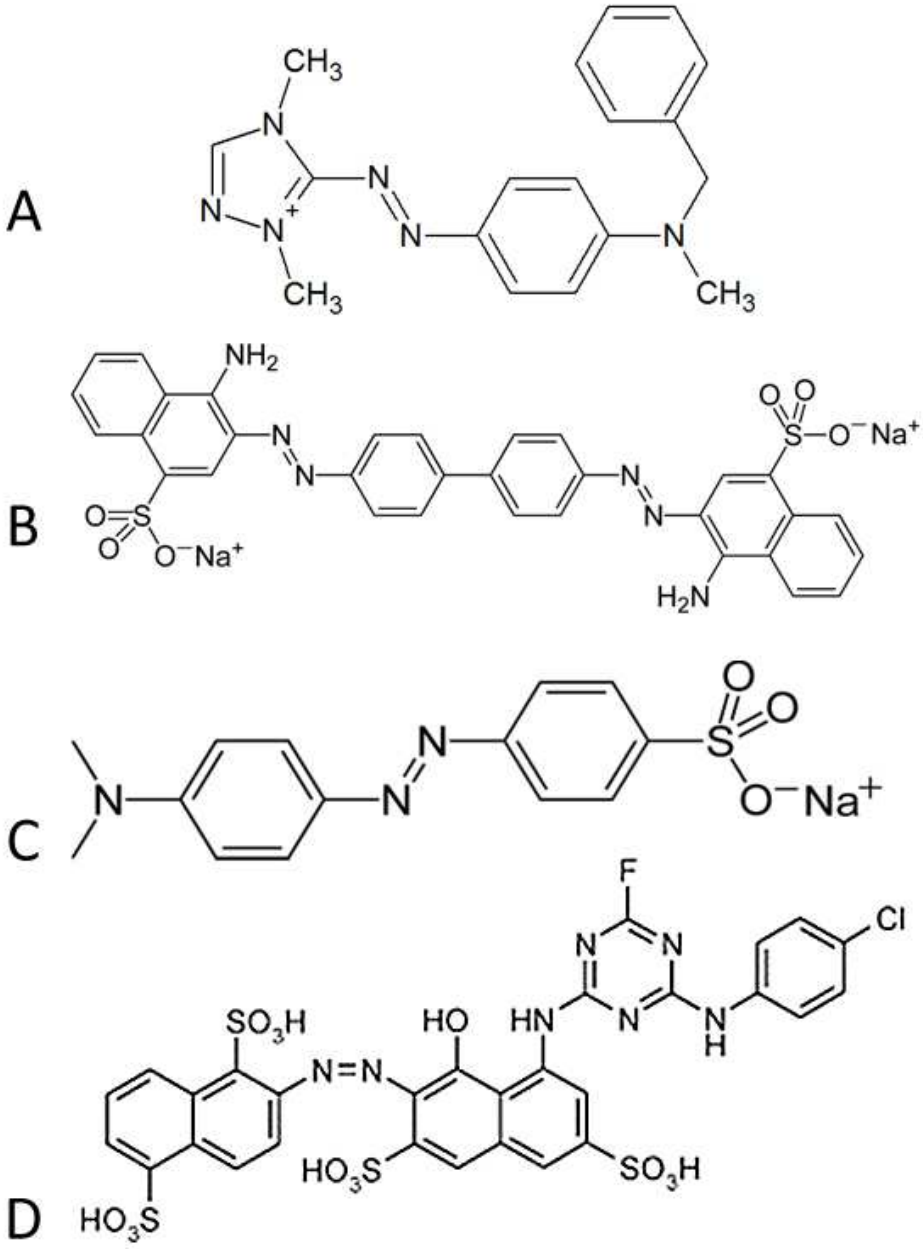

Figure A.5.1 Structural formulas of used dyes: Astrazon Red (A), Congo Red (B), Methyl Orange (C), Reactive Red 184 (D).

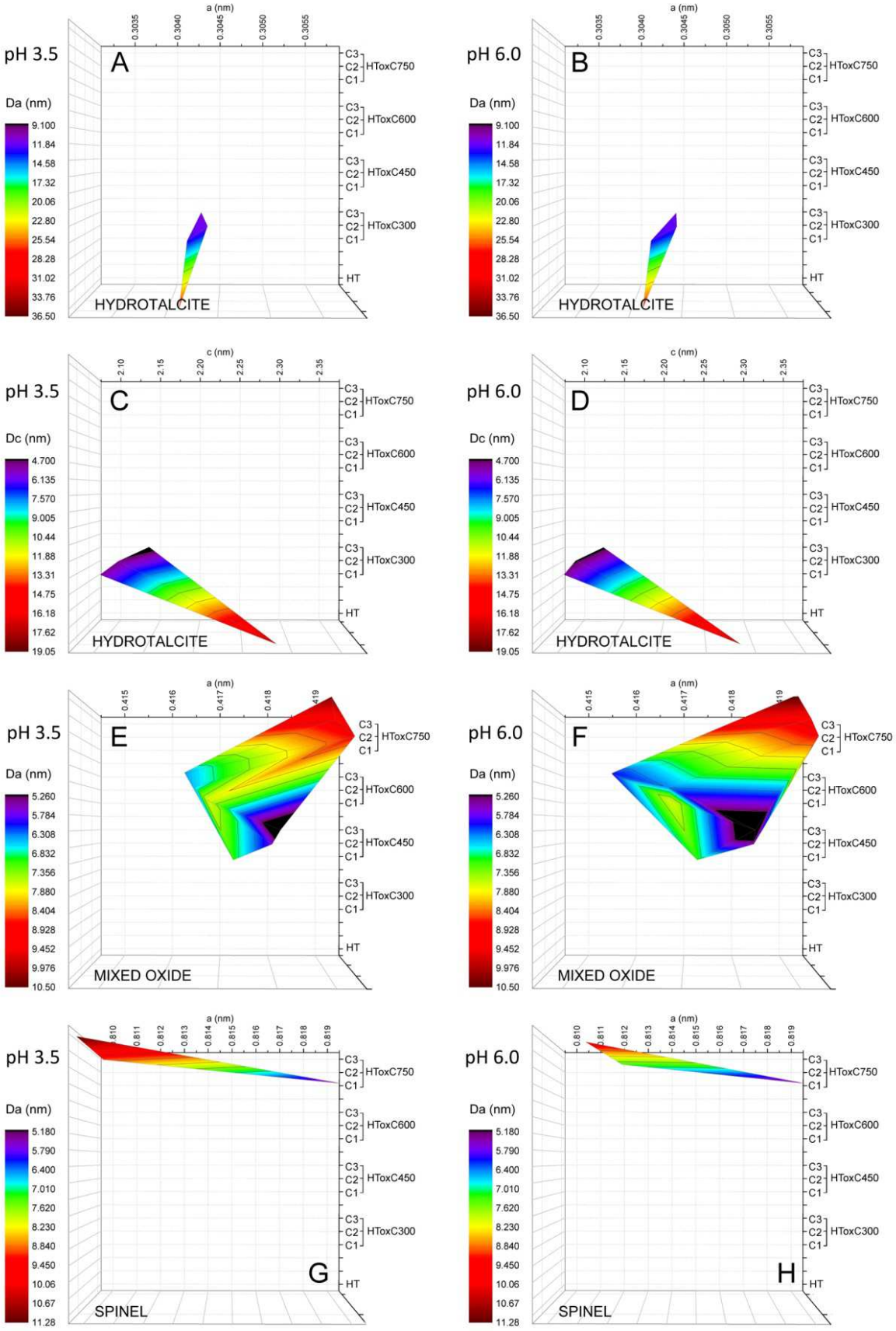

Figure A.5.2 Evolution of cell parameters for materials after calcination in different temperatures after adsorption of AMB.

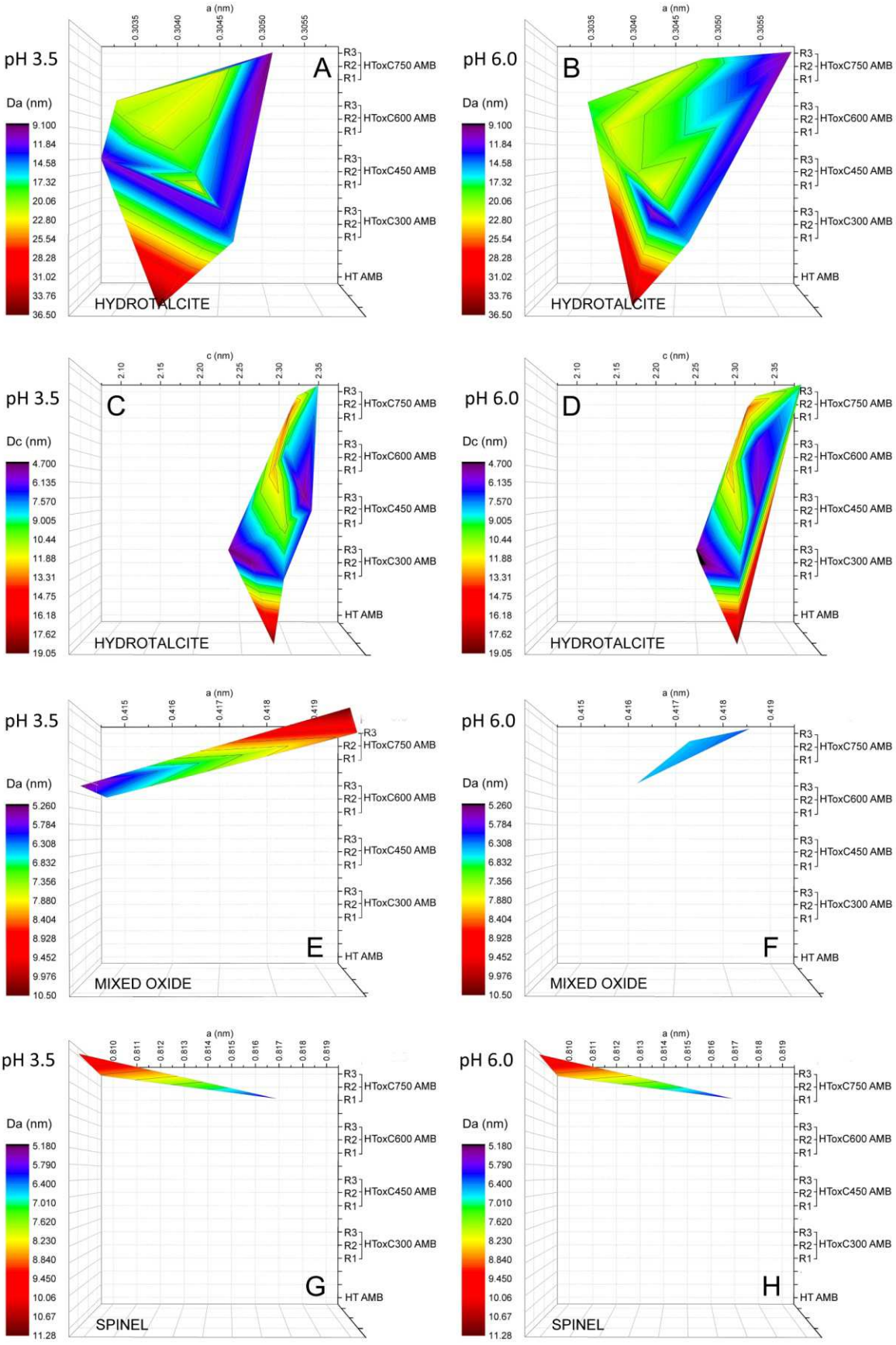

Figure A.5.3 Evolution of cell parameter for materials after adsorption of AMB after calcination in different temperatures.

Supporting materials S.5

S.5.1 Kinetics and equilibrium models

To describe the adsorption kinetics two models were adjusted to the experimental data. Pseudo 1st order model (Lagergren, 1898) is given by Eq. 1 (Ho, 2004) and pseudo 2nd order model (Ho and McKay, 1999) is expressed by Eq. 2:

$$q_t = q_e\left(1 - e^{-k_1 t}\right) \quad (1)$$

$$q_t = \frac{q_e^2 k_2 t}{1 + q_e k_2 t} \quad (2)$$

q_e and q_t (mg g^{-1}) are adsorption capacities at equilibrium and at time t (min), respectively, k_1 (min^{-1}) and k_2 (g mg^{-1} min^{-1}) are the pseudo 1st and pseudo 2nd order kinetic rate constants, respectively.

Two models were fitted to the data obtained in equilibrium studies. The Langmuir's model (Langmuir, 1918) model is expressed by Eq.3. and the Freundlich's model (Freundlich, 1906) (Freundlich, 1906) is given by Eq. 4.

$$q = \frac{q_m K_L C_e}{1 + K_L C_e} \quad (3)$$

$$q = K_F C_e^{\frac{1}{n}} \quad (4)$$

The parameters used in the models are: q (mg g^{-1}) the amount of dyestuff adsorbed per unit weight of adsorbent, C_e (mg L^{-1}) the equilibrium concentration, q_m (mg g^{-1}) and K_L (L mg^{-1}) are the Langmuir's model constants related to the maximum adsorption capacity considering monolayer coverage, and energy of adsorption, respectively; n and K_F ((mg g^{-1})(L mg^{-1})$^{1/n}$) are the Freundlich's model constants related to adsorption intensity and adsorption capacity, respectively.

S.5.2 References

Freundlich, H.M.F., 1906. Über die adsorption in läsungen. Z. Phys. Chem. 57, 385-470.

Ho, Y.S., 2004. Citation review of Lagergren kinetic rate equation on adsorption reactions. Scientometrics 59, 171-177.

Ho, Y.S., McKay, G., 1999. Pseudo-second order model for sorption processes. Process Biochem. 34, 451-465.

Lagergren, S., 1898. About theory of so-called adsorption of soluble substances. Kongl. Vetenskaps Academiens Handlingar 24, 1-39.

Langmuir, I., 1918. The adsorption of gases on plane surfaces of glass, mica and platinum. J. Am. Chem. Soc. 40, 1361-1403.

CHAPTER 6

Hybrids

Sustainable adsorbent obtained from by-product of acid activation of vermiculite and composite clay-LDH hybrid adsorbent for removal of industrial dyes and metal cations

Wojciech Stawiński[a*], Agnieszka Węgrzyn[b*], Grzegorz Mordarski[c], Zofia Piwowarska[b], Michał Skiba[d], Olga Freitas[a], Sónia Figueiredo[a]

[a] *REQUIMTE, LAQV, Instituto Superior de Engenharia do Porto, Instituto Politécnico do Porto, Rua Dr. António Bernardino de Almeida 431, 4200-072 Porto, Portugal*
stawor@gmail.com; omf@isep.ipp.pt; saf@isep.ipp.pt

[b] *Faculty of Chemistry, Jagiellonian University, ul. Ingardena 3, 30-060 Kraków, Poland*
wegrzyn@chemia.uj.edu.pl
zofia.piwowarska@uj.edu.pl

[c] *Jerzy Haber Institute of Catalysis and Surface Chemistry Polish Academy of Sciences, ul. Niezapominajek 8, 30-239 Kraków, Poland*
nbmordar@cyf-kr.edu.pl

[d] *Jagiellonian University, Institute of Geological Sciences, Department of Mineralogy, Petrology and Geochemistry, ul. Oleandry 2a, 30-063 Kraków, Poland*
michal.skiba@uj.edu.pl

Abstract

Hydrotalcite-like double-layered hydroxide (LDH) materials were synthesized from liquid waste byproduct of acid activation of raw and expanded vermiculites. Other adsorbents were obtained by combining acid activated vermiculites and the by-products to form novel hybrid vermiculite-hydrotalcite-like composite materials. All materials were characterized by ATR, XRD, SEM-EDS, XRF and TGA. Adsorption experiments were performed on original and calcined (at 450 °C) materials, in batch system using two anionic dyes, Congo Red (CR) and Reactive Red 184 (R), a cationic dye, Astrazon Red (AR), and copper cations. The result revealed that calcination significantly increased adsorption capacity of all materials, and that materials obtained from raw vermiculite had higher adsorption capacity compared to their counterparts derived from expanded mineral. In the case of composites, a strong synergic effect on adsorption was observed, especially in the materials derived from expanded vermiculite. Those adsorbents had higher adsorption capacity than if they were prepared by mixing ex situ appropriate amounts of activated vermiculite and hydrotalcite-like material.

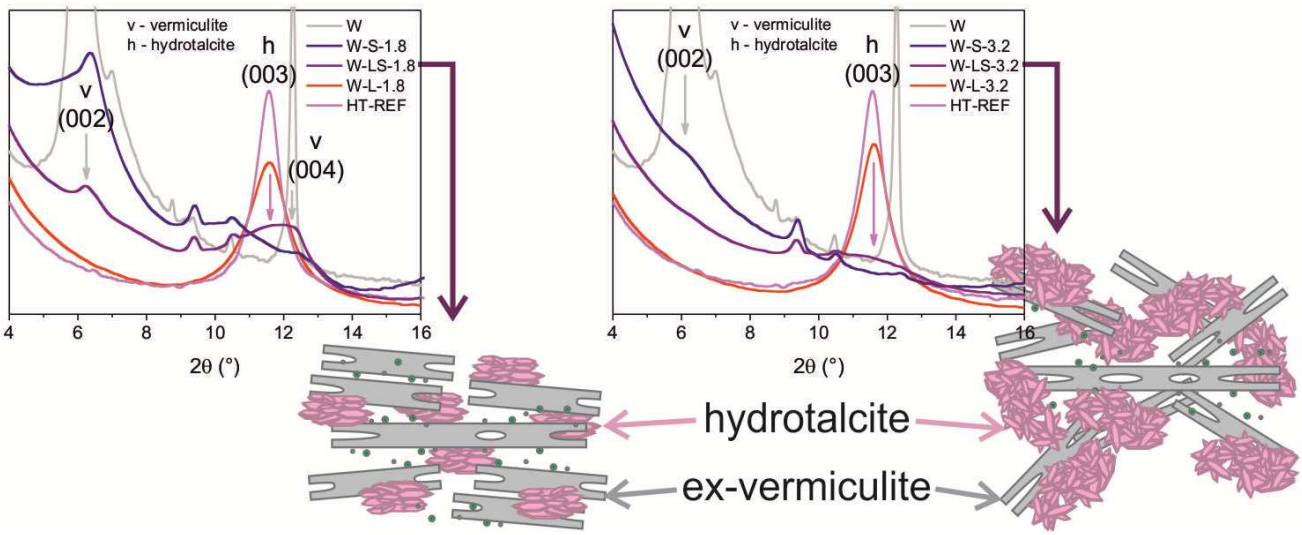

Key words: acid activation, dye removal, hybrid adsorbent, metal removal, vermiculite

6.1 Introduction

Water is an essential resource, without it life as we know it would not exist. Water quality is a highly important issue essential to maintain the environment and to human health. However, as a consequence of fast development of the industry, science and technology, together with rapid growth of the humankind, water quality endures deterioration. It has been reported by a study of United Nations that only 8% of the waste is treated in low-income developing countries, while 70% receives treatment in high-income developed nations (Monsalvo, 2016).

Dyes are common pollutants generated in various industries, such as paper, plastics, food, cosmetics and textile (Rozada et al., 2003; Angın et al., 2013). They are often accompanied by heavy metals in wastewaters (Pereira and Alves, 2011). Dyes are usually the first to be noticed in water bodies owning to their intense color, they exhibit ecotoxicity and by reduction of light penetration in aquatic environments hinders photosynthetic activity. Moreover, due to their complex molecular structure and chemical stability they are resistant to conventional treatment methods (Reife and Freeman, 1996; Forgacs et al., 2004; Bhatnagar and Jain, 2005). Heavy metals affect cellular organelles and components, and interact with some metabolic enzymes. Furthermore, they pose threat to human beings and animal even at low concentrations due to their bioacumulative nature (Wang and Shi, 2001).

It is important to eliminate pollutants from wastewaters, to take preventive measures against discharge of contaminants to the environment, and to reduce, recycle and dispose of wastes in a sustainable way. Decreasing of the environmental impact of wastewaters to acceptable levels has become the first and major concern of the uttermost importance together with the demand on efficient, economic and environmentally friendly technologies of removing pollutants at affordable costs has been rising (Sevekow, 2003; Pereira and Alves, 2011).

Among various processes adsorption has been getting more interest in the application in that field (Leitão and Serrão, 2005). Due to its broad applicability, ease of operation, insensibility to toxicants, high removal efficiency and possibility of recycling many adsorbents, it is considered to be one of the best wastewaters treatment methods (Pan et al., 2009; Ali et al., 2012). One of the widely used adsorbents is activated carbon (Duman and Ayranci, 2006; Ayranci and Duman, 2009; Duman and Ayranci, 2010) however, it is relatively expensive. The desired adsorbent should be derived from materials that are easily available in nature, inexpensive and non-hazardous (Ali et al., 2012; Ummartyotin and Pechyen, 2016).

Layered materials show promising perspectives in this field. From the numerous families of laminar solids, few of them exhibit good adsorption properties due to ability of intercalation of guest molecules. At the forefront of such materials are clays and layered double hydroxides (LDH) (Pinnavaia, 2004). The first family consists of minerals with its structure built of phyllosilicate sheets that may carry a negative charge which is balanced by a counter ion located between the layers. The second family, the LDHs, or hydrotalcite-like materials have similar, layered structure, however the sheets are built of hydroxides of two (sometimes more) different kinds metal cations and the layer has a positive charge which is balanced by interlayer anionic species (Braterman et al., 2004). Those charge balancing ions can be exchanged, which gives the materials good ion-exchange properties (Bergaya and Lagaly, 2006). Vermiculite is a very abundant clay that is much cheaper than other clays and it is commonly used in agricultural, industrial and environmental applications (Duman and Tunç, 2008; Duman et al., 2015). Due to its structure it exhibits good adsorption properties towards cationic species. The LDHs, on the other hand, have good adsorption properties towards anionic compounds and find continuous increase in their use in decontamination, with emphasis on compositions containing other adsorbents for the simultaneous removal of more than one chemical class of contaminant (Braterman et al., 2004; de Roy et al., 2006; Rives, 2006a).

Layered minerals can be a subject to various modifications in order to change their properties (Ruiz-Hitzky et al., 2004; Bergaya and Lagaly, 2006; Heller-Kallai, 2006; Komadel and Madejova, 2006; Lagaly et al., 2006). In the case on the clays, one of the most common modifications is their acid activation, which results in an increase of the maximum adsorption capacity of the material due to increasing its specific surface area and formation of new adsorption centers (Komadel and Madejova, 2006; Steudel et al., 2009; Santos et al., 2015; Stawiński et al., 2016). However, this process is not sustainable and does not fulfill the premise of Green Chemistry (Anastas and Warner, 1998) as it usually produces highly acidic waste containing metals leached during the process. In previous studies, treatment of vermiculite in order to enhance its adsorption capacity for dyes was developed. Nonetheless, this process created substantial amounts of waste. The aim of current research was to make the acid activation of clays more sustainable by application of the waste produced during the production process as a precursor for another adsorbent. The waste was successfully used to create a layered hydrotalcite-like material that was characterized by good adsorption properties for anionic dyes and metal cations. Moreover, by using the waste and the acid treated clay, a hybrid vermiculite-hydrotalcite adsorbent was prepared, which is able to adsorb metal ions and both, anionic and cationic dyes. Such prepared adsorbents were subjected to

thermal modification that resulted in increased maximum adsorption capacity for all aforementioned pollutants.

6.2 Experimental

6.2.1 Materials

6.2.1.1 Adsorbates

The cationic dye Astrazon Red FBL 200% (AR), CAS 12221-69-1, and two anionic dyes, Reactive Red 184 (R), CAS 85496-37-3 and Congo Red (CR), CAS 573-58-0, supplied by Dystar, were used for adsorption experiments. Analytical grade salt, $CuCl_2 \cdot 2H_2O$ obtained from Sigma-Aldrich was employed for preparation of Cu^{2+} solutions.

6.2.1.2 Adsorbents

6.2.1.2.1 Nomenclature

The first part of sample's name stands for the material used in the synthesis (W for the raw vermiculite, Ve for the expanded vermiculite). It is followed by either L or LS meaning that only liquid fraction after the acid treatment was used to form a hydrotalcite-like material, or both, liquid and solid fractions were utilized to obtain a hybrid composite material, respectively. Alternatively in the second part of the name, a single letter S denotes solid residual fraction after the acid treatment without formation of hydrotalcite-like material. The third part of the name indicates the concentration of nitric acid used during the synthesis (M). The last part, if present, stands for calcination at 450 °C.

6.2.1.2.2 Materials preparation

A volume of 100 mL of 1.8 M HNO_3 was placed in a round bottom reactor equipped with a condenser and heated in an oil bath. When the temperature reached 98 °C, a portion of 10 g of raw vermiculite (W) was added to the reactor and stirred (Velp, Multistirrer 15) at 400 r.p.m. for 2 h while the temperature was maintained constant. After that the material was centrifuged (Sartorius, Sigma 2-16) for 10 min at 4500 r.p.m. and the supernatant collected. The sediment was washed in 5 cycles of mixing with distilled water and centrifuged (10 min at 4500 r.p.m. in each cycle) and dried at 40 °C overnight originating the material W-S-1.8. The supernatant was placed in another round bottom reactor with a condenser, heated to 60 °C at constant stirring (400 r.p.m.), alkalinized with ammonium carbonate to pH 10 and stirred for 24 h. After that time the material was centrifuged (10 min at 4500 r.p.m.), washed 5 times following the procedure described

above, left to dry overnight at 40 °C and ground in a mortar, originating the material W-L-1.8. Similar procedure was applied using 3.2 M HNO_3 to form materials W-S-3.2 and W-L-3.2, respectively. The experiment was repeated with expanded vermiculite (Ve), creating materials Ve-S-1.8, Ve-L-1.8, Ve-S-3.2 and Ve-L-3.2, respectively. In another part of the experiment, after treating both vermiculites in 1.8 M and 3.2 M HNO_3 the whole content of the reactor was alkalinized without previous separation of the factions. The content was left at constant stirring for 24 h, then centrifuged, washed and left to dry and ground in a mortar in a manner described above. In this part the following materials were obtained: W-LS-1.8, W-LS-3.2, Ve-LS-1.8 and Ve-LS-3.2, respectively. Reference hydrotalcite (REF-HT), with formula $[Mg_{0.666}Al_{0.235}Fe_{0.097}(OH)_2](CO_3)_{0.165}\cdot 0.5H_2O$, was prepared by co-precipitation method. A solution of 0.666 M $MgCl_2$, 0.235 M $Al(NO_3)_2\cdot 9H_2O$ and 0.097 M $Fe(NO_3)_3\cdot 9H_2O$ was added drop-wise from one dropping funnel, and a solution of 2 M NaOH from another one to a 0.160 M solution Na_2CO_3. The pH was maintained at 10 and temperature at 60 °C under constant stirring (400 r.p.m.). Prepared material was centrifuged and washed five times in water (10 min at 4500 r.p.m. in each cycle), left to dry for 24 h at 40 °C and ground with a mortar. The materials were divided into two portions; one of them was calcined in a muffle furnace at 450 °C during 6 h with heating rate of 2 °C min^{-1} originating materials with the c450 suffix.

6.3 Methods

6.3.1 Characterization of materials

The structure of the materials was studied by analysis of XRD patterns recorded using a X-ray powder diffractometer (Bruker, D2 PHASER) equipped with CuKα radiation source. Infrared spectra of the materials were recorded using attenuated total reflectance technique (ATR) (Nicolet 6700 FT-IR, Thermo Scientific). The textural parameters of the materials were determined by adsorption of N_2 at −196 °C using a 3Flex (Micromeritics) surface characterization analyzer on outgassed materials. Cation exchange capacity was determined using the ammonium acetate method (Steudel, 2008). X-ray fluorescence (XRF) analysis was performed using Skayray Instrument EDX 3600H - Alloy Analyzer. A field emission scanning electron microscope (FESEM) Hitachi S-4700 equipped with a Vantage Noran EDS system was used. Surfaces of the materials were prepared by carbon coating..

6.3.2 Adsorption experiments

Weighted portions of 20 mg of each material were placed in an Erlenmeyer's flasks, mixed with 40 mL of solution containing AR, R, CR or Cu^{2+} ions of concentrations equal 200 mg L^{-1} in the case of dyes and 30 mg L^{-1} in the case of Cu^{2+}. Flasks were closed with a cap and stirred (Velp, Multistirrer 15) at 400 r.p.m. during 2 h, at room temperature (24 °C) without pH correction. Each experiment was triplicated. At the end, materials were centrifuged and concentration of adsorbates in the supernatant determined. The dyestuff concentration was measured using an UV-VIS spectrometer (Thermo Scientific, Evolution 300) at the maximum absorbance wavelength of each dyestuff (540 nm for R, 531 nm for AR, and 495 nm for CR). Concentration of Cu^{2+} was determined using atomic absorption spectroscopy (AAS) using the line 327 nm line (Analitic Jena High-Resolution Continuum Source Atomic Absorption Spectrometer, ContrAA 700).

The adsorption capacity was calculated according to Eq.1:

$$q_{=}\frac{(C_0-C_{eq})V}{m} \qquad (1)$$

where q is adsorption capacity (mg g^{-1}), C_0 and C_{eq} initial and final concentrations (mg L^{-1}) respectively, V, volume of adsorbate (L) and m, adsorbent mass (g).

6.4 Results

6.4.1 Synthesis efficiency

The analysis of the reaction yield showed that proposed procedures allowed to obtain desired materials with satisfying efficiency. In the case of hybrid hydrotalcite-vermiculite materials the yield was close to 100% (Fig.6.1 materials Ve-LS-1.2, Ve-LS-3.2, W-LS-1.8 and W-LS-3.2), which means that vermiculites can be efficiently and totally transformed on a way of acid and base into versatile composite.

The yield of the solid fraction after acid treatment was equal to 44 and 38% in the case of raw vermiculite (W) after treatment with 1.8 and 3.2 M nitric acid, respectively (Fig.6.1 material W-S-1.8 and W-S-3.2). At the same time application of 1.2 and 3.2 M nitric acid activation of expanded vermiculite (Ve) (Fig.6.1 materials Ve-S-1.2 and Ve-S-3.2) resulted in 63.5 and 48.4% yield, respectively. Higher yield for this type of adsorbent compared to the yield for W, meaning that more W is dissolved at given concentration than Ve, implies that expanded mineral has higher resistance to acid attack than its raw version, and dissolution intensity is highly dependent on acid concentration.

The yield for the material obtained from liquid residue after acid treatment of vermiculites does not sum up to 100% with the yield of the material derived from solid

fraction (Fig.6.1 materials Ve-L-1.2, Ve-L-3.2, W-L-1.8 and W-L-3.2). This may be due to removal of some impurities present in the starting materials which are further not incorporated in neither of the fractions. Also the derived adsorbents had diminished amount of physically adsorbed water (Table 6.4). Also there is a small loss of material in every cycle of centrifugation and washing as each time it becomes less susceptible to settling. This can also explain not 100% yield of the synthesis of the reference hydrotalcite (Fig.6.1 material HT-REF). The yield of the hybrid material obtained from W after treatment in 3.2 M acid exceeded 100%. In the case where LDH (layered double hydroxide) is formed, additional substrates are incorporated into the structure, e.g., CO_3^{2-} or NO_3^- anions, which are not present in the starting material. Thus it is normal to obtain yields greater than 100%.

According to the XRF analysis (section 3.2.2) of the materials a share of each phase in the hybrid material was calculated. All materials except Ve-LS-1.2 were characterized by quite homogeneous composition with equally distribution of both phases (Fig.6.1).

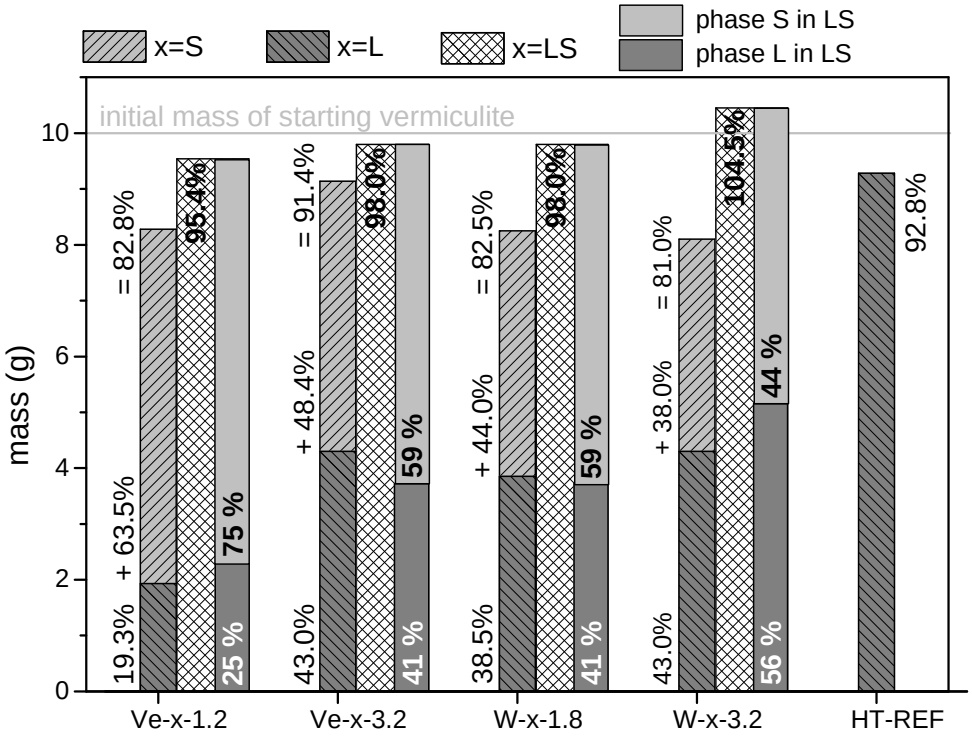

Figure 6.1 Synthesis efficiency and phase composition of hybrid hydrotalcite-vermiculite materials.

6.4.2 Material characterization

6.4.2.1 Scanning Electron Microscopy with Energy Dispersive Spectroscopy (SEM-EDS)

Element distribution was quantified in materials obtained from raw vermiculite (W) treated with 3.2M nitric acid. The analysis of the material formed from solid fraction (Fig.6.2 material W-S-3.2) showed significant concentration of Si in amorphous silica created during the treatment. Distribution of small amounts of Mg, Al and Fe which were not leached from the material was homogenous. Some aggregation of Mg and Al in one grain is most probably due to incomplete dissolution of the layers and partial redeposition of degradation product. The material obtained from liquid fraction (Fig.6.2 material W-L-3.2) was characterized by uniform distribution of Al, Mg and Fe, which are its main components, however some Si leached from the starting material was also incorporated into the structure. The material synthesized with both, liquid and solid phases (Fig.6.2 materialW-LS-3.2), contained Si, Al and Mg with random, homogeneous distribution in most of the surface; however, Mg, and Al occurred in some regions in higher concentration, which might be attributed to bulk accumulated LDH (regions marked as HT, Fig.6.2).

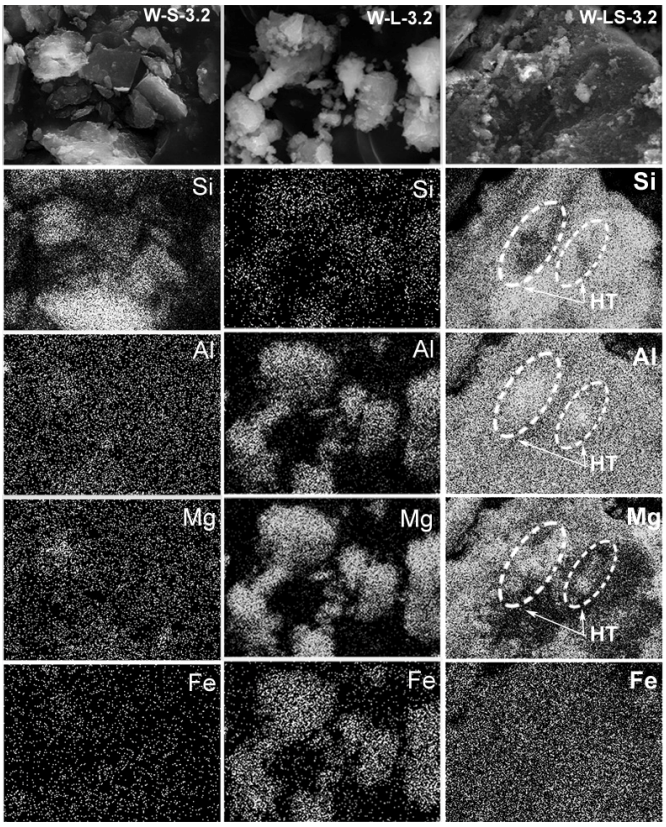

Figure 6.2 SEM images and elemental mapping of the material W-X-3.2.

6.4.2.2 X-ray fluorescence (XRF)

Both straining vermiculites had similar chemical composition, with Si, Al, Mg and Fe being the dominant components. The results are presented in Fig. 6.3. Expanded material (Ve), however, contained more K and Ca than the raw mineral (W). In both cases acid treatment caused leaching of all metal cations except for Si, with intensity proportional to used concentration. Ve was more resistant to acid dissolution which was manifested in the presence of Al and K in the material after treatment with 3.2 M HNO_3 (Ve-S-3.2) whereas its raw vermiculite counterpart (W-S-3.2) did not contain those cations. The reference hydrotalcite (REF-HT) had similar composition to the materials obtained from the liquid fractions (L) however, they had slightly varying content of Fe and some amounts of Ca and K incorporated in the structure in the case of both materials from W (W-L-1.2 and W-L-3.2) and Ve-L-3.2. Moreover, the material obtained from cations leached after treatment of Ve with 1.2 M acid (Ve-L-1.2) stood out from its counterparts with its higher amount of Ca and Si. The composite vermiculite-hydrotalcite materials synthesized from both liquid and solid fractions (LS) were characterized by similar chemical composition to the corresponding starting vermiculites..

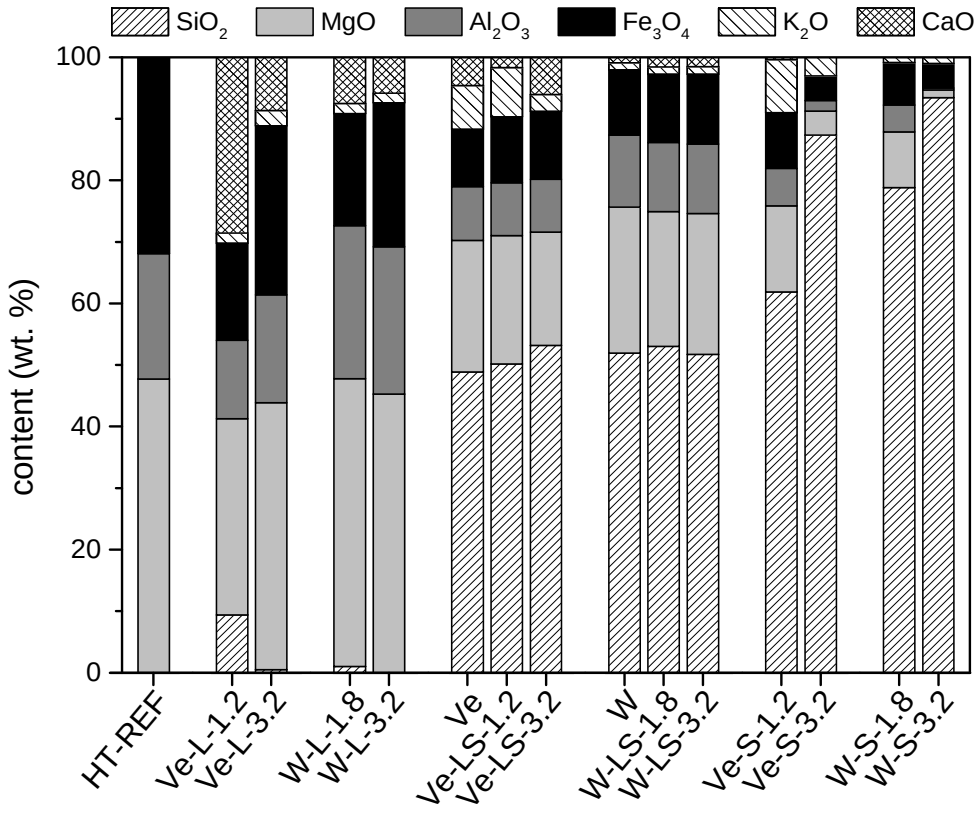

Figure 6.3 XRF analysis of chemical composition of adsorbents.

6.4.2.3 Attenuated Total Reflectance (ATR)

In the infrared spectra analysis of the materials (Fig.6.4) some peaks were identified using the second derivative method (data not shown). Every material exhibited a peak assigned to vibrations of inner OH groups at around 3620 cm^{-1} (Somasundaran, 2006). The peak associated with OH stretching vibration in weakly bonded water molecules (Chmielarz et al., 2012) was present in the spectrum of the raw vermiculite at 3340 cm^{-1}, however in the case of other materials it is shifted towards higher wavenumbers to around 3400 cm^{-1}. Such change might be explained by an increase in the interlayer O-OH distance (Somasundaran, 2006) as a result of leaching of the vermiculite base materials and different structure of hydrotalcite like materials. Another peak associated with water vibrations was detected at around 1640 cm^{-1} (Chukanov, 2014) in the spectra of every material. The peak assigned to stretching vibration of Al_2OH in vermiculite at 3326 cm^{-1} (Madejová and Komadel, 2001) was present in the spectra of the materials formed using solid (S), and solid and liquid fractions (LS), however it was not detected in the case of the materials made of only from the liquid residue (L) obtained after the acid treatment of vermiculites. The materials obtained from the solid fraction after treatment in 3.2 M nitric acid (W-S-3.2 and Ve-S-3.2) did not show in their spectra a peak at around 3555 cm^{-1} attributed to Fe_2OH or AlFeOH vibrations (Besson and Drits, 1997; Parikh et al., 2014), which suggests strong leaching of the octahedral layers when more concentrated acid was used in the treatment.

The peak at around 3030 cm^{-1} assigned to CO_3-H_2O (Kloprogge and Frost, 2006) or salvation water molecules highly condensed in micropores (Kuśtrowski et al., 2004) was present in the spectrum of the reference hydrotalcite and in every material made of only liquid fraction (L). Two peaks at 1750 cm^{-1} and 1480 cm^{-1} were detected in the spectra of every material containing the hydrotalcite material (L and LS) and are associated with NO_3^- (Kloprogge and Frost, 2006). Interlayer carbonate gave a peak at around 1360 cm^{-1} (Kloprogge et al., 2004; Kloprogge and Frost, 2006) with high intensity in the case of pure hydrotalcite materials (L). This peak was not observed in vermiculite and materials obtained from solid fractions (S), however in the case where both solid and liquid fractions were used for the synthesis, this peak exhibits moderate intensity. Another peak associated with carbonate species was found at the range between 1500 – 1400 cm^{-1} (El Gaini et al., 2009; Santos et al., 2013).

The materials formed from solid fraction (S) gave reflections at around 1200 cm^{-1} attributed to Si-O stretching in amorphous silica (Chmielarz et al., 2012; Barabaszová and Valášková, 2013). In the spectra of the materials where additionally hydrotalcite

phase was present (LS) this reflection was less intense, and it was not observed in the case of hydrotalcite and materials synthesized from liquid residue (L).

The starting vermiculites exhibited a sharp reflection at 955 cm^{-1} ascribed to Si-O stretching in the clay layer (Stubičan and Roy, 1961; Madejova, 2003; Ritz et al., 2014). This reflection is present as a shoulder on reflections at 1045 cm^{-1} and 1020 cm^{-1} assigned to amorphous silica (Chmielarz et al., 2012; Barabaszová and Valášková, 2013) in the case of materials made from solid fraction (S), with an exception for the material Ve-S-1.2 where the peak at around 955 cm^{-1} remained almost the same. These results suggest intensive transformation of vermiculites after acid treatment and stronger resistance to such modification of expanded vermiculite. In the spectra of the materials formed from both phases (LS) the Si-O vibration is manifested by a reflection at around 1000 cm^{-1} (Stubičan and Roy, 1961; Ritz et al., 2014) without the shoulder at 955 cm^{-1}. Both starting vermiculites showed in their spectra a peak at 650 cm^{-1} assigned to Si-O bending (Stubičan and Roy, 1961; Madejová and Komadel, 2001). This peak is no longer present in the spectra of the materials derived from solid fraction (S) after the acid activation where a peak at 670 cm^{-1} corresponding to Fe-O out-of-plane vibrations (Madejova, 2003) appeared together with a peak at around 800 cm^{-1} assigned to amorphous silica (Madejova, 2003). The 670 cm^{-1} band was also detected in the materials formed with liquid and solid phase (LS).

In the spectra of the reference hydrotalcite and the materials formed from only liquid fraction (L) a peak at 860 cm^{-1} is present and assigned to Fe-OH vibrations (Ovejero et al., 2013). Those materials also showed a peak at 940 cm^{-1} that might be due FeO-OH vibrations (Qwabe et al., 2015), 745 cm^{-1} assigned to a translational mode of M-OH moieties (Sobhana et al., 2016) and at around 610 cm^{-1} that did not appeared in the case where both phases were used (LS). Every material, except those from solid residue and raw material, gave reflection at around 850 cm^{-1} suggesting formation of AlFeOH units (Madejová and Komadel, 2001).

Each material containing hydrotalcite showed reflections in the range of 600-550 nm associated with stretching and bending vibrations of M-O, M-O-Me, and O-M-O bonds (Madejova, 2003; Nakamoto, 2009) and hydroxyl group associated mainly with Al, which are influenced by probably one Mg in its coordination environment (Kloprogge and Frost, 2006).

After calcination no significant alternations of the ATR spectra were observed. However, all peaks in the range of higher wavenumbers associated with OH groups vibrations appeared with reduced intensity. The intensity was also lowered in the case of peak related to vibration of CO_3^{2-} in materials containing hydrotalcite phase.

Peaks and their assignment are presented in Table 6.1.

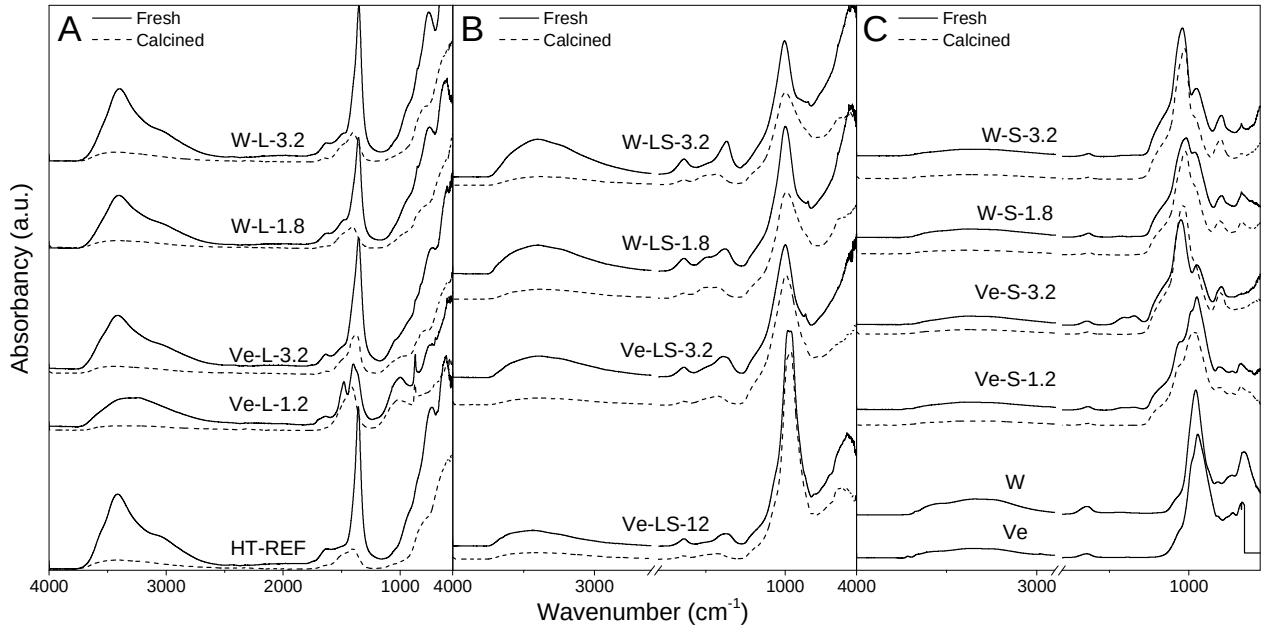

Figure 6.4. ATR spectra of material obtained from liquid phase after acid treatment of vermiculites (A), hybrid vermiculite-hydrotalcite adsorbents from liquid and solid phase (B) and solid phase remained after the treatment (C).

Table 6.1 Peak assignment and IR spectra of synthesized adsorbents.

Peak (cm^{-1})	Assignment	Reference
3720	Si-OH	(Ahlrichs et al., 1974)
3670-3680	Mg_3OH	(Parikh et al., 2014)
3620	inner OH groups	(Somasundaran, 2006)
3550- 3555	Fe_2OH or AlFeOH	(Parikh et al., 2014) (Besson and Drits, 1997)
3230	stretching vibration of Al_2OH	(Madejová and Komadel, 2001)
3035	H_2O-CO_3^{2-} or salvation water molecules highly condensed in micropores	(Kloprogge and Frost, 2006) (Kuśtrowski et al., 2004)
1700, 1230, 1480-1497	interlayer NO_3^-	(Kloprogge and Frost, 2006)
1635-1640, 3398- 3415	HOH bending vibrations	(Stubičan and Roy, 1961; Chmielarz et al., 2012; Chukanov, 2014)
1350-1360 1405-1410	interlayer carbonate	(Kloprogge et al., 2004; Kuśtrowski et al., 2004; Kloprogge and Frost, 2006)
800, 1045, 1080, 1196-1190	amorphous silica	(Belver et al., 2002; Madejova, 2003; Chmielarz et al., 2012; Barabaszová and Valášková, 2013; Ritz et al., 2014)
955-966, 1000	stretching vibrations of Si-O	(Stubičan and Roy, 1961; Ritz et al., 2014)
860, 940	FeO-OH vibrations	(Ovejero et al., 2013; Qwabe et al., 2015)
850	AlFeOH	(Madejová and Komadel, 2001)
817	tetrahedral Al–O out-of-plane or amorphous silica	(Madejová and Komadel, 2001) (Chmielarz et al., 2012; Barabaszová and Valášková, 2013)
750-760	Al–O–Si in-plane	(Madejová and Komadel, 2001)
730-745	translational mode of Me-OH moieties	(Sobhana et al., 2016)
672	Fe-O out-of-plane vibrations	(Madejova, 2003)
650	Si-O bending	(Stubičan and Roy (1961); Madejová and Komadel (2001))
610 580	stretching and bending vibrations of M-O, M-O-M, and O-M-O bonds	(Nakamoto, 2009)
550-552	hydroxyl group associated mainly with Al, which are influenced by probably one Mg in its coordination	(Kloprogge and Frost, 2006)

6.4.2.4 X-ray Diffraction (XRD)

The XRD patterns of reference hydrotalcite showed typical reflections characteristic of that material at 11.71° (d_{003}= 7.55 Å), 23.31° (d_{006}= 3.82 Å), 34.8° ($d_{009+012}$= 2.57 Å), 39.40° (d_{015}= 2.29 Å), 47.00° (d_{018}= 1.93 Å), 60.90° (d_{110}= 1.52 Å) and 62.19° (d_{112}= 1.49 Å) (de Roy et al., 2006). Those reflections were also present in the patterns of the materials obtained from liquid fractions (L), proving that the material was indeed layered double hydroxide (Fig.6.5A). The basal reflection d_{003} was sharper in the case of the materials derived from raw vermiculite compared to materials obtained from expanded mineral, what suggests better crystallinity of the first ones. Moreover, a series of other sharp reflections appeared in the diffractograms with material Ve-L-1.2 having their highest number. Based on the XRF analysis (Fig.6.3) the high calcium content of that material may be ascribed to the different calcium species present. Calcination of those materials resulted in their complete transformation in mixed oxides, which is reflected in the patterns with three characteristic reflections at 35.20° (d_{111}= 2.55 Å), 43.30° (d_{200}= 2.09 Å) and 62.50° (d_{220}= 1.48 Å), as shown in Fig.6.6A.

Both starting vermiculites showed characteristic reflection at 6.2° (d=14.2 Å, 002), 12.3° (d=7.2 Å, 004), 18.5° (d=4.8 Å, 006), 24.8° (d=3.6 Å, 008), 31.2° (d=2.9 Å, 0010), 37.5° (d=2.4 Å, 0012), 44.1° (d=2.05 Å, 0014) in the case of W (Santos et al., 2015) and additional two reflections at 7.19◦ (d=1.23 nm) and 8.60◦ (d=1.03 nm) in the case of Ve (Lagaly, 2006). The patterns for the materials obtained from solid fractions (S) showed typical image of vermiculites subjected to acid treatment, with decreased crystallinity, formation of significant amount of amorphous silica, especially in the case where higher concentration were used, and gradual lowering of basal reflections intensity with increasing acid concentration (Fig.6.5C) (Stawiński et al., 2016). Thermal treatment of those materials did not result in any significant changes in their crystalline structure, besides lowering of the intensity of the reflection d_{003} of W-S-1.8 (Fig.6.6C).

In the patters the hybrid materials (Fig.6.5B), obtained from liquid and solid fractions (LS), characteristics peaks of both vermiculite and hydrotalcite phases were identified. The hydrotalcite basal reflection d_{003} overlaps with d_{004} reflection of vermiculite what results in broad asymmetric reflection in the case of the materials derived from W. Other reflections assigned to hydrotalcite located in higher angles were sharper and also asymmetric. The results allowed to state that LS materials indeed contain both vermiculite and hydrotalcite phases, however the latter one, as being crystallized on the surface of degraded vermiculite layers, has lower crystallinity compared to pure hydrotalcite materials. Nonetheless, the pattern on of the crystallinity of this phase being depending on the starting vermiculite and acid concentration used in the synthesis is

kept and visible in the diffractogram of the hybrid materials. After calcination it was impossible to identify the d_{111} reflection of mixed oxide, however the reflections d_{200} and d_{220} were present in the patterns. Moreover, hydrotalcite phase was still present in the case of the materials derived from W. In the case of W-LS-1.8-C450 the d_{003} reflection was identified at the usual angle, and in the case of W-LS-3.2-C450 this reflection is shifted toward higher angles, which corresponds to formation of an intermediate dehydrated layered phase (Fig.6.6B). This fact could suggest in this certain combination of phases hydrotalcite exhibits better thermal stability.

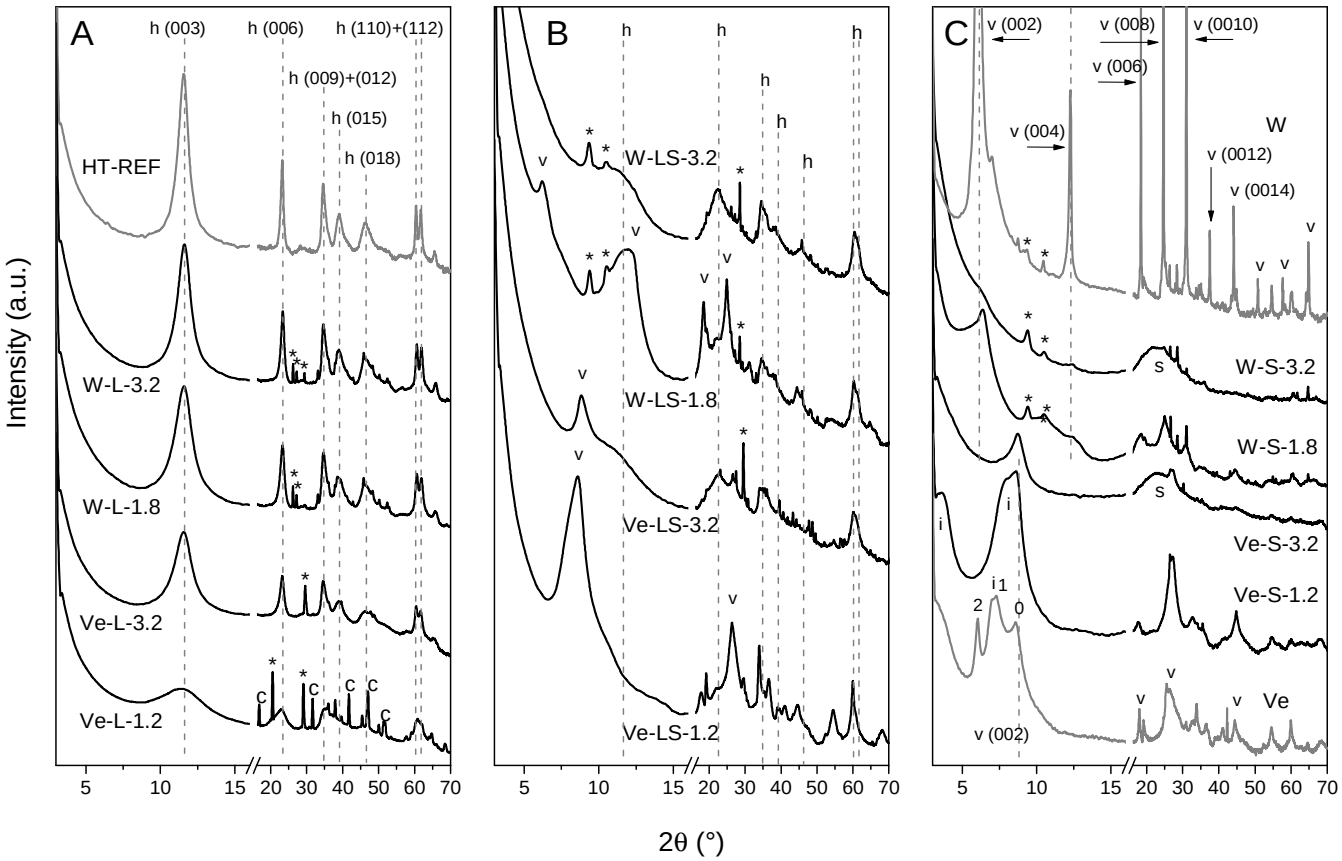

Figure 6.5 Phase composition of material obtained from liquid phase after acid treatment of vermiculites (A), hybrid vermiculite-hydrotalcite adsorbents from liquid and solid phase (B) and solid phase remained after the treatment (C).

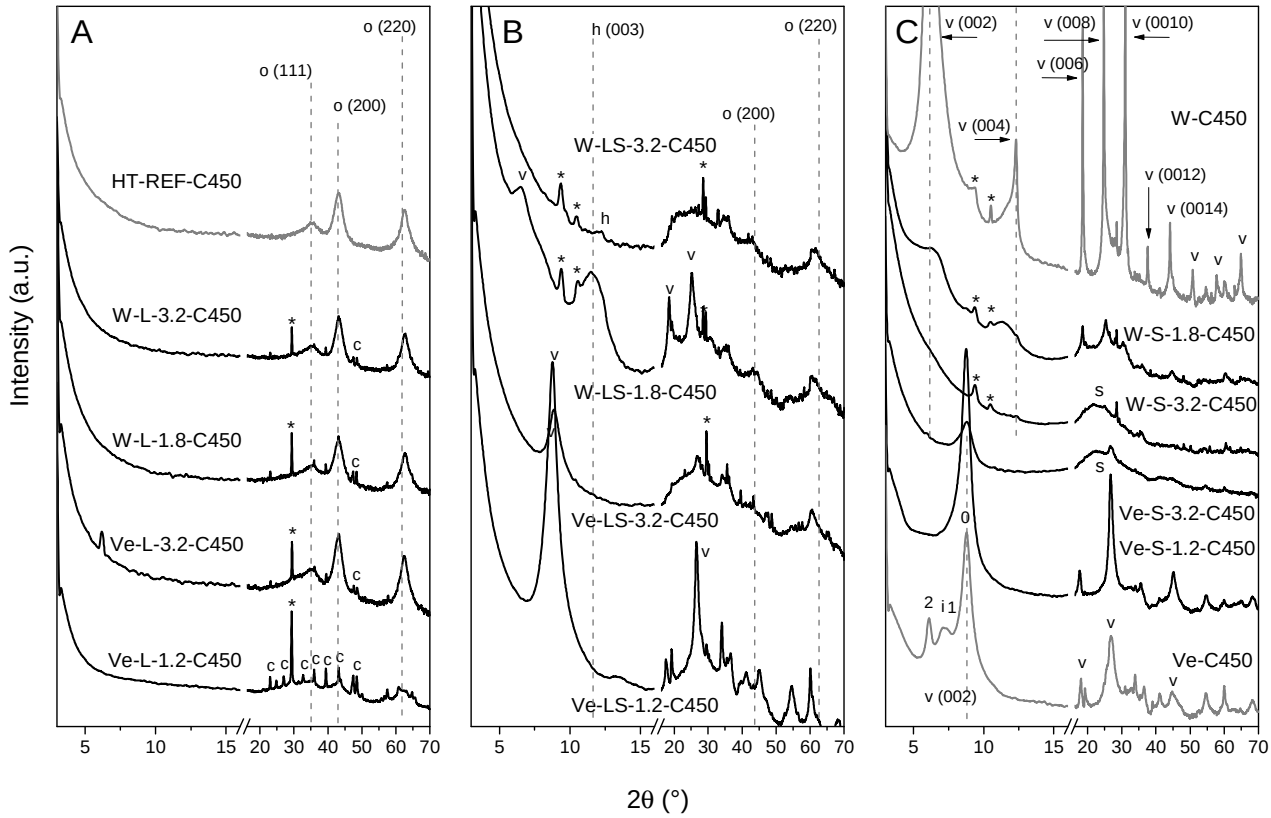

Figure 6.6 Phase composition of material after calcination at 450 °C obtained from liquid phase after acid treatment of vermiculites (A), hybrid vermiculite-hydrotalcite adsorbents from liquid and solid phase (B) and solid phase remained after the treatment (C).

The *c* parameter of the materials obtained from liquid fractions (L) diminished when higher acid concentration was used in the preparation in comparison to their adequate counterparts. The parameter decreases when the *x* (ratio M^{2+} to M^{3+}) increases. In that case, more concentrated acid causes more intense leaching of the layers thus more available Fe and Al was present in the solution, resulting in higher ratio. The *a* parameter corresponding to the distance between metal cations in the layers corresponds to the calculated ratio of Mg:Al:Fe in the material. The material V-L-3.2 has higher *a* parameter compared to its counterpart, resulting in higher concentration of Mg, which has the highest ionic radius of the three cations. The materials obtained from W have a similar parameter value, which is in accordance with their chemical composition.

The crystallites dimensions parallel to the *c* and *a* length (*Dc* and *Da* parameter, respectively) were lower compared to the reference hydrotalcite and formation of LDH from the liquid fraction after acid treatment of expanded vermiculite generally resulted in smaller crystallites compared to the material obtained from raw mineral. Moreover, the dimensions were smaller when less concentrated acid was used during the synthesis.

However, in the case of composite materials the opposite was true and lower acid concentration gave larger crystallites. Furthermore, in this case the crystallites were much smaller compared to their counterparts from pure hydrotalcite phase. Although the crystallites were smaller, the *c* and *a* parameters are higher than in the case of pure hydrotalcite, which suggests that the presence of digested phyllosilicate in the solution promoted growth of LDH species with thicker brucite-like layer and higher distance between the metal cations.

After calcination of the pure LDH materials the product maintained the differences in the *a* parameters observed in the uncalcined materials, however the calcined hybrid materials exhibited an increased cation-cation distances compared to their counterparts, and a difference in the parameter between materials obtained from W, with the parameter of W-LS-3.2 being higher than W-LS-1.8. In this case the grain size was also higher in the material obtained after treatment in more concentrated acid, however the general trend of the crystallite was smaller than in materials derived from liquid fraction. The parameters are shown in Table 6.2.

It has to be noticed that most of the differences in the parameters may be originated by the fact that the materials were obtained from different starting materials, which are characterized by different chemical composition. Also the treatment conditions were different in each case resulting in varying composition of the fractious used in the synthesis. All this is reflected in slightly different materials.

Table 6.2 Cell parameters of synthesized adsorbents.

	Original				Calcined	
Material	***c* (nm)**	***Dc* (nm)**	***a* (nm)**	***Da* (nm)**	***a* (nm)**	***Da* (nm)**
Ve-LS-1.2	2.40917	4.25484	0.30829	10.2255	0.41907	1.25485
Ve-LS-3.2	2.36583	3.40993	0.3079	9.64817	n.o.	n.o
W-LS-1.8	2.34818	5.85247	0.30708	15.70858	0.42076	1.22655
W-LS-3.2	2.37611	4.00201	0.30665	11.90136	0.42507	3.54133
Ve-L-1.2	2.3213	5.69386	0.30455	10.57884	0.41796	4.26558
Ve-L-3.2	2.29587	13.65912	0.3061	21.33075	0.42016	6.89952
W-L-1.8	2.29084	14.94044	0.30524	23.10736	0.4192	6.38213
W-L-3.2	2.28425	19.08008	0.30528	29.51805	0.41877	7.43632
HT-REF	2.29786	24.53256	0.3062	34.84188	0.41956	6.9525

6.4.2.5 Thermogravimetric. Analysis (TGA)

Peaks' maxima corresponding to H_2O emission during the thermal decomposition of materials are presented in Table 6.3. Dehydratation of the materials started at a temperature range below 100 °C, from desorption of water adsorbed on the surface (Földvári, 2011). Due to increased specific surface area, as a result of acid leaching (Stawiński et al., 2016), the temperatures were elevated in the case of materials W-S-1.8 and W-S-3.2, and their hybrid counterparts, as the diffusion was impeded. All materials, containing layered structure material, lost the water adsorbed between the layers in temperature between 100 and 140 °C (Földvári, 2011). This peak was not observed in the case of the materials obtained from solid fraction of acid treated vermiculite as their structure is highly distorted, layer charge and cation exchange capacity diminished (Stawiński et al., 2017), thus it might be assumed that the water from that region escaped in lower temperature range. In the case of materials containing layered-double hydroxides (LDHs) this peak might be ascribed to loss of water from the interlayer gallery that resulted only in partial dehydration on the interlayer (Rives, 2006b). As last escaped the water bound to interlayer cations in the case of the material W, and in the case LDH the dehydratation of interlayer gallery was completed (Rives, 2006b; Földvári, 2011). This peak was not observed in the case of the materials obtained from solid fraction (S) what might be attributed to the acid leaching that caused intensive removal of the interlayer species (Chmielarz et al., 2010). Additionally the peak at 220 °C, seen in the case of the W-S-3.2 material, may be attributed to dehydratation of amorphous silica (Zhuravlev, 2000) since this material contains it in significant amounts (Stawiński et al., 2016).

The dehydroxylation of OH groups bonded to Al stated in the temperature range between 323 and 327 °C, in the case of the materials containing LDH phase (Rives, 2006b). Next peak, in higher temperatures, might be due to dehydroxylation of OH groups bounded to Mg in the case of materials obtained from liquid fraction (L) and to dehydroxylation of amorphous silica in the case of the materials derived from solid fraction (S) (Zhuravlev, 2000; Rives, 2006b). For hybrid materials (LS) this peak most probably resulted from the combination of both abovementioned processes. Dehydroxylation of the structural layers occurs at around 500 °C (Földvári, 2011; Smykatz-Kloss, 2012). This peak was observed in the case of all materials containing the solid fraction (materials S and LS). The last peak in higher temperature range may be attributed to destruction of the material's structure and crystallization of a new phase – enstatite (Földvári, 2011) or mullite (El Mouzdahir et al., 2009; Smykatz-Kloss, 2012).

Table 6.3 Peaks maxima for evolved water in decomposition of synthesized materials.

Material	Peak maximum (°C)						
W	53	100	196			502	860
W-S-1.8	70				356	504	850
W-S-3.2	80		221		360	512	840
W-LS-1.8	75	117	166	323	365	510	810
W-LS-3.2	70	140	166	320	360	530	820
W-L-1.8	56	120	203	327	379		
W-L-3.2	55	135	203	314	366		
HT-REF	53	120	202	325	376		

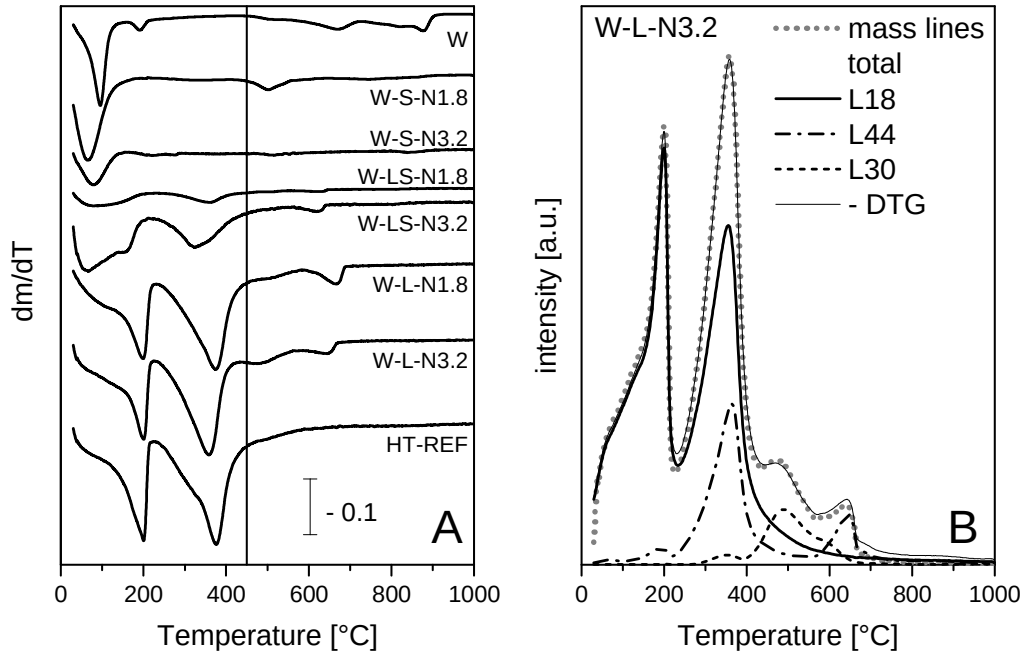

Figure 6.7 Thermal decomposition of leached vermiculite, hybrid vermiculite-hydrotalcite materials, and hydrotalcite like adsorbents; A – derivatives of thermogravimetric curves (DTG); B – mass lines evolution in the course of material W-L-N3.2 decomposition.

The loss of water contributed the most to the total loss of mass of the materials (Table 6.4) however, CO_2 and NO were also found in the decomposition products. The presence of the first one may be due to the fact that the materials adsorbed some of CO_2 from the atmosphere. Its content is the highest in the materials containing pure LDH since carbonate can be incorporated between the layers acting as charge balancing anion. The content of this compound is diminished in the case of hybrid adsorbents due to relatively lower percentage of LDH in their composition (Fig.6.1). Moreover, small amounts of NO were found during the analysis what should be due to traces of HNO_3 used during the synthesis that was not fully washed off from the materials or adsorbed in the interlayers, in the case of materials containing LDH (Table 6.4). Additionally, in the raw vermiculite emission of CO_2 and NO may be associated with presence of impurities

such as alkali and earth alkali nitrates, hydrocarbonates or carbonates or some other organic impurities (Post and Henderson, 2012). Derivatives of thermogravimetric curves of investigated materials are presented in Fig.6.7A and the mass lines of a model material in Fig.6.7B.

Table 6.4 Total mass loss and contribution of decomposition products for hybrid vermiculite-hydrotalcite materials

Material	total mass loss [%]	H_2O [%]	CO_2 [%]	NO [%]
W	17.28	15.18	1.49	0.61
W-S-1.8	16.58	15.34	0.95	0.29
W-S-3.2	10.15	7.93	1.5	0.73
W-LS-1.8	26.07	22.83	3.18	0.07
W-LS-3.2	30.22	26.58	3.57	0.06
W-L-1.8	42.53	32.1	9.18	1.25
W-L-3.2	43.53	31.68	8.52	3.33
HT-REF	43.54	35.39	7.15	1

6.4.3 Batch adsorption experiments

The raw vermiculite (W) exhibited moderate adsorption properties for the cationic dye Astrazon Red (AR) and copper cations, however in the case of anionic dyes, Congo Red (CR) and Reactive Red 184 (R), the capacities were negligible (Table 6.5). Similar behavior was observed in the case of the expanded vermiculite (Ve), however adsorption capacity for AR was lower. After calcination no significant changes occurred in the capacities, however a reduction of capacity of calcined W was observed for AR. The increase of acid concentration used in the treatment of the materials obtained from the solid fractions (S) of both vermiculites caused a decrease in the adsorption capacity of copper ions, which increased upon calcination to approximately the level of the starting materials. The capacity for AR increased after treatment with lower acid concentrations, which already had been proven to be optimal for that purpose (Stawiński et al., 2016) and decreased when higher concentrations were used. In relation to adsorption of R the capacity of the materials derived from both vermiculites initially increased upon the treatment with less concentrated acids but did not change when higher concentrations were applied. Calcination of those materials resulted in a drastic decrease in the capacity to the levels of the starting materials. For adsorption of CR no significant changes were observed.

The material formed solely of the liquid fraction (L) exhibited good adsorption capacity for the anionic dyes and copper ions. Adsorption of AR on them was insignificant as well as on the reference hydrotalcite (HT-REF), however after the thermal

treatment enabled all materials to adsorb that dye. The adsorption levels for CR were comparable to the reference material and similar for all materials. After calcination the capacities were significantly enhanced with more distinctive increase in the case of the materials treated in more concentrated acid. Regarding adsorption of R the capacities were influenced by acid concentration used in the treatment, with application of more concentrated acid resulting in higher capacity. Contrarily to adsorption of CR, after thermal treatment only materials derived from Ve and treated with higher concentrations of acid exhibited an increase in the adsorption capacity, whereas the opposite was true in the case of the materials obtained from W. Moreover, the material W-L-1.8 exceeded the capacity of the reference hydrotalcite. Every material obtained from that fraction showed higher adsorption capacity towards Cu^{2+} compared to the reference material. No statistically significant difference was observed between the materials obtained from the raw vermiculite however, the material formed from expanded vermiculite treated in 3.2 M nitric acid reached higher adsorption levels compared to the one treated in 1.2 M nitric acid. The thermal treatment resulted in an increase in the adsorption capacity of each material.

The composite materials obtained from liquid and solid fractions (LS) exhibited intermediate properties between both above described materials and were able to adsorb both types of dyes, and copper ions. In the case of AR the capacity was higher than the capacity of materials L and lower than of materials S, and it increased after calcination. For CR and R the maximum adsorption capacities for those dyes were lower than for those materials formed exclusively from liquid fraction (L) nonetheless significantly higher than those containing sole solid fraction (S). Adsorption of R on raw vermiculite has reached higher adsorption capacities compared to their counterparts obtained from the expanded material, and in each case the treatment with 3.2 M nitric acid resulted in better adsorption properties. However, such relation did not exist for adsorption of CR where no significant differences were observed between the materials. Calcination resulted in high increase in the capacities for CR in all cases and for R in the materials derived from W, however it decreased for this dye in the case of the material obtained from Ve. For adsorption of Cu^{2+} the materials obtained from both vermiculites revealed similar maximum adsorption capacities of values between those of the materials S and L, and upon annealing the capacity increased around two times in each case.

The experiments performed revealed a few phenomena occurring with the material on different stages of preparation related to adsorption capacities of different kind of adsorbates. First of all, acid activation of vermiculites results in an increase in their adsorption capacity for cationic dyes, with a certain optimal acid concentration that

gives the best adsorption properties. The highest increase was in the case of the material obtained after treatment of W with 1.8 M nitric acid, where the capacity increased from 48.5 ± 0.6 to 76 ± 11 mg g^{-1}. This is attributed to changes occurring in the material's structure when it is exposed to acid as a result of corrosion of the sheets, namely: leaching of octahedral layers by protonating the oxygen atoms; delamination of the structure and development of porosity what together with creation of amorphous silica phase provide new adsorption sites in the form of surface hydroxyls groups and make those already existing more accessible; a decrease in the layer charge, thus changing cation exchange capacity (CEC), which facilitate migration of dye molecules in between the layers (Schoonheydt and Johnston, 2006; Maqueda et al., 2009; Steudel et al., 2009; Stawiński et al., 2017). Regarding adsorption of metal cations the lowering of CEC resulted in decreased adsorption capacity for that adsorbate. Nonetheless, it was reported that nitric acid up to concentration 0.05 M can be used to treat vermiculite without a loss in the adsorption capacity (Stawiński et al., 2017). Moreover, calcination of such materials results in regeneration of the capacity for metal cations without any significant changes in the capacity regarding cationic dyes. The thermal modification of aluminosilicates changes their composition, structure and sorption ability and changes of those properties observed with the increasing temperature and individual and specific feature of given clay (Stefanova, 2001). One of the changes is lowering of cation exchange capacity (CEC) due to migration of cations into the layer structure, where they become basically non-exchangeable, which facilitates penetration of other species into the interlayer space *(Heller-Kallai, 2006)*. Other changes in the structure is that breaks and an amorphous phase is formed (Perez-Maqueda et al., 2012) at temperature range e.g. 550 to 650 °C for illite (Gerasimov and Bachvarov, 1977) and 450 to 650 ° in the case of kaolinite (Peters and Iberg, 1978). A decrease in the XRD reflection d_{002} the materials derived from W suggest the formation of an amorphous phase, however the temperature used during treatment was not high enough to affect the starting material, thus no changes in its capacity was observed for Cu^{2+}. Expanded vermiculite, Ve, had been subjected to thermal treatment in the process of exfoliation thus treatment at 450 °C did not manifest in any structural changes, except hydration state in the case of the materials Ve-C450 and V-S-1.2-C450 (Fig.6.6). However activation in stronger acid conditions rendered it more susceptible to further thermal modification i.e., decrease of CEC with no visible in the XRD patterns changes in the crystallinity thus the capacity of the materials Ve-S-3.2 also increased. Also the amorphous silica formed during acid activation is dehydroxylated at temperature around 350 °C (TG), which created new adsorption sites for metal cations (Goyne et al., 2002). However, thermal treatment greatly influenced the adsorption properties of some of the materials towards anionic

dyes and copper cations. The biggest change regarding CR was in the material W-L-3.2 where the capacity changed from 41.6 ± 0.4 mg g^{-1} to 289 ± 3 mg g^{-1} followed by W-LS-3.2 with a change from 42.3 ± 0.9 to 238 ± 3 mg g^{-1}, regarding R in the material W-LS-1.8 and W-L-1.8 with changes from 29 ± 2 to 219 ± 1 mg g^{-1} and from 58.4 ± 0.8 to 158 ± 2 mg g^{-1}, respectively. In the case of Cu^{2+} the change was the most prominent in the materials W-LS-3.2 and Ve-LS-3.2 with almost similar increase for 37 ± 2 mg g^{-1} reaching average level of 73.5 ± 2 mg g^{-1}. In the case of LDH bearing materials the hydrotalcite-like phase was transformed in mixed oxides after calcination. This material has an unique property and is able to reconstruct the LDH structure when in contact with water, and incorporate between the layers anions available in the solution (de Roy et al., 2006). In this case removal of dyes is more efficient since there is no need for diffusion between the layers that would be impeded due to the presence of interlayer species in the as prepared LDHs. Hydrotalcite-like materials despite their positive layer charge are also able to adsorb metal cations. The positive charge of the layers attracts hydroxide ions around the surfaces of LDH crystals in aqueous solution and metal hydroxides are formed. Furthermore the carbonates that are unavoidable present in the edges of the interlayer space and attached to the surface can come into contact with metal cations and form insoluble carbonates (Barnabas et al., 2016).

Furthermore, based on the data about composition of the composite materials obtained from liquid and solid fractions (LS) provided in Fig.6.1, it can be stated that in some cases a strong synergic effect on the adsorption took place. This assumption is based on comparison of a hypothetical capacity of an adsorbent obtained from both fractions mixed ex situ in adequate proportions with the capacities of the composites obtained during the experiment. It can be seen that the strongest effect was in the case of adsorption of CR and R onto the material Ve-LS-1.2 with an increase by 400 and 300%, respectively. This effect did not occur for adsorption of AR onto Ve-LS-3.2, and it the case of remaining materials the capacities were lower than the calculated ones with W-LS-1.8 having the lowest value of only 34%. The value was also below 100% in the case of adsorption of R onto the materials derived from the raw vermiculite and 105% for the material Ve-LS-3.2. Adsorption of Cu^{2+} was enhanced by 131 to 168%. This relation slightly changes after calcination, this effect was also most visible in adsorption of CR however, onto the material W-LS-1.8 with an increase by 339%. Moreover, the situation reversed and in the case of adsorption of R the materials derived from Ve reached values below 100% and the ones obtained from W showed strong synergic effect, on the level of 196 and 179% for the lower and higher acid concentration, respectively. Also adsorption of AR is enhanced onto all materials by 108 to 135%, and an increase of 176 to 214% was observed in the case of Cu^{2+}.

Table 6.5 Results of batch adsorption experiments of Astrazon Red (AR), Congo Red (CR), Reactive Red 184 (R) and copper cations (Cu) onto original and calcined materials.

Material	Adsorption capacity (mg g^{-1})							
	Original				Calcined			
	AR	CR	R	Cu	AR	CR	R	Cu
Ve	27.2 ± 0.7	5 ± 2	6 ± 2	19 ± 1	21.0 ± 0.5	4 ± 1	1 ± 1	17 ± 3
Ve-S-1.2	31 ± 2	1.02 ± 0.03	1.3 ± 0.4	22 ± 1	33.6 ± 0.6	1 .3 ± 0.3	1.3 ± 0.4	22 ± 1
Ve-LS-1.2	18 ± 1	43 ± 1	22.6 ± 0.6	35 ± 1	36 ± 1	84 ± 1	14 ± 1	62 ± 3
Ve-L-1.2	5 ± 2	39.7 ± 0.7	26 ± 1	40.7 ± 0.6	33 ± 1	155 ± 3	92 ± 1	49.5 ± 0.8
Ve-S-3.2	26 ± 2	4 ± 2	25.9 ± 0.1	3.2 ± 0.7	29 ± 1	1.1 ± 0 .3	1.1 ± 0.1	26.6 ± 0.7
Ve-LS-3.2	17 ± 2	36.3 ± 0.4	49.0 ± 0.4	38.1 ± 0.5	43 ± 2	75.3 ± 0.5	34.1 ± 0.5	75 ± 1
Ve-L-3.2	3.8 ± 0.6	37 ± 2	77.5 ± 0.5	51 ± 1	35.9 ± 0.7	21 4 ± 2	119.5 ± 0.3	66 ± 3
W	48.5 ± 0.6	7 ± 1	8 ± 3	19 ± 2	14.4 ± 0.5	9 ± 3	9 ± 4	17 ± 2
W-S-1.8	76 ± 1	4.7 ± 0.2	47 ± 2	9 ± 1	73 ± 2	0.44 ± 0.02	0 .44 ± 0.02	15 ± 1
W-LS-1.8	15.7 ± 0.3	41.1 ± 0.5	29 ± 2	37 ± 1	38.1 ± 0.9	2 19 ± 1	110 ± 2	70 ± 1
W-L-1.8	2.4 ± 0.4	39.7 ± 0.4	58.4 ± 0.5	48 ± 3	38.2 ± 0. 6	158 ± 2	137 ± 2	60 ± 3
W-S-3.2	35.1 ± 0.2	7 ± 1	47.8 ± 0.7	2.4 ± 0.8	31 ± 2	1.1 ± 0.3	1.11 ± 0.01	15 ± 2
W-LS-3.2	15.62 ± 0.03	42.3 ± 0.9	61 ± 1	35 ± 1	44 ± 1	238 ± 3	111 ± 2	72 ± 3
W-L-3.2	0.9 ± 0.2	41.6 ± 0.4	96.0 ± 0.4	44 ± 3	35.4 ± 0. 5	289 ± 3	109 ± 1	64 ± 2
HT-REF	0.63 ± 0.06	40 ± 2	75 ± 2	31 ± 3	35.6 ± 0.6	297 ± 3	125 ± 1	61.2 ± 0.7

6.5 Conclusions

Acid activation of clays is a common treatment in order to increase their adsorption properties; however the issue of generation waste by-product to authors' best knowledge has not been raised.

Waste by-products of acid activation of vermiculites were used as a substrate for synthesis of hydrotalcite-like layered double hydroxides (LDHs). Depending on starting material and acid concentration used in the activation, obtained materials were characterized by different levels of adsorption capacities towards different adsorbates. The anionic dyes, Congo Red (C) and Reactive Red 184 (R), and a metal cation, Cu^{2+}, were adsorbed better than the cationic dye Astrazon Red (AR). Materials derived from raw vermiculite (W), which was more susceptible to acid leaching than the expanded version (Ve), were characterized by higher adsorption capacities. Thermal treatment of the materials resulted in significant increase in their adsorption capacities for all investigated adsorbates. The highest levels were obtained on the material derived from W after treatment in 3.2 M nitric acid for CR and Cu^{2+}, reaching 289 ± 2 and 64 ± 2 mg g^{-1} respectively, however, adsorption of AR and R was better in the case of the counterpart of that material, obtained after treatment with 1.8 M HNO_3 with 38.2 ± 0.6 and 137 ± 2 mg g^{-1}, respectively. Moreover, both, the waste by-product and acid activated vermiculite, were successfully used to form hybrid vermiculite-hydrotalcite-like composite materials. The adsorbents obtained on that way exhibited very good adsorption properties towards cationic and anionic adsorbates. Also in this case the materials

derived from W had better capacities than the ones obtained from Ve and they were greatly increased on the way of thermal treatment reaching levels of 44 ± 1, 238 ± 3, 111 ± 2 and 72 ± 3 mg g^{-1} respectively for AR, CR, R and Cu^{2+} on the material W-LS-3.2 (i.e. hybrid material obtained from raw vermiculite treated with 3.2M HNO_3). Furthermore, in these materials, a strong synergic effect on the adsorption was observed. Based on their composition analysis, hybrid adsorbents adsorbed more of the above-mentioned species than theoretical adsorbents obtained by mixing ex situ acid activated vermiculite and material obtained from liquid fraction produced during that activation. Although present in the materials derived from both vermiculites, the synergic effect was more visible in the case of materials obtained from Ve, where the capacity reached up to 400% of the theoretically calculated on the material Ve-LS-1.2 (i.e. hybrid material derived from expanded vermiculite treated with 1.2M HNO_3).

The proposed synthesis of an adsorbent using the waste, stand as a solution for the problem of waste management and allows their valorization. Moreover, synthesized hybrid materials are able to efficiently remove both anionic and cationic pollutants, which makes them useful for pollution control, especially when the composition of wastewater is complex. Furthermore, the synthesis does not produce any waste and all elements of dissolved vermiculite are used in the procedure. Such prepared materials are not toxic, nor require toxic or hazardous substrates to their manufacturing, also no solvents or auxiliaries, nor high temperatures or pressures are needed in the process fulfilling the principles of Green Chemistry.

6.6 References

Ahlrichs, J.L., Serena, C., Serratosa, J.M., 1974. Structural hydroxils in sepolites. Clays Clay Miner. 23, 119-124.

Ali, I., Asim, M., Khan, T.A., 2012. Low cost adsorbents for the removal of organic pollutants from wastewater. J. Environ. Manage. 113, 170-183.

Anastas, P.T., Warner, J.C., 1998. Green Chemistry: Theory and Practice. Oxford University Press.

Angın, D., Köse, T.E., Selengil, U., 2013. Production and characterization of activated carbon prepared from safflower seed cake biochar and its ability to absorb reactive dyestuff. Appl. Surf. Sci. 280, 705-710.

Ayranci, E., Duman, O., 2009. In-Situ UV-Visible Spectroscopic Study on the Adsorption of some Dyes onto Activated Carbon Cloth. Sep. Sci. Technol. 44, 3735-3752.

Barabaszová, K.Č., Valášková, M., 2013. Characterization of vermiculite particles after different milling techniques. Powder Technol. 239, 277-283.

Barnabas, M.J., Parambadath, S., Mathew, A., Park, S.S., Vinu, A., Ha, C.-S., 2016. Highly efficient and selective adsorption of In3+ on pristine Zn/Al layered double hydroxide (Zn/Al-LDH) from aqueous solutions. J. Solid State Chem. 233, 133-142.

Belver, C., Bañares Muñoz, M.A., Vicente, M.A., 2002. Chemical Activation of a Kaolinite under Acid and Alkaline Conditions. Chem. Mater. 14, 2033-2043.

Bergaya, F., Lagaly, G., 2006. General introduction: clays, clay minerals, and clay science. in: Bergaya, F., Theng, B.K.G., Lagaly, G. (Eds.). Handbook of Clay Science. Elsevier Ltd.

Besson, G., Drits, V.A., 1997. Refined relationships between chemical composition of dioctahedral fine-grained mica minerals and their infrared spectra within the oh stretching region. Part I: identification of the oh stretching bands. Clay and Clay Minerals 45, 158-169.

Bhatnagar, A., Jain, A.K., 2005. A comparative adsorption study with different industrial wastes as adsorbents for the removal of cationic dyes from water. J. Colloid Interface Sci. 281, 49-55.

Braterman, P.S., Xu, Z.P., Yarberry, F., 2004. Layered double Hydroxides (LDHs). in: Auerbach, S.M., Carrado, K.A., Dutta, P.K. (Eds.). Handbook of Layered Materials. Marcel Dekker, U.S.A.

Chmielarz, L., Kowalczyk, A., Michalik, M., Dudek, B., Piwowarska, Z., Matusiewicz, A., 2010. Acid-activated vermiculites and phlogophites as catalysts for the DeNOx process. Appl. Clay Sci. 49, 156-162.

Chmielarz, L., Wojciechowska, M., Rutkowska, M., Adamski, A., Węgrzyn, A., Kowalczyk, A., Dudek, B., Boroń, P., Michalik, M., Matusiewicz, A., 2012. Acid-activated vermiculites as catalysts of the DeNOx process. Catal. Today 191, 25-31.

Chukanov, N.V., 2014. Infrared spectra of mineral species. Extended library.

de Roy, A., Forano, C., Besse, J.P., 2006. Layered double hydroxides: synthesis and post-synthesis modification. in: Rives, V. (Ed.). Layered Double Hydroxides: Present and Future Nova Science Publishers, Inc., New York.

Duman, O., Ayranci, E., 2006. Adsorption Characteristics of Benzaldehyde, Sulphanilic acid, and p-Phenolsulfonate from Water, Acid, or Base Solutions onto Activated Carbon Cloth. Sep. Sci. Technol. 41, 3673-3692.

Duman, O., Ayranci, E., 2010. Adsorptive removal of cationic surfactants from aqueous solutions onto high-area activated carbon cloth monitored by in situ UV spectroscopy. J. Hazard. Mater. 174, 359-367.

Duman, O., Tunç, S., 2008. Electrokinetic Properties of Vermiculite and Expanded Vermiculite: Effects of pH, Clay Concentration and Mono- and Multivalent Electrolytes. Sep. Sci. Technol. 43, 3755-3776.

Duman, O., Tunç, S., Polat, T.G., 2015. Determination of adsorptive properties of expanded vermiculite for the removal of C. I. Basic Red 9 from aqueous solution: Kinetic, isotherm and thermodynamic studies. Appl. Clay Sci. 109–110, 22-32.

El Gaini, L., Lakraimi, M., Sebbar, E., Meghea, A., Bakasse, M., 2009. Removal of indigo carmine dye from water to Mg–Al–CO3-calcined layered double hydroxides. J. Hazard. Mater. 161, 627-632.

El Mouzdahir, Y., Elmchaouri, A., Mahboub, R., Gil, A., Korili, S.A., 2009. Synthesis of nano-layered vermiculite of low density by thermal treatment. Powder Technol. 189, 2-5.

Földvári, M., 2011. Handbook of Thermogravimetric System of Minerals and Its Use in Geological Practice. Geological Institute of Hungary (=Magyar Állami Földtani Intézet).

Forgacs, E., Cserháti, T., Oros, G., 2004. Removal of synthetic dyes from wastewaters: a review. Environ. Int. 30, 953-971.

Gerasimov, E., Bachvarov, S.J., 1977. Technology of Ceramic Products. Technics, Sofia.

Goyne, K.W., Zimmerman, A.R., Newalkar, B.L., Komarneni, S., Brantley, S.L., Chorover, J., 2002. Surface Charge of Variable Porosity Al2O3(s) and SiO2(s) Adsorbents. J. Porous Mater. 9, 243-256.

Heller-Kallai, L., 2006. Thermally Modified Clay Minerals. in: Bergaya, F., Theng, B.K.G., Lagaly, G. (Eds.). Handbook of Clay Science. Elsevier Ltd.

Kloprogge, J.T., Frost, R.L., 2006. Infrrared and Raman Spectorscopic Studies of Layered Double Hydroxides (LDHs). in: Rives, V. (Ed.). Layered Double Hydroxides: Present and Furure. Nova Science Publishers, pp. 153-215.

Kloprogge, J.T., Hickey, L., Frost, R.L., 2004. FT-Raman and FT-IR spectroscopic study of synthetic Mg/Zn/Al-hydrotalcites. J. Raman Spectrosc. 35.

Komadel, P., Madejova, J., 2006. Acid Activation of Clay Minerals. in: Bergaya, F., Theng, B.K.G., Lagaly, G. (Eds.). Handbook of Clay Science. Elsevier Ltd.

Kuśtrowski, P., Chmielarz, L., Bożek, E., Sawalha, M., Roessner, F., 2004. Acidity and basicity of hydrotalcite derived mixed Mg–Al oxides studied by test reaction of MBOH conversion and temperature programmed desorption of NH3 and CO2. Mater. Res. Bull. 39, 263-281.

Lagaly, G., 2006. Colloid Clay Science. in: Bergaya, F., Theng, B.K.G., Lagaly, G. (Eds.). Handbook of Clay Science. Elsevier Ltd.

Lagaly, G., Ogava, M., Dekany, I., 2006. Clay Mineral Organic Interactions. in: Bergaya, F., Theng, B.K.G., Lagaly, G. (Eds.). Handbook of Clay Science. Elsevier Ltd.

Leitão, A., Serrão, R., 2005. Adsorption of phenolic compounds from water on activated carbon: prediction of multicomponent equilibrium isotherms using single-component data. Adsorption 11, 167-179.

Madejova, J., 2003. FTIR techniques in clay mineral studies. Vib. Spectrosc. 31, 1-10.

Madejová, J., Komadel, P., 2001. Baseline studies of the clay minerals society source clays: infrared methods. Clays Clay Miner. 49, 410-432.

Maqueda, C., Perez-Rodriguez, J.L., Šubrt, J., Murafa, N., 2009. Study of ground and unground leached vermiculite. Appl. Clay Sci. 44, 178-184.

Monsalvo, V.M., 2016. Introduction. in: Monsalvo, V.M. (Ed.). Water treatment in developed and developing nations. An international perspective. CRC Proess, Apple academic Proess.

Nakamoto, K., 2009. Infrared and Raman Spectra of Inorganic and Coordination Compounds, Part A, Theory and Applications in Inorganic Chemistry, 6th Edition. Wiley, New Jersey.

Ovejero, G., Rodríguez, A., Vallet, A., García, J., 2013. Ni/Fe-supported over hydrotalcites precursors as catalysts for clean and selective oxidation of Basic Yellow 11: Reaction intermediates determination. Chemosphere 90, 1379-1386.

Pan, B., Pan, B., Zhang, W., Lv, L., Zhang, Q., Zheng, S., 2009. Development of polymeric and polymer-based hybrid adsorbents for pollutants removal from waters. Chem. Eng. J. 151, 19-29.

Parikh, S.J., Goyne, K.W., Margenot, A.J., Mukome, F.N.D., Calderón, F.J., 2014. Chapter One - Soil Chemical Insights Provided through Vibrational Spectroscopy. in: Donald, L.S. (Ed.). Advances in Agronomy. Academic Press, pp. 1-148.

Pereira, L., Alves, M., 2011. Dyes-Environmental Impact and Remediation. in: Malik, A., Grohmann, E. (Eds.). Environmental Protection Strategies for Sustainable Development. Springer Science & Business Media.

Perez-Maqueda, L.A., Maqueda, C., Perez-Rodriguez, J.L., Subrt, J., Cerny, Z., Balek, V., 2012. Thermal behaviour of ground and unground acid leached vermiculite. J. Therm. Anal. Calorim. 107, 431-438.

Peters. T., Iberg, R., 1978. Mineralogical changes during firing od calcium-rich clays. The American Ceramic Society Bulletin 5, 503-509.

Pinnavaia, T.J., 2004. Foreword. in: Auerbach, S.M., Carrado, K.A., Dutta, P.K. (Eds.). Handbook of Layered Materials. Marcel Dekker, U.S.A.

Post, E., Henderson, J.B., 2012. Characterization of Two Different Clay Materials by Thermogravimetry (TG), Differential Scanning Calorimetry (DSC), Dilatometry (DIL) and Mass Spectrometry (MS) - 12215. WM2012: Waste Management 2012 conference on improving the future in waste management, United States.

Qwabe, L.Q., Friedrich, H.B., Singh, S., 2015. Preferential oxidation of CO in a hydrogen rich feed stream using Co–Fe mixed metal oxide catalysts prepared from hydrotalcite precursors. J. Mol. Catal. A: Chem. 404–405, 167-177.

Reife, A., Freeman, H.S., 1996. Environmental Chemistry of Dyes and Pigments. John Wiley & Sons, New York.

Ritz, M., Zdrálková, J., Valášková, M., 2014. Vibrational spectroscopy of acid treated vermiculites. Vib. Spectrosc. 70, 63-69.

Rives, V., 2006a. Preface. in: Rives, V. (Ed.). Layered Double Hydroxides: Present and Future. Nova Science Publishers, Inc., New York.

Rives, V., 2006b. Study of Layered Double Hydroxides by Thermal Methods. in: Rives, V. (Ed.). Layered Double Hydroxides: Present and Future. Nova Science Publishers, Inc., New York.

Rozada, F., Calvo, L.F., García, A.I., Martín-Villacorta, J., Otero, M., 2003. Dye adsorption by sewage sludge-based activated carbons in batch and fixed-bed systems. Bioresour. Technol. 87, 221-230.

Ruiz-Hitzky, E., Aranda, P., Saerratosa, J.M., 2004. Clay-organic interactions: organoclay complexes and polymer-clay nanocomposites. in: Auerbach, S.M., Carrado, K.A., Dutta, P.K. (Eds.). Handbook of layered materials. Marcal Dekker, New York.

Santos, R.M.M., Gonçalves, R.G.L., Constantino, V.R.L., da Costa, L.M., da Silva, L.H.M., Tronto, J., Pinto, F.G., 2013. Removal of Acid Green 68:1 from aqueous solutions by calcined and uncalcined layered double hydroxides. Appl. Clay Sci. 80–81, 189-195.

Santos, S.S.G., Silva, H.R.M., de Souza, A.G., Alves, A.P.M., da Silva Filho, E.C., Fonseca, M.G., 2015. Acid-leached mixed vermiculites obtained by treatment with nitric acid. Appl. Clay Sci. 104, 286-294.

Schoonheydt, R.A., Johnston, C.T., 2006. Surface and interface chemistry of clay minerals. in: Bergaya, F., theng, B.K.G., Lagal, G. (Eds.). Handbook of Clay Science. Elsevier.

Sevekow, U., 2003. Health and safety aspects. in: Hunger, K. (Ed.). Indystrial Dyes. Chemistry, Properties, Applications. Wiley-Vch, Weinheim.

Smykatz-Kloss, W., 2012. Differential Thermal Analysis: Application and Results in Mineralogy. Springer Berlin Heidelberg.

Sobhana, L.S.S., Mehedi, R., Malmivirta, M., Paturi, P., Lastusaari, M., Dîrtu, M.M., Garcia, Y., Fardim, P., 2016. Heteronuclear nanoparticles supported hydrotalcites containing Ni(II) and Fe(III) stable photocatalysts for Orange II degradation. Appl. Clay Sci. 132–133, 641-649.

Somasundaran, P., 2006. Encyclopedia of Surface and Colloid Science. Taylor & Francis.

Stawiński, W., Freitas, O., Chmielarz, L., Węgrzyn, A., Komędera, K., Błachowski, A., Figueiredo, S., 2016. The influence of acid treatments over vermiculite based material as adsorbent for cationic textile dyestuffs. Chemosphere 153, 115-129.

Stawiński, W., Węgrzyn, A., Freitas, O., Chmielarz, L., Mordarski, G., Figueiredo, S., 2017. Simultaneous removal of dyes and metal cations using an acid, acid-base and base modified vermiculite as a sustainable and recyclable adsorbent. Sci. Total Environ. 576, 398-408.

Stefanova, R.Y., 2001. Metal removal by thermally activated clay marl. Journal of environmental science and health. Part A, Toxic/hazardous substances & environmental engineering 36, 293-306.

Steudel, A., 2008. Selection Strategy and Modification of Layer Silicates for Technical Applications. Univ.-Verlag Karlsruhe.

Steudel, A., Batenburg, L.F., Fischer, H.R., Weidler, P.G., Emmerich, K., 2009. Alteration of swelling clay minerals by acid activation. Appl. Clay Sci. 44, 105-115.

Stubičan, V., Roy, R., 1961. Infrared Spectra of Layer-Structure Silicates. J. Am. Ceram. Soc. 44, 625-627.

Ummartyotin, S., Pechyen, C., 2016. Strategies for development and implementation of bio-based materials as effective renewable resources of energy: A comprehensive review on adsorbent technology. Renewable and Sustainable Energy Reviews 62, 654-664.

Wang, S., Shi, X., 2001. Molecular mechanisms of metal toxicity and carcinogenesis. Mol. Cell. Biochem. 222, 3-9.

Zhuravlev, L.T., 2000. The surface chemistry of amorphous silica. Zhuravlev model. Colloids Surf. Physicochem. Eng. Aspects 173, 1-38.

CHAPTER 7

General conclusions
and suggestions for future work

General conclusions

Clays, due to their specific structure are able to exchange cations, which gives them good properties and makes them interesting for application in wastewater treatment. Acid treatment of clays is a well-known procedure to increase their adsorption capacity. During the process the material is subjected to various changes, the interlayer cations are exchanged by protons, and metals from the layers are leached what results in delamination of the structure and weakening of interaction between layers, decrease of cation exchange capacity (CEC) and appearance of an amorphous phase with consequent increase of porosity and specific surface area. An additional step of activation, washing with citric acid, causes further leaching from the layers and removal of interlayer cations as well as and chelating of metals present in the solution preventing their redeposition in the structure of final product. All these phenomena facilitate adsorption of dyes and create new adsorption sites in the material. The treatment with 1.8 M nitric acid and 10% citric acid was able to increase the adsorption capacity of vermiculite for two cationic dyes, Astrazon Red (AR) and Methylene Blue (MB). The capacity changed from 54 ± 1 to 100.8 ± 0.8 mg g^{-1} in the case of adsorption of AR, and from 55 ± 2 to 150 ± 4 mg g^{-1} in the case of MB, based on results obtained in column operation, respectively for raw and treated material (feed concentration 50 mg L^{-1}) Although an enhanced adsorption of dyes was achieved, the capacity for metal cations was significantly diminished from 15 ± 1 to 5.28 ± 0.09 mg g^{-1}, respectively for raw and acid activated material in batch system with the initial Cu^{2+} concentration equal to 25 mg L^{-1}.

However, if a base activation (with NaOH) is added at the end of such acid activation, two changes are observed in the properties of the adsorbent: first, the adsorption capacity for dyes increases even more; second, the capacity for metal returns to the level of the untreated clay. This treatment removes the amorphous phase formed during acid activation, which in spite of, creating new adsorption sites, it also works as cementing agent impeding access to interlayer space and disaggregation of the material. Moreover, the remaining interlayer cations (Mg^{2+}) are exchanged by Na^{+} and, together with other metal cations that remained in the material after acid leaching, are redeposited in the form of hydroxides both in the interlayers and on the surface. The acid-base treatment leaves the material with highly distorted layers with multiple adsorption sites on broken edges and with Na^{+} as charge balancing ion, which is easier to exchange than any divalent cation. Moreover, CEC has decreased, thus migration between the layers is easier and there is no amorphous phase clogging the entrances between them. The adsorption capacity on such prepared material reached a level of 127 ± 2 mg g^{-1}, 203 ± 4

mg g^{-1} and 24 ± 1, respectively for AR, MB and Cu^{2+}, in column operation with the feed concentration of 50 mg L^{-1} in the case of the dyes, and 25 mg L^{-1} in the case of Cu^{2+}.

The modified material above described may find use in case of wastewaters leaden with moderate amount of dyes, without heavy metals present or at low concentration levels, which is typical in textile effluents. However, to treat a wastewater that contains more metal cations than dyes, vermiculite modified with 2 M sodium hydroxide solution should be used. This alkaline treatment does not change material's CEC or its specific surface area, nor significantly alter its composition. However interlayer cations are exchanged by Na^{+} and some of the amorphous phase appears due to removal of Si from the structure. Moreover, every species that is leached from the material is redeposited in it, in the form of hydroxides, which gives the material a coating of hydroxides. The alkaline activated material enhances its adsorption capacity for metal ions due to the presence of interlayer species that are easier to exchange than the original cations, keeping an high CEC due to the formation of new adsorption sites on coating of hydroxides. In this case the capacity for dyes remained unchanged in comparison with the raw material but the capacity for copper cations increased from 23 ± 3 to 51 ± 1 mg g^{-1}, in column operation with the feed concentration equal to 25 mg L^{-1}.

An in-depth study was carried on desorption and regeneration of modified vermiculites. It was found out that a mixture of ethanol and 1M sodium chloride (1:1 v/v) has good desorbing properties in the case of dyes, and a 0.5 M nitric acid solution efficiently desorbs metal cations, moreover it was feasible to separate metal cations from dyes during desorption in column operation.

Vermiculite based adsorbents were proven to be efficient in removal of cationic dyes and metal cations, however this group of material does not remove anionic species. For this purpose very interesting become layer-double hydroxides (LDHs) that are good anion exchangers. Moreover this group of materials upon thermal treatment transforms into mixed oxides that can regenerate their layer structure in water. An LDH material, hydrotalcite, was subjected to thermal modification in order to increase its adsorption properties. The optimal conditions were found upon annealing at 450°C, resulting in the formation of mixed oxides characterized by high specific surface area and high adsorption capacity. The maximum adsorption capacity for an anionic dye, based on the equilibrium studies, Levafix Amber (AMB), increased from 179 ± 5 on uncalcined material to 291 ± 8 mg g^{-1} on the thermally treated. Adsorption in this case was strongly pH dependent and at lower pH values removal of the anionic dye was the highest; in the range of higher pH values the material was able to remove cationic AR on the level of 6 ± 2 mg g^{-1} before calcination and 48 ± 2 mg g^{-1} after annealing. Thermal treatment was also used for regeneration of this materials and it was found that products of

decomposition of AMB, sulfuric compounds, were accumulated in the adsorbent upon each cycle of adsorption/regeneration, which can be considered as an additional advantage since it prevents the release of toxic sulfates to the environment.

Although the production of wastes could be the major drawback of the chemical modification processes their use in the synthesis of new materials allowed their valorization. Another LDH material was synthesized from the waste by-product of acid activation of raw (W) and expanded vermiculite (Ve). Also in this case, calcination at 450 °C resulted into a great increase of the adsorption capacities of these adsorbents. The highest levels were obtained on the material derived from W after treatment with 3.2 M nitric acid, reaching 289 ± 2 and 64 ± 2 mg g^{-1}, respectively for the anionic dye Congo Red (CR) and Cu^{2+}. However, adsorption of the cationic AR and another anionic dye, Reactive Red 184 (R), was better in the case of the counterpart of that material obtained with 1.8 M nitric acid, 38.2 ± 0.6 and 137 ± 2 mg g^{-1}, respectively.

Finally a composite hybrid vermiculite-LDH adsorbent was obtained in one-pot synthesis by combining the waste by-product with acid activated vermiculite. Also in this case the materials derived from raw vermiculite exhibited better adsorption capacities than the ones obtained from expanded mineral. They were greatly increased on the way of thermal treatment reaching levels of 44 ± 1, 238 ± 3, 111 ± 2 and 72 ± 3 mg g^{-1}, respectively for AR, CR, R and Cu^{2+} on the material obtained from the waste of acid activation with 3.2 M nitric acid. Furthermore, a strong synergic effect on the adsorption was observed in these materials. The hybrid adsorbents, obtained by mixing ex situ acid activated vermiculite and the LDHs, adsorbed more pollutants than it was theoretically expected based on their composition analysis. Although observed in materials derived from both vermiculites (W and Ve), the synergic effect was more pronounced in the materials obtained from Ve, where the capacity of the material obtained from the waste of acid activation with 1.2 M nitric acid was four times higher when compared to the theoretical one predicted from the capacities of the original materials. The results were obtained in batch system with concentration of200 mg L^{-1} for dyes and 30 mg $L^{-1}$for Cu^{2+} .

Developed adsorbents were obtained on a sustainable way that does not require application of high concentrated substances, nor high temperature or high pressures. The syntheses are easy and do not need highly qualified staff or advanced facilities. Adsorbents themselves are efficient in removal of pollutants, can be regenerated and reused. They also give possibility of separation of the adsorbates for their potential further use. The feasibility of application of the synthesized materials for cation (organic and inorganic) and anion removal has been proven. All that features make the technology readily available for applications not only in developed countries that have already advanced solutions, but also in developing countries where water pollution and a lack of advanced treatment facilities are still major problems.

Future work

The presented research opened a wide range of further interesting possibilities for scientific investigation and various practical applications of the developed materials. Some particularly intriguing examples are briefly described below.

Truly interesting appear their application for adsorption of pollutants from the gaseous phase. It was already successfully tested on a preliminary level and convincingly shown that such materials are fully capable to adsorb smoke of several cigarettes until it reached its capacity. This topic sounds exquisitely appealing because there in not much available literature addressing the serious subject of application of clays for remediation of the air, not to mention their modifications for that sole purpose.

To face a worrisome problem of emerging contaminants the materials were applied to remove from aqueous solution an antidepressant pharmaceutical, venlafaxine. Although, all the materials were able to adsorb that compound to some extent, some exhibited approximately 5 times greater adsorption capacity compared to the others. Thus very promising and hopeful seems extending their use for removal of other pharmaceuticals.

The catalysis is another domain where the materials could find a successful application. Some of the materials subjected to various modifications were used as catalysts for α-pinene isomerization. The main products of the reaction are desired feedstocks for e.g. pharmaceutical and cosmetic industry, also in syntheses of fine chemicals (e.g. camphene, limonene, terpinolene, α-terpinene, etc.). The catalytic properties of acid activated expanded vermiculite were used for the purposes of the $DeNO_x$ processes, different hydrotalcite-like materials are applied to catalytic N_2O reduction. Hence, studies on catalytic properties of already developed materials and on their modifications for that purpose should be truly fascinating.

Broadening the range of the species to which adsorption the materials can be applied could be achieved by their modifications by organic species (e.g. surfactants).

Another key issue that could be addressed is the adsorbent's form. The developed materials have a form of a powder what exhorts using filtration of some kind, provided the adsorbents are not used in a column system. To the effective solution of this practical problem comes encapsulation of those materials. Preliminary tests were performed on the samples derived from hydrotalcite. The material was successfully encapsulated in beads formed from a polysaccharyde. It was perfectly possible to obtain beads that could withstand moderate mechanical stress occurring during agitation and demonstrated general adsorption properties.

Due to the tremendous amount of arduous work it would required and strictly limited time, any further research must have been temporarily abandoned. It is abundantly evident the there is still a lot of research work to be carried out and the author fervently believes that there will be time and resources to continue it.